Sérgio Abílio Pereira Gonçalves

New generation of interactive platforms based on novel printed smart materials

novembro de 2021

Universidade do Minho
Escola de Engenharia

Sérgio Abílio Pereira Gonçalves

**New generation of interactive platforms
based on novel printed smart materials**

Tese de Doutoramento
Programa Doutoral em Engenharia
Eletrónica e de Computadores
Área de Instrumentação e Microssistemas Eletrónicos

Trabalho efetuado sob orientação de
Professor Doutor Pedro Sérgio Oliveira Branco
Professor Doutor Senentxu Lanceros-Méndez
Professor Doutor José Gerardo Vieira Rocha

novembro de 2021

DIREITOS DE AUTOR E CONDIÇÕES DE UTILIZAÇÃO DO TRABALHO POR TERCEIROS

ACKNOWLEDGEMENTS

I am grateful to my adviser Dr. Pedro Branco for his guidance on this project and his creative ideas. My special tanks to Dr. Senentxu Lanceros-Méndez for the technological support on this research and for all the supporting moments which were essential in giving me determination towards the next objective. Additionally, I would like to express my gratitude to Dr. José Gerardo Rocha.

I also want to thank Nélson Pereira and Nélson Castro for the nice partnership and for helping to develop several electrical systems. And likewise, for Vítor Correia, Pedro Costa, Carlos Costa and Jivago Nunes.

It is my intention to thank to both engageLab and ESM research group members for always providing me with a comfortable environment where I could work, socialize and have fun. I also am very grateful to Armando Ferreira who really helped me toward the final steps of my PhD.

My special thanks to João Pedro Ferreira and José Gomes Dias. They were a great inspiration in several moments for sharing their points of view, for guiding me into improving my arguing skills, for all the philosophical conversations, and for the emotional support on my weaker moments.

Quero expressar a minha gratidão aos meus pais e irmãos, pois nunca me abandonaram mesmo quando estava errado ou fui mais duro com eles. Sempre confiaram nas minhas capacidades, foram quem mais contribuiu para todas as oportunidades da minha vida e a quem todo o meu sucesso devo.

And the last intention of this list of thankfulness goes to the most recent person that entered my intimate life, yet contributing significantly to the person I am and to whom I purposely wrote this paragraph with a particular vocabulary with the intent of whetting the craving for English. I highly appreciate all those moments shared together, the concern and admiration for my work, the eagerness in trying to understand it despite the difficulty, the patience to endure the bad moments, and also for the caused deviations and distractions from my objectives... because they are also part of the run.

Smiling, open-minded, faithful, intense, amorous.

STATEMENT OF INTEGRITY

I hereby declare having conducted this academic work with integrity. I confirm that I have not used plagiarism or any form of undue use of information or falsification of results along the progress leading to its elaboration.

I further declare that I have fully acknowledged the Code of Ethical Conduct of the University of Minho.

STATEMENT OF INTEGRITY

ABSTRACT

The last decade was marked by the computer-paradigm changing with other digital devices suddenly becoming available to the general public, such as tablets and smartphones. A shift in perspective from computer to materials as the centerpiece of digital interaction is leading to a diversification of interaction contexts, objects and applications, recurring to intuitive commands and dynamic content that can proportionate more interesting and satisfying experiences.

In parallel, polymer-based sensors and actuators, and their integration in different substrates or devices is an area of increasing scientific and technological interest, which current state of the art starts to permit the use of smart sensors and actuators embodied within the objects seamlessly. Electronics is no longer a rigid board with plenty of chips. New technological advances and perspectives now turned into printed electronics in polymers, textiles or paper. We are assisting to the actual scaling down of computational power into everyday use objects, a fusion of the computer with the material. Interactivity is being transposed to objects erstwhile inanimate.

In this work, strain and deformation sensors and actuators were developed recurring to functional polymer composites with metallic and carbonaceous nanoparticles (NPs) inks, leading to capacitive, piezoresistive and piezoelectric effects, envisioning the creation of tangible user interfaces (TUIs). Based on smart polymer substrates such as polyvinylidene fluoride (PVDF) or polyethylene terephthalate (PET), among others, prototypes were prepared using piezoelectric and dielectric technologies. Piezoresistive prototypes were prepared with resistive inks and restive functional polymers. Materials were printed by screen printing, inkjet printing and doctor blade coating. Finally, a case study of the integration of the different materials and technologies developed is presented in a book-form factor.

Keywords: Interactive books, polymer sensors and actuators, printed electronics, smart materials, TUI.

RESUMO

A última década foi marcada por uma alteração do paradigma de computador pelo súbito aparecimento dos *tablets* e *smartphones* para o público geral. A alteração de perspetiva do computador para os materiais como parte central de interação digital levou a uma diversificação dos contextos de interação, objetos e aplicações, recorrendo a comandos intuitivos e conteúdos dinâmicos capazes de tornarem a experiência mais interessante e satisfatória.

Em simultâneo, sensores e atuadores de base polimérica, e a sua integração em diferentes substratos ou dispositivos é uma área de crescente interesse científico e tecnológico, e o atual estado da arte começa a permitir o uso de sensores e atuadores inteligentes perfeitamente integrados nos objetos. Eletrónica já não é sinónimo de placas rígidas cheias de componentes. Novas perspetivas e avanços tecnológicos transformaram-se em eletrónica impressa em polímeros, têxteis ou papel. Neste momento estamos a assistir à redução da computação a objetos do dia a dia, uma fusão do computador com a matéria. A interatividade está a ser transposta para objetos outrora inanimados.

Neste trabalho foram desenvolvidos atuadores e sensores e de pressão e de deformação com recurso a compostos poliméricos funcionais com tintas com nanopartículas (NPs) metálicas ou de base carbónica, recorrendo aos efeitos capacitivo, piezoresistivo e piezoelétrico, com vista à criação de interfaces de usuário tangíveis (TUIs). Usando substratos poliméricos inteligentes tais como fluoreto de polivinilideno (PVDF) ou politereftalato de etileno (PET), entre outos, foi possível a preparação de protótipos de tecnologia piezoelétrica ou dielétrica. Os protótipos de tecnologia piezoresistiva foram feitos com tintas resistivas e polímeros funcionais resistivos. Os materiais foram impressos por serigrafia, jato de tinta, impressão por aerossol e revestimento de lâmina *doctor blade*. Para terminar, é apresentado um caso de estudo da integração dos diferentes materiais e tecnologias desenvolvidos sob o formato de um livro.

Palavras-chave: Eletrónica impressa, livros interativos, materiais inteligentes, sensores e atuadores poliméricos, TUI.

CONTENTS

LIST OF ACRONYMS

Acronym	Meaning
μC	Microcontroller
3D	Three-dimensional
AC	Alternating current
ACP	Anisotropic conductive paste
ADC	Analog-to-digital converter
AMux	Analog multiplexer
ASCII	American Standard Code for Information Interexchange
AWG	American wire gauge
Ba	Barium
BaTiO$_3$	Barium titanate
BLE	Bluetooth Low Energy
BOPP	Biaxially oriented polypropylene
BPF	Band-pass filter
bps	Bits per second
CD-DEG	Circular diaphragm dielectric elastomer generator
CNT	Carbon nanotube
CPME	Cyclopentyl methyl ether
CTE	Coefficient of thermal expansion
DC	Direct current
DCM	Dichloromethane
DE	Dielectric elastomer
DEG	Dielectric elastomer generator
DIW	Direct ink writing
DMF	N,N-dimethylformamide
DOD	Drop-on-demand
dpi	Dots per inch
ECATT	Electrically conductive adhesive transfer tape
EAP	Electroactive polymer
EPAM	Electric poling-assisted additive manufacturing

Acronym	Meaning
FFC	Flexible flat cable
FFF	Fused filament fabrication
FG	Fluorinated graphene
FSR	Force-sensing resistor
FTDI	Future Technology Devices International Ltd.
GIG	Gold/ITO/gold
GND	Electrical ground
GUI	Graphical user interface
H	Hydrogen
HCI	Human-computer interaction
HPF	High-pass filter
HT	High temperature
HV	High voltage
I^{2}C	Inter-Integrated Communication
IA	Instrumentation amplifier
IAR	Ion assisted reaction
IC	Integrated circuit
IR	Infrared
ITO	Indium tin oxide
LED	Light-emitting diode
LiNbO$_3$	Lithium niobate
LPF	Low-pass filter
LT	Low temperature
ME	Magnetoelectric
MEMS	Microelectromechanical systems
MFC	Micro fiber composite
MIDI	Musical Instrument Digital Interface
MIT	Massachusetts Institute of Technology
MWCNT	Multi-walled carbon nanotube
N/A	Not applicable

Acronym	Meaning
NFC	Near-Field Communication
NP	Nanoparticle
O	Oxygen
OCR	Optical character recognition
OUI	Organic user interface
OWC	Oscillating water column
P(VDF-CTFE)	Poly(vinylidene fluoride-co-chlorotrifluoroethylene)
P(VDF-HFP)	Poly(vinylidene fluoride-co-hexafluoropropylene)
P(VDF-TrFE)	Poly(vinylidene fluoride trifluoroethylene)
P(VDF-TrFE-CFE)	Poly(vinylidene fluoride-trifluoroethylene-chlorofluoroethylene)
P(VDF-TrFE-CTFE)	Poly(vinylidene fluoride-trifluoroethylene-chlorotrifluoroethylene)
PAN	Polyacrylonitrile
PBAT	Polybutylene adipate terephthalate
PC	Polycarbonate
PCB	Printed circuit board
PCT	Projected capacitive touch
PDLA	Poly-D-lactic acid
PDMS	Polydimethylsiloxane
P-E	Polarization P (C/m2)/electric field E (V/m)
PEDOT	Poly(3,4-ethylenedioxythiophene)
PEDOT:PSS	Poly(3,4-ethylenedioxythiophene) polystyrene sulfonate
PEH	Piezoelectric energy harvester
PEN	Polyethylene naphthalate
PES	Polyethersulfone
PET	Polyethylene terephthalate
PhD	Doctor of Philosophy
PI	Polyimide

Acronym	Meaning
PLA	Polylactic acid
PLLA	Poly-L-lactic acid
PMMA	Poly(methyl methacrylate)
PMN-PT	Lead magnesium niobate-lead titanate
PP	Polypropylene
PPEN	Poly(phenyl ether nitrile)
PPS	Polyphenylene sulfide
PTFE	Polytetrafluoroethylene *(vulgarly known as Teflon)*
PU	Polyurethane
PUA	Polyurethane acrylate
PUI	Physical user interface
PVA	Poly(vinyl alcohol)
PVAc	Polyvinyl acetate
PVC	Poly(vinyl chloride)
PVDCN/VAc	Poly(vinylidene cyanide-vinyl acetate)
PVDF	Polyvinylidene fluoride
PWM	Pulse-width modulation
PWV	Pulse wave velocity
PZN-PT	Lead zinc niobate-lead titanate
PZT	Lead zirconate titanate
QR	Quick response
RF	Radio frequency
rGO	Reduced graphene oxide
rpm	Revolutions per minute
RRFC	Reversing ramping field capacitive
RT	Room temperature
SAW	Surface acoustic wave
SEBS	Styrene-*b*-(ethylene-co-butylene)-*b*-styrene
SF	Silk fibroin
SI	International System of Units

Acronym	Meaning	Acronym	Meaning
SiO_2	Silicon dioxide *or* silica	Ti	Titanium
SMA	Shape-memory alloy	TPU	Thermoplastic polyurethane
SMT	Surface-mount technology	TUI	Tangible user interface
SNW	Silver nanowire	TV	Television
sps	Samples per second	UART	Universal asynchronous receiver-transmitter
SSSEP	Simultaneous stretching and static electric poling	USB	Universal Serial Bus
SWCNT	Single-walled carbon nanotube	UV	Ultraviolet
		V_{cc}	Voltage common collector
TEM	Transmission electron microscopy	ZnO	Zinc oxide

LIST OF ABBREVIATIONS

Abbreviation	Meaning
&	and
@	at
©	copyright
®	registered trademark
a. u.	arbitrary units
approx.	approximated
Dr.	Doctor
e.g.,	*exempli gratia* (from Latin, meaning "for example", "for instance")
ed.	editor
eds.	editors
et al.	*et alias* (from Latin, meaning "and others")
etc.	*et cetera* (from Latin, meaning "and other things")
i.e.	*id est* (from Latin, meaning "that is", "in other words")
mol.%	mole percentage
n.d.	no date
p.	page
para.	paragraph
pp.	pages
sec.	section
vol.	volume
wt.%	weight percentage

LIST OF SYMBOLS

Symbol	Description	SI unit
μ	Viscosity	Pa·s
A	Area	m^2
C	Capacitance	F
d	Distance	m
d_{ij}	Piezoelectric coefficient	C/N
E	Electric field	V/m
E	Energy	J
F	Force	N
f	Frequency	Hz
GF	Gauge factor	–
I	Electric current	A
k^2	Electro-thermal coupling factor	–
k_{ij}	Electromechanical coupling factor	–
l	Length	m
$\varnothing$	Diameter	m
P	Polarization	C/m2
P	Power	W
p	Pyroelectric coefficient	C/m^2/K
Q	Electric charge	C
R	Resistance	Ω
T	Temperature	K
T_c	Curie temperature	K
T_g	Glass transition temperature	K
T_m	Melting temperature	K
V	Voltage	V
w	Width	m
γ	Surface tension	N/m
δ	Partial charge	–
ε	Strain	–
ε_0	Vacuum permittivity (constant $8.8541878128(13) \times 10^{-12}$)	F/m
ε_r	Relative permittivity *or* dielectric constant	–
η	Efficiency	–

Symbol	Description	SI unit
η	Energy density	J/m^3
ρ	Electrical resistivity	$\Omega \cdot$m
σ	Electrical conductivity	S/m
φ	Phase	rad
ω	Angular frequency	rad/s

LIST OF FIGURES

LIST OF TABLES

Dedicated to

my beloved wife Sofia, whose love, patience and understanding
have helped make this possible

my beloved daughter Sùria, that pure creation of God

"Growth is an endlessly iterative process.

When we learn something new, we don't go from "wrong" to "right."

Rather, we go from wrong to slightly less wrong.

And when we learn something additional, we go from slightly less wrong to slightly

less wrong than that, and then to even less wrong than that, and so on.

We are always in the process of approaching truth and perfection without actually

ever reaching truth or perfection." [1]

(Mark Manson)

1. INTRODUCTION

The revolution of digital devices in the last decade, particularly with smartphones and tablets suddenly becoming available to the general public, completely changed the traditional keyboard and mouse interface. A wave of developments within the human-computer interaction (HCI) field, riding on paradigms such as ubiquitous computing, tangible user interfaces (TUIs) and physical computing lead to a very recent perspective of a computer fused with the material (Ishii et al., 2012). The phenomenon was predicted by Weiser (1991) who started his article in the Scientific American magazine with:

> "The most profound technologies are those that disappear. They weave themselves into the fabric of everyday life until they are indistinguishable from it." [1]

(Mark Weiser)

He further continued by stating that computers were still a very recent technology in terms of humankind presence, but that in the future computation and computer interaction will be so ubiquitous that their presence will not be identifiable anymore. Just like writing once was such a new technology that required tremendous effort to operate such as making ink or baking clay, but that nowadays it has fused with our quotidian in newspapers, street signs, graffiti, or even in the candy wrapper (Weiser, 1991).

Digital technology is seamlessly woven within materials, displaying information through shape, color and texture (Coelho & Maes, 2009; Coelho & Zigelbaum, 2011), sensing interaction floors, walls, multitouch surfaces or textiles, enabling diverse and radically new forms of interactivity ranging from TUIs (Ishii & Ullmer, 1997), to organic user interfaces (OUIs) (Holman & Vertegaal, 2008) and computational composites (Vallgårda & Redström, 2007), among others.

The technological scaling down of the computer electronics and the availability of a number of novel material possibilities, such as conductive ink, conductive thread and fabric, electroactive materials, shape-memory alloys (SMAs), among others, lead to the exploration of materials embedded in paper, textiles or polymers with computational behaviors (Boem & Troiano, 2019). Some examples of such technology are the Electronic Popables, a paper book that integrates traditional pop-up mechanisms with thin, flexible, paper-based electronics (Qi & Buechley, 2010); Shutters, a fabric-made curtain with individually controlled louvers for information display and ventilation and daylight incidence control (Coelho & Maes, 2009); and Keppi, a compressible pressure sensor stick for self-reporting of pain intensity on patients (Adams et al.,

---

2018). Pressure detection is being introduced as the third dimension of user control, in addition to touch and location, using technologies such as piezoelectric, piezoresistive or capacitive (Dempsey et al., 2015).

Regarding material developments, polymers and polymer composites have been target of important advances recently. Composite materials is a class of materials composed by several constituent materials with different properties so that the combination of them results in a new material with properties that cannot be observed in any of the materials individually (Vallgårda & Redström, 2007). In turn, there is also a classification of smart materials, which represents a material or composite capable of changing one or more properties when in presence of a stimulus (Harrison & Ounaies, 2002).

With focus on the development of smart materials, a great deal of effort has been devoted to smart polymer-based materials, understanding, modifying, processing and characterizing (P Costa et al., 2017; Dias et al., 2015; P. Martins et al., 2014; Pedro Martins & Lanceros-Méndez, 2013; L. Wu et al., 2014). They present important characteristics such as flexibility, transparency, lightweight, low-cost and durability, among others. Polymer composites can also be tailored to exhibit smart response, such as dielectric, triboelectric, piezoelectric, pyroelectric, magnetostrictive or magnetoelectric, among others. All these have made of polymer composites one of the bases of the latest generation of physical interfaces (Vyas et al., 2012; Wessely et al., 2016).

In simultaneous, strong advances have also recently occurred in smart and functional materials based on the inclusion of nanoparticles (NPs), such as carbon nanotubes (CNTs), metallic NPs, magnetic NPs, or others, in order to improve the active response of materials (Georgakilas et al., 2007; Paiva et al., 2010). Piezoelectric, piezoresistive, magnetic and magnetoelectric properties, among others, have thus been developed to reach specific target applications (P. Costa et al., 2015; P. Martins et al., 2013, 2014; Pedro Martins & Lanceros-Méndez, 2013).

The tailoring of smart materials' properties for printing applications is, nevertheless, a very recent field and just few smart materials for printed technologies exist yet. There are suitable conductive, semiconductive and dielectric inks (H. F. Castro et al., 2014), which properties still deserve improvements.

Some examples of base technologies used in the development of polymer application interfaces are piezoelectric (Rendl et al., 2016), piezoresistive (Y.-J. Yang et al., 2008), pyroelectric (Rendl et al., 2012), capacitive (Grosse-Puppendahl et al., 2017), among others, promising enormous future developments in transforming computer interaction ubiquitous, along with sensors and actuators, of course.

Polymer composites allow for increased tangibility, as referred by Follmer et al. (2012):

"Malleable and organic user interfaces have the potential to enable radically new forms of interactions and expressiveness through flexible, free-form and computationally controlled shapes and displays." [1]

(Sean Follmer et al.)

Therefore, this work aims to evolve the state of the art by interconnecting materials and interaction, integrating new printed smart and functional materials, such as conductive inks and piezoelectric materials, among others, with interaction technologies. Electric circuits printed on polymers is still a brand-new field where innovations are increasingly expected and needed.

1.1. CONTEXT AND MOTIVATION

Probably, there is no simpler way to classify today's computer interaction experience with the user than as Ishii et al. (2012) did:

"Humans have evolved a heightened ability to sense and manipulate the physical world, yet the digital world takes little advantage of our capacity for hand-eye coordination." [2]

(Hiroshi Ishii et al.)

Traditional user interaction with computers through keyboard, mouse and screen lack many experience factors for our mind to grasp on, requiring much effort from our brain (Schmidt, 2017). It is not surprising the appearing of new paradigms that consider physical intuitive interactions as interfacing with computers (Ratti et al., 2004). Virtualization has never been present in our genesis up until

---

1 Republished with permission of ACM (Association for Computing Machinery), from "Jamming user interfaces: Programmable particle stiffness and sensing for malleable and shape-changing devices", (Follmer et al., 2012), copyright © 2012 ACM; permission conveyed through Copyright Clearance Center, Inc.

2 Republished with permission of ACM (Association for Computing Machinery), from *Interactions*, vol. *19*(1), "Radical Atoms: Beyond Tangible Bits, toward transformable materials", (Ishii et al., 2012), copyright © 2012 ACM; permission conveyed through Copyright Clearance Center, Inc.

computers appeared. Maybe that is the reason why we can easier recall the position of the pages in our notebook than in a digital file.

The difficulty of creating forms of interaction that are intuitive has been identified by (Cartwright et al., 2001):

> *"Using representations requires the availability of interfaces that work, and ones that work with different "representation machines" and with different users. The challenge is to provide flexible access to increasingly powerful geospatial (and related) representation software."* [1]

(William Cartwright et al.)

In a caricature of the problem in Figure 1.1, the cartoonist Dan Piraro poses the implicit question of how do traditional inanimate objects such as books and digital technology relate to each other, and how are users (in)capable to differentiate it.
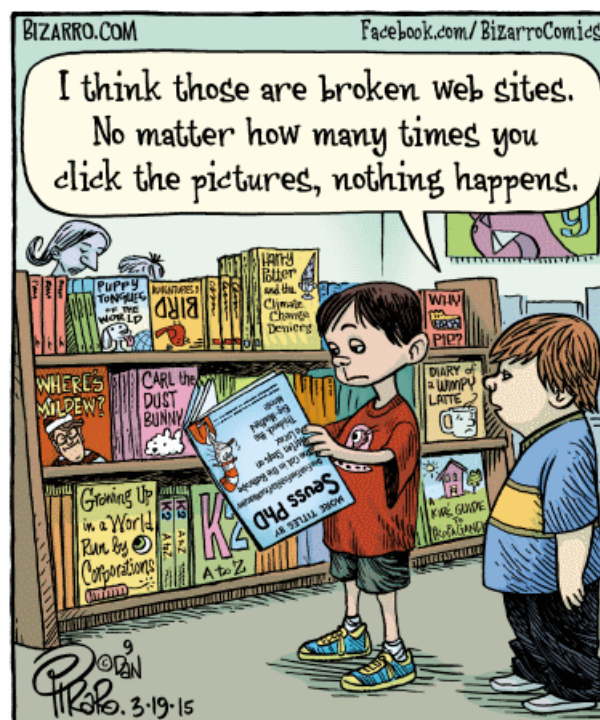
Figure 1.1.   Ironic illustration of the fusion of interfaces. Reproduced from bizarro.com, 3-19-15, copyright © 2015 Dan Piraro, by written permission.

---

1 Reprinted from *Cartography and Geographic Information Science*, vol. *28*(1), "Geospatial information visualization user interface issues", (Cartwright et al., 2001), Rights managed by Taylor & Francis.

Prior to the current project, the candidate had experience in the development of TUIs within the research team of engageLab[1], from University of Minho, and had several scientific papers published relating the development of new TUIs for children to playfully engage in narrative games and enhance their speech and storytelling capabilities (Sylla, Gonçalves, Branco, et al., 2012, 2013; Sylla, Gonçalves, Brito, et al., 2012, 2013). The research team was target of some prizes, from which two stand out particularly: the ACE 2012 Gold Creative Showcase Award, in Kathmandu, Nepal (Porto Canal, 2012), and the World Technology Award 2013 for the category of Entertainment, in New York (Centro ALGORITMI, 2013).

Moreover, when the candidate integrated another research team, ESM[2] (Electroactive Smart Materials Group), also at University of Minho, acquired experience in the development of printed electronics using electroactive and smart polymer materials for sensors and actuators, as well as learning the screen-printing technique. During this period, there was the prospect of visiting BCMaterials[3] (Basque Center for Materials, Applications & Nanostructures) in Bilbao, Spain, to gain experience with inkjet printing. This surely was another reason of motivation towards the polymer-topic research. And, in fact, an internship in this institution took place during the current PhD project.

These two research experiences allowed for the candidate to get in touch with the state of the art of each of the areas and the gap between them, to know experts in the field and acquire their knowledge, and were essential in identifying the statement of the problem and to trace a solution.

Therefore, the current project is supported by multidisciplinary teams, working on interaction technologies, electronics and materials. Several technologies were implemented with different materials, always envisioning the initial problem of interaction. At the end, a case study is presented as form-factor of aggregation of technologies.

Several projects were sources of inspiration for the current work. But one in particular was more motivational than the rest: Bridging Book, developed by the lab team (A. C. Figueiredo, Pinto, Branco, et al., 2013; Pinto et al., 2013). It consists in a printed book that works in conjugation with a tablet, showcasing the support for new interactions and the deep integration of interaction design and materiality. For better understanding, watch the video showcase[4] (A. C. Figueiredo, Pinto, Zagalo, et al., 2013).

This project represents strong scientific and technological innovation, as well as potential for technology transfer.

---

1 engageLab official website: http://engagelab.org
2 ESM official website: https://esmg.pt
3 BCMaterials official website: https://www.bcmaterials.net
4 Demo video also available at: https://vimeo.com/engagelab/bridgingbook

1.2. OBJECTIVES

The objectives of the current project were to explore, develop and incorporate new printed smart materials, such as conductive inks, piezoresistive inks and piezoelectric materials, among others, into digital platforms, as well as to develop new printable interaction platforms that could be explored in a proof-of-concept.

Regarding the development of novel materials oriented for applications, the first objective was to develop printable sensors and actuators based on capacitive, piezoelectric and piezoresistive materials, namely:

–   The development of strain and deformation sensors based on polymer composites with specific fillers such as carbonaceous filler and/or metallic nanoparticles (NPs);

–   The development of electronic sensors and actuators based on electroactive composites.

–   The development of green solutions for sensors, using natural polymers/fibers, such as paper;

–   The development of electronic solutions to interface printed devices.

It is to notice that several of the responsive materials were developed within the research team and that the main focus was the development of devices with printable inks (by screen printing and/or inkjet printing, among others).

The second main objective was the integration of materials and digital technology through interaction design methodology. The approach was to rely on off-the-shelf devices such as computers, smartphones or tablets combined with piezoelectric, piezoresistive and capacitive embedded materials to create sensors and actuators.

The third main objective was the development of hybrid physical/digital solutions as proof of concept showcasing the deep integration between devices and materials. This allowed for conceptualization, design and testing of interactive materials, leading to a proof-of-concept demonstrator.

Given the amount of work and the expected innovations, most of the effort will be devoted to the first objective.

1.3. SCIENTIFIC PUBLICATIONS

In the context of the current project there were published several documents, in a total of 10 journal articles, 2 conference posters and 1 cover artwork, listed in Table 1.1, Table 1.2 and Table 1.3, respectively.

Complete list of publications of the candidate can be accessed in the ORCID record of the candidate.[1]

Table 1.1.   List of published journal articles.

Journal publication
Pereira, N., Gonçalves, S., Barbosa, J. C., Gonçalves, R., Tubio, C. R., Vilas-Vilela, J. L., Costa, C. M. & Lanceros-Mendez, S. (2021). High dielectric constant poly(vinylidene fluoride-trifluoroethylene-chlorofluoroethylene) for capacitive pressure and bending sensors. *Polymer*, *214*, 123349. https://doi.org/10.1016/j.polymer.2020.123349
Dios, J. R., Gonzalo, B., Tubio, C. R., Cardoso, J., Gonçalves, S., Miranda, D., Correia, V., Viana, J. C., Costa, P., & Lanceros-Méndez, S. (2020). Functional piezoresistive polymer-composites based on polycarbonate and polylactic acid for deformation sensing applications. *Macromolecular Materials and Engineering*, 2000379. https://doi.org/10.1002/mame.202000379
Reizabal, A., Gonçalves, S., Pereira, N., Costa, C., Perez-Alvarez, L., Vilas, J. L., & Lanceros-Mendez, S. (2020). Optically transparent silk fibroin/silver nanowire composites for piezoresistive sensing and object recognitions. *Journal of Materials Chemistry C*. https://doi.org/10.1039/D0TC03428B
Mendes-Felipe, C., Barbosa, J. C., Gonçalves, S., Pereira, N., Costa, C. M., Vilas-Vilela, J. L., & Lanceros-Mendez, S. (2020). High dielectric constant UV curable polyurethane acrylate/indium tin oxide composites for capacitive sensing. *Composites Science and Technology*, *199*, 108363. https://doi.org/10.1016/j.compscitech.2020.108363
Costa, P., Gonçalves, S., Mora, H., Carabineiro, S. A. C., Viana, J. C., & Lanceros-Méndez, S. (2019). Highly sensitive piezoresistive graphene-based stretchable composites for sensing applications. *ACS Applied Materials & Interfaces*, *11*(49), 46286–46295. https://doi.org/10.1021/acsami.9b19294
Gonçalves, S., Serrado-Nunes, J., Oliveira, J., Pereira, N., Hilliou, L., Costa, C. M., & Lanceros-Méndez, S. (2019). Environmentally friendly printable piezoelectric inks and their application in the development of all-printed touch screens. *ACS Applied Electronic Materials*, *1*(8), 1678–1687. https://doi.org/10.1021/acsaelm.9b00363

---

[1] Sérgio Gonçalves https://orcid.org/0000-0002-3189-863X

Journal publication
Reizabal, A., Gonçalves, S., Brito-Pereira, R., Costa, P., Costa, C. M., Pérez-Álvarez, L., Vilas-Vilela, J. L., & Lanceros-Méndez, S. (2019). Optimized silk fibroin piezoresistive nanocomposites for pressure sensing applications based on natural polymers. *Nanoscale Advances*, *1*(6), 2284–2292. https://doi.org/10.1039/C8NA00417J
Dios, J. R., Garcia-Astrain, C., Gonçalves, S., Costa, P., & Lanceros-Méndez, S. (2019). Piezoresistive performance of polymer-based materials as a function of the matrix and nanofiller content to walking detection application. *Composites Science and Technology*, *181*, 107678. https://doi.org/10.1016/j.compscitech.2019.107678
Costa, P., Nunes-Pereira, J., Pereira, N., Castro, N., Gonçalves, S., & Lanceros-Mendez, S. (2019). Recent progress on piezoelectric, pyroelectric, and magnetoelectric polymer-based energy-harvesting devices. *Energy Technology*, *7*(7), 1800852. https://doi.org/10.1002/ente.201800852
Nunes, J. S., Castro, N., Gonçalves, S., Pereira, N., Correia, V., & Lanceros-Mendez, S. (2017). Marked object recognition multitouch screen printed touchpad for interactive applications. *Sensors*, *17*(12), 1–9. https://doi.org/10.3390/s17122786

Table 1.2.   List of conference posters.

Conference poster
Gonçalves, S., Pereira, N., Correia, V., & Lanceros-Méndez, S. (2019, March 19–21). *Multitouch printed touchscreens based on piezoelectric polymers* [Poster presentation]. LOPEC 2019, Munich, Germany. http://program.lopec.com/#!contentsessions/36021
Castro, N., Gonçalves, S., Nunes, J. S., Pereira, N., Correia, V., & Lanceros-Méndez, S. (2017, February 21–22). *Development of printed interactive surfaces based on electroactive polymers* [Poster presentation]. Printed and Flexible Electronics Congress 2017, London, United Kingdom. http://www.globalengage.co.uk/electronics/pr17.html#posters

Table 1.3.   List of published artwork journal covers.

Artwork cover
Gonçalves, S., Serrado-Nunes, J., Oliveira, J., Pereira, N., Hilliou, L., Costa, C. M., & Lanceros-Méndez, S. (2019). *ACS Applied Electronic Materials, 1*(8) [Cover image]. https://pubs.acs.org/pb-assets/images/_journalCovers/aaembp/aaembp_v001i008-3.jpg

1.4. OUTLINE OF THE THESIS

In the scheme of Figure 1.2 is represented the structure of the organization of this document.
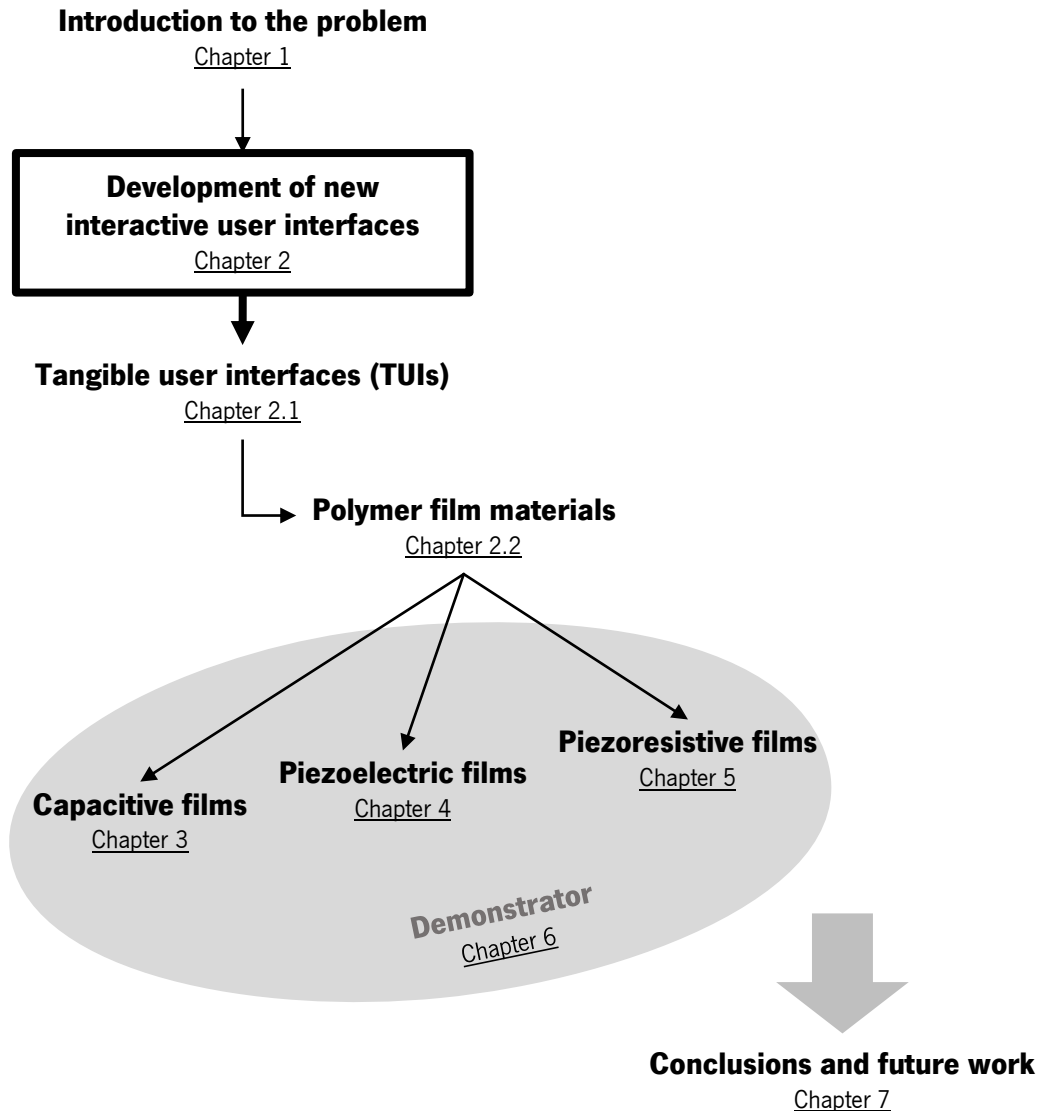
Figure 1.2.   Scheme of the thesis structure.

Each of the several chapters address a specific subject, namely:

– Chapter 1 introduces the inspiration for the current project and the urge for new interactive interfaces, referring polymer films as means to attain it. The research goals are indicated and it is listed the produced scientific publications.

– Chapter 2 presents the literature review relatively to the user interfaces and the solution to improve interfaces through tangible user interfaces (TUIs). It is also presented the literature review relative to polymer films with printed electronics, available materials and printing techniques.

– Chapter 3 introduces polymer film sensors based on capacitive sensing, mentioning relevant literature for single and multitouch surfaces, particularly those implemented polymer films. Next, it is showed the implemented systems for touch sensing, as well as the obtained results and conclusions.

– Chapter 4 is relative to the piezoelectric polymer film sensors and actuators. It is presented a brief historical context and the relationship between dielectric, piezoelectric, pyroelectric and ferroelectric materials. It is presented the methods for poling ferroelectric materials. Furthermore, it is explained the designed systems for piezoelectric sensor and actuators.

– Chapter 5 addresses piezoresistive materials, discussing the corresponding literature in the creation of sensors for touch, bending, deformation and multitouch surfaces. It is explained the developed systems and their implementation, along with the obtained results.

– Chapter 6 shows the application of the developed capacitive, piezoelectric and piezoresistive materials into a demonstrator, which is a hybrid book, exposing the tangibility of the interface and the potential for new exploitations.

– Chapter 7 presents conclusions of the developed work and points out future implementations and improvements.

– Chapter 8 lists the supporting bibliography of the document.

– Chapter 9 contains the appendices.

2. INTERACTION AND MATERIALS

The first part of this chapter presents the relevant state of the art of human-computer interaction (HCI) and the urge of tangibility in the design of (future) interfaces. The concept of tangible user interfaces (TUIs) has been long introduced, but a lack of smart materials and designs has limited the tangibility of devices (Ishii et al., 2012). For this reason, representative works on TUIs have been scattered over the last decade or so, and the emergence of novel forms of interface concepts has been somewhat stagnated, since visions published more than two decades ago are still deemed futuristic (Holman & Vertegaal, 2008; Ishii, 2008; Ishii et al., 2012; Ishii & Ullmer, 1997; Weiser, 1991).

Smart and electroactive polymer films with printed electronics represent a high potential for tangible materials to exhibit digital properties through a seamless technology. The advantages of such materials lie in the low-cost manufacturing, flexibility, physical robustness and lightweight, among others, which has led to an increase in applications as sensors and actuators (Briand et al., 2011; Song et al., 2014).The second half of this chapter focuses on those polymer film materials and fabrication techniques.

2.1. INTERFACES OF INTERACTION

The traditional interface based on display with keyboard and mouse was long questioned about how good this modality was for us to manipulate information (Ishii & Ullmer, 1997; Weiser, 1991). Digital technology often takes little advantage from the humans' ability to sense and manipulate physical objects (Ishii et al., 2012; Ishii & Ullmer, 1997; Schmidt, 2017). A wave of developments within HCI field, riding on paradigms such as ubiquitous computing, TUIs, physical computing and organic user interfaces (OUI), led to a very recent perspective of a computer fused with the material (Ishii et al., 2012).

The rigidity imposed by graphical user interfaces (GUIs) made researchers pursue new and more natural modalities of HCI. In the nineties, Mark Weiser introduced the concept of ubiquitous computing, suggesting that computer interaction must evolve and that the computer should stop being a box on a desk and become something we can carry to the beach, and something that vanishes into a digital

chalkboard wall (Weiser, 1991). Moreover, he defends that the computer must become invisible to the user.

Then, Hiroshi Ishii came along. It is not possible to talk about TUIs without saying the name of this professor of Massachusetts Institute of Technology's (MIT). The shared vision from the passage of GUIs to TUIs and beyond, alongside with his vast supporting work, makes Ishii a pilar of TUIs field. Ishii and Ullmer (1997) took on the Weiser's concept of the ubiquitous computer and published the notion of tangibility of digital objects. The approach suggests new design topologies for interfaces to allow users to directly grasp and manipulate the bits and pixels with bare hands (Ishii, 2008; Ishii & Ullmer, 1997). Consequently, the proposed approach envisioned three main measures: the transformation of ordinary architectural surfaces (walls, desktops, ceilings, doors, windows, etc.) into active interfaces; the coupling of everyday use objects (cards, books, models, etc.) with pertaining digital information; and the use of ambient media for background as cyberspace interface (sound, light, airflow, water movement, etc.) (Ishii & Ullmer, 1997). But, ultimately, TUIs means more than that.

2.1.1. Tangible user interfaces (TUIs) and beyond

Nowadays, TUIs is synonym of physical manipulation of objects loaded of digital information, and geolocation awareness of those objects (Ishii, 2008). This is based on the fact that humans have developed sophisticated skills to manipulate the physical environment they live in, doing specific actions such as carrying an object from a point to another. But GUIs require an abstract capability to manipulate information in a way that cannot be found anywhere else in nature (Ishii, 2008; Ishii et al., 2012). A study conducted by Xie et al. (2008) to compare children's performance and enjoyment in games using a physical user interface (PUI), a TUI and a GUI found no difference in the reported enjoyment, but the game using the GUI took more time for users to complete than for the PUI and the TUI.

In TUIs, the possibility of executing physical operations in specific objects allows for a more immersive experience. Digital information gets physical forms. Physical objects can be used to control information or to represent information (Ishii, 2008). This is explained by the diagram in Figure 2.1.

The sudden spread of touchscreens in smartphones and tablets in the last decade worked as a push to new forms of interaction. By freeing some of the rigidity of the traditional GUI, applications quickly immerged that transformed it into a TUI, such as Flexibles, a set of physical objects to be used with a tablet (Schmitz et al., 2017), depicted in Figure 2.2. Touch interfaces are now starting to consider

pressure sensing along with touch multitouch position, using piezoelectric, piezoresistive or capacitive technologies (Dempsey et al., 2015).
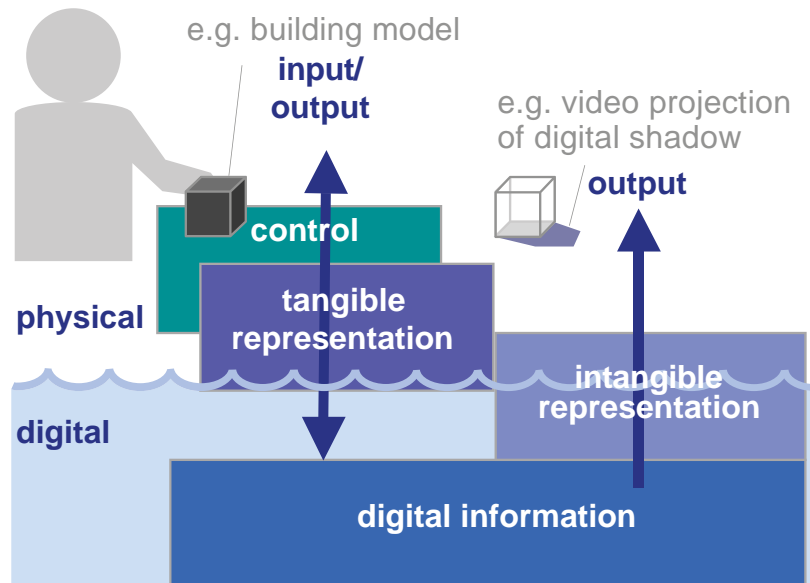
Figure 2.1.   Representation of tangible user interfaces (TUIs). Republished with permission from ACM (Association for Computing Machinery), from *Proceedings of the 2nd International Conference on Tangible and Embedded Interaction*, "Tangible Bits: Beyond pixels", (Ishii, 2008), copyright © 2008 ACM; permission conveyed through Copyright Clearance Center, Inc.

Figure 2.2.   Flexibles: tangible objects to use in a tablet. Republished with permission of ACM (Association for Computing Machinery), from *Proceedings of the 2017 CHI Conference on Human Factors in Computing Systems*, "Flexibles: Deformation-aware 3D-printed tangibles for capacitive touchscreens", (Schmitz et al., 2017), copyright © 2017 ACM; permission conveyed through Copyright Clearance Center, Inc.

Ishii et al. (2012) make a very interesting and self-explanatory analogy of the evolution of interfaces, representing digital technology as an iceberg, in Figure 2.3. A GUI is something similar to interacting with a sunken iceberg only through the surface of the water, or, if we must, giving commands through a keyboard and mouse while the information is shown on a screen. Likewise, a TUI, which foresees direct

manipulation of physical objects, can be thought of as if the iceberg has its tip out of the water, allowing the user to interact directly with some part of it more intuitively, while the remaining digital world stays hidden under beneath. Advances in materiality interaction tend to expose that digital world into more physical and natural interfaces, as if the iceberg is rising from the depths and becoming completely manipulable, something that the authors call Radical Atoms. It contemplates a new hypothetical generation of materials capable of changing appearance (color, texture) and shape (Schmidt, 2017).

a) A graphical user interface only lets users see digital information through a screen, as if looking through the surface of the water. We interact with the forms below through remote controls such as a mouse, a keyboard, or a touchscreen.

b) A tangible user interface is like an iceberg: There is a portion of the digital that emerges beyond the surface of the water – into the physical realm – that acts as physical manifestations of computation, allowing us to directly interact with the "tip of the iceberg."

c) Radical Atoms is our vision for the future of interaction with hypothetical dynamic materials, in which all digital information has physical manifestation so that we can interact directly with it – as if the iceberg had risen from the depths to reveal its sunken mass.

Figure 2.3.   Iceberg metaphor – from *(a)* **GUI (painted bits) to** *(b)* **TUI (tangible bits) to** *(c)* **Radical Atoms.** Republished with permission of ACM (Association for Computing Machinery), from *Interactions*, vol. *19*(1), "Radical Atoms: Beyond Tangible Bits, toward transformable materials", (Ishii et al., 2012), copyright © 2012 ACM; permission conveyed through Copyright Clearance Center, Inc.

In an interview with Anne Roudaut, Kasper Hornbæk, and Hiroshi Ishii it becomes evident the presence that shape-changing interfaces will take in the future of TUIs (Schmidt, 2017). Some authors have made efforts to attain such goals (Coelho & Maes, 2009; Coelho & Zigelbaum, 2011; Ou et al., 2016), but more material developments are necessary for a broader availability of materials to facilitate the design of applications.

Since nearly the beginning of computers' age that computers are not only of use during design and simulation of composite materials, but they also take major role during execution in dynamically controlling such materials. Some authors even defend that computational power itself is a constituent of composites (Vallgårda & Redström, 2007). The understanding that the computational power can be used

in conjugation with electrical properties, optical properties, tensile properties, thermal properties, deformations, etc. highlights the fact that computers have other modalities to present information other than through screens (Vallgårda & Redström, 2007).

Meanwhile, an intertwined more advanced topology for interfaces arises up. We live in a world of "blobjects" (contraction of "blob" and "object"), word for an object tool with smooth curves and no sharp edges. These are the types of objects that we find in nature, not flat screens, and they advocate that user interfaces should be based on such objects, creating organic user interfaces (OUIs). The concept of OUIs emphasizes on the employment of non-planar displays, often capable of changing form (Shaer & Hornecker, 2010, sec. 10.2). Holman and Vertegaal (2008) present the following comparison that gives us a glimpse of tomorrow's idea of computation:

"For example, the leaves of plants form resilient solar panels that bend rather than break when challenged. They are not just flexible to adapt to their environment, they also grow and adjust shape to maximize solar efficiency. Computers may one day do just that." [1]

(David Holman & Roel Vertegaal)

That results in the concept of the computer fused with the material, and altogether will be a form of user interface.

2.1.2. Some examples of applications

The Mark Weiser's vision of ubiquitous computing (Weiser, 1991) in which he defends that the computer must become more and more invisible to the user, has made researchers to create platforms with virtual touchscreens that can be applied to any surface regardless of size, using cameras and projectors (Soleimani et al., 2011), or mid-air gesture recognition, using capacitive and acoustic technologies together (Braun et al., 2016).

Grosse-Puppendahl, Berghoefer, et al. (2013) have presented a prototype which they named OpenCapSense, consisting in a toolkit for capacitive sensing for easy user interface configuration. The

---

[1] Republished with permission of ACM (Association for Computing Machinery) from *Communications of the ACM*, (Holman & Vertegaal, 2008), vol. *51*(6), copyright © 2008 ACM; permission conveyed through Copyright Clearance Center, Inc.

authors present four case-study scenarios, namely a gesture recognition platform, a wearable device capable of monitoring muscle activity or identifying user actions such as drinking, a fall detection floor, and a smart couch capable detecting posture, depicted in Figure 2.4. Pohl et al. (2015) followed up on the interactive couch and used it as form of control over the environment solely based on the user's posture, such as turning lights on for reading, playback music to relax, turn the television on, and so on.
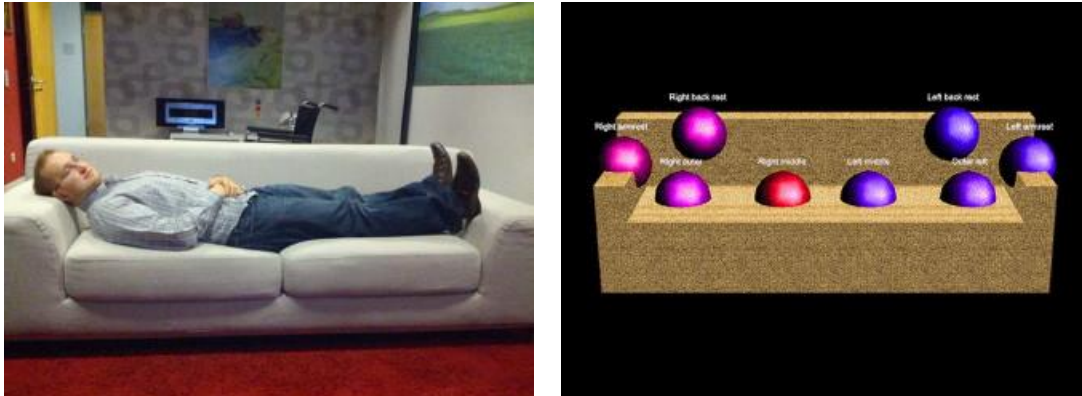
Figure 2.4.   Smart couch, capable of recognizing different postures. Reprinted from (Grosse-Puppendahl, Berghoefer, et al., 2013), copyright © 2013, IEEE.

To achieve similar operations, Schoessler et al. (2015) instead relied on cable control to grant interaction, in a project they called Cord UIs, shown in Figure 2.5. The cables were equipped with pressure sensors to detect user actions such as touch, sliding, pinching, stretching, swinging, kinking, swinging, etc.. For example, tightening a knot in the cord changes intensity of the lamp, or pulling the Universal Serial Bus (USB) cable performs safe-removal.

(a)   *(b)*   *(c)*
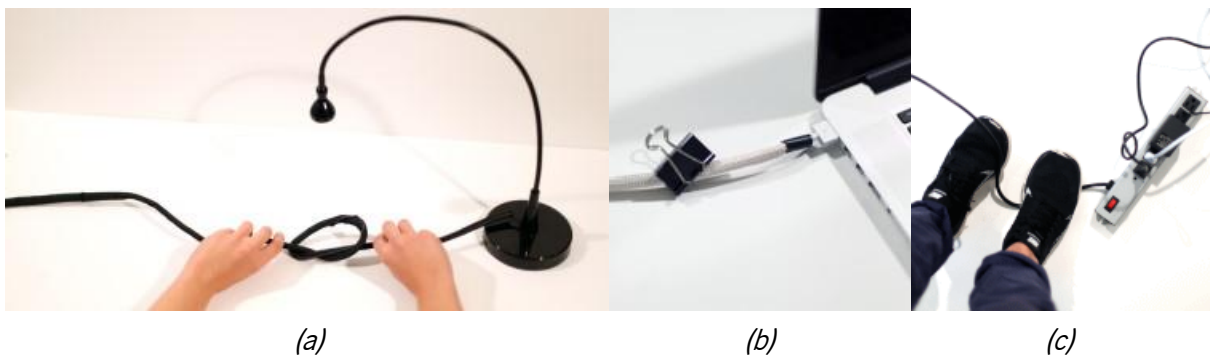
Figure 2.5.   Cord UIs prototype that allows to control devices through the cable interaction: *(a)* knot detection for light intensity control, *(b)* clamp pression to put computer to sleep, and *(c)* kink cable to power energy off. Republished with permission of ACM (Association for Computing Machinery), from *Proceedings of the Ninth International Conference on Tangible, Embedded, and Embodied Interaction*, (Schoessler et al., 2015), copyright © 2015 ACM; permission conveyed through Copyright Clearance Center, Inc.

The following project is a true advance in technology, combining material science, electronic sensing techniques and interaction. Yang Zhang et al. (2017) proposed Electrick, a low-cost system capable of transforming any surface in a touch surface, whether it is small or large, flat or not. The authors rely on conductive materials such as polymer films, coatings or paints, but mostly carbonaceous ink spray to apply on the desired surface. Then, using electrodes distributed regularly around the edges of the surface, an electronic scanning system detects the finger touches, based in tomography, in a manner that resembles mutual-capacitance matrix sensing (described in section 3.1.2.2. Mutual-capacitance). In Figure 2.6 is shown a guitar prepared by Electrick. The touch buttons and sliders can be virtually placed on any position of the surface. Prior to use, the system requires the user to setup the sensitive locations, since every surface must be calibrated to overcome the lack of homogeneity of the conductive deposition.

Figure 2.6. **Electrick: a low-cost technique to assess touch input on objects or surfaces, even in non-flat ones. Illustration shows a guitar that was sprayed with carbonaceous ink to create touch buttons and sliders.** Republished with permission of ACM (Association for Computing Machinery), from *Proceedings of the 2017 CHI Conference on Human Factors in Computing Systems*, (Yang Zhang et al., 2017), copyright © 2017 ACM; permission conveyed through Copyright Clearance Center, Inc.

TUIs have been used for educational purposes, allowing for better comprehension of hard-to-understand concepts. One of such examples is the platform propose by Schneider et al. (2013) for neuroscience learning. The authors identified difficulties in visualizing and understanding complex multidimensional relationships between brain regions even by students of the area, a followed a TUI approach for a less constrained system and that can also encourage wider exploration. The built prototype consisted on a tabletop with a projector and a camera underneath the table, shown in Figure 2.7. A replica of the brain is manipulated on the table. It is possible to deconstruct and reconstruct it, as well as manipulate it. The camera underneath the table tracks the position of each brain regions. Then, the projector creates an augmented reality layer by showing the connections between each part of the brain.

The authors claim that students who engaged in the platform interaction outperformed those who used traditional book reading learning method.

Figure 2.7.   BrainExplorer, a TUI for neuroscience teaching and learning. Reprinted from (Schneider et al., 2013), copyright © 2013, IEEE.

The technological scaling down of the computer electronics and the availability of a number of novel material possibilities, such as conductive ink, conductive thread and fabric, shape-memory alloys (SMAs), among others, lead to the exploration of materials embedded in paper or textiles with computational behaviors. One example of such technology is Electronic Popables from Qi and Buechley (2010), a paper book that integrates traditional pop-up mechanisms with thin and flexible paper-based electronics, as shown in Figure 2.8. The construction of the book seeks blending electronics invisibly with paper through the creation of switches, sensors and actuators while keeping circuitry as thin as possible. It combines the use of copper tape, conductive fabric and conductive paint with light-emitting diodes (LEDs), magnets, magnetic paint, SMAs, piezoresistive elastomers, and other electronic components. Energy is usually provided by a small circuit containing a battery, which attaches magnetically to the book in a specific slot. According to the authors, the differential factor from Electronic Popables to the majority of the similar projects is that the development of Electronic Popables focuses on a stand-alone paper book, which grants it some advantage by its autonomy.
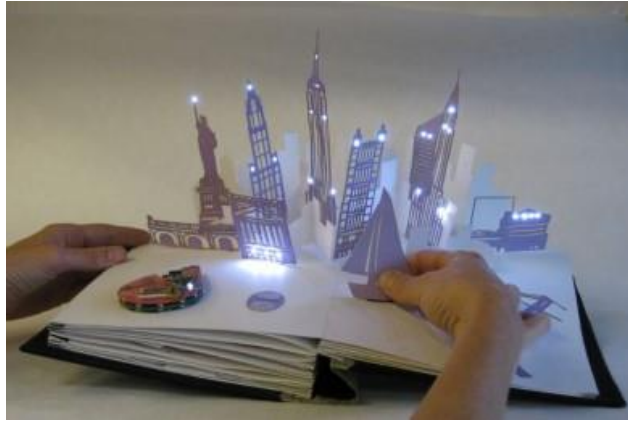
Figure 2.8. **Electronic Popables: an electronic pop-up book.** Republished with permission of ACM (Association for Computing Machinery), from *Proceedings of the Fourth International Conference on Tangible, Embedded, and Embodied Interaction*, (Qi & Buechley, 2010), copyright © 2010 ACM; permission conveyed through Copyright Clearance Center, Inc.

Nonetheless, the use of a computational system can come out with some benefits too, as Węgrzyn (2012) demonstrated in his diploma project where he presented Elektrobiblioteka[1] (in Polish, Electrolibrary in English), a physical book with printed circuits with conductive ink. It detects when the book is opened and in what page and a computer adds hybrid functionality to the book, displaying complementary information to the book's content. Attached to the book is a microcontroller that detects the page through mechanical switches, and in some cases, also the finger touches in specific spots. That information is sent to the computer via USB, which triggers actions on the screen of the computer.

It has been noticed that page detection in hybrid books is an important feature, but the existence of wires and cables coming out of the book might end up creating an undesired notion of complexity for an object best-know for simplicity. This issue was successfully overcame by Figueiredo, Pinto, Branco, et al. (2013) in their project Bridging Book through the incorporation of thin magnets in the book sheets that can be read by the tablet's internal compass. The book and the device must be placed next to each other, as shown in Figure 2.9, and as the user flips the pages, the tablet updates content, requiring no batteries or wires. The digital device provides further interaction with the user, particularly designed for educational purposes (A. C. Figueiredo, Pinto, Branco, et al., 2013; A. C. Figueiredo, Pinto, Zagalo, et al., 2013; Pinto et al., 2013).

1 Elektrobiblioteka presentation video: https://vimeo.com/prtscr/elektrobiblioteka

Figure 2.9.   Bridging Book, a hybrid book that combines a physical book with an iPad.
Republished with permission of ACM (Association for Computing Machinery), from
*Proceedings of the 2014 Workshops on Advances in Computer Entertainment
Conference*, (Sylla et al., 2014), copyright © 2014 ACM; permission conveyed through
Copyright Clearance Center, Inc.

Masunaga et al. (2017) implemented Navigation Book, an interface for physically manipulating page navigation in a digital book. The interface is based on a physical book, which commands the digital book to display the same page than it is opened in the physical one, allowing the user to perform intuitive operations otherwise not possible in digital books such as inserting the finger among pages to keep a temporary bookmark, back-and-forth page flipping without losing attention, randomly opening a page, bookmarking a page by folding its corner, or half-flipping a page to take a peek on the next one, among others. The implementation of the system uses Quick Response (QR) codes printed on the corner of each page of the book to identify its page number, and a camera to recognize the current page.

Electronics have also been embedded in educational touch-and-feel books. Moorthy et al. (2017) present Hello World prototype, a metaphor for children having their first contact with an interactive book. It consists in a textile touch-and-feel with embedded electronic circuits, including LEDs, light sensors and acoustic actuators, among others, as visible in Figure 2.10. The aim of the project was to keep children using their senses enthusiastically and while keeping motivated to explore. Very similarly, Posch (2021) also introduces Crafting Stories, a touch-and-feel book with increased interaction, containing elements such as a furry cat with vibration to simulate a real cat when the children pet it, among others.

Figure 2.10. Hello World book prototype, a textile touch-and-feel book with embedded electronics (two dots in the firefly are a light sensor, and stars are LEDs).
Reprinted from Moorthy et al. (2017) with permission, copyright © 2017 Owner/Author.

On the other hand, Flexibles (previously shown in Figure 2.2) are deformable objects that can interact with a tablet's touchscreen, adding deformation awareness to passive objects (Schmitz et al., 2017). The objects are three-dimensional (3D)-printed, containing embedded conductive structures for touchscreen identification via capacitive coupling effect. The objects can recognize deformations such as pressing, squeezing or bending. The authors developed three interactive application examples. One of the examples, called Angry Trees, is a game where two users fight against each other throwing fruits by bending and releasing their own tree. The system takes into account the orientation and position of the trees.

Another good project of demonstration of TUIs is the work presented by Villar et al. (2018), Zanzibar. It consists in a mat capable of detecting the objects placed on it and their location. It uses capacitive sensing to detect the objects and hover gestures, and Near-Field Communication (NFC) over a large area to identify the pieces. The authors present different case scenarios, one of them the Movie Maker, shown in Figure 2.11, which allows the user to create a shooting scene with tangible objects. The objects are passed to the computer, generating a 3D construction of the set-up scenario. After using, it is possible to simply wrap the entire mat and carry it around, since the mat is composed by two outer layers of fabric with two inner layers of flexible substrates: a stretchable NFC antenna array and a flexible printed circuit board (PCB) capacitive layout. This prototype has been designed as a toy for children storytelling as they play with the objects, but other uses are possible.

Figure 2.11.   Project Zanzibar: a flexible mat capable of detecting objects placed on it via NFC, and their location via capacitive sensing. Republished with permission of ACM (Association for Computing Machinery), from *Proceedings of the 2018 CHI Conference on Human Factors in Computing Systems*, (Villar et al., 2018), copyright © 2018 ACM; permission conveyed through Copyright Clearance Center, Inc.

The design of projects for the construction of the narratives for storytelling by children has also been including TUIs, as it was particularly noticeable in the works developed by in the project TOK (Sylla, Branco, & Coutinho, 2011; Sylla, Branco, Coutinho, et al., 2011), where an initial setup of pre-made cardboards helped children creating a story, later developed into a hybrid system complimented by an electronic platform called t-books (Sylla, Ângelo, et al., 2011; Sylla, Gonçalves, Brito, et al., 2012, 2013). Figure 3.14 shows the t-books prototype.

Similarly, t-words follows the blocks concept for the creation of narratives and language exploitation (Sylla, Gonçalves, Branco, et al., 2012, 2013). It comprises a set of blocks where children can record sounds. The blocks are attachable to each other magnetically, which triggers the playback of the recorded sounds according to the order that they are associated. A sequence of t-words blocks is shown in Figure 2.12.

TUIs can be employed in nearly every area fields. A new prototype named Keppi for medical science can help the health of those suffering from chronical pain by more precisely reporting it to the healthcare provider. Keppi is a TUI for patients to self-report pain levels by the means of a pressable device that they hold on their hands and measures the amount of force exerted (Adams et al., 2018). The stronger the pain, the higher the natural contraction the patient's muscles. A photograph of the device and its internal diagram representation are shown in Figure 2.13. The device is deformable, containing a thick layer of rubber, but the top cap is rigid and holds a battery and a Bluetooth Low Energy (BLE) communication module, so there is no wiring connecting to the device.

Figure 2.12. t-words: a set of audio record and playback blocks for language exploitation. Reprinted by permission from Springer Nature, *Creativity in the Digital Age*, (Sylla et al., 2015), copyright © 2015, Springer-Verlag London.
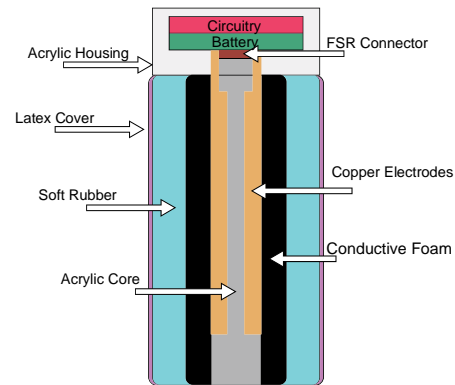
(a)   *(b)*

Figure 2.13. Keppi: *(a)* TUI for self-reporting pain and *(b)* schematic representation of the device. Republished with permission of ACM (Association for Computing Machinery), from *Proceedings of the 2018 CHI Conference on Human Factors in Computing Systems*, (Adams et al., 2018), copyright © 2018 ACM; permission conveyed through Copyright Clearance Center, Inc.

Another project in the health domain is the work presented by Rus et al. (2014) which consists in a system to recognize bed postures using capacitive sensing. The system is targeted to elderly people to prevent prolonged bad bed postures and therefore avoid further health complications such as the decubitus ulcer. The proposed approach was a grid of crossed wires to be placed on top of the mattress, below the bedsheets.

The concept of organic user interfaces (OUIs) presupposes the use of non-planar displays to present information to the user (Holman & Vertegaal, 2008; Shaer & Hornecker, 2010, sec. 10.2). OUIs are strongly linked to the shape changing interfaces. One example of such approach is the kinetic window display of Shutters by Coelho and Maes (2009). It consists in a fabric surface of levered windows electrically controlled with shape-memory alloy (SMAs). Figure 2.14 shows a fabric prototype and the

detail of the levered window. It can be of use for efficient light control in buildings or for shadow image projection.

Nevertheless, in a more recent work, Coelho and Zigelbaum (2011) improved Shutters by trying a more generic approach, by using thick fabric and foamy parts together with SMAs, which permitted operations such as elongations and compressions in specific places that resulted in bends and twists, therefore transforming the object into something more complex with dynamic shape. Figure 2.15 shows Surflex, one of the developed prototypes. A process somewhat related to origami. However, as the authors pointed out, the power requirements of the SMAs are considerably high, making their untethered use impractical.

(a)   (b)

Figure 2.14.   Shutters: *(a)* kinetic shadow window display and *(b)* detail of the levered windows using SMAs. Republished with permission of ACM (Association for Computing Machinery), from *Proceedings of the 3rd International Conference on Tangible and Embedded Interaction*, (Coelho & Maes, 2009), copyright © 2009 ACM; permission conveyed through Copyright Clearance Center, Inc.

Figure 2.15.   Surflex: transformable and programmable physical surface. Reprinted by permission from Springer Nature Customer Service Centre GmbH: Springer Nature, *Personal and Ubiquitous Computing* (Coelho & Zigelbaum, 2011), copyright © 2010, Springer Nature.

A similar shape-changing device based on paper was implemented by G. Wang et al. (2018), as shown in Figure 2.16. The electric layout is printed on paper with a fused filament fabrication (FFF) 3D printer, using conductive polylactic acid (PLA) filament. The conductivity of the filament is provided by graphene particles, which expands when heated. The bilayer actuator relies on the Joule heating of the conductive PLA filament to get deformed when an electric current flows through the printed filament. Additionally, the system also implements capacitive touch sensing, and self-angle detection based on the resistance change of the filament, which broadens the range of applications, including paper robots, artistic demonstrations, pop-up book mechanisms and volumetric transformation, among others.

(a)   *(a)*
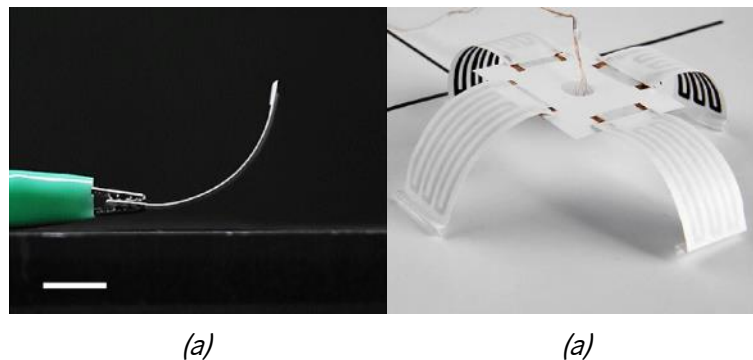
Figure 2.16. Paper-based actuators: *(a)* single actuator and *(b)* four actuators in the legs of a robot. Republished with permission of ACM (Association for Computing Machinery), from *Proceedings of the 2018 CHI Conference on Human Factors in Computing Systems*, (G. Wang et al., 2018), copyright © 2018 ACM; permission conveyed through Copyright Clearance Center, Inc.

Relatively to the actuation mechanism, Ou et al. (2016) pursued a different approach in their project aeroMorph to achieve performance as a shape-changing material, with recourse to airflow and inflatable materials. A specifically pre-designed pattern of air canals in a polymer sheet defines how the polymer behaves and what shape it acquires when getting inflated. Figure 2.17 displays the classical crane-shaped origami molded by aeroMorph. In comparison with Shutters and Surflex, aeroMorph lacks the ability to control individually each of the hinges, limiting the possibilities for different shapes.

Figure 2.17.   aeroMorph: a crane origami using pneumatic actuation. Republished with permission of ACM (Association for Computing Machinery), from *Proceedings of the 29th Annual Symposium on User Interface Software and Technology*, (Ou et al., 2016), copyright © 2016 ACM; permission conveyed through Copyright Clearance Center, Inc.

Furthermore, Purnendu et al. (2021) also achieved similar type of operation, but employing electrohydraulic actuators, and which are low-power and require no external fluid supply source.

2.2. SMART POLYMERS AND PRINTED ELECTRONICS

So far, the different forms of user interaction have been discussed and specific applications from the user's point of view have been presented. Now we will focus on how those platforms are made in terms of materials and technical engineering, particularly using smart polymers films and the recent science field of printed electronics.

Larger-sized tangible user interfaces (TUIs) often rely on ordinal non-responsive mechanical materials, or structural materials (e.g., mechanical switches) (Qi & Buechley, 2010; Sylla, Gonçalves, Branco, et al., 2012). But thin film devices for TUIs must rely on the intrinsic properties of the materials themselves, such as piezoresistive, piezoelectric, dielectric or magnetoelectric properties, among others (Dempsey et al., 2015).

For terminology, materials can be classified in several categories. For example, functional materials, smart materials and electroactive materials, as shown in the diagram of Figure 2.18.
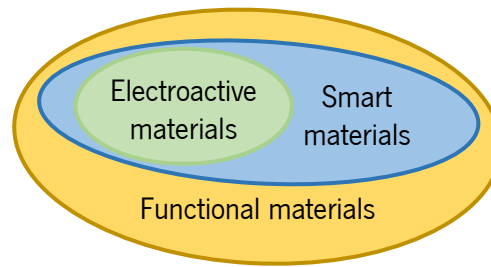
Figure 2.18. Electroactive materials as a subgroup of smart materials.

Functional materials are materials that exhibit native chemical and physical properties, which are altered by external factors from the surrounding environment, such as pressure, temperature, electric or magnetic field, pH, etc. However, functional materials might or might not be predictable in how they change towards a stimulus. Some examples of functional materials are, piezoelectric, ferroelectric, or ferromagnetic materials, superconductor or metallic conductors (Z. L. Wang & Kang, 1998, Chapter 1).

Smart materials are functional materials that exhibit a large change of their properties when submitted to the external stimulus, and producing a predictable outcome (Harrison & Ounaies, 2002). Most of smart materials are actually result of an engineering process for an intended purpose, but some smart materials exist naturally as well (Z. L. Wang & Kang, 1998, Chapter 1). All the smart materials are functional materials. Some examples of smart materials are piezoelectric, pyroelectric, thermoelectric, piezoresistive, chromatic, shape-memory or magnetorheological materials.

Electroactive materials are a subset of smart materials with the specification that they must produce a significant change in size or shape when the external stimulus is electrical (Lantada, 2012, sec. 3.3.4). Some examples of electroactive materials are dielectric, piezoelectric or magnetoelectric materials, or some ionic composites.

Smart and electroactive materials are often the base of sensors, allowing changes in the environment to be converted to electrical signals. It is not uncommon for the principles that these materials work on to be reversible, such as the piezoelectric or magnetoelectric. Therefore, actuators can also be produced (Tzou et al., 2004).

2.2.1. Why polymers?

Additive manufacturing of polymer-based sensors and sensor matrices is seeing an increasing number of applications due to the cost-effective production and the capacity for large-scale production, which represents a great potential (Song et al., 2014). Polymer films can be printed with conductive inks

through printing techniques without significantly impacting on the polymer properties. Printed electronics using polymer substrates possess a series of advantages such as flexible, thin, bendable, lightweight, low-cost, transparent and wearable, among others (Briand et al., 2011). An example of the potential of printed polymer films is shown in Figure 2.19, where a polymer sensor matrix is perfectly wrapped around an endoscope to detect its real form when inside the body during endoscopy. Therefore, it is expected that the market for these materials will continue to grow (Briand et al., 2011).

Figure 2.19.   Example of the versatility of polymer films: Sensor matrix wrapped around an endoscope.

Many applications have surged recently recurring to polymer films, ranging from sensors (S. Khan, Lorenzelli, et al., 2015), to actuators (Correia et al., 2019), circuits (H. F. Castro et al., 2014), batteries (C. M. Costa et al., 2019), among many others.

However, despite being target of intense research in the recent years, the fabrication of printed polymer films is still not a simple process. The quality and functionality of manufactured prototype circuit films highly depends on three major components (Gerard & Desmulliez, 2012): the printing technique, the inks used, and the substrate. In the detail of Figure.2.20, for instance, are shown some flaws that have occurred in the printing of an inductor via inkjet printing using silver ink on a polyethylene terephthalate (PET) substrate.
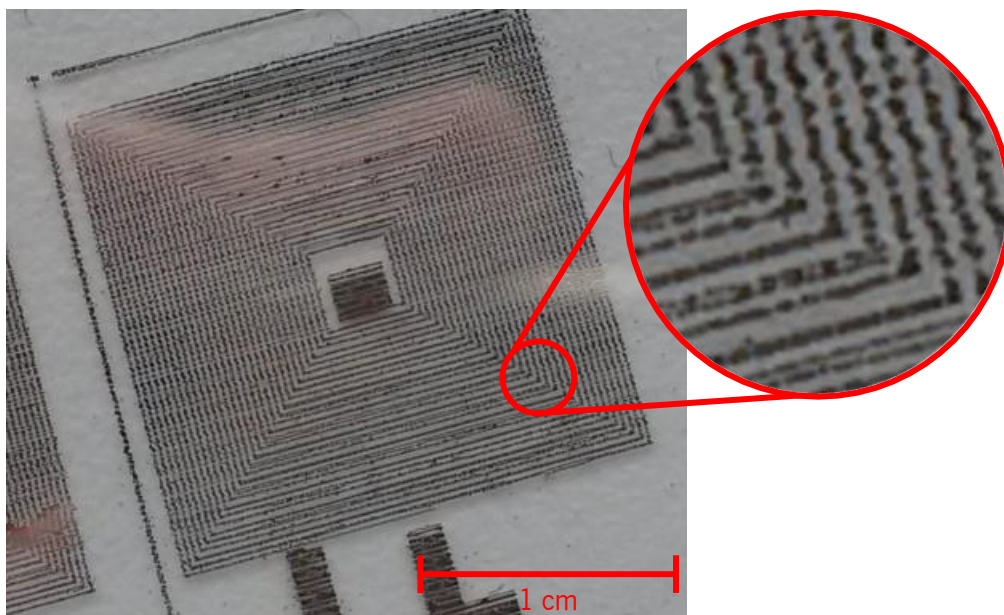
Figure.2.20.   Detail of a faulty inductor due to inkjet printing inaccuracies using silver ink on a PET substrate.

As an example, it is possible to identity the cuts in the conductive vertical traces, caused by the mechanical imprecision of the printer; the formation of small ink droplets in the horizontal traces, possibly indicating that the solvent of the ink is taking too long to dry out, giving the ink time to move due to superficial tension; and the merge of some horizontal traces, probably as a result of the interaction between the surface tension of the substrate with the ink's, i.e., hydrophobic behavior.

Adding to that, the connection of the film with the external electronics is often problematic (Nunes et al., 2017). The films are generally not solderable, and mechanical terminals must guarantee good contact without scratching the conductive layer. The use of conductive glues or tapes can be useful to overcome this problem.

Thus, next will be presented a brief review of some important printing techniques for prototyping, some accessible inks and substrates, as well as some solutions for terminal contacts of printed polymer films.

2.2.2. Printing techniques

The use of printing techniques has been a contribution for the development of flexible electronics. Many polymer printing techniques exist for both prototyping and industrial production, such as screen printing (Suikkola et al., 2016), inkjet printing (de Gans et al., 2004), spray printing (Reale et al., 2015),

bar-coating (also known as doctor blade) (Berni et al., 2004), among many others (Huang & Zhu, 2019; S. Khan, Lorenzelli, et al., 2015; Rim et al., 2016). The constant pursuit towards the much desired of fully printed electronics has led to the maturation of inks and their properties for the different printing techniques, namely to the development of conductive, semiconductive and dielectric inks, among others, enabling the fabrication of inkjet-printed transistors (H. F. Castro et al., 2014), sensors with integrated signal conditioning filters (H. F. Castro et al., 2016), audio circuits (Street et al., 2020), screen-printed piezoelectric matrices (Rendl et al., 2012, 2014), electrochromic displays (Xuan Cao et al., 2016), etc.

Projects often recur to a combination of several printing techniques to print different layers in different materials (Ko et al., 2007; Krebs, 2009). In Table 2.1 are shown some comparative technical specifications of the more commonly used printing techniques for prototyping, which are going to be explained next.

Table 2.1.   Comparison of the technical specifications of some printing techniques used in prototyping.

Characteristic	Screen	Inkjet	Spray	Doctor blade
Maximum Resolution (µm)	30 – 100	15 – 100	10 – 100	N/A
Wet thickness (µm)	> 10	> 1	> 1	10 – 500
Ink viscosity µ (Pa·s)	0.5 – 5	0.002 – 0.025	0.01 – 1[a]	< 0.1
Ink surface tension γ (mN/m)	38 – 47	15 – 25	[a]	[a]
References	*(1)*	*(2)*	*(3)*	*(4)*

[a]   Not a strict parameter.

(1)   (Aleeva & Pignataro, 2014; S. Khan, Lorenzelli, et al., 2015; Subramanian et al., 2008)

(2)   (Aleeva & Pignataro, 2014; Hösel et al., 2013; S. Khan, Lorenzelli, et al., 2015)

(3)   (Guo et al., 2014; Jang et al., 2006; Y. Khan et al., 2020; Krebs, 2009; X. Zhao et al., 2017)

(4)   (Berni et al., 2004; Darcovich & Kutowy, 1988; Y. Khan et al., 2020; Krebs, 2009)

2.2.2.1. <u>Screen printing</u>

Screen printing is the most used and mature printing technology for electronic applications. It started to be used in the beginning of the 20th century (Aleeva & Pignataro, 2014), and it contemplates a screen mask with the desired layout to be printed. A squeegee presses against the screen and forces ink through the mask and onto the substrate, as shown in Figure 2.21. The mask consists in a mesh made of nylon

or stainless steel fibers, usually with 30 to 200 threads per cm, which defines the maximum resolution of the printed pattern (Aleeva & Pignataro, 2014).
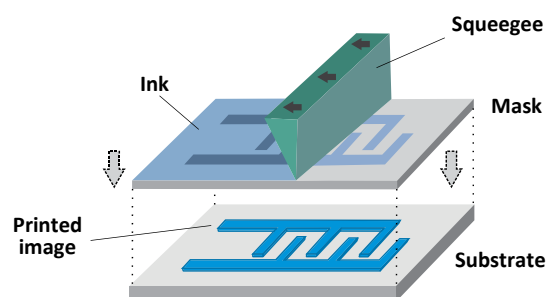
Figure 2.21. Screen-printing apparatus. Adapted with permission from (S. Gonçalves, Serrado-Nunes, et al., 2019b), copyright © 2019 American Chemical Society.

Inks prepared for screen printing must have high viscosity and surface tension because the ink has to be freestanding in the mesh until it gets pushed down by the squeegee. Inks with low surface tension would be dripping from mesh and low viscous inks would excessively spread in the substrate (Subramanian et al., 2008). Many of inks for screen printing actually come in the form of a paste. However, this can have an impact on the performance of the ink, especially in conductive and semiconductive inks composed of nanoparticles (NPs) because, to increase viscosity, it is usually added a polymer binder, which can degrade or destroy the ink behavior (Subramanian et al., 2008).

2.2.2.2. Inkjet printing

Inkjet printing, on the other hand, is a novel and complex system for printing. It consists of a nozzle that moves over the substrate, while pushing the ink down in little droplets, creating the desired pattern. Figure 2.22 shows the inkjet-printing apparatus. This process can easily print at 300 dots per inch (dpi), and can reach up to 1200 dpi at the mechanical level (Krebs, 2009). Although, the theoretical resolution during the printing process does not mean that the final printed pattern is the same resolution, because ink might spread after landing on the substrate.
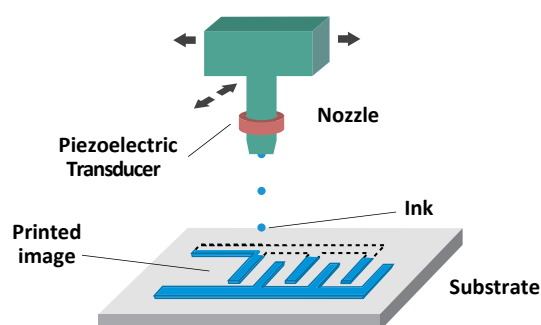
Figure 2.22. Inkjet-printing apparatus.

Inkjet ink must be highly tuned in terms of viscosity and surface tension (Aleeva & Pignataro, 2014). The output of the nozzle is microperforated, thus the ink must have very low viscosity to exit the nozzle properly, and simultaneously possess low surface tension to not stick to the nozzle tip, but not to the point where it starts dripping, yet still facilitating the formation of droplets. There is also a constraint for high volatility of one or more of the solvents of the ink for so that it dries out quickly in the landing place and to not move on the substrate due to surface tension (Krebs, 2009). Usually, inkjet printers are equipped with a controllable heating printing head which allows to adjust the viscosity of the ink, and substrate bed that can also be heated for quicker solvent evaporation (de Gans et al., 2004).

Inkjet printers can be designed to operate in one of two different modes: drop-on-demand (DOD) or continuous operation (Aleeva & Pignataro, 2014; Krebs, 2009). In continuous operation, the nozzle evacuates ink droplets at a constant pace during the whole printing, and to create the desired pattern, an electric field deviates the jet into a reservoir, preventing the ink from landing on the substrate. On the other hand, in DOD the nozzle transducer is actuated only when desired. It is a less ink consuming method and more versatile since it can use non-electrostatic inks, but might be more faulty due to clogging, jet variation and ink flow related to start and stop events (Krebs, 2009).

2.2.2.3. <u>Spray printing</u>

The spray coating technique has been widely used in the painting industry, but recently it started to be used in the context of printed electronics, and together with a pre-designed mask it has been possible spray printing (Guo et al., 2014; Jang et al., 2006). It consists of a high-pressure gas that exits a nozzle at very high speed, and forming a fine aerosol before landing on the substrate, as presented in Figure 2.23. As the gas leaves the nozzle at high speed, it picks ink particles from a reservoir that land spread on the substrate. A mask is firmly attached to the substrate to create the desired printing pattern (X. Zhao et al., 2017).

The ink for spray printing should be designed to allow pulverization and leveling off on the substrate, and then the evaporation of one or more solvents turns the ink solid or partially solid (Krebs, 2009). One of the main advantages of this technique is the possibility to be applied on almost any surface, either smooth or rough (X. Zhao et al., 2017). Nevertheless, in the final result it can be very hard to obtain a smooth surface, and the wet thickness is mostly uncontrollable with precision (Krebs, 2009). Thicker depositions are attained through longer exposition time (Reale et al., 2015). Irregularities in the dispersion can also pose a challenge in homogeneity.
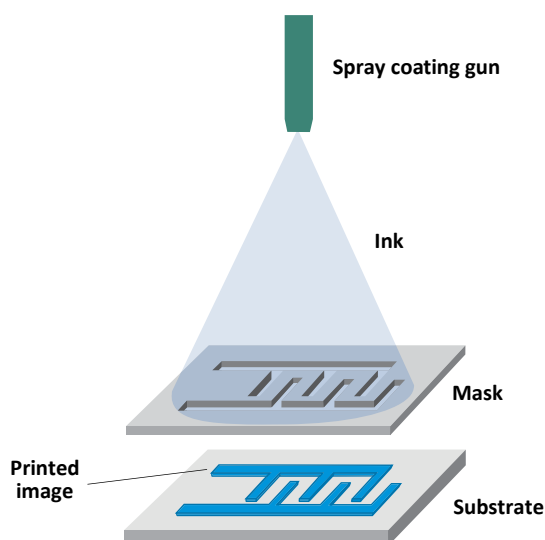
Figure 2.23. Spray-printing apparatus. Adapted with permission from (S. Gonçalves, Serrado-Nunes, et al., 2019b), copyright © 2019 American Chemical Society.

Another large advantage of this method is that the ink preparation can be fairly simple because the range for viscosity and surface tension is wide (Krebs, 2009). The mask and the used ink set the precision of this technique, which is typically about 100 μm (Guo et al., 2014), but it is possible to reach up to 10 μm (T. Zhao et al., 2017).

2.2.2.4. Doctor blade coating

Bar coating, often referred to as doctor blade technique, is a method for the creation of thin films and membranes, originally developed in the 1940's (Berni et al., 2004). This system works by depositing an arbitrary amount of ink on the substrate, often using a reservoir, and then swiping longitudinally a blade over the substrate at a fixed distance, as demonstrated in Figure 2.24, usually in the 10 to 500 μm range (Krebs, 2009). This is a coating method, not a printing method. Consequently, it is not possible to create any pattern in the resulting film (S. Gonçalves, Serrado-Nunes, et al., 2019b).
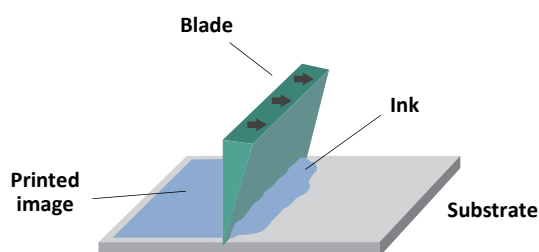
Figure 2.24. Doctor blade coating apparatus. Adapted with permission from (S. Gonçalves, Serrado-Nunes, et al., 2019b), copyright © 2019 American Chemical Society.

Contrarily to the expected, the wet layer thickness in doctor blading is not the same as the doctor blade gap because the wet layer is sheared by the interaction of the doctor blade with the ink, especially

for lower thicknesses (Berni et al., 2004; Krebs, 2009). In fact, several factors also affect the wet thickness such as the ink viscosity, surface tension of the ink and the substrate, speed of the passage, solvent volatility, among others. In practice, the real wet thickness is about $60\,\%$ to $70\,\%$ of the doctor blade gap (Berni et al., 2004; Darcovich & Kutowy, 1988).

The ink constraints for this method in terms of viscosity and surface tension are not very important, although inks are generally low viscous, with viscosity lower than 100 Pa·s (Y. Khan et al., 2020).

2.2.2.5. <u>Final remarks on printing techniques</u>

Many printable inks require post treatment in order to attain the designed electrical properties, including temperature curing (Dearden et al., 2005; S. Gonçalves, Pereira, et al., 2019), ultraviolet (UV) radiation exposition (Rajan et al., 2016) or solvent evaporation at room temperature (Dehsari et al., 2017; S. Gonçalves, Pereira, et al., 2019), among other more radical approaches such as X-ray exposition (H.-T. Tung et al., 2012). It is a process necessary for two main reasons: solvent evaporation, and, in nanoparticles (NPs) ink, to sinter metal particles. In traditional NPs ink, a non-conductive material binds the conductive particles, i.e., a ligand. Normally, high-temperature annealing or UV exposure are needed to reach suitable conductivity values (Minari et al., 2014). Nevertheless, new inks have been formulated that require no annealing by the use of new types of ligand materials that facilitate the contact between metal NPs at room temperature (Minari et al., 2014).

To achieve a smooth surface in the print usually it is required a long recovery time to allow the ink to move. However, when the substrate presents hydrophobic behavior overall or locally due to irregular surface tension or surface contamination, the ink might form little cuts in traces, resulting in faulty imprints (Aleeva & Pignataro, 2014). Nevertheless, a study by (C. S. Lee et al., 2003) indicates that the surface of the substrate, namely polyvinylidene fluoride (PVDF), can be treated with ion assisted reaction (IAR) to make the surface of PVDF hydrophilic, which highly increases the adhesion between the film and the ink. This grants better durability of electrodes.

2.2.3. Inks for printing technologies

There exist some suitable inks in the market for the more basic electrical behaviors such as conductive, dielectric and resistive inks (Aleeva & Pignataro, 2014; Rim et al., 2016), but the continuous research on those fields is also allowing for the creation of more complex mechanisms, as is the case of

transistors (H. F. Castro et al., 2014), solar cells (Krebs, 2009; Reale et al., 2015) or phosphorescent components (Jung et al., 2012), among others. Inclusively, there are inks and polymer composites developed for self-healing printed electronics (J. Kim et al., 2017; Q. Zhang et al., 2018).

The formulation of smart inks results from a mixture of a solvent and active particles, such as silver for conductive inks, carbon for resistive or polyimide (PI) for dielectric (Subramanian et al., 2008), together with other minor components to stabilize the ink, improve printability of adhesion, among others. Thus, a binder can be used to control the viscosity of the ink, especially in inks for screen printing (Subramanian et al., 2008). Surfactants are also used to prevent agglomeration in NPs-based inks (W. Wu, 2017).

The polymer binder has a very important role in the development of stretchable inks, because it is the binder who dictates the form how smart particles attach and connect to each other (Mohammed & Pecht, 2016). Therefore, it is not unusual for stretchable inks to be composed of two or more binding polymers. The same study also suggests that using only silver nanospheres increases conductivity and reduces the sintering temperature, in comparison with other metal powders, but ohmic stability during stretching is lost. This has been overcome by the use of a mixture of silver flakes with large and fine diameters, whereas the large particles promote conductivity during stretching, and smaller particles also improve conductivity while reducing sintering temperature (Mohammed & Pecht, 2016). This concept is illustrated in Figure 2.25.
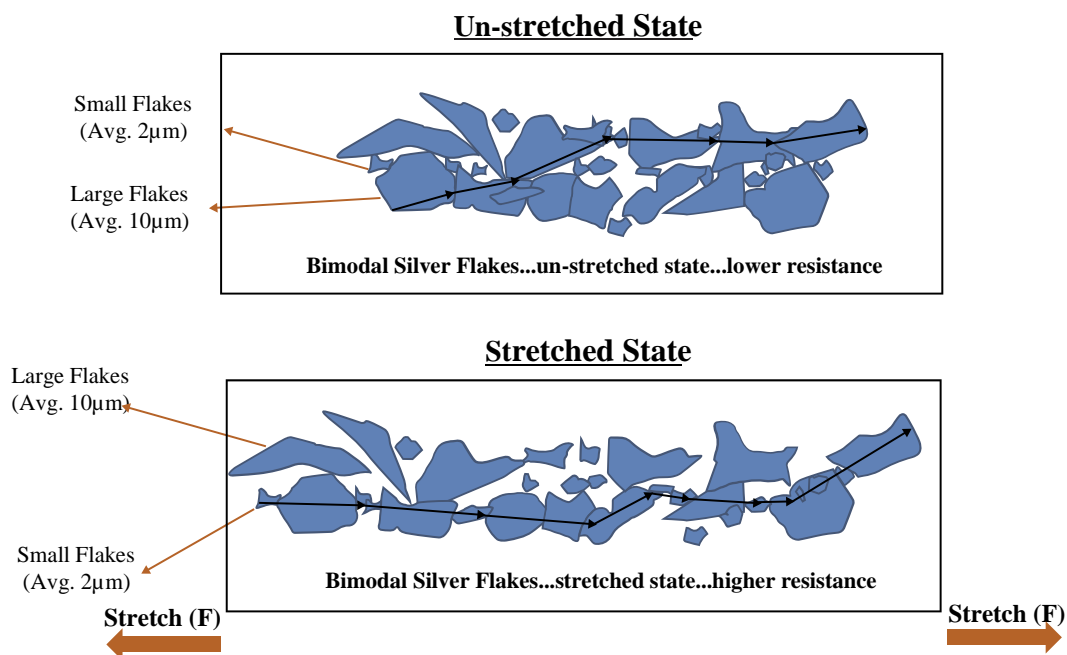
Figure 2.25. Bimodal flake distribution maintaining ohmic connectivity during stretching – a conceptual approach. Reprinted from (Mohammed & Pecht, 2016), with the permission of AIP Publishing, copyright © 2016 Authors.

The use of nanotubes instead of simple NPs is often an option in the formulation of differentiated inks, such as silver nanowires (SNWs) in transparent inks, or carbon nanotubes (CNTs) in piezoresistive inks. The interaction between the long conductive chains can make it change resistance under stress (P. Costa et al., 2015), or facilitate the creation of transparent inks (Reizabal et al., 2020).

Table 2.2 lists a bunch of commercial inks with different properties for conductive, resistive and dielectric functions.

Table 2.2.   Example of some commercial inks for printing.

Characteristic	NovaCentrix HPS-21LV[1]	Poly-Ink PolyBioWire[2]	Nanopaint PR-2 Ink[3]	Sigma-Aldrich 736465[4]	Creative Materials 125-17M[5]
Type of ink	Conductive	Conductive	Piezoresistive	Conductive	Dielectric
Active material	Silver NPs	SNWs	CNTs	Silver NPs	(not provided)
Color	Silver	Clear	Black	Silver	Matte, colorless
Substrates	Plastics, glass	Plastics	Plastics, glass	Porous plastics	Plastics, glass
Printing method	Screen	Screen, inkjet, doctor blade	Screen, doctor blade	Inkjet	Screen
Resistivity ρ ($\Omega \cdot m$)	$10.4 – 33.8 \times 10^{-9}$	900×10^{-9}	(not provided)	11×10^{-9}	71×10^{12}
Dielectric constant εr	N/A	N/A	N/A	N/A	4.3
Post-treatment	60 min @ 80 °C	30 s @ 110 °C	10 min @ 60 °C	100 – 150 °C	1 min @ UV

When developing an ink for printed electronics, the choice for the solvent is also very important since it directly controls the rheological properties of the ink (W. Wu, 2017). Many inks use highly hazardous solvents, such as toluene (Gerard & Desmulliez, 2012) or N,N-dimethylformamide (DMF) (C. S. Lee et al., 2003), but environmental concerns have been giving significance to environmentally friendly solvents such as water-based inks. Yet, the elaboration of water-based inks for application on plastic films is a

---

1 NovaCentrix official website: https://www.novacentrix.com
2 Poly-Ink official website: http://www.poly-ink.fr
3 Nanopaint official website: https://nanopaint-tech.com
4 Sigma-Aldrich official website: https://www.sigmaaldrich.com
5 Creative Materials official website: http://creativematerials.com

limited one, resulting in poor wetting print due to the high surface energy of the water when compared to the plastics' (W. Wu, 2017).

2.2.3.1. Post-printing treatments

Printed polymer inks with NPs usually require subsequent treatments to attain the desired electrical properties, due to three main reasons:

- – The presence of solvent in the printed ink;
- – The inexistence of a tridimensional polymeric network, only non-interconnected monomers;
- – The lack of interconnection between NPs.

Thus, inks normally suffer thermal treatments after being printed, which are curing and sintering treatments (Huang & Zhu, 2019; W. Wu, 2017).

The curing process is a form of heat treatment that works as chemical reaction accelerator. Its main purpose is to foment the change of the chemical structure of the composite from dispersed monomers into a tridimensional polymeric network chain, also often referred to as polymerization (Callister & Rethwisch, 2010, sec. 15.22), and represented in Figure 2.26. It also has a second purpose of easing solvent evaporation. This gives the ink mechanical strength, makes it adhere stronger onto the substrate and makes it more flexible. Thermal curing can be achieved with different techniques such as traditional oven heating, ultraviolet (UV) and infrared (IR) exposure, laser, radiation curing, electron beams, radioactive curing, ultrasonic heating, electrical and magnetic heating, among others (Abliz et al., 2013). Nevertheless, curing is a polymer treatment, not a NPs treatment, and alone does not endow any substantial electrical properties due to the lack of conductive paths in the ink nanostructure.

| Uncured | Moderately cured | Completely cured |
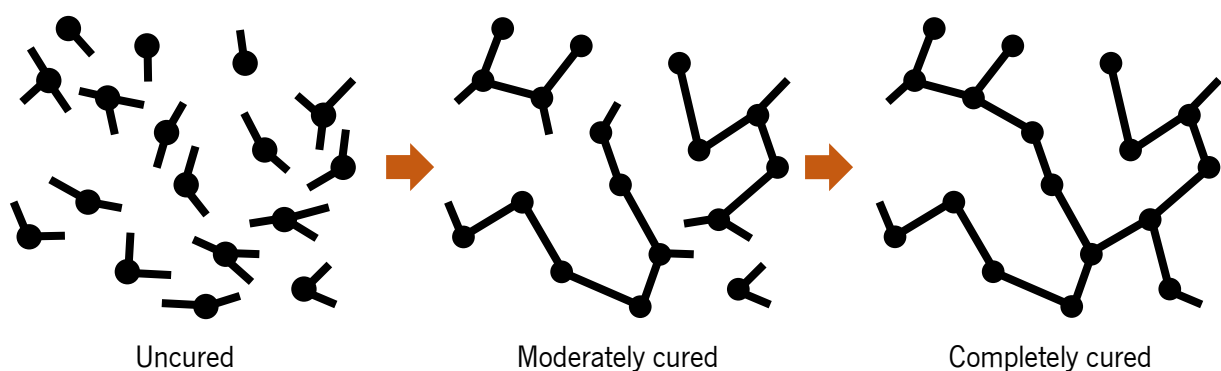
Figure 2.26. Creation of polymer network during curing.

The sintering process creates conductive necks between the metal NPs as shown in Figure 2.27 (W. Wu, 2017). Similarly to the curing process, despite sintering being a thermal process, the thermal treatment can be achieved not just using a traditional oven, but also through several treatment techniques,

depending on the formulation of the ink, such as UV or IR light exposure, laser sintering, plasma, microwave and electrical or chemical sintering techniques, among others (Rajan et al., 2016; W. Wu, 2017).

The treatment of metallic nano inks in terms of electrical conductivity is called sintering. The sintering treatment is also a thermal treatment that consists in the heating of the ink up to the point where the outer layers of the NPs fuse with of their neighbors', below the melting point, creating conductive paths.
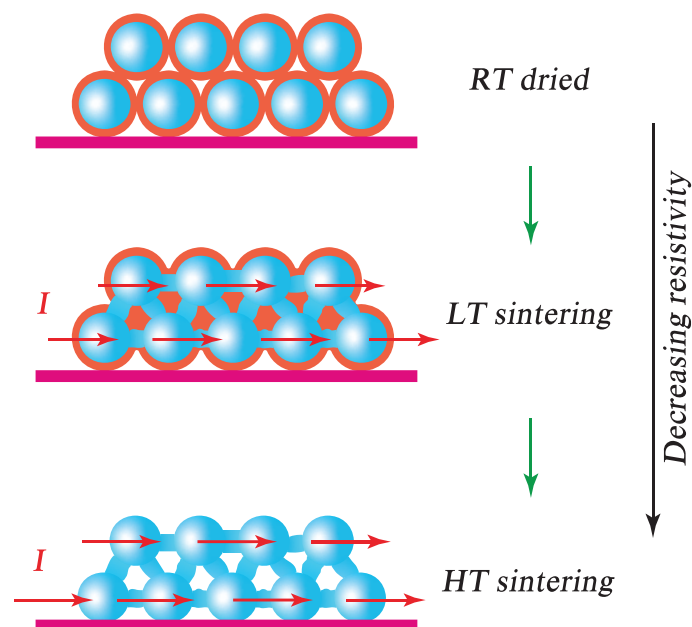
Figure 2.27.   Fusion of particles during sintering process (room temperature (RT), low temperature (LT), high temperature (HT)). Republished with permission of Royal Society of Chemistry, from Nanoscale, vol. *9*(22), (W. Wu, 2017), "Inorganic nanomaterials for printed electronics: A review", copyright © 2017 The Royal Society of Chemistry; permission conveyed through Copyright Clearance Center, Inc.

Curing and sintering are both post-printing thermal treatments, but they differ in the temperature magnitude and process duration. It is also possible to obtain inks with different thermal-induced treatments for curing and sintering. However, in many inks, particularly in NPs inks with low sintering temperature (< 150 °C), curing and sintering often take place at the same time. For this reason, there is a misconception between curing and sintering, and the "curing" term usually englobes both curing and sintering treatments.

2.2.4. Flexible substrates

Flexible polymer films are the base of flexible electronics. The substrate limits the adhesion of the printed ink and the curing possibilities. Also, the properties of the substrate determine the applicability of the system, in terms of transparency and curvature radius (Rim et al., 2016).

Many polymer films exist for flexible electronics, being the polyimide (PI) film among the most used ones, more known as Kapton film. Kapton film is much used by the industry in the fabrication of flexible PCBs. It has a high usable temperature, which is a major advantage, but the low transparency, intrinsic color and high manufacturing cost give room for the selection of alternative types of films (Rim et al., 2016). Prototype applications often recur to other substrates such as PET (W. Kim et al., 2015) or polyethylene naphthalate (PEN) (H. F. Castro et al., 2014) due to the low production cost and transparency, or PVDF and its copolymers in piezoelectric systems (S. Khan, Dang, et al., 2015; Rajeev et al., 2020). In Table 2.3 are listed some polymers used in flexible electronics alongside with their characteristics.

Table 2.3.   Specifications of some flexible substrates (Pedro Costa, Nunes-Pereira, et al., 2019; L. Hu et al., 2019; A Nathan et al., 2012; Ramadan et al., 2014; Rim et al., 2016; Y Wang et al., 2010; P. Yang et al., 2014)**.**

Material	Maximum deposition temperature (°C)	Dielectric constant εr	Piezoelectric coefficient d_{33} (pC/N)	Color
Polyimide (PI)	220 – 275	3.4	N/A	Orange
Polyethersulfone (PES)	190 – 230	4.1	N/A	Light yellow
Polycarbonate (PC)	125	2.8	N/A	Clear
Polyethylene naphthalate (PEN)	150 – 160	4.2	N/A	Clear
PET	120	3.3	N/A	Clear
P(VDF-TrFE)	100	12	38	Clear
PVDF	90	12	24 – 34	Clear

A proper choice of the substrate must consider the final application, the adhesion of the ink to be printed, and the curing and sintering temperature of the ink. The combination of the chosen ink and substrate must ensure that the substrate can endure the curing and sintering processes, as well as to be

resistant to the solvents present in the ink. Other requirements for substrates normally include low cost, moisture resistance, and, not so often, good thermal conduction and low coefficient of thermal expansion (CTE) (A Nathan et al., 2012).

The maximum usable temperature of the substrates shown in Table 2.3 is linked to the glass transition temperature, Tg, of the polymer. The glass transition temperature is a limit occurring in many amorphous polymers, always below the melting temperature, Tm, at which the polymer begins transiting from a solid and hard state to a softer and possibly gummy state, and thereupon acquiring a new form and not recovering to the original one anymore. Non-stretchable polymer films for flexible electronics are used well below Tg, but stretchable polymers such as elastomers are used above Tg (Ellingford et al., 2020). Furthermore, the maximum usable temperature of piezoelectric polymer substrates[1] are also restrained by the Curie temperature, Tc, which is the temperature at which the material loses the permanent magnetization and polarization. This effect is explained in section 4.1.4. Ferroelectrics.

Available piezoelectric film substrates for practical uses are mostly restrained to PVDF and its copolymers and terpolymers, such as poly(vinylidene fluoride trifluoroethylene) (P(VDF-TrFE)), poly(vinylidene fluoride-co-chlorotrifluoroethylene) (P(VDF-CTFE)), poly(vinylidene fluoride-co-hexafluoropropylene) (P(VDF-HFP)), poly(vinylidene fluoride-trifluoroethylene-chlorotrifluoroethylene) (P(VDF-TrFE-CTFE)), from which PVDF and P(VDF-TrFE) are the most well studied and used in applications (Pedro Costa, Nunes-Pereira, et al., 2019). The cost of production of these materials is still relatively high, having commercial PVDF and P(VDF-TrFE) films seen a significant drop in production cost over the recent years.

More recently, pushed by environmental concerns towards the use of plastics and versatility of applications, natural materials have been more and more studied, such as cellulose (Hoeng et al., 2016) or silk (Tulachan et al., 2014), among others. The potential of paper substrates for flexible electronics has enabled applications such as transistors and batteries (Ferreira et al., 2011), sensors, antennas and circuits (Tentzeris, 2013), and piezoelectric applications (Sappati & Bhadra, 2018). This comes up with the potential for reduced environmental impact and recyclable electronics (A Nathan et al., 2012).

---

1 Piezoelectric material is explained in section 4.1.2. Piezoelectrics.

2.2.5. Terminals

The terminal joints between the polymer film and the external electrical circuit is a reason of concern by nature. Polymer materials usually are not solderable and the thin conductive layers restrain the insertion of mechanical terminals (Measurement Specialties Inc., 1999; Nunes et al., 2017). In more extreme situations solutions have inclusively passed by the use of wireless intercommunication (Ageyeva et al., 2019).

Typical commercial solutions for interconnecting rigid electronics with polymer films in prototyping are based on clincher connectors (Nunes et al., 2017), conductive glues (M. Martins et al., 2012; Mendes-Felipe et al., 2020; Suikkola et al., 2016), and *z*-axis conductive adhesive tape (Reizabal et al., 2020), among others, each with its pros and cons, as shown in Table 2.4.

Table 2.4.   Comparison between connecting the terminals.

Characteristic	Clincher	Conductive glue	*z*-axis conductive adhesive tape
Flexible	No	No	Yes
Resistance of contact	Very low	Low	Low
Thickness	Large	Thin	Very thin
Supports flat cable	Yes	No	Yes
Pitch	2.54 mm	–	Yes
Mechanical strength	Poor	Very good	Good
Rough materials	Yes	Yes	No
Bad contacts	Very susceptible	Not susceptible	A little susceptible
Notes	Conducting traces might crack during crimping	Might be reactive	Requires ultra-flexible cables

2.2.5.1. <u>Clinchers</u>

Connecting clinchers is a type of connector that pierces the substrate and clamps onto the conductive paths. It is a versatile option that can be used on flexible printed circuit boards (PCBs), printed polymer films or even fabric. It requires a specific clamping tool, usually supplied by the manufacturer. The major downside of this connector is that, as it pierces the substrate, it might crack the conductive

traces weakening the joint's conductivity and often resulting in bad connections (Nunes et al., 2017). Also, due to the same reason, it is a connector not recommended if the film is going to be moving or bending. If connected properly, this type of connector presents very little electrical resistance because of the metal-to-wire contact. In Figure 2.28 is shown a Clincher Flex Connector from Amphenol ICC[1].

Figure 2.28.   Clincher connector.

2.2.5.2. <u>Conductive glue</u>

Conductive glues are mostly used when connecting single terminals, since the precision and size of the contact are rough and limited to manual application and viscosity of the glue. Nevertheless, precision and size of the contacts can be enhanced through the use of the screen-printing technique (Bare Conductive, 2017). In fact, using screen-printing technique it is not only possible to make the connections but also print an entire film panel. Some projects use anisotropic conductive paste (ACP) to bond electronic components directly to a printed polymer film (Street et al., 2020).

Conductive glues use a polymer binder material in conjunction with conductive material particles, e.g., carbon (Figure 2.29*a*) or silver (Figure 2.29*b*), and a solvent. However, the presence of the solvent has a potential for reacting with the printed material creating unexpected results.

---

1 Amphenol ICC official website: https://www.amphenol-icc.com

(a)   *(b)*
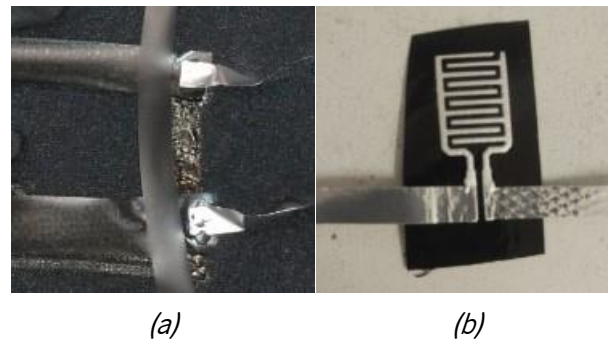
Figure 2.29. Connections made with *(a)* conductive carbon glue and *(b)* conductive silver glue.

In this type of connection, the resistance of the connection highly depends on the glue formulation, but it is usually low, at about of a few dozen Ω or less. The glue must dry before become conductive. The major advantage of conductive glues is the mechanical strength of the contact, which is strong. On the other hand, the downside of most conductive glues is that they become rigid once dried. However, flexible conductive glues have also been developed, at the cost of lower conductivity (L. Wang et al., 2018).

As example of commercial conductive glues there is Colloidal Silver from Agar Scientific[1], Electric Paint from Bare Conductive[2], or Wire Glue[3].

2.2.5.3. *z*-axis conductive tape

A type of electrically conductive adhesive transfer tape (ECATT) is the *z*-axis conductive adhesive tape, that has the particularity of being conductive only in the *z*-axis direction, i.e., along its thickness, without conducting sideways. This is the major advantage of this type of material because material can be deposited over an entire row of pins without short-circuiting parallel pins (3M, 2009). It is one of the neatest methods for connecting polymer films, as shown in Figure 2.30.
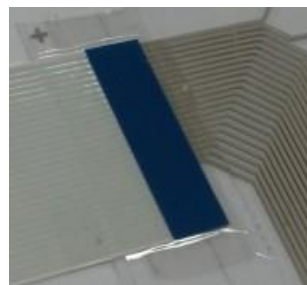
Figure 2.30. Connection made with *z*-axis conductive adhesive tape.

---

1 Agar Scientific official website: https://www.agarscientific.com
2 Bare Conductive official website: https://www.bareconductive.com
3 Wire Glue official website: http://www.wireglue.us

The thickness of the connection is minimal, and the connection is flexible, ideal to connect printed polymer films with flexible flat cables (FFCs) or PCBs (J.R. Dios et al., 2019). The connection can be better secured with a sealing material such as epoxy resin or adhesive tape.

This type of *z*-axis ECATT is composed of small conductive particles, usually metal particles, that are large enough to make vertical contact with each other, but slightly separated horizontally. When pressed against a surface, it reinforces the vertical connection. Therefore, one downside of this connection is that it is not constant in terms of electrical conductivity, which usually sits around at a dozen Ω, just similar to conductive glues. Conductive particles can be copper, nickel, carbon, or, the most used, silver, as is the case of 3M 9703[1].

2.3. CONCLUSIONS

This chapter presents a literature review for the current project, explaining the initial problem of interfaces, the need of TUIs in the future designs, and the possibility of smart polymers with printed electronics to be the solution.

An introduction of the different forms of interface with the user has been presented, explaining that the GUI is giving way to other more intuitive forms of interaction such as TUIs, shape-changing interfaces or OUIs. An exhaustive literature review was made on the state of the art, showing several applications, their forms of interaction, types of sensors and actuators used, and functioning methodology.

Then, the use of polymer films with printed electronics was proposed in the development of new interfaces, namely smart or electroactive polymers. The advantages of such materials was listed, and the necessary processes in the production of sensors and actuators: a review on some printing techniques (screen printing, inkjet printing, spray printing, doctor blade coating); a review on some existing inks for printing (conductive, resistive, dielectric) as well as the post-treatments needs (sintering, curing); a review on some substrates available in the market for dielectric and piezoelectric operation; and a review on the terminals to perform the electric interface between printed polymer films and rigid electronic circuits.

---

1 3M official website: https://www.3m.com

3. CAPACITIVE FILMS

Capacitive sensing is a technology that uses the capacitive coupling effect between materials in order to detect proximity, touch and/or pressure (D. Wang, 2014). Its range of applications is quite large. Besides the well-known digital devices brimming capacitive touchscreens (Davison, 2010; Kwon et al., 2018; Schmitz et al., 2017), other applications also comprise gesture recognition (Kellogg et al., 2014), liquid level sensing (D. Wang, 2014), pressure sensors (Joo et al., 2017; McIntosh et al., 2006), distance sensors (Zaitsev et al., 2019), vibration sensors (Y. Wu & Huang, 2018), humidity sensors (Hajian et al., 2019), electrostatic actuators (Tausiff et al., 2020), energy harvesters, (Moretti et al., 2018, 2020), virus biomarkers (Cecchetto et al., 2017), pH sensors (Arefin et al., 2014), gas/liquid measure (Ji et al., 2014), and radio frequency (RF) tuning (Achenbach et al., 2014), and so on. Among the reasons for the popularity of capacitive sensors are their versatility, easy manufacturing, and also the low-power requirements (Hussaini et al., 2018).

It is a technology that appeared in the 1970s–80s for touch detection, along with several other concurring technologies such as resistive sensing, light interruption, or surface acoustic waves (SAWs), among others (Buxton, 2010). More recently, in digital devices, capacitive touchscreens came as replacement of resistive touchscreens, and nowadays it is possible to find capacitive touchscreens in almost every daily use equipment, such as in laptops, smartphones, smartwatches, tablets, televisions (TVs), automobiles, laundry machines, and so on (Du, 2016; Walker, 2012).

Capacitive sensing has been gaining popularity over other technologies, e.g., optical detection, in applications that require contactless sensing, such as proximity and gesture detection, liquid level sensing or material analysis (D. Wang, 2014). Its main advantages lies in being a low cost technology, the ability to sense large distances with small sensors, and high resolution (D. Wang, 2014).

With the advent of the smartphones, the market and applications for capacitive touchscreens have highly grown, especially since the launch of the iPhone® by Apple in 2007 (Luo et al., 2012; Walker, 2012).

Traditional transparent capacitive touchscreens are typically rigid, constituted by a transparent substrate such as glass or acrylic, and transparent electrodes, usually made of a very thin layer of indium tin oxide (ITO) which is highly conductive. However, the ITO deposition technology is expensive and new replacing printing solutions are being researched (W. Kim et al., 2015; Ma et al., 2015).

Nonetheless, there is also an increasing demand for opaque capacitive touchscreens for applications such as touchpads (Choi et al., 2011), keyboards (Y.-C. Tung et al., 2015), proximity buttons (Kaneswaran

& Arshak, 2009), position tracking surfaces (Grosse-Puppendahl, Braun, et al., 2013; Valtonen et al., 2012), and pen-shaped haptic devices (Tian et al., 2017). Opaque capacitive sensors are often built-in the printed circuit board (PCB) using the copper or aluminum layers (Hong et al., 2013).

However, advances in printed electronics and materials now allow for printed flexible capacitive sensing films, by using a polymer substrate with printed conductive ink (Molina-Lopez et al., 2012; Rivadeneyra et al., 2015). Capacitive sensing films are going to be further discussed.

This chapter is mostly covered by the publications of the candidate (N. Castro et al., 2017; Mendes-Felipe et al., 2020; Nunes et al., 2017; Pereira et al., 2021).

3.1. CAPACITIVE SENSING PRINCIPLE

Capacitive sensing is based on the capacitive coupling effect, which represents the electrical capacitance between conductors (Du, 2016). Two parallel conductive plates as shown in Figure 3.1 form an electrical capacitance, capable of storing electric charge.
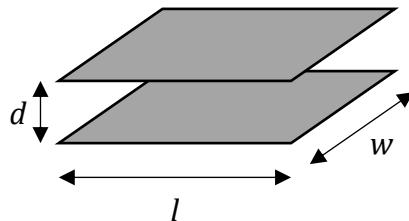
Figure 3.1.   Schematic representation of a parallel plate capacitor.

The capacitance C (F), given by:

$$C = \varepsilon_\mathrm{r}\varepsilon_0 \frac{lw}{d}$$
(3.1)

where $\varepsilon_0 = 8.8541878128(13) \times 10^{-12}$ (F/m) is the permittivity of vacuum, ε_r is the dielectric constant of the material between the plates, and l (m), w (m) and d (m) are the length, width and distance of the plates, respectively (Callister & Rethwisch, 2010, sec. 18.18). The stored charge in the capacitor

Q (C) can be calculated as function of the capacitance C (F) and the voltage differential developed across plates V (V):

$$Q = CV \tag{3.2}$$

The energy stored in the capacitor E (J) is given by:

$$E = \frac{1}{2}CV^2 \tag{3.3}$$

However, Equation (3.1) does not take into account the fringing effect that occurs on the outside of the parallel plates, as shown in Figure 3.2, due to the difficulty of modeling this effect (D. Wang, 2014). In common capacitive applications, the fringing effect can be neglected, but capacitive sensors often rely on it to operate.

Fringing effect
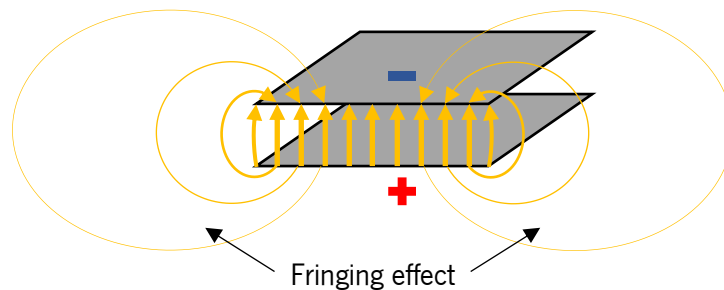
Figure 3.2.   Electric field in a capacitor.

Capacitive sensors can consider the change of any of the variables from the Equation (3.1) to take measurements, such as the deformation of the plates (McIntosh et al., 2006), the deformation of the dielectric (S. W. Park et al., 2017), or the alteration of the dielectric to another material (Ji et al., 2014). Nevertheless, the fringing effect is the most used one in practical applications, e.g., in capacitive touch, proximity and gesture detection sensors, liquid level sensing and material analysis (D. Wang, 2014).

Capacitive touch sensing can be divided in two categories: surface capacitance and projected capacitance. Projected capacitance can be further subcategorized in self-capacitance and mutual capacitance. These technologies are going to be explained next.

3.1.1. Surface capacitance

Surface capacitance technology consists in the creation of a uniform electric field between some electrodes, usually four, over the surface of a panel. Surface capacitance touch panels are made of a rigid substrate material, usually glass, with a layer of conductive material deposited on the glass, as

shown in Figure 3.3, being the electrodes placed on the corners of the panel (Akhtar et al., 2017; Walker, 2012). It is not uncommon for systems based on this technology to also implement a linearization pattern to correct the inherent nonlinearity of dispersion of the electric field (Bauman, 2007; Walker, 2012).
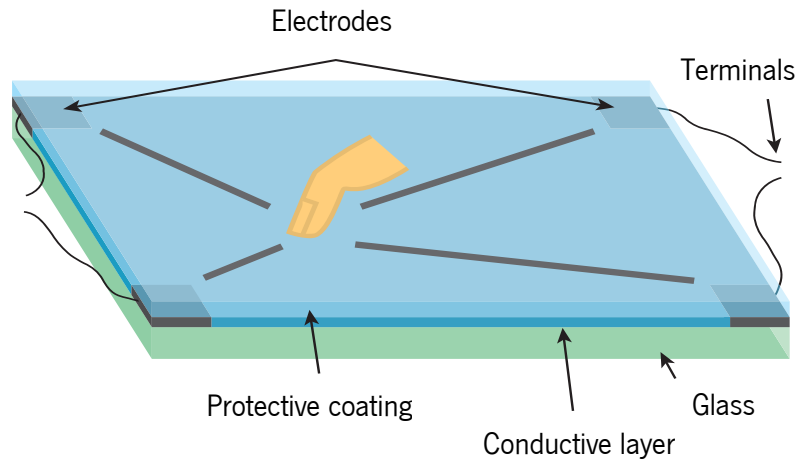
Figure 3.3.   Surface capacitance panel for touch detection. The human finger draws current from the electrodes due to capacitive coupling, allowing to triangulate the touch position.

Surface capacitance touchscreens apply an AC (alternating current) voltage on the electrodes and measure the current on each electrode, comparing it with the baseline of when the touchscreen is not touched, to determine the touch location (Akhtar et al., 2017; Walker, 2012, 2014). The system requires a very stable reference to ground to set the threshold for touch or no touch events. Thus, for the application of surface capacitance touchscreens in mobile devices, a system using reversing ramped field capacitive (RRFC) technology was developed (Walker, 2012, 2014), consisting in alternating pin functions with symmetry.

Surface capacitance devices require simple controllers and need less electric power than other capacitive technologies, but they suffer from limited resolution and the inability for multitouch detection, being this last one the reason why they never took off as application for tablets and smartphones, and ultimately, the cause of their decline (Akhtar et al., 2017).

3.1.2. Projected capacitance

In projected capacitance touch (PCT), electrodes can function as transmit or as receive. The transmit sends out an electric signal that is sensed by the receive. To evaluate human hand or object proximity, it

is measured the amount of time that the signal takes to travel from the transmit to the receive, or the amount of current flowing in the circuit, which varies according to the environment (Zimmerman et al., 1995).

PCT can be categorized according to the form of operation, as shown in Figure 3.4. There are several forms of operation of projected capacitive sensing, namely the loading, shunt, receive, and transmit modes (Grosse-Puppendahl et al., 2017; Grosse-Puppendahl, Braun, et al., 2013; Zimmerman et al., 1995).
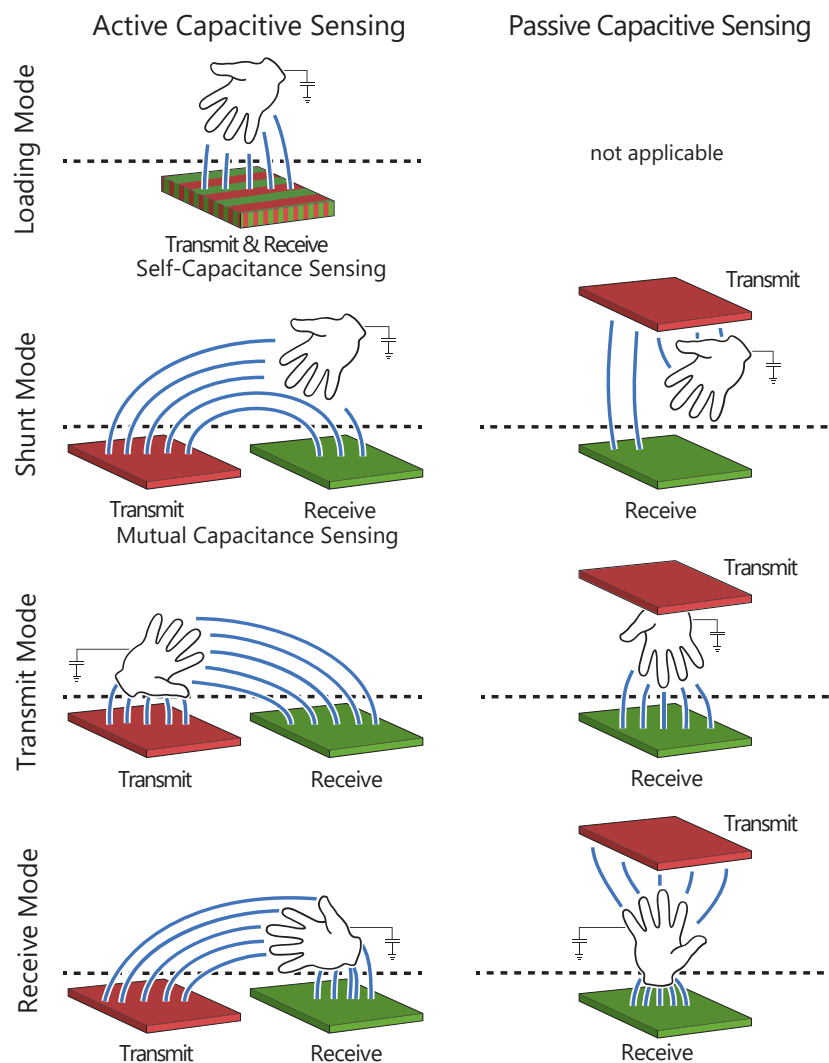
Figure 3.4.   Capacitive sensing techniques. The dashed line represents the limit between the sensor, on bottom, and the external environment, on top.
Republished with permission of ACM (Association For Computing Machinery), from *Proceedings of the 2017 CHI Conference in Human Factors in Computing Systems*, (Grosse-Puppendahl et al., 2017), copyright © 2017 ACM; permission conveyed through Copyright Clearance Center, Inc.

PCT can also be classified in terms of signal source as active or passive (Grosse-Puppendahl et al., 2017). In active capacitive sensing, the transmit pin exists physically in the device. But, in the arising concept of passive capacitive sensing, the system relies on external and ambient electric fields, such as power lines, appliances, Wi-Fi and other radio signals for the transmit function. It is a less reliable method, but that requires minimal power and infrastructure (Grosse-Puppendahl et al., 2017).

The performance of PCT in noisy environments can be compromised, thus, a shield layer is usually applied, at the cost of less sensitivity (Cleary, 2019).

3.1.2.1. <u>Self-capacitance</u>

In loading mode, the transmit and receive are actually the same electrode, operating with alternating functions. For this reason, this is known as self-capacitance.

This system operates by applying an electric charge on the electrode, and measuring the amount of time it takes to stabilize. Conductive bodies nearby change the recovering time, as shown in Figure 3.5 (Barrett & Omote, 2010; Grosse-Puppendahl et al., 2017; Grosse-Puppendahl, Braun, et al., 2013).
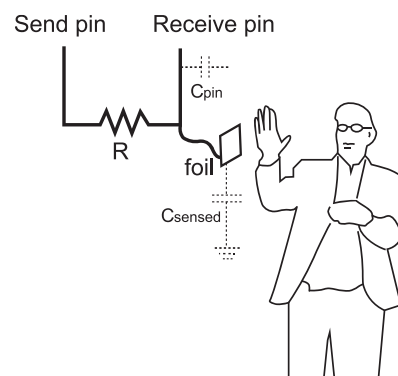
Figure 3.5.   Self-capacitance sensor operation circuit. Reproduced from arduino.cc website, copyright © 2020 Arduino, under Creative Commons BY-SA 3.0 license (https://creativecommons.org/licenses/by-sa/3.0).

Self-capacitance is the most common type of capacitive single-touch button sensors due to its robustness, easy application and cheap manufacturing. For multiple touch buttons, it is possible the implementation of individual multi-pads, as indicated in Figure 3.6. However, as the amount of pads increases quadratically with the dimension, it becomes impractical for larger touch panels (3M, 2013; Luo et al., 2012).
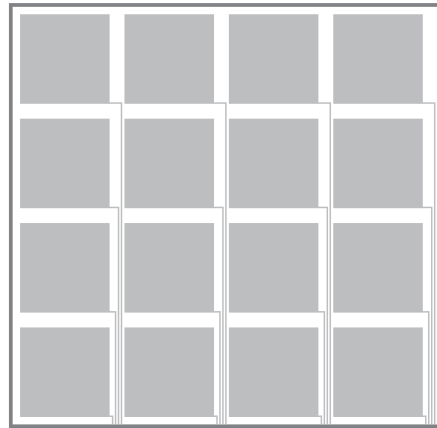
Figure 3.6.   Self-capacitance multi-pad touchscreen.

Interpolation between adjacent self-capacitance electrodes can be attained using specific electrodes' shapes that promote finger touch crossover on two or more electrodes simultaneously (Cleary, 2019). Figure 3.7 compares the implementation of non-interpolating and interpolating electrodes. The interpolated design allows to gradually swipe the finger from one electrode to the other.

(a)   *(b)*

Figure 3.7.   Self-capacitive electrodes: *(a)* two non-interpolated electrodes and *(b)* two interpolated electrodes.

Matrices are implemented using electrodes arranged in rows and columns in two separated conductive layers, as illustrated in Figure 3.8.

● Real touch   ✖ Ghost touch
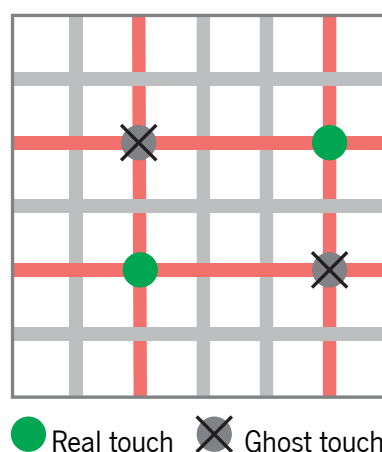
Figure 3.8.   Self-capacitance matrix made of rows and columns, causing the perception of ghost touches during simultaneous touches.

To improve performance of self-capacitance matrices, systems normally use enhanced patterns such as the diamond pattern or the flower pattern (Cleary, 2019), among others, increasing electrode overlapping by finger, reducing the electrode overlapping between each other, permitting best interpolation, and reducing noise susceptibility. However, as the electrodes are sensed individually with reference to ground, multitouch detection is not possible due to the appearing of ghost touches (3M, 2013; Barrett & Omote, 2010).

3.1.2.2. <u>Mutual-capacitance</u>

In mutual-capacitance, always two electrodes are necessary, one driving an electric signal and the other sensing it (Cleary, 2019; Ho et al., 2009). In this topology there is no ground referencing. A touching finger overlaps the two electrodes, facilitating the passage of electric charge, as shown in Figure 3.9. The capacitor between electrodes C_{DS} is low, and the capacitors C_{DF} and C_{SF} increase when a finger is placed nearby.
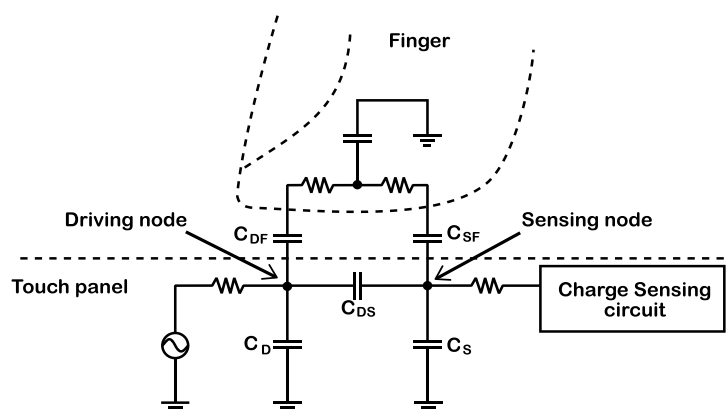
Figure 3.9.   Theoretical model of mutual-capacitance sensors. Reprinted from (Ho et al., 2009), *SID Symposium Digest of Technical Papers*, vol. *40*(1), copyright © 2009 Society for Information Display, with permission from John Wiley and Sons.

Several layouts can be employed for mutual-capacitance, such as interdigitated, serpentine, spiral, or meandered electrodes, among others (Ho et al., 2009; Rivadeneyra et al., 2015). In Figure 3.10 are shown two possible layouts for mutual-capacitance single sensors. It is also possible to implement interpolation in mutual-capacitance sensors using multiplex design, as observable in Figure 3.11, which highly increases the resolution of the measurements, ideal for sliders or touchscreens (Ho et al., 2009).

(a) (b)
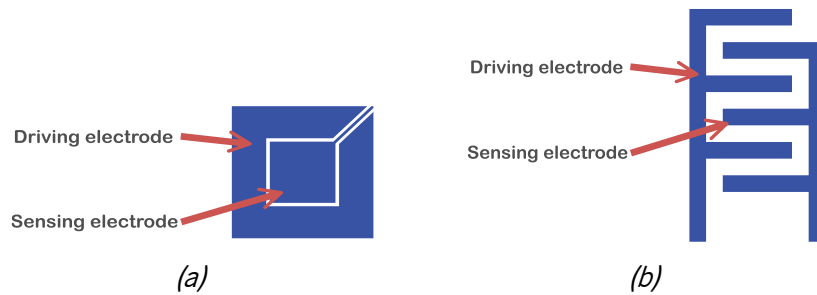
Figure 3.10. Example of mutual-capacitance sensors: *(a)* Square pad and *(b)* interdigitated pad. Reprinted from (Ho et al., 2009), *SID Symposium Digest of Technical Papers*, vol. *40*(1), copyright © 2009 Society for Information Display, with permission from John Wiley and Sons.
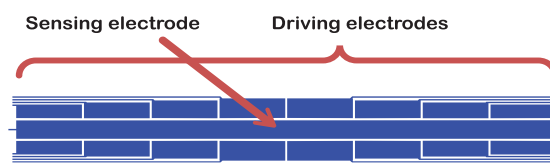
Figure 3.11. Multiplex design mutual-capacitance sensor. Reprinted from (Ho et al., 2009), *SID Symposium Digest of Technical Papers*, vol. *40*(1), copyright © 2009 Society for Information Display, with permission from John Wiley and Sons.

Mutual-capacitance matrices measure the intersections between electrodes individually, which allows for multitouch detection. For this reason, mutual-capacitance matrices is the most used technology nowadays in touch sensing (Du, 2016).

The most common type of geometry for mutual-capacitance matrices is the diamond shape, shown in Figure 3.12 (Akhtar & Kakarala, 2014; Barrett & Omote, 2010).
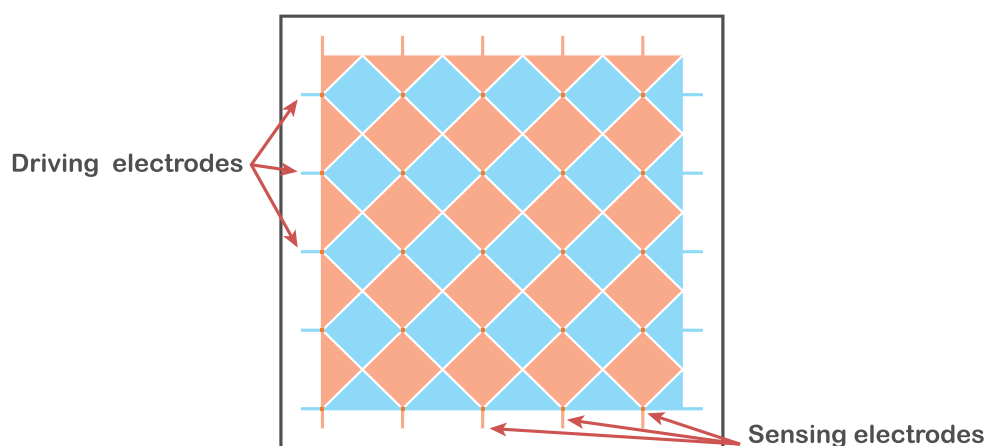
Figure 3.12. Diamond-shaped mutual-capacitance matrix. Only one driving electrode is transmitting at a time, and the sensing electrodes sense the capacitance towards that electrode.

This layout features minor intersecting electrodes and maximum electrode area exposed to finger touch. Nevertheless, many other patterns exist, such as the sunflower (Cleary, 2019), or the diamond outer frame (Peng, 2019), among others (Akhtar & Kakarala, 2014; Harley & Orsley, 2009; Hoch & Badaye, 2017), some of them patented.

3.2. APPLICATIONS WITH CAPACITIVE POLYMER FILMS

For years, capacitive sensing required rigid and non-transparent materials. Touchscreens in tablets and smartphones banalized transparent capacitive devices in the last decade, but the concept of a flexible capacitive touchscreen is still mostly an unheard concept for the general public (Y. Khan et al., 2020).

Grosse-Puppendahl, Braun, et al. (2013) presented a rigid platform for hand detection and gesture recognition, as shown in Figure 3.13. It uses projected mutual capacitance technology, employing shunt mode measurements, and has several large round electrodes: eight driving electrodes located in the device's edges, and two sensing electrodes in the center. According to the authors, the main advantage of this prototype is the small number of sensors necessary.
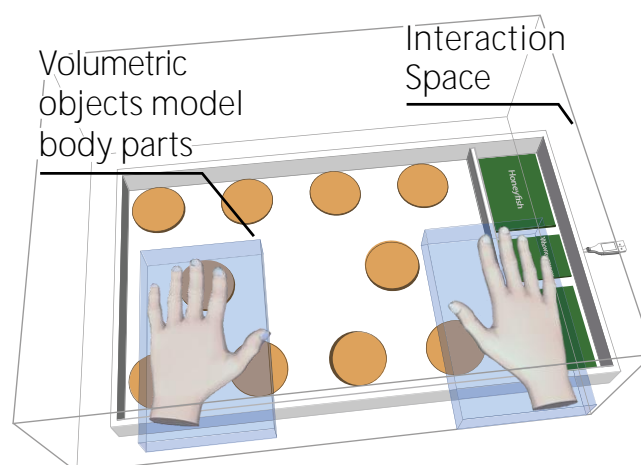
Figure 3.13.   Multi-hand and gesture recognition prototype, using few capacitive sensors.
Republished with permission of ACM (Association for Computing Machinery), from
Proceedings of the SIGCHI Conference on Human Factors in Computing Systems,
(Grosse-Puppendahl, Braun, et al., 2013), copyright © 2013 ACM.

Similarly, Sylla, Gonçalves, Brito, et al. (2012) also presented a prototype called t-books to identify different block pieces using capacitive sensors, for educational purposes. The system consists in a book with slots in its pages, and an electronic board on the back cover, as visible in Figure 3.14. The user inserts cardboards with capacitive tags in the slots, which attach to the electronic circuit magnetically, allowing it to detect what card has been inserted. The information of the placed cards is then sent to a computer where it triggers actions based on which card has been inserted, and allows children to create their own narratives. It uses self-capacitance measurements, with several sensors per slot. The combination of the activated sensors indicates which card has been inserted on it, and, contrarily to the previously presented gesture recognition prototype (Grosse-Puppendahl, Braun, et al., 2013), here hand detection from accidentally touching the sensors is not useful, thus that is filtered out by the use of a checksum.

(a) (b)

Figure 3.14. t-books prototype, *(a)* an adventure book with cards that are *(b)* placed in slots and detected through capacitive sensing. Republished with permission of ACM (Association for Computing Machinery), from *Proceedings of the 11th International Conference on Interaction Design and Children*, (Sylla, Gonçalves, Branco, et al., 2012), copyright © 2012 Authors.

The field of flexible printed electronics now allows researchers to develop non-rigid smart materials for electronic sensing based on capacitive technology (J. Kim et al., 2017; Nunes et al., 2017). The two prototypes presented before are perfect examples of rigid platforms that would highly benefit from printed and flexible electronics: in the gesture recognition prototype (Grosse-Puppendahl, Braun, et al., 2013), using the same topology, it would be possible to sensorize any surface, even non-planar ones, and in the t-books prototype (Sylla, Gonçalves, Branco, et al., 2012, 2013) it would eliminate the need for the thick back cover of the book, and the sensors could be easily fitted inside the pages of the book seamlessly.

The work conducted by Fan et al. (2017) shows the result of multi-layer screen-printed capacitive sensors on a PET film using silver paste for the opaque electrodes and poly(3,4-ethylenedioxythiophene)

(PEDOT) for the transparent ones, as shown in Figure 3.15. Several designs were implemented, such as single buttons, matrix buttons, and linear and radial sliders. To achieve multi-layer, the top and bottom layers were printed on the same side of the PET film intercalated with a UV-curable dielectric ink layer. Since the produced films were intended to be used with backlight illustration for user feedback on touch, the sensing areas were printed with PEDOT, a blueish transparent ink.
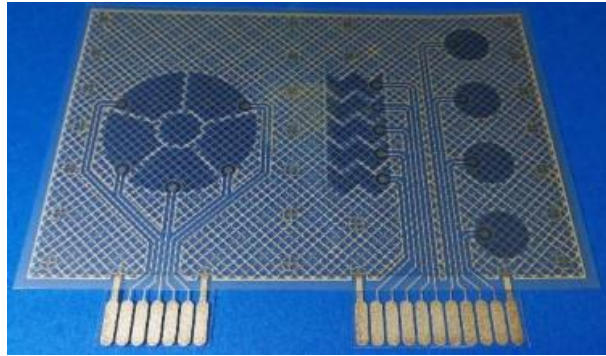
Figure 3.15.   Multi-layer screen-printed capacitive touch buttons and sliders on a PET film. The traces made of silver paste, and the touch sensing areas are transparent PEDOT for backlight illustration upon finger touch. Reprinted from (Fan et al., 2017), copyright © 2017, IEEE.

To achieve high transparency in commercial touch devices, electrodes are usually made of ITO, deposited in a glass substrate (Ho et al., 2009; Ma et al., 2015), but the use of ITO is becoming more and more expensive because both the slow manufacturing process based on lithography and the drop in indium reserves, not to mention the toxicity of indium (Ma et al., 2015). Also, ITO is susceptible to deformation, which restricts its range of applications to rigid devices (Ma et al., 2015).

To counteract these, the work presented by W. Kim et al. (2015) proposed the use of single-walled carbon nanotubes (SWCNTs) instead of ITO to take advantage of the SWCNTs' flexibility. Their prototype envisioned the creation of a capacitive multitouch touchscreen capable of detecting the force applied on each touch. Instead of relying on the fringing effect, an elastic silicone gel material was used as dielectric to separate the two conductive layers, which gets deformed when a finger presses it. In Figure 3.16 is shown the layers composing the device. The bottom layer is made of glass with transparent and conductive columns printed on it, and in the top layer a PET substrate with printed rows. The authors claim to have attained a transmittance of the transparent SWCNT electrodes of 85 %, and a 25 % variation in capacitance when applying 500 gf on the touchscreen over a 3 mm diameter tip.

Receive line (19 Active line + 1 Ground line)
Dimension of channel (Length/Width: 52.85/4.35 mm

→ **Transparent Electrode on PET film**

→ **Force Sensing layer (elastic material) with thickness of 1.4 mm**

→ **Transparent Electrode on Glass**

Transmit line (11 Active line + 1 Ground line)
Dimension of channel(Length/Width): 87.4/4.39 mm

*Gap between channels : 0.02 mm
*Active touch area of touchscreen: 52.85 × 87.4mm

Figure 3.16. Diagram of force sensing capacitive touchscreen. Reprinted from *Sensors*, vol. *15*(11), (W. Kim et al., 2015), copyright © 2015 by the authors, under Creative Commons BY 4.0 license (https://creativecommons.org/licenses/by/4.0).

Nevertheless, B. Zhang et al. (2014) also came up with a similar prototype to achieve dual operation, proximity and pressure sensing, but using transparent silver nanowires (SNWs) electrodes. The diagram of the designed film composite is visible in Figure 3.17. The same principle was used for the dielectric, made of an elastic layer of polydimethylsiloxane (PDMS). The optical transmittance of the developed film was 77 % at the worst point.

Elastic PDMS

PET substrate

Silver nanowires network electrode
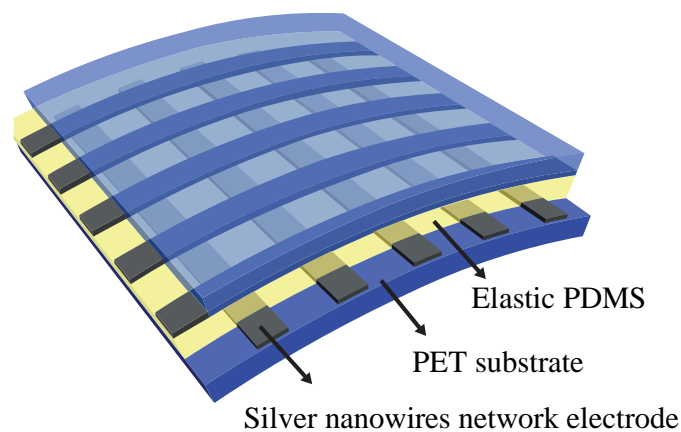
Figure 3.17. Schematic illustration of a flexible proximity and pressure sensing film.
Reprinted by permission from Springer Nature: Springer Nature, *Nano Research*, vol. *7*(11), "Dual functional transparent film for proximity and pressure sensing", (B. Zhang et al., 2014), copyright © 2014, Tsinghua University Press and Springer-Verlag Berlin Heidelberg.

Figure 3.18. Transparent and flexible interdigitated capacitive sensor. Republished with permission of IOP Publishing, Ltd., from *Flexible and Printed Electronics*, (Nair et al., 2019), vol. *4*(4), copyright © 2019 IOP Publishing Ltd.; permission conveyed through Copyright Clearance Center, Inc.

Nair et al. (2019) have developed a new ink formulation based on SNWs which was used in the fabrication of an interdigitated capacitive touchpad, envisioning flexibility and transparency, as shown in Figure 3.18. The ink was prepared for an unconventional printing method: direct ink writing (DIW), a 3D printing technology, very similar to 3D fused filament fabrication (FFF) printing, which can create 3D structures by depositing ink, layer after layer (Yubai Zhang et al., 2019). The prototype consisted of three layers. The bottom layer was a PET film, the middle layer was the printed SNW ink, and the top layer was composed of PDMS. When bending the device, the PET layer suffers compressive stress and the PDMS layer tensile stress. According to the authors, this construction facilitates the device to recover the original shape. The authors claim to have achieved a level of transmittance of 94 %.

When compared to traditional physical touch buttons, capacitive touch buttons lack the ability to provide feedback to the user that the button has been pressed. However, the approach pursued by Kisić et al. (2017) might be on the way to solve this issue. It does mutual-capacitance measurements between two electrodes that are separated by an air gap. When the user pushes against the touch button, the top electrode deflects itself as shown in Figure 3.19, bringing the two electrodes closer together, while the user gets a slight sensation that the button has been pushed. The substrate polymer used in this prototype was polyimide (PI) film. The electrodes had 2 cm of diameter and were inkjet-printed with silver nanoparticles (NPs) ink. The spacer was simply made by stacking 3 PI films with open holes attached with glue, resulting in a total thickness of 700 μm. The author executed performance measurements on the developed device and found out that the response fitted a linear approximation with sensitivity of 4.14 pF/mm.
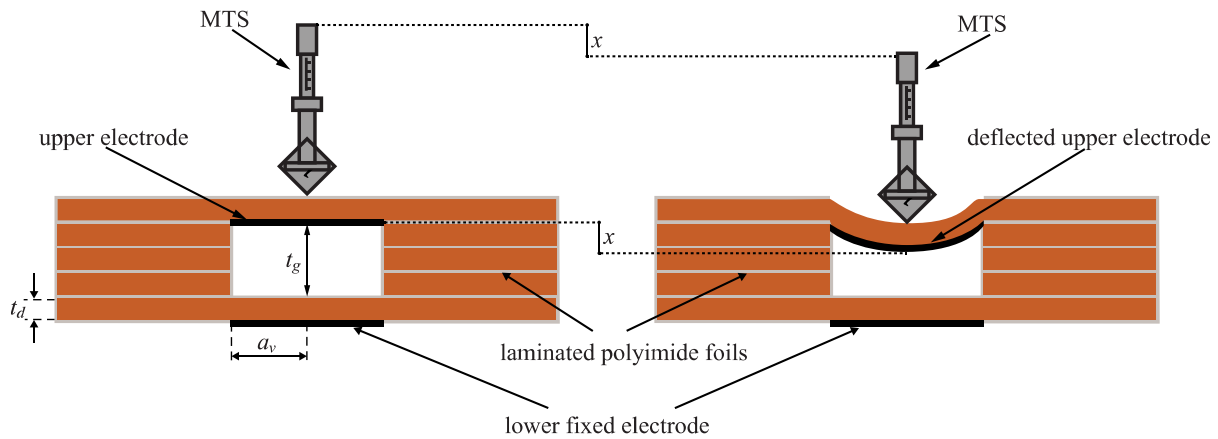
Figure 3.19. Deformable touch button with spacers and an air gap. Reprinted from (Kisić et al., 2017), copyright © 2017, IEEE.

A fragility of touch sensors, by nature, is the mechanical stiffness of the electrodes, especially the bendable ones. Continuous bending operation or systematic hitting the sensor with fingers might cause the electrodes to degrade over time, affecting the performance of the sensor. To face this problem, Q. Zhang et al. (2018) have created a conductive self-healing polymer that could fit flexible circuits and wearables. The polymer is highly flexible and can achieve an efficiency of up to 98 % after 48 h of thermal treatment at 25 °C. The authors show two demonstrations: first with an LED by deliberately damaging one of its terminals, and second with a capacitive sensor. In both case scenarios the system recovered from the damage and became functional again.

So far, most attention was given to touch sensors. But capacitive technology goes much beyond, such as the humidity sensor developed by Hajian et al. (2019). It is a fully printed flexible sensor based on fluorinated graphene (FG) as active humidity sensitive material. A silver-based ink was screen-printed on PI substrate with interdigitated electrodes, and then the FG solution was drop-casted on top of the electrodes. The sensor produced a capacitance change of more than 300 % for levels of relative humidity between 20 % to 70 %. Nevertheless, in other works more patterns have also been investigated such as the serpentine, spiral or meandered electrodes using the humidity susceptibility of the PI substrate itself (Rivadeneyra et al., 2015).

Capacitive sensors have also found their way into wearable devices. The work presented by Park et al. (2017) contemplates the creation of a capacitive film sensor for a wearable respiration monitoring system. The sensor is worn in the waistbelt of the user's waist to measure the exerted pressure on it during inhale and exhale movements, as shown in Figure 3.20. The sensor is composed by a dielectric elastomer and two flexible electrodes. The dielectric elastomer was a 36 % porous polybutylene adipate terephthalate (PBAT), more known under the brand name Ecoflex, and the flexible electrodes were made

of PDMS with SNWs and carbon fibers for increased conductivity. The result is a very flexible device that could fit the waistbelt and be compressed when the pressure increases without the risk of breaking or cracking. The signal measured from the sensor was filtered by a 20 Hz low-pass filter, following to an instrumentation amplifier, then converted to digital and analyzed in a computer. The researchers were able to successfully identify the breathing frequency, inhales, exhales and the intentional holding breath moments in several subjects.
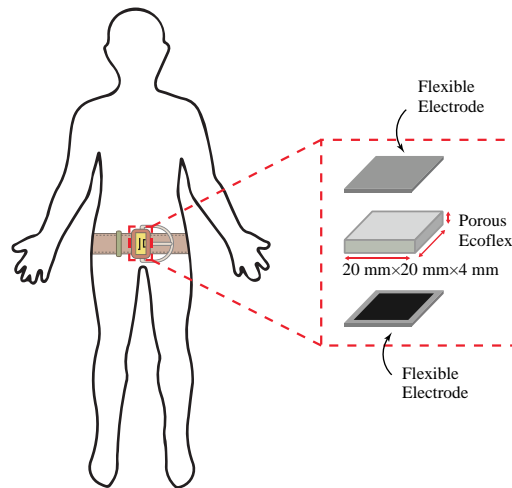
Figure 3.20. Diagram of breathing sensor attached to the user's waistbelt. The inset image represents the constitution of the sensor. Reprinted from (S. W. Park et al., 2017), copyright © 2017, IEEE.

Other applications of capacitive films can be based on changing the dielectric material, allowing to measure measure a pipe, for example. Thus, Ji et al. (2014) have designed a capacitive film system to measure the amount of air bubbles existing in a flowing liquid inside a micropipe. The capacitive electrodes are placed around the pipe, and the fluid acts as dielectric, as demonstrated in Figure 3.21. When a gas slog passes the sensing area, the dielectric permittivity of the mean decreases, resulting in lower capacitance of the sensor. The system is composed by two sensors to detect the velocity of the gas slog inside the pipe. Prior to use, it is necessary to perform calibration of each sensor for empty and full case scenarios, since the mutual capacitance between electrodes extremely low.

Nonetheless, dielectric elastomers can also be used in capacitive energy harvesters (Moretti et al., 2020) as is the case of the dielectric elastomer generator (DEG) built by Moretti et al. (2018) to scavenge electrical energy from water waves in oceans, as shown in Figure 3.22.
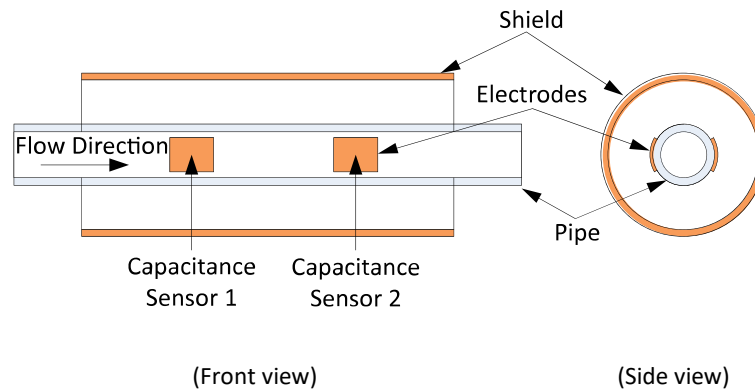
Figure 3.21.   Capacitive sensing for detection of gas slogs inside a liquid-flowing micropipe. Adapted from *Sensors*, (Ji et al., 2014), vol. *14*(12), copyright © 2014 by the authors, under Creative Commons BY 4.0 license (https://creativecommons.org/licenses/by/4.0).
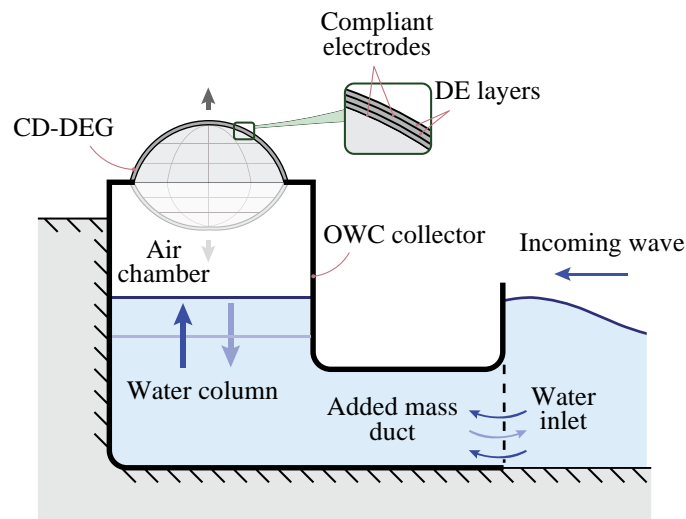
Figure 3.22.   Schematic representation of a dielectric elastomer generator (DEG) for water wave energy scavenge. Republished with permission of IOP Publishing, Ltd., from *Smart Materials and Structures*, (Moretti et al., 2018), vol. *27*(3), copyright © 2018 IOP Publishing Ltd.; permission conveyed through Copyright Clearance Center, Inc.

The DEG is constituted by a highly flexible polyacrylate film with a pair of carbon grease-coated electrodes. DEG systems work by combining the preloading of the DEG's capacitor with stretch movements. Initially, the DEG is stretched and some charge is loaded into its capacitor. Then, when the DEG returns to the unstretched state with the same pre-loaded charge Q (C) distributed on a smaller capacitance C (F). The voltage V (V) rises accordingly to Equation (3.2), which results in a higher energy stored in the capacitor, E (J), due to the quadratic relationship between voltage V and energy E in Equation (5.1). Elastomer energy harvesters often use a flyback circuit, or a dual active bridge to attain that (Moretti et al., 2020).

For a long time that the use of paper as substrate in printed electronics has been a very tempting alternative to the other polymers, for being environmentally friendly and of low-cost production. The experiments conducted by R.-Z. Li et al. (2014) allowed the prototyping of paper-based capacitive touch pads by direct ink writing (DIW) technique. The large amount of conductive ink deposited through the needle on paper enables the ink to easily fill in the roughness of the paper and form conductive traces. Figure 3.23 shows a capacitive sensor printed by DIW on paper. Vella et al. (2019) have also proposed the imprint of capacitive sensors directly on the 3D objects without the need for a film substrate.

(a)   *(b)*
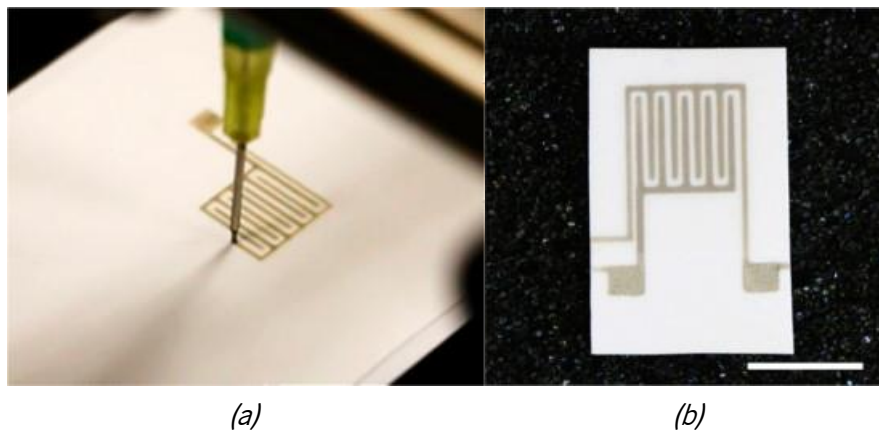
Figure 3.23.   Paper printing: *(a)* **Interdigitated capacitive sensor printed by direct ink writing (DIW) technique on paper substrate;** *(b)* **The sensor fully printed.**
Reprinted with permission from (R.-Z. Li et al., 2014), copyright © 2014, American Chemical Society.

An older idea by Mazzeo et al. (2012) but still valid nowadays proposes the implementation of capacitive touch pads out of ordinary metalized paper used in packaging, e.g., in beverages, and therefore making use of the existing aluminum foil in the cardboard. To create the electrodes and the electric connections, a laser cuts the aluminum in the respective regions of the in the cardboard. This can give discardable packaging a new life that otherwise would end up in the trash.

Though not much usual, some electrostatic actuators have been developed. One of such examples is the paper robot developed by Shigemune et al. (2017), shown in Figure 3.24. It consists is in sheet of paper where an interdigitated pattern was inkjet-printed with silver ink. Then, a water-based ink was also printed on the paper to induce self-folding of the paper into the desired 3D curved L-shape. When applying a strong electric field between the electrodes, it causes the robot to slightly straighten up, and, due to the uneven form of the robot, the longer segment pushes the other forward, resulting in the locomotion of the robot. To produce electrostatic actuation, the robot was powered by an AC 2.83 kV, and to enhance the robot's velocity it was operated at 100 Hz. Each pulse creates a micromovement, but the fast-alternating electric field made the robot travel up to 56 mm in 15 s.
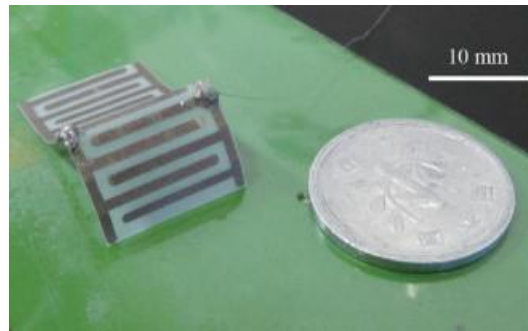
Figure 3.24. Electrostatic printed actuator for paper robot. Reprinted from (Shigemune et al., 2017) copyright © 2017, IEEE.

3.3. EXPERIMENTAL WORK

Three different prototypes were prepared based on the capacitive technology:

- A touch sensor made of a resin/ITO composite (Mendes-Felipe et al., 2020);
- A diamond-patterned mutual capacitive matrix, printed on a PET substrate with silver ink (N. Castro et al., 2017; Nunes et al., 2017);
- A pressure and bending sensor based on the deformable dielectric poly(vinylidene fluoride-trifluoroethylene-chlorofluoroethylene) (P(VDF-TrFE-CFE)) (Pereira et al., 2021).

These prototypes are going to be discussed next.

3.3.1. Polyurethane acrylate/ITO composite touch sensor prototype

UV-curable polymers and polymer composites are growing interest in the scientific community. Polyurethane composites, in combination with zinc oxide, have demonstrated excellent antibacterial

properties, in special for *Escherichia coli* and *Bacillus subtilis* (J. H. Li et al., 2009). However, polyurethane acrylate (PUA) has been rarely investigated with respect to its dielectric properties.

In this work, a PUA composite was developed with the inclusion of indium tin oxide (ITO) for capacitive sensing, using UV-curing, and requiring no solvents or high temperature procedures.

The development of this prototype resulted in a scientific publication (Mendes-Felipe et al., 2020), and a video demonstration was submitted along with the document, available as supplementary material[1].

3.3.1.1. Materials and sample preparation

UV-curable PUA resin was acquired from SPOT-A Materials, reference SPOT-E. ITO nanoparticles (NPs) with size between 20 to 70 nm were purchased from SkySpring Nanomaterials, Inc., with a purity of 99.99 %. Sample cleaner 2-propanol with 99.5 % of purity was used from Alfa Aesar.

The ITO nanoparticles (NPs) were mixed with the PUA resin to obtain a concentration of 25 wt.%, placed in an ultrasound bath (ATU ATM model ATM3L) for 3 h at 30 °C, and then stirred for 2 h at room temperature. The solution was bar-coated on a glass substrate, and then cured on a UV chamber (Honle UV America, Inc., reference UVACUBE 400) for 90 s with a 1000 W/m2 irradiation exposure. The composite was peeled off from the glass and cleaned with the 2-propanol. The produced film was 200 µm thick. Two pairs of gold electrodes were deposited on the sample, two electrodes on each side and overlapping each other, forming two capacitors, as shown in the inset of Figure 3.25. The electrodes were circular with 5 mm of diameter, and were sputter-coated using equipment Quorum Q150T SC502.

PUA is transparent, but ITO is blueish, which makes the sample to lose transparency with the increase in the concentration of ITO. The prepared sample was nearly opaque due to the concentration of 25 wt.% (transmittance of 1 %), but in turn the dielectric constant becomes higher (εr = 33). Further characterization of the composite is available in (Mendes-Felipe et al., 2020).

3.3.1.2. Electrical circuit

The terminals of the sample were created by two strips of aluminum foil, which were attached to the gold electrodes using Electric Paint from Bare Conductive. The device was properly isolated with adhesive tape to prevent fingers from directly touching it.

The implemented circuit to read the capacitance of the sensor was a very simple one, for convenience. Instead of relying in an analog-to-digital converter (ADC) (Tan et al., 2021), a high-value

---

1 Link of the demo video available as supplementary material: https://www.sciencedirect.com/science/article/pii/S0266353820316961#mmc1

resistor was used (10 MΩ) to limit the rate of charge of the of the sensor's capacitor, and this way, determining if it was being touched or not. This is the same technique as used in self-capacitance sensors. Two digital pins of a microcontroller are connected, one acting as source, and the other as sensing, as visible in Figure 3.25.
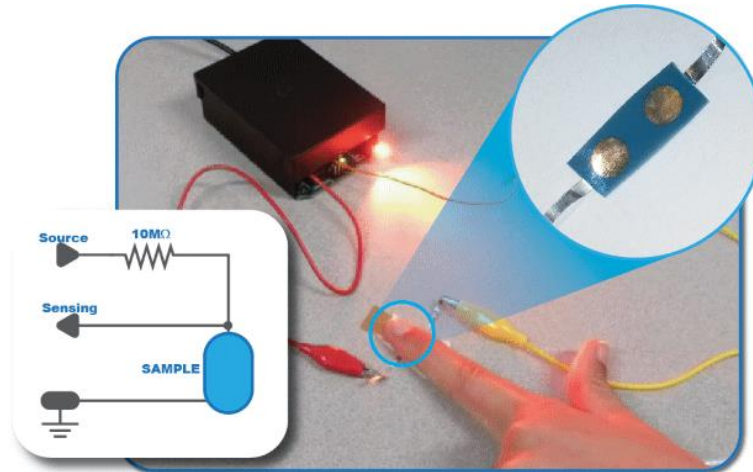
Figure 3.25. Developed prototype for capacitive sensing with PUA/ITO composite film.
Reprinted from *Composites Science and Technology*, vol. *199*, (Mendes-Felipe et al., 2020), copyright © 2020 Elsevier Ltd. All rights reserved.

The electric circuit was composed by a microcontroller (Microchip ATmega328P) running at 16 MHz and with 5 V supply. The microcontroller was connected to a computer via USB, but since the microcontroller has universal asynchronous receiver-transmitter (UART) interface, in between was inserted a USB to UART converter (FT232RL from Future Technology Devices International Ltd. (FTDI)). An LED in series with a 330 Ω resistor was used to provide user feedback.

The diagram of Figure 3.26 shows the algorithm used to calculate the state of the sensor. Initially, the pin of the microcontroller acting as sensing is connected to ground to completely discharge the sensor. Then, it changes to high-impedance state, and the pin operating as source rises to 5 V level, providing the electrical charge to charge up the sensor through the resistor. During this process, the sensing pin is closely monitoring its state until it detects that it has changed from *low* to *high* level. The elapsed time for that to happen determines the capacitance of the sensor. Yet, to measure the time, instead of setting a timer in the microcontroller running, it was used a pooling method, incrementing the variable `Count` endlessly. The result of `Count` will not be time itself, but proportional to time. In fact, the resulting value will change with the frequency of the microcontroller, or even with the selected pin of the microcontroller as operating as sensing. To reduce noise susceptibility, this operation is executed 50 times and the values of `Count` simply added.
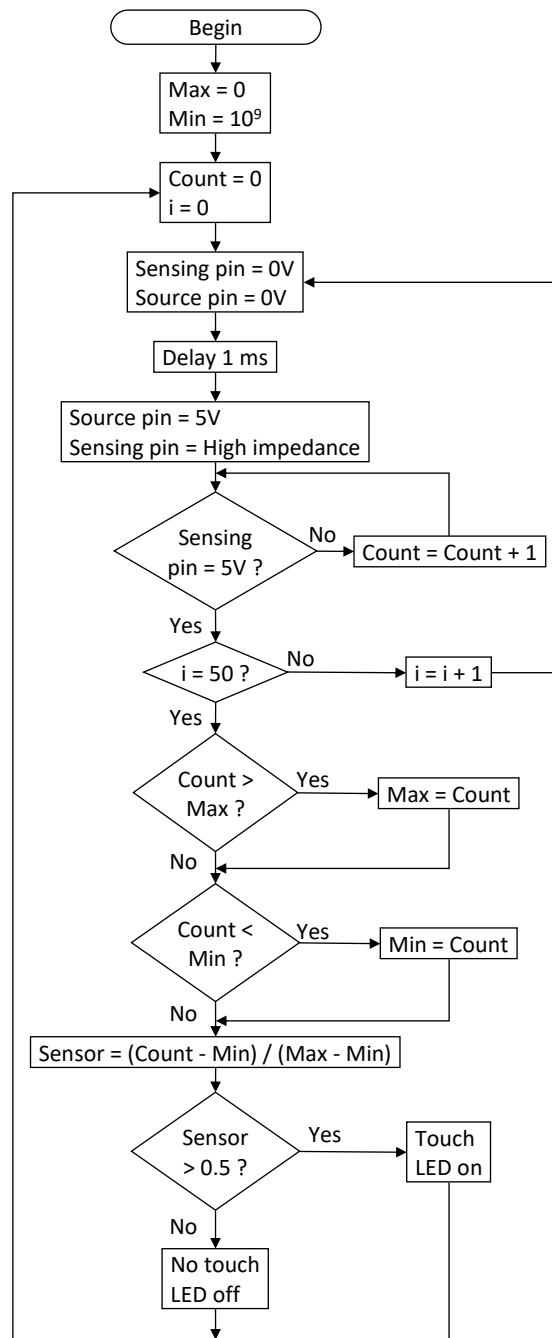
Figure 3.26. Algorithm implemented to acquire the measurements from the self-capacitive sensor, with self-calibration. Reprinted from *Composites Science and Technology*, vol. *199*, (Mendes-Felipe et al., 2020), copyright © 2020 Elsevier Ltd. All rights reserved.

To cancel the effect of `Count` being only proportional to the real charging time of the sensor, two variables called `Min` and `Max` keep tracking of the minimum and maximum values obtained. After the user has touched and released the sensor for at least once, the `Min` variable will contain the obtained value of `Count` for when the sensor is not being touched, and the `Max` variable the value for when being touched. A simple mathematical operation allows to remove the offset of `Count` and convert it to

a scale from 0 to 1, allowing the microcontroller to perform self-calibration during execution. It is considered a touch if the obtained value is higher than 0.5. To data log the measurements, this value is further converted to the range from 0 to 255 (range of a byte) and sent to the computer by the UART interface of the microcontroller.

3.3.1.3. <u>Results and discussion</u>

Based only on the implemented system, it was not possible to indicate capacitance of the sensor. Instead, the system acquired a waveform of amplitudes with arbitrary units (a. u.) resulting from the touching and releasing events by the user, as shown in the plot of Figure 3.27. It is easily identifiable the peaks, corresponding to the user touching the sensor.
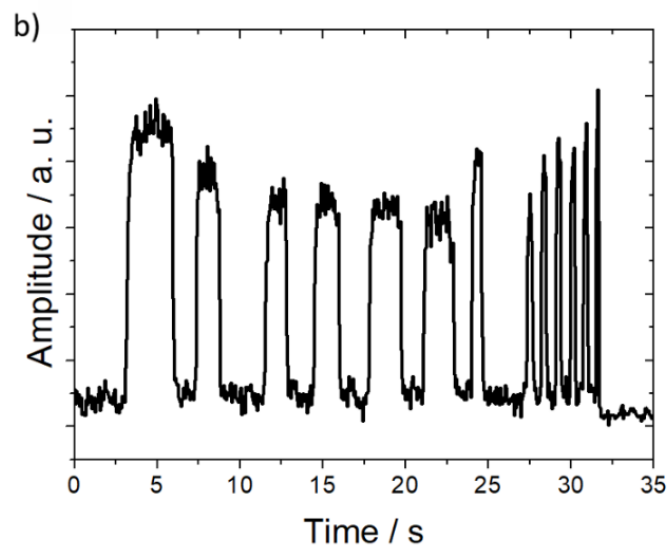
Figure 3.27. Waveform acquired by the microcontroller from the developed PUA/ITO capacitive sensor. Reprinted from *Composites Science and Technology*, vol. *199*, (Mendes-Felipe et al., 2020), copyright © 2020 Elsevier Ltd. All rights reserved.

The demonstration of the functioning of the system is furnished as supplementary material of the respective publication (Mendes-Felipe et al., 2020)[1].

Despite of the toxicity of ITO, which future developments might consider replacing, the developed PUA/ITO film sensor is a step on the development of environmentally friendlier materials, recurring to UV curing and additive manufacturing, without the use of solvents or high temperature processing.

---

1 Link of the demo video available as supplementary material: https://www.sciencedirect.com/science/article/pii/S0266353820316961#mmc1

3.3.1.4. <u>**Conclusions**</u>

In this work, a material based on the photopolymer PUA resin was developed, with the inclusion of ITO with a concentration of 25 wt.%. The prepared solution was UV-cured, involving no high temperature annealing. When compared with the PUA alone, the developed material presented high dielectric constant $\varepsilon r = 33$ at the trade of loss of transparency. An electric circuit based on self-capacitance technology was implemented to perform capacitance measurements on the sensor, for human touch applications. The system worked flawlessly, presenting high reproducibility and performance, which demonstrates the good application of the developed material as a new solvent-free for coatings with electronic sensing.

3.3.2. **Flexible capacitive touchpad prototype**

The objective of this prototype was to demonstrate the applicability of a low-cost fabrication method for the development of a flexible touchpad matrix capable of multitouch detection. Therefore, it was created a flexible touchpad made of a PET film with conductive silver ink printed on it by screen-printing technique. To achieve multitouch, it was employed the mutual-capacitance technology for the sensing circuit. Nevertheless, if one wants to use this prototype with self-capacitance technology, it is only necessary to change the developed electronic circuit, since the sensing matrix can be interchanged between both technologies. The fabricated capacitive matrix was of $220 \, \mu m$ thick, containing 10 rows × 15 columns. Upon finger touch, a variation of 30 -50 pF was obtained.

The development of this prototype resulted in a scientific publication (Nunes et al., 2017), and a video demonstration was submitted along with the document, available as supplementary material[1].

3.3.2.1. <u>**Materials and methods**</u>

There exist many pattern geometries for capacitive matrices, as was previously discussed (Akhtar & Kakarala, 2014). For this work, the diamond pattern was chosen. It consists of two layers of conductive material arranged in a diamond-like structure (Cleary, 2019; Ma et al., 2015). A dielectric film material was used, with rows printed on one side and columns on the other, providing capacitance intersection which allows to determine the touch location due to the capacitance change when a conductive material

---

[1] Link of the demo video available as supplementary material: https://www.mdpi.com/1424-8220/17/12/2786/s1

such as the human fingers is close to the matrix. In Figure 3.28 is shown the layout of designed matrix, 10 rows × 15 columns, with an area of 102×67 mm. Each of the squares of the electrodes has a side of 4 mm, which is adequate for fingertip detection.

(a)   (b)
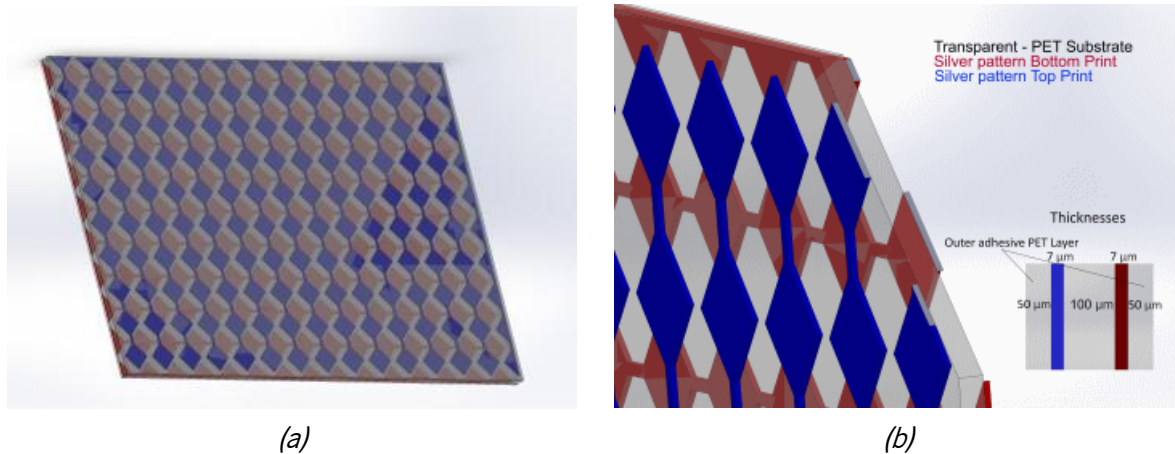
Figure 3.28.   Illustration of the geometry used for the capacitive touchscreen from *(a)* front view and *(b)* perspective view. Reprinted from *Sensors*, vol. *17*(12), (Nunes et al., 2017), copyright © 2017 by the authors, under Creative Commons BY 4.0 license (https://creativecommons.org/licenses/by/4.0).

To print the conductive layout, silver ink is a suitable solution because of the low-temperature necessary for currying and sintering, as well as the good conductivity of the final imprint. The ink selected for this work was the HPS-21LV ink from Novacentrix[1], prepared for screen printing. The used substrate was Melinex with 100 μm of thickness from Lohmann Technologies UK Ltd.[2], a PET film with treatment for better ink adhesion. The thermal treatment of the printed material was performed in a JP Selecta oven, model 2005165. The screen-printing apparatus was homemade, and the polyester mesh used for screen printing had 62/64 threads/cm.

3.3.2.2. Touchpad fabrication

The touchpad was screen-printed on both sides, one side at a time. First, the top of the layer was printed with silver ink, and to prevent shrinkage of the PET film during thermal annealing, it was only dried for 6 h at room temperature. Then the same procedure was performed for the bottom layer of the polymer with the aid of guiding marks. Once printed, the composite film was heated to 120 °C for 30 min to cure and sinter the ink.

---

1 Novacentrix official website: https://www.novacentrix.com

2 Lohmann Technologies UK Ltd. Official website: https://www.lohmann-tapes.co.uk

Next, a clincher connector was inserted with 25 terminals and pitch of 2.54 mm, from Amphenol FCI[1] with reference 65801-125LF. Finally, a layer of ordinary adhesive PET was applied on each side of the film as protection against scratches and oxidation. The appearance of the developed sensing film is shown in Figure 3.29.
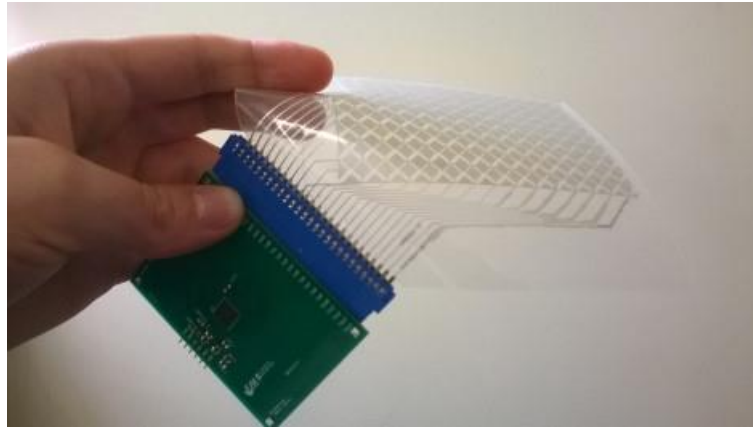
Figure 3.29.   Developed touchpad prototype, attached to a multitouch capacitive controller. Reprinted from *Sensors*, vol. *17*(12), (Nunes et al., 2017), copyright © 2017 by the authors, under Creative Commons BY 4.0 license (https://creativecommons.org/licenses/by/4.0).

The overall thickness of the printed film was 220 µm, and it is such a flexible device that can easily fit on any curved surface without getting damaged.

3.3.2.3. Capacitive detection circuit

The developed matrix can be used for self-capacitance or mutual-capacitance sensing. It is the external electrical circuit whose dictates the mode of operation. However, self-capacitance is limited to single touches, while mutual-capacitance is capable of multitouch detection (Walker, 2012). Capacitive controllers detect an AC signal based on its amplitude (Baglio et al., 2004) or frequency (Pintér & Dénes, 2015). To measure the capacitance of all of the intersections between rows and columns it is necessary a multiplexing system, allowing to access one intersection at a time. This task is eased through the use of a commercial capacitive controller integrated circuit (IC). It was chosen the IQS550 from Azoteq Ltd., a capacitive controller IC capable of analyzing 10 rows × 15 columns. The typical circuit recommended by the manufacturer is shown in Figure 3.30*b*. The digital interface of communication of the IQS550 is Inter-Integrated Circuit (I2C), which was connected to the microcontroller dsPIC33F128GP804 from Microchip Technology Inc., shown in Figure 3.30*a*.

---

1 Amphenol FCI official website: https://www.amphenol-icc.com
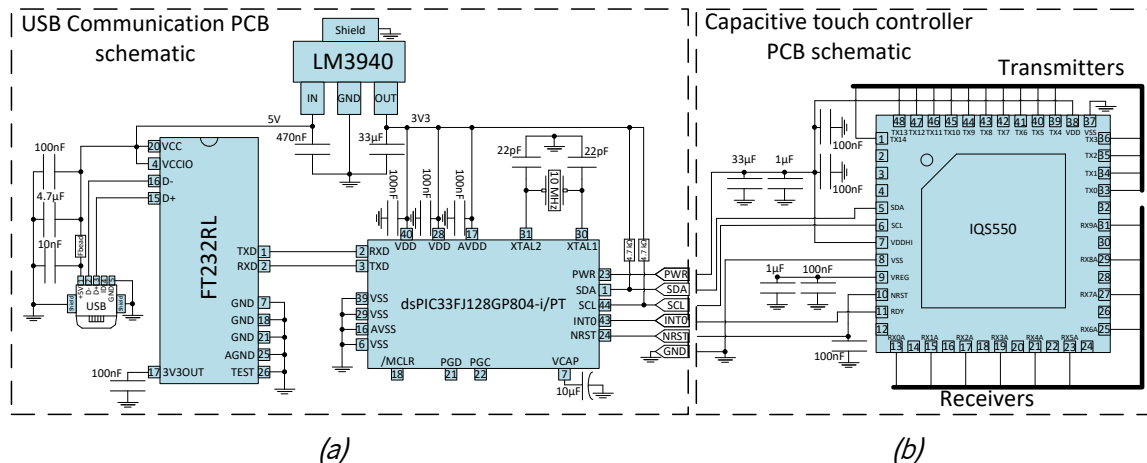
Figure 3.30. Circuit implemented: *(a)* a microcontroller stablishes communication between the computer and *(b)* the capacitive controller. Reprinted from *Sensors*, vol. *17*(12), (Nunes et al., 2017), copyright © 2017 by the authors, under Creative Commons BY 4.0 license (https://creativecommons.org/licenses/by/4.0).

The interface of communication of the microcontroller to the computer was UART, therefore a USB to UART converter was included, which was the FT232RL from FTDI. Also, since the used microcontroller needs a 3.3 V supply, but the USB provides 5 V level, the conversion of level was performed by an LM3940 voltage regulator from Texas Instruments Inc.

The circuit was assembled in two different PCBs, according to the modules shown in Figure 3.30*a* and *b*, so that the microcontroller could be bypassed and the programmer CT210A-S from Azoteq Inc. could be directly connected to the IQS550 integrated circuit.

3.3.2.4. <u>Results and discussion</u>

To assess the performance of the system, it was necessary to perform the calibration of the matrix, using the software tool provided by Azoteq Ltd. together with the CT210A-S programmer. The system presented a suitable response, but it was noticed that the capacitive controller would easily saturate when the fingers touched the film. By adding a separator on top of the film with a few mm, such as a glass, the precision was greatly improved. Figure 3.31*a* shows the system working with the matrix fitting the curved border of a table and in Figure 3.31*b* the matrix with a 5 mm glass overlay.

The used capacitive controller is capable of reading up to 5 simultaneous touches. The scanning frequency of the matrix is 100 Hz, though it decreases with each touch, to the lowest of 88 Hz with 5 touches. The initial capacitance for every of the 150 points is roughly of 40 pF, and a variation of 30 -50 pF is found on the touches, which gives a good sensitivity range for the capacitive controller. Despite the designed matrix had 10 rows × 15 columns, the capacitive controller implements

interpolation between traces, resulting in an actual resolution of 2304 × 3584 points, which is about 36 point/mm. This allows high precision measurements.

<div align="center">(a)   (b)</div>
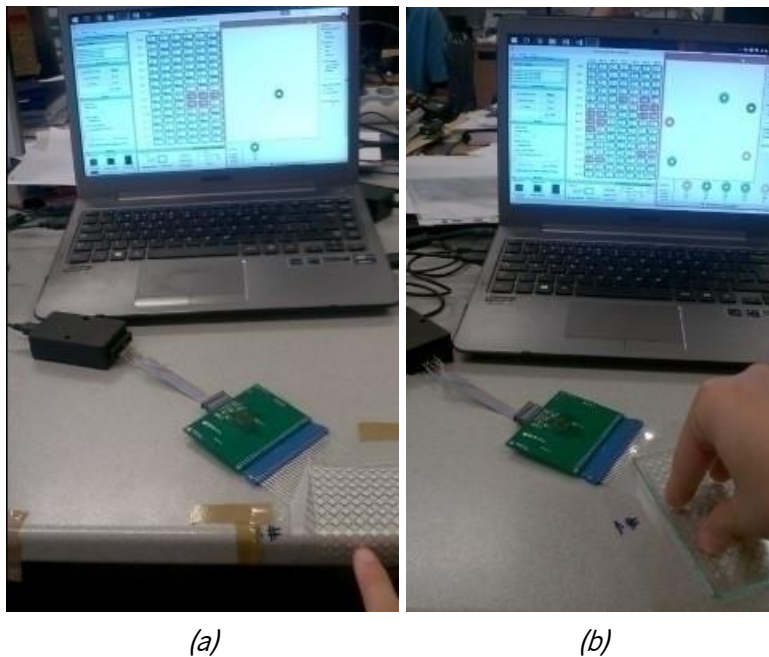
Figure 3.31. Performance of the system: *(a)* fitting a curved surface; *(b)* with 5 mm glass overlay; *(c)* capacitance distribution map, using the glass overlay. Reprinted from *Sensors*, vol. *17*(12), (Nunes et al., 2017), copyright © 2017 by the authors, under Creative Commons BY 4.0 license (https://creativecommons.org/licenses/by/4.0).

The connector using the clincher proved to be a critical point of failure of the whole system, probably because the clincher punctures through the film and cracking the silver ink deposition. The connector had to be stabilized and placed in a way that it would not move while utilizing the system. In this situation, the glass overlay also gave improved mechanical stabilization of the contacts.

Furthermore, to be used as a demonstrator, a C# application was also developed to show the capacitive touchpad capability in detecting objects with conductive elements shown in Figure 3.32, based on the number of touching points and the distance between them.
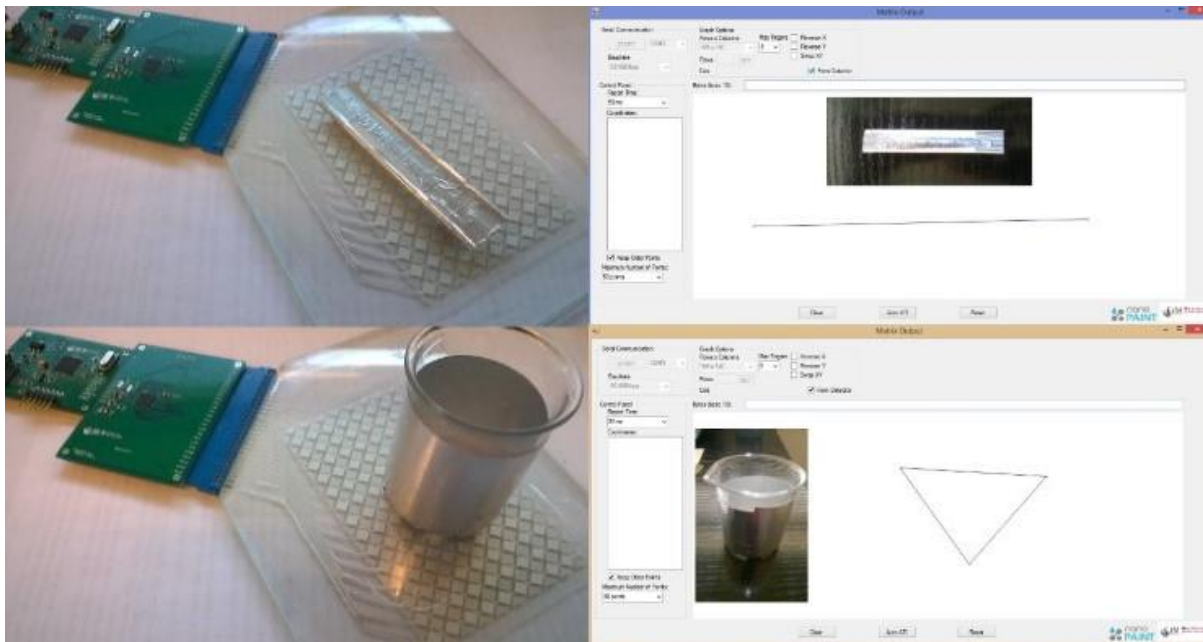
Figure 3.32. Demonstration of recognition of objects with conductive elements, based on number of touching points and distance between them. Reprinted from *Sensors*, vol. *17*(12), (Nunes et al., 2017), copyright © 2017 by the authors, under Creative Commons BY 4.0 license (https://creativecommons.org/licenses/by/4.0).

3.3.2.5. Conclusions

It has been presented the fabrication of a low-cost printed capacitive matrix on a flexible PET film with an overall thickness of 220 µm. The diamond pattern was printed in both sides with silver ink through screen printing. A capacitive controller IC was used to acquire the touches from the matrix, sending the data to a microcontroller via I2C, and then to a computer via USB. The matrix had 10 rows × 15 columns, and the capacitive controller was capable to reach a resolution of 2304 × 3584 points through interpolation, at a scanning frequency of 100 Hz. Each point showed a capacitance below 40 pF with no touch, and a 30 -50 pF capacitance change on finger touch.

To conclude, the capability of the capacitive matrix to fit on curved surfaces was demonstrated, as well as the possibility to detect, not only human fingers, but objects with conductive materials as well, which contributes for the possibility of implementing TUIs with flexible multitouch sensing areas.

3.3.3. Deformable P(VDF-TrFE-CFE) dielectric prototype

The objective of this prototype was to create sensors capable of reading the real finger pressure instead of the estimated pressure based on the area of finger contact (Nunes et al., 2017) and to avoid the usually slow-to-recover piezoresistive sensors (Pedro Costa, Gonçalves, et al., 2019) by creating dielectric deformable sensors that do not rely on the fringing effect.

The terpolymer P(VDF-TrFE-CFE) is a dielectric non-ferroelectric material that exhibits high dielectric constant, $\varepsilon r = 40$, and excellent mechanical properties, which makes it suitable for capacitive sensing applications. In this work, pressure and deformation sensors were fabricated using P(VDF-TrFE-CFE), on a PET substrate. The P(VDF-TrFE-CFE) dielectric film was prepared by solvent casting technique, and the sensors were assembled using bar-coating and screen-printing techniques. The respective signal conditioning electronics was designed, and measurements were broadcasted via Bluetooth.

Performance tests were completed on the sensors and curves of linearity and repeatability were traced. The good response obtained and the reproducibility potential of this technology represents an advance in polymer film materials for electronic applications.

The development of this prototype resulted a scientific publication (Pereira et al., 2021). Demo video is also available in the footnote link[1].

3.3.3.1. Materials and sample preparation

The P(VDF-TrFE-CFE) (62.5/29/8.5 mol.% of VDF, TrFE and CFE, respectively) was acquired from Piezotech, with reference RT-FS, and the DMF solvent was furnished by Merck. PET film with 100 μm of thickness was acquired from DuPont (Melinex ST506), and silver ink was supplied from Novacentrix (Metalon HPS-021LV). The utilized PDMS silicone elastomer used was obtained from DOW (reference SYLGARD™ 184 Silicone Elastomer Kit). Screen-printing apparatus was homemade, and used meshes were $100/105$ threads/cm with 55 μm gaps. Used oven was a JP Selecta 2005165, and the hot-pressing apparatus was a VERSAPRESS FC480.

The preparation of the solution was made by dissolving P(VDF-TrFE-CFE) powder in DMF with a concentration of 15 wt.% and stirred for 2 h. The solution was deposited on a glass substrate through doctor blade coating with a 50 μm spacer. Then, it underwent a three-phase thermal treatment to fully evaporate solvent: 10 min at 210 °C in an oven, followed by 2 h at 90 °C, and then 15 days at room

---

1 Link of the demo video: https://youtu.be/jevyGvo1LrE

temperature. Lastly, the produced P(VDF-TrFE-CFE) film was peeled off from the glass. Further characterization of the prepared samples is available in (Pereira et al., 2021).

3.3.3.2. Sensor fabrication

A PET film was used to support the sensor, as shown in Figure 3.33. First, it was screen-printed a 1 cm diameter circular shape on the substrate with silver ink to create the bottom electrode, along a 2 cm straight line for the terminals. The imprint was annealed in the oven for 60 min at 80 °C. Afterwards, the P(VDF-TrFE-CFE) film was overlaid on the PET substrate on top of the cured electrode and adhered by hot pressing for 15 min at 100°C. The top electrode was also screen-printed, and again the whole device was put in the oven for 60 min at 80 °C to cure and sinter the top electrode. The whole sensor was 127 um thick: 100 um for the PET film, 20 um for the dielectric, and 7 um for the electrodes (3.5 um each).
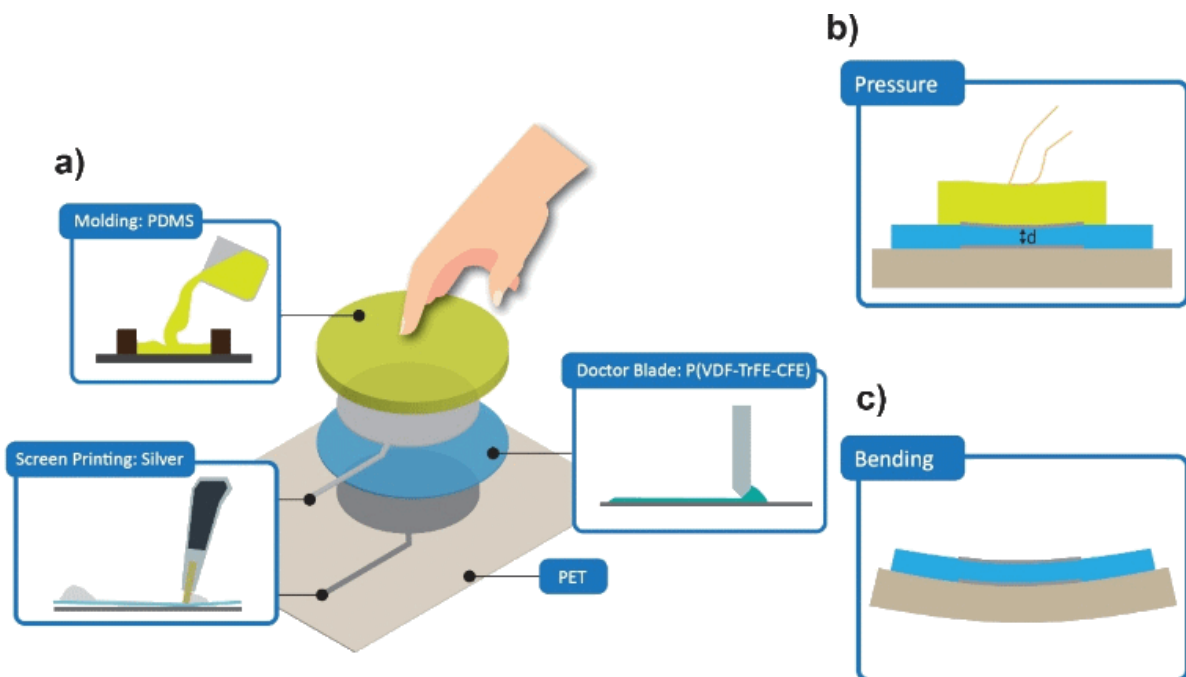
Figure 3.33. P(VDF-TrFE-CFE) dielectric deformable capacitive sensor: a) screen printed silver electrodes, doctor blade coated P(VDF-TrFE-CFE) and molded PDMS cap; b) pressure sensor operation, and c) bending sensor operation.
Reprinted from *Polymer*, vol. *214*, (Pereira et al., 2021), copyright © 2020 Elsevier Ltd. All rights reserved.

Bending sensor was covered with a protective piece of ordinary adhesive PET tape to prevent oxidation. But for the pressure sensor it was fabricated a 2 mm-thick elastic cap in PDMS through molding

process, using a 3D-printed polylactic acid (PLA) mold made by fused filament fabrication (FFF). This elastic cap creates the sensation of a press button to the user, while protecting the device from scratches.

The terminals were printed parallel to each other, facilitating the application of a conductive *z*-axis tape (3M 9703) and a 1 mm-pitch flexible flat cable (FFC).

Contrarily to the two previous presented prototypes, this sensor does not rely on the fringing effect happening between the electrodes and human fingers. Instead, it takes into account the variation of the thickness of the dielectric (Figure 3.33*b*) and the alteration of the overlapping area between electrodes (Figure 3.33*c*), according to Equation (3.1).

3.3.3.3. <u>Electric circuit</u>

The implemented circuit to read this type of sensors was very simple, similar to as implemented in the first prototype (section 3.3.1). The instrumentation is done by the digital interface of the microcontroller (µC), recurring to a resistor in series with the capacitive sensor, as shown in Figure 3.34*a*. A high-value resistor (1 MΩ) limits the rate at which the capacitor charges. The principle of operation is that the time the sensor takes to charge up depends on its capacitance. The sequence of execution of the microcontroller is shown in the flowchart of Figure 3.34*b*. Instead of sending every single sample acquired, an overall addition of each 50 measurements was made to stabilize the signal and reduce noise. The value returned by the variable `Count` is proportional to the capacitance measured, in arbitrary units. Since this system sets a counter in the microcontroller in pooling mode, the produced `Count` value will also change with the clock speed of the microcontroller.

The used microcontroller was a Microchip ATmega328P running at 12 MHz, powered at 5 V level. To broadcast the measurements of the sensor, the microcontroller was connected to a Bluetooth module (HC-06) via UART. The Bluetooth module was also supplied with 5 V, but its UART interface operated in the 3.3 V logic, thus, a voltage divider made of a 10 kΩ and a 20 kΩ resistors was placed on the receive data (RXD) of the Bluetooth module to convert the 5 V signal into 3.3 V. The opposite was not necessary because the microcontroller is tolerant to 3.3 V logic. The baud rate of the communication was set to 9600 bps.

(a) (b)
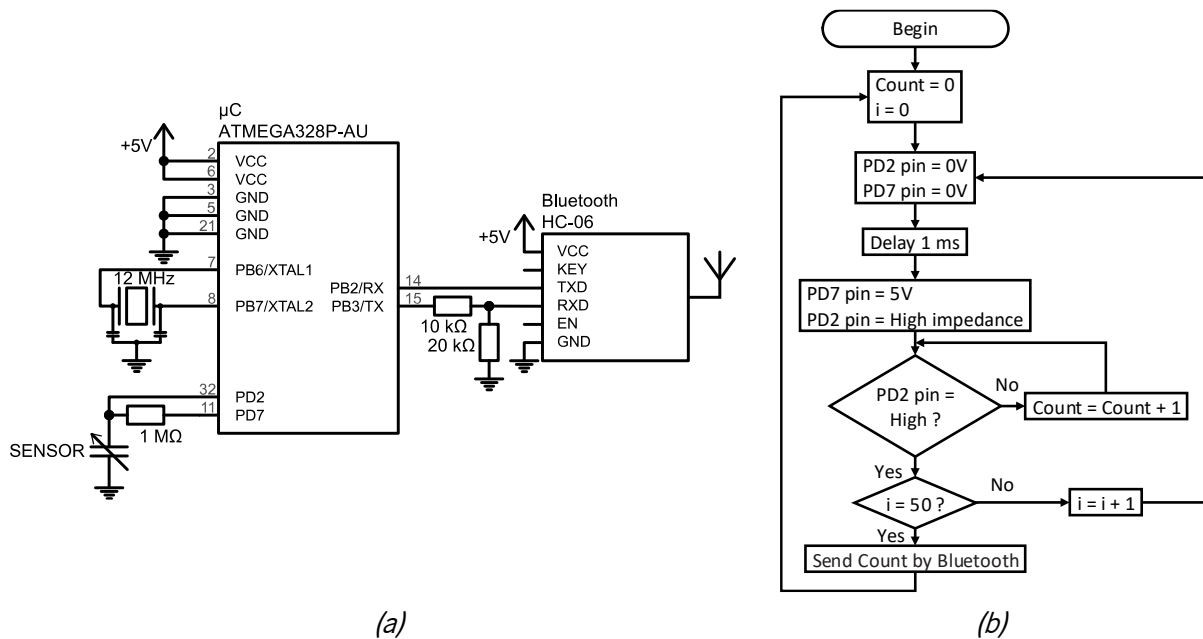
Figure 3.34. *(a)* **Readout circuit for the capacitive sensor with a microcontroller and a Bluetooth module;** *(b)* **flowchart of the execution of the microcontroller.**
Reprinted from *Polymer*, vol. *214*, (Pereira et al., 2021), copyright © 2020 Elsevier Ltd. All rights reserved.

3.3.3.4. <u>Results and discussion</u>

Since the system makes the data available through Bluetooth, a smartphone was connected to plot the response of the sensors, using an application developed in Qt 5. The sensors were tested manually by a user executing pressure and bending operations, as shown in Figure 3.35*a* and *b*, respectively. The plots of the capacitance of the sensors for pressure and bending are shown in Figure 3.35*c* and *d*, respectively.

The amplitude transmitted by Bluetooth has arbitrary units, as visible in the scale on the screen of the smartphone. To convert that arbitrary amplitude to the capacitance shown in the plots, the sensor was replaced by an ordinary fixed-value capacitor, and the received constant value by Bluetooth was noted down to serve as the conversion factor.

When the sensor is pressed, the elastic dielectric layer is compressed and the electrodes are brought closer together, therefore the capacitance drops. When bending, the same happens, but due to a compressive force on the PET film and a tensile force on the elastomer. This cannot squeeze the dielectric as much as pressing, thus it is expected a smaller change in the capacitance. Also, during normal operation of the bending sensor, that difference of compressive and tensile forces causes the elastomer to become slightly longer than the substrate, which facilitates the separation between them. In practical

terms, the capacitance shows a descendent tendency in first few bending operations, as seen in Figure 3.35*d*.
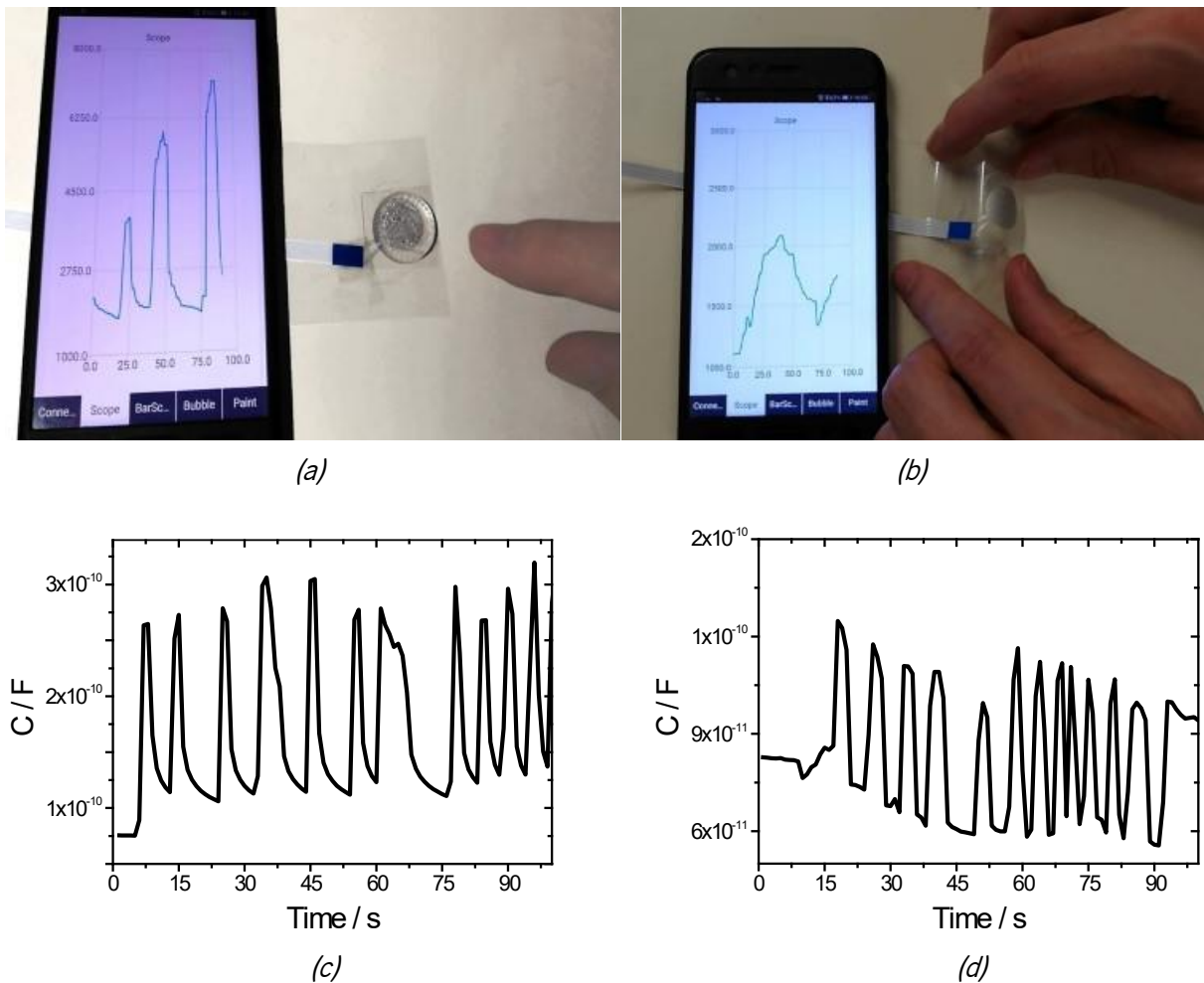
Figure 3.35. **Demonstration of *(a)* the pressure sensor and *(b)* the bending sensor. Data acquired during user manipulation of *(c)* the pressure sensor and *(d)* the bending sensor.** Reprinted from *Polymer*, vol. *214*, (Pereira et al., 2021), copyright © 2020 Elsevier Ltd. All rights reserved.

The theoretical value of the capacitance of the sensors, calculated through Equation (3.1), is ≈ 1.4 nF, but the real measured capacitance with the sensors at rest is somewhere between 60 to 100 pF, which is explained by the loss of adherence of the dielectric to the substrate and the existence of tiny air bubbles stuck in between the bottom electrode and the dielectric, particularly due to the rough finish of the silver ink's surface. However, when pressed, the sensors can get up to 500 pF or more, which is more than a third of the theoretical value. When heavily and quickly pressed by the user, the pressure sensor shows a little delay to recover, which is linked to the dielectric remaining bit more adhered to the substrate than usual.

The pressure sensor was submitted quantitative and cyclic tests with testing equipment (autograph universal testing machine Shimadzu AG-IS, and multimeter Agilent 34401A), and in Figure 3.36a and b are shown obtained curves for linearity and repeatability, respectively. The force applied in the sensor F (N) is distributed all over the area of the sensor.

(a)   *(b)*
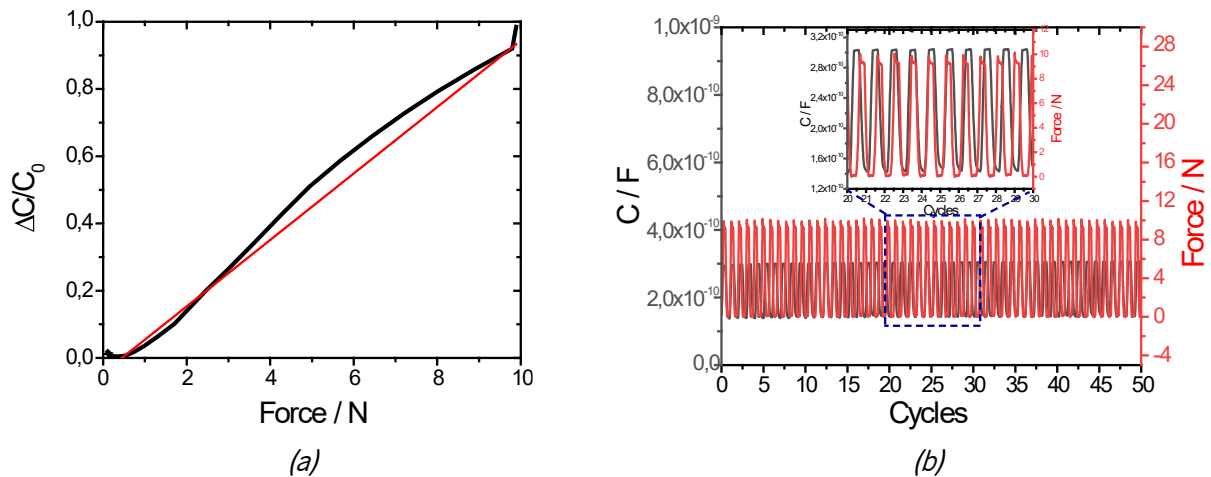
Figure 3.36. **Performance of the pressure sensor:** *(a)* **linearity and repeatability over 50 cycles.** Reprinted from *Polymer*, vol. *214*, (Pereira et al., 2021), copyright © 2020 Elsevier Ltd. All rights reserved.

The rate of change of the capacitance over its initial value $\Delta C/C_0$ fits a linear curve with the increase of the applied force F (N), and the sensor shows a sensitivity of 0.03/kPa. For the testing conditions, the sensor showed no memory effect. The developed pressure sensor does not require stretching prior to use, unlike some piezoresistive sensors (Pedro Costa, Gonçalves, et al., 2019; Pruvost et al., 2019). Further, the sensitivity of the developed pressure sensors is better than other PDMS composites with a thin PET isolating layer (Pruvost et al., 2019) or electrospun PVDF nanofiber membrane with CNTs (X. Yang et al., 2019).

The developed sensors can be processed from solution melt and printing techniques, and taking into account the excellent response potential of this technology, a proof-of-concept matrix was also fabricated using the same methodology as the pressure and bending sensors developed, shown in Figure 3.37.

It produced very similar results to the pressure sensor when reading individual points, with the difference that the electrodes were smaller, and, in order to the keep the same time constant, the series resistor was changed to 10 MΩ.
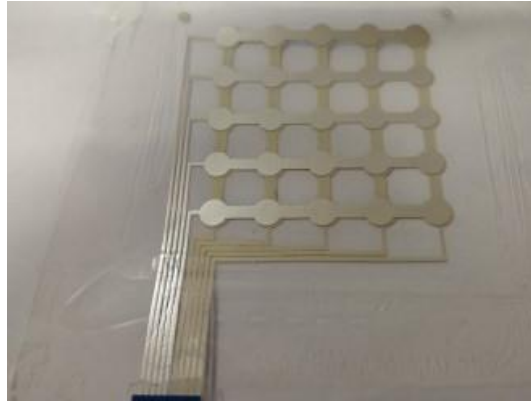
Figure 3.37.   Proof of the concept matrix with elastomer P(VDF-TrFE-CFE) dielectric.

3.3.3.5. <u>Conclusions</u>

Pressure and bending sensors were prepared based on deformable dielectric using P(VDF-TrFE-CFE) terpolymer. The polymer film material was prepared by solvent casting, and the fabrication of the sensors was supported on a PET substrate, recurring to printing techniques. The electronic circuit designed to acquire the sensors were just a high-value resistor in series with the sensor, and connected to the digital pins of a microcontroller. Readout values from the sensors were broadcast via Bluetooth and plotted in a smartphone. The sensors presented excellent performance in terms of linearity and repeatability, and due to that factor, a matrix was also manufactured, envisioning future applications. This prototype enables the implementation of TUIs with proportional pressure sensing buttons.

4. PIEZOELECTRIC FILMS

Piezoelectric materials are a class of materials that shows an electrical charge displacement when the material is deformed, resulting in the appearing of a voltage and/or current (Callister & Rethwisch, 2010, sec. 18.25). It is a reversible process, meaning that a piezoelectric material when subjected to an electric stimuli will also deform itself (T.-B. Xu, 2016).

This electrical property is interesting for the development of sensors, actuators (Dias et al., 2015) and energy harvesters (S. Li & Lipson, 2009; Nunes-Pereira et al., 2018). Some applications range from touchscreens (Reis et al., 2010), microphones (Ramadan et al., 2014), loudspeakers (C. S. Lee et al., 2003; Street et al., 2020; Sugimoto et al., 2009), bending and vibration sensors (Rendl et al., 2016, 2014), strain sensors (T. Wu et al., 2020), IR sensors (Scheipl et al., 2009), etc.

The brothers Pierre Curie and Jacques Currie first discovered piezoelectricity in 1880 when experimenting with some natural minerals, namely tourmaline, topaz, sphalerite, quartz, calamine and boracite (Pedro Costa, Nunes-Pereira, et al., 2019; Curie & Curie, 1880), and also Rochelle salt (Andrusyk, 2011; Kao, 2004, sec. 4.1). During the World War II, in 1941, barium titanate (BaTiO3) was developed, the first non-natural piezoelectric material, and in 1952 lead titanate zirconate (PZT) was engineered (Jaffe & Berlincourt, 1965). Figure 4.1 shows some PZT discs still at use nowadays. Applications for PZT range from vibration, pressure or acceleration sensors, to acoustic and ultrasonic transducers, ignition sparkers and gas lighters, actuators for lenses and mirror positioning systems (King et al., 1990), and printing heads (Ricoh Europe PLC, 2016), among others.
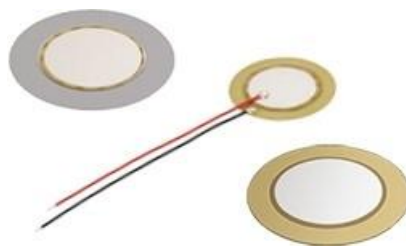
Figure 4.1.   Some PZT piezoelectric diaphragms for acoustic transducers.

Piezoelectricity was also reported in polymers, such as poly(vinyl chloride) (PVC), and poly(methyl methacrylate) (PMMA) (Greaves & Lamb, 1971), but in 1969, a new piezoelectric material was discovered by Heiji Kawai named polyvinylidene fluoride (PVDF), which presented a piezoelectric coefficient about ten times higher than the other polymers, and with important properties such as good chemical stability, transparency, flexibility and physical robustness (Pedro Costa, Nunes-Pereira, et al., 2019; Fukada, 2000; Kawai, 1969). In Figure 4.2 is shown the aspect of a piezoelectric PVDF polymer film.
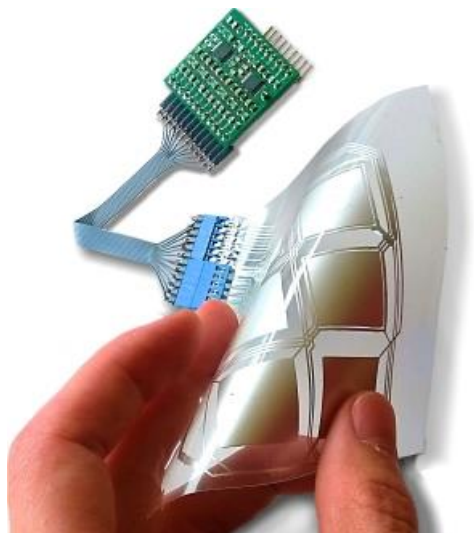
Figure 4.2.   A piezoelectric PVDF polymer film with six silver ink printed electrodes.

Since then, piezoelectric polymers were a target of large research to enhance their properties and piezoelectric response, from which copolymers and terpolymers of PVDF were developed, with particular emphasis to poly(vinylidene fluoride trifluoroethylene) (P(VDF-TrFE)) that appeared in the late 1970's, among others (Higashihata et al., 1981; Yagi et al., 1984; Yagi & Tatemoto, 1979). Nowadays, both the homopolymer PVDF and the copolymer P(VDF-TrFE) have been broadly used for applications, ranging from sensors (Katsuura et al., 2017; Rendl et al., 2016, 2014), to actuators (Dias et al., 2016; Frecker & Aguilera, 2003), ultrasonic transducers (M. S. Martins et al., 2017), audio transducers (Reis et al., 2010; Street et al., 2020; Sugimoto et al., 2009), energy harvesters (Dutta et al., 2018; Nunes-Pereira et al., 2018; Rajeev et al., 2020), biomaterials (Ribeiro et al., 2015), and energy storing systems (C. M. Costa et al., 2019), among others (Pedro Costa, Nunes-Pereira, et al., 2019; Heywang et al., 2008, sec. 6).

This chapter is covered by the publications of the candidate (Pedro Costa, Nunes-Pereira, et al., 2019; S. Gonçalves, Pereira, et al., 2019; S. Gonçalves, Serrado-Nunes, et al., 2019b). The artwork displayed in Figure 4.3 was published as cover of the journal *American Chemical Society (ACS) Applied Electronic Materials* (S. Gonçalves, Serrado-Nunes, et al., 2019a).

Figure 4.3. Artwork published as cover of the volume 1, issue 8 of the journal *ACS Applied Electronic Materials*[1]. Abstract image depicts a piezoelectric material and a screen-printed layout, capable of detecting the finger touch. Reproduced with permission from (S. Gonçalves, Serrado-Nunes, et al., 2019a), copyright © 2019, American Chemical Society.

---

1 Available online at: https://pubs.acs.org/toc/aaembp/1/8

4.1. ORIGIN OF PIEZOELECTRICITY IN MATERIALS

Piezoelectric materials are electrical insulators by nature. Within insulators, several subgroups exist, namely dielectrics, piezoelectrics, pyroelectrics and ferroelectrics, according to the diagram of Figure 4.4. All of these directly influence the piezoelectricity of materials (Pedro Costa, Nunes-Pereira, et al., 2019; Jiangyu Li et al., 2013). Therefore, they are going to be explained in the following.
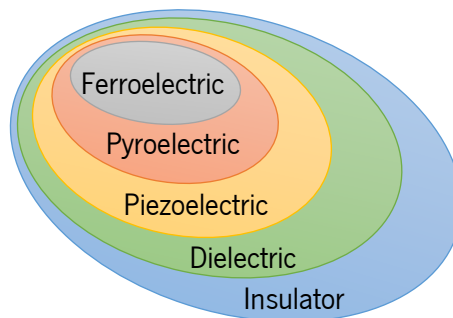
Figure 4.4.   Diagram of relationships between insulator, dielectric, piezoelectric, pyroelectric and ferroelectric materials.

4.1.1. Dielectrics

Dielectric materials are not ordinary insulators. They suffer polarization when subjected to an electric field. This is a consequence of the presence of electric dipoles in the material (Callister & Rethwisch, 2010, sec. 2.7). As an example, the uneven shape of a water molecule makes it highly polar, as shown in Figure 4.5. Thus, it can be represented as a dipole, for simplicity. Since the dipoles have freedom of movements, they become aligned to an external electric field E, as demonstrated in Figure 4.6, resulting in an increase of the dielectric permittivity εr. Many dielectrics lose polarization when the external electric field is removed. Yet, some retain part of it – they are ferroelectric materials, explained in section 4.1.4.
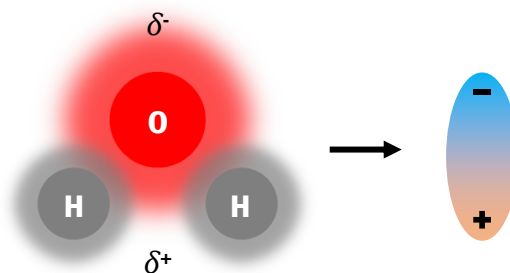
Figure 4.5.   Schematic representation of a polar molecule: *(a)* charges in a water molecule; *(b)* simplified representation of a dipole.
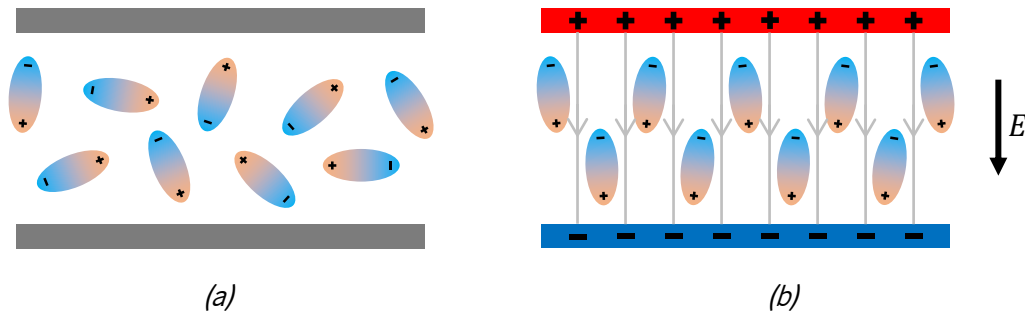
Figure 4.6. Representation of the dipoles of a dielectric material: *(a)* in the absence of an electric field, the dipoles are randomly aligned to the minimum energy state, but when an electric field E crosses through the dielectric material (*b),* the dipoles will tend to get aligned with that electric field.

Dielectric materials are very usefull on the manufactoring of capacitors because they easily propagate the electrid field through it, allowing capacitors to have higher capacities and/or smaller size (Y Wang et al., 2010). The capacitance of a capacitor can be calculated by any of the Equations (3.1) or (3.2). Table 4.1 shows a list of some dielectric polymers, together with their main functional characteristics.

Table 4.1. Comparison of the properties of some dielectric polymers. Reprinted from (Y Wang et al., 2010), copyright © 2010, IEEE.

Material	Dielectric constant εr	Maximum temperature T_{MAX} (°C)	Breakdown strength E_{BR} (MV/m)	Energy density η (J/m3)
Biaxially oriented polypropylene (BOPP)	2.2	105	720	5
PET	3.3	125	570	1 – 1.5
Polycarbonate (PC)	2.8	125	528	0.5 – 1
Polyphenylene-sulfide (PPS)	3	200	550	1 – 1.5
Polyimide (PI)	3.4	250	300	1 – 1.5
PVDF	12	125	590	2.4
P(VDF-CTFE)	13	125	620	25
P(VDF-HFP)	15	125	700	25
P(VDF-TrFE-CFE)	52	125	400	10
Aromatic polyurea	4.2	200	800	12

4.1.2. Piezoelectrics

The piezoelectric effect is the capacity of certain dielectric materials to generate an electric field E (V/m) upon the application of an external deforming force F (N). The physical rearrangement of the dipoles inside the material causes the electric charges to migrate inside the material, and, if the material is polarized, some charge differential Q (C) builds up at the surface of the material, as exemplified in Figure 4.7 (Callister & Rethwisch, 2010, sec. 18.25; Ramadan et al., 2014; Rendl et al., 2012). Furthermore, the converse piezoelectric effect is also true: the application of an external electric field on a piezoelectric material produces a deforming force (Q. Li & Wang, 2016; Ramadan et al., 2014).
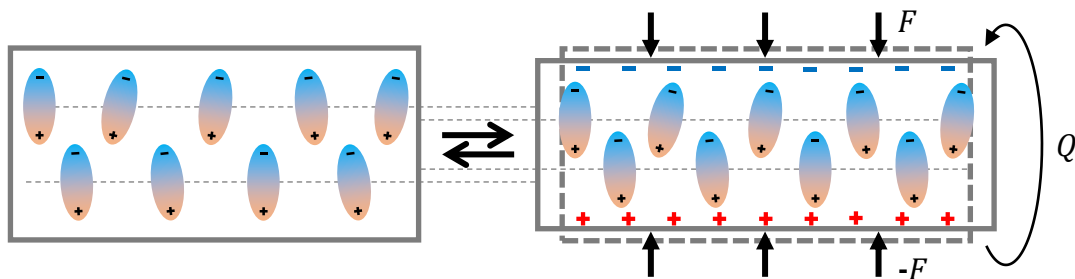
Figure 4.7. The direct and converse piezoelectric effects: exerting a force F on a poled piezoelectric material produces an electric charge variation Q, or vice-versa.

The displaced charge Q (C) on a piezoelectric material is given by:

$$Q = d_{ij} \cdot F \qquad (4.1)$$

where F (N) is the applied force on the material and dij (C/N) is the piezoelectric constant of the material. The i subscript indicates the direction in which the charge builds up, and j subscript the direction of the applied force, according to the convention shown in Figure 4.8 (Mishra et al., 2019; T.-B. Xu, 2016; Zhu, 2010). In this notation, the z-axis is always made coincident with the direction of positive polarization of the material.

Through the application of electrodes on the surface of a piezoelectric material it is possible to extract the accumulated charge in the surface. The voltage generated on the electrodes of a piezoelectric material can be calculated using Equation (3.2) or (4.1).
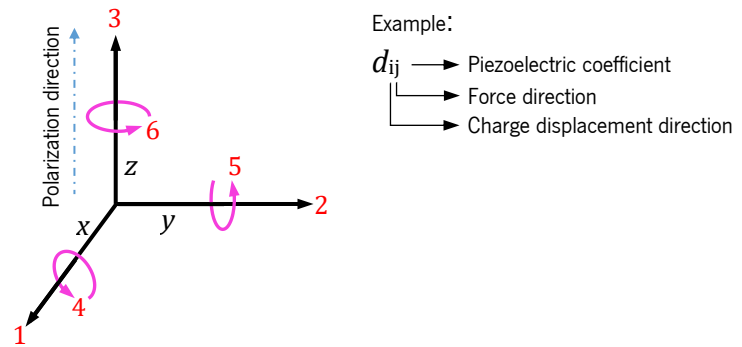
Figure 4.8.   Correspondence between axis and directions for piezoelectric elements.
Reprinted from *Structural Health Monitoring (SHM) in Aerospace Structures*, (T.-B. Xu, 2016), "7 - Energy harvesting using piezoelectric materials in aerospace structures", pp. 175-212, copyright © 2016, with permission from Elsevier.

The electromechanical coupling factor kij is an indicator in piezoelectric materials that specifies the efficiency of the mechanical-to-electrical transformation, or vice-versa (Pedro Costa, Nunes-Pereira, et al., 2019). Piezoelectric polymers present lower piezoelectric coefficient than some piezoelectric ceramic materials, and also lower stability for higher temperatures, but a whole bunch of other properties give piezoelectric polymers great advantage, such as flexibility, transparency, stretchability, softness and light weight (Pedro Costa, Nunes-Pereira, et al., 2019).

Table 4.2 lists some piezoelectric ceramics and their properties, and Table 4.3 some polymers. Most piezoelectric polymers only present a d_{31} piezoelectric coefficient, which limits the type of applications to 3D. However, PVDF and PVDF copolymers stand out from the remaining piezoelectric polymers for exhibiting higher piezoelectric coefficient, and in the d_{33}, as observable in Table 4.4.

Table 4.2.   Properties of some piezoelectric ceramics (C) and single crystals (SC) (Pedro Costa, Nunes-Pereira, et al., 2019; Jaffe & Berlincourt, 1965).

Material	Piezoelectric coefficient		Electromechanical coupling factor k_{33}	Dielectric constant εr
	d_{31} (pC/N)	d_{33} (pC/N)		
BaTiO3 (C)	-115	483	0.5	3000
PZT (C)	-274	590	0.75	1000
PMN-PT (SC)	-100	2000	0.9 - 0.94	5000
PZN-PT (SC)	-1400	1400	0.92 - 0.94	6800

Table 4.3.   Properties of some piezoelectric polymers. Reprinted with permission from (Pedro Costa, Nunes-Pereira, et al., 2019), copyright © 2019 WILEY-VCH Verlag GmbH & Co. KGaA, Weinheim.

Material	Piezoelectric coefficient d_{31} (pC/N)	Electromechanical coupling factor k_{31}	Dielectric constant εr
Polyurea	< 10	–	≈ 4
Nylon-7	17	0.054	–
Nylon-11	14	0.049	–
PAN	2	0.01	38
PVDCN/VAc	10	0.05	3
PPEN	–	–	5
PVC	0.5 - 5	0.001	10
PVAc	–	–	6.5
PI	< 5	–	4

Table 4.4.   Piezoelectric properties of polymers from the PVDF family (Pedro Costa, Nunes-Pereira, et al., 2019; P. Martins et al., 2014).

Material	Piezoelectric coefficient		Electromechanical coupling factor k_{33}	Dielectric constant εr
	d_{31} (pC/N)	d_{33} (pC/N)		
PVDF	8 – 12	-24 – -34	0.2	6 – 12
P(VDF-TrFE)	12	-38	0.37	18
P(VDF-CTFE)	–	-140	0.39	13
P(VDF-HFP)	30	-24	0.36	5.6
P(VDF-TrFE-CTFE)	–	–	0.28	80

Additionally, Fulay and Lee (2016) make an extensive list of piezoelectric materials and their properties.

4.1.3. Pyroelectrics

Pyroelectricity is the ability of some piezoelectric materials of suffering an electric charge variation when the temperature of the material changes over time (Pedro Costa, Nunes-Pereira, et al., 2019).

The second law of thermodynamics limits the theoretical maximum of thermal energy that can be converted to work, through the Carnot efficiency η_{Carnot}:

$$\eta_{\text{Carnot}} = 1 - \frac{T_{\text{H}}}{T_{\text{C}}} \tag{4.2}$$

where T_{H} and T_{C} (K) are the temperature of the hot and cold states, respectively (Pedro Costa, Nunes-Pereira, et al., 2019). However, the pyroelectric energy conversion is very ineffective due to the energy necessary to actually heat the material. So, the real efficiency η is given by:

$$\eta = \frac{\pi}{4} k^2 \eta_{\text{Carnot}} \tag{4.3}$$

where $k2$ is the thermoelectric coupling factor (Q. Li & Wang, 2016).

The pyroelectric coefficient p (C/m2/K) relates the generated electric charge Q (C) with the temperature variation by:

$$Q = pA(T_{\text{f}} - T_{\text{i}}) \tag{4.4}$$

in which A (m2) is the area of the overlapping electrodes, and T_{i} and T_{f} (K) are the initial and final temperatures of the pyroelectric material, respectively (Bowen et al., 2014).

Table 4.5 shows some pyroelectric materials and their properties, and Bowen et al. (2014) present a more detailed list of pyroelectric materials.

Table 4.5.   Some pyroelectric materials and their properties (Bowen et al., 2014).

Material	Pyroelectric coefficient p (µC/m2/K)	Thermoelectric coupling factor $k2$
PVDF	-27	0.001194
P(VDF-TrFE) 50/50	-40	0.001310
P(VDF-TrFE) 80/20	-31	0.002023
PZT	-380	0.006752
BaTiO3	-200	0.000452

4.1.4. Ferroelectrics

Ferroelectricity is the capability of some materials to retain polarization in the absence of an external electric field, which can be reversed through the application of an opposed external electric field (Callister & Rethwisch, 2010, sec. 18.24; Fulay & Lee, 2016, sec. 10.1). This is caused by the lack of mobility for of the dipoles (Fulay & Lee, 2016, sec. 10.1.1).

For better understanding, let us take the example of barium titanate (BaTiO3), which structure is shown in Figure 4.9. Due to the attractive and repulsive forces between ions, the titanium ion (Ti^{4+}) cannot assume a center position in the unit cell (Callister & Rethwisch, 2010, sec. 18.24; Fulay & Lee, 2016, sec. 10.1.1). Therefore, each unit cell must adopt one of the six possible configurations from Figure 4.10, resulting in the corresponding polarization P.
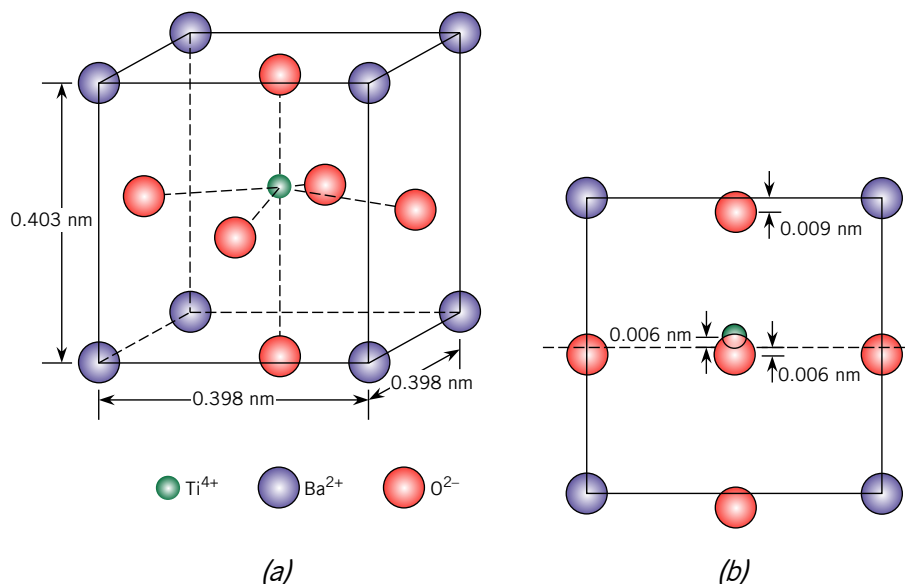
Figure 4.9.   A BaTiO3 unit cell: *(a)* isometric projection, *(b)* front view. The structure is not symmetrical due to the Ti^{4+} and O^{2-} ions. Republished with permission of John Wiley & Sons – Books, from (Callister & Rethwisch, 2010), "Material science and engineering: An introduction", 8th edition, copyright © 2010, 2007, 2003, 2000 John Wiley & Sons, Inc.; permission conveyed through Copyright Clearance Center, Inc.

However, when a ferroelectric material is heated above the Curie temperature Tc, mobility of dipoles is reestablished, and it becomes centrosymmetric and nonpolar (Fulay & Lee, 2016, sec. 10.1.1). Table 4.6 presents the Curie temperature of some ferroelectric materials.
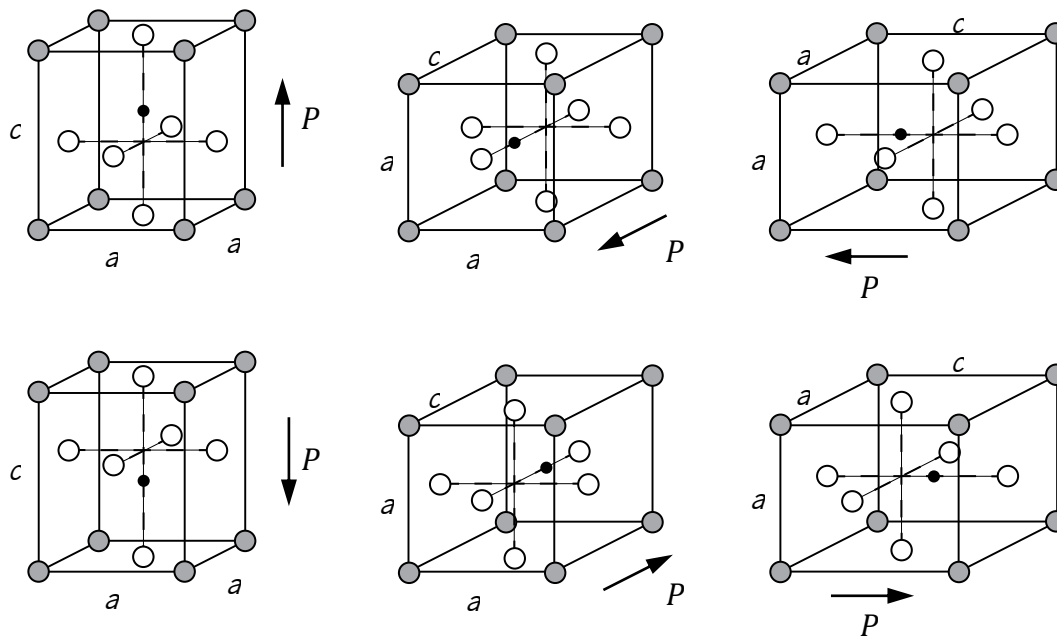
Figure 4.10. Six different structures for BaTiO3, resulting in six spontaneous polarizations _P_. Reprinted from _Journal of the Mechanics and Physics of Solids_, vol. _55_(10), (Mehling et al., 2007), "Phenomenological model for the macroscopical material behavior of ferroelectric ceramics", pp. 2106–2141, copyright © 2007 Elsevier Ltd., with permission from Elsevier.

Below the Curie temperature Tc, the interaction between adjacent unit cells propitiates the emergence of domains, where groups of dipoles become mutually aligned. This is called spontaneous polarization (Callister & Rethwisch, 2010, sec. 18.24). In Figure 4.11 it is visible the electric domains in a BaTiO3 micrography.

Table 4.6.   Comparison of the main properties of some ferroelectric materials. Adapted from "Handbook of active materials for medical devices: Advances and applications", (Lantada, 2012), copyright © 2012 by Taylor & Francis Group, LLC, reproduced with permission of Taylor and Francis Group LLC (Books) US through PLSclear.

Material	Density (g/cm³)	Curie temperature Tc (°C)	Type
Silica (SiO2)	2.7	570	Ceramic
Lithium Niobate (LiNbO3)	4.6	1200	Ceramic
BaTiO3	5.7	140	Ceramic
PZT	7.4	300	Ceramic
PVDF	1.8	80 – 100	Polymer
P(VDF-TrFE)	1.8	100 – 160	Polymer
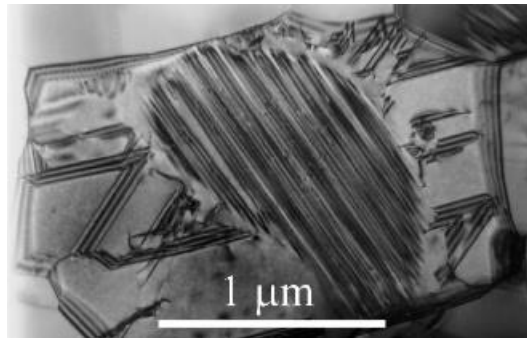
Figure 4.11. Ferroelectric domains in a BaTiO3 micrograph by transmission electron microscopy (TEM). Reproduced from DoITPoMS, University of Cambridge, "Full Record for Micrograph 199" [1], Prof. W. E. Lee, copyright © 2002 University of Cambridge, under Creative Commons BY-NC-SA 2.0 UK license (https://creativecommons.org/licenses/by-nc-sa/2.0/uk/).

Domains often cancel each other's out, but through a poling process it is possible to induce polarization at a macroscopic level.

4.1.4.1. <u>Poling of ferroelectric materials</u>

Unpoled materials have a domain structure that resembles Figure 4.12*a*. By the application of an external direct current (DC) electric field E, domains will suffer fusion and reorientation (Hartono et al., 2016; Kamel & de With, 2008), as shown in Figure 4.12*b*. For certain high electric fields, below the breakdown strength, it is even possible to obtain a single domain, as represented in Figure 4.12*c* (Fulay & Lee, 2016, sec. 10.1.2). When the external electric field is removed, ferroelectric materials retain part of their domains and respective polarization, as in Figure 4.12*d*. This is called reminiscing polarization (Hartono et al., 2016).

The poling cycle can be described in a hysteresis graph that plots the polarization of the material P (C/m2) as function of the external electric field E (V/m), as shown in Figure 4.13 (Chen et al., 2010).

There are several techniques for poling ferroelectric materials, such as contact poling (Marshall et al., 2008), corona poling, (Marshall et al., 2008), corona poling with stretching (Kaura et al., 1991), surface poling (Ting et al., 2013), simultaneous stretching and static electric poling (SSSEP) (Huan et al., 2007), electric poling-assisted additive manufacturing (EPAM) (C. Lee & Tarbutton, 2014), liquid contact poling (Tang et al., 1997), among others. The apparatus of contact and corona poling are shown in Figure 4.14, which are two of the most commonly used techniques for polymers.

---

1 Downloaded from: https://www.doitpoms.ac.uk/miclib/full_record.php?id=199
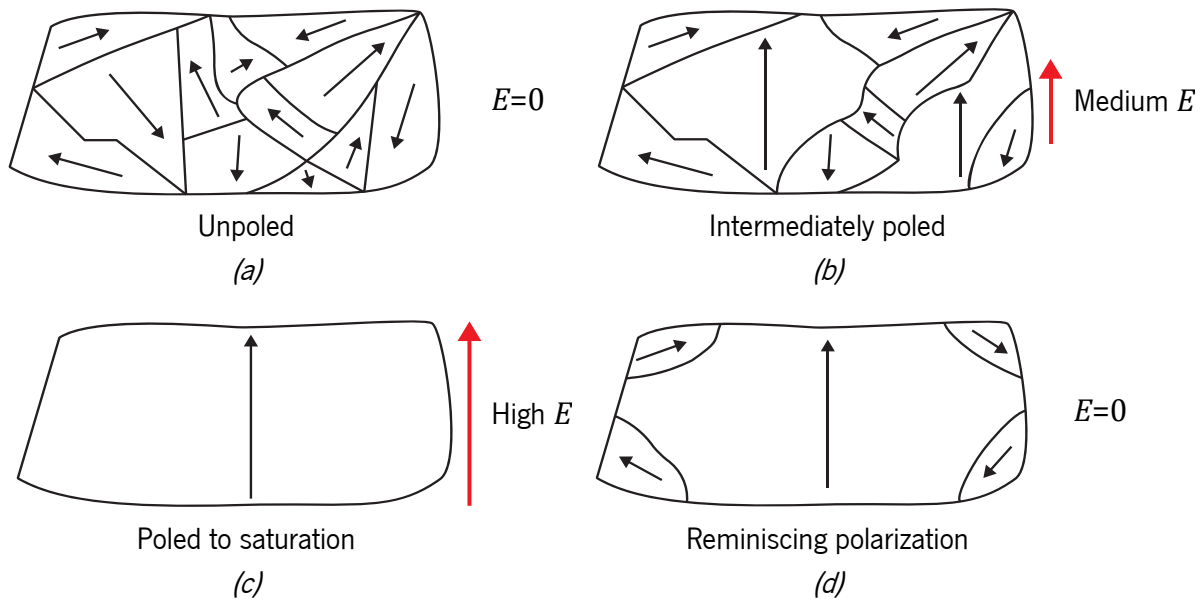
Figure 4.12. **Representation of the domains and their polarities in a ferroelectric material:** *(a)* **unpoled material at rest,** *(b)* **external electric field causes partial polarization of the material,** *(c)* **saturation,** *(d)* **reminiscing polarization after external electric field has been removed.**
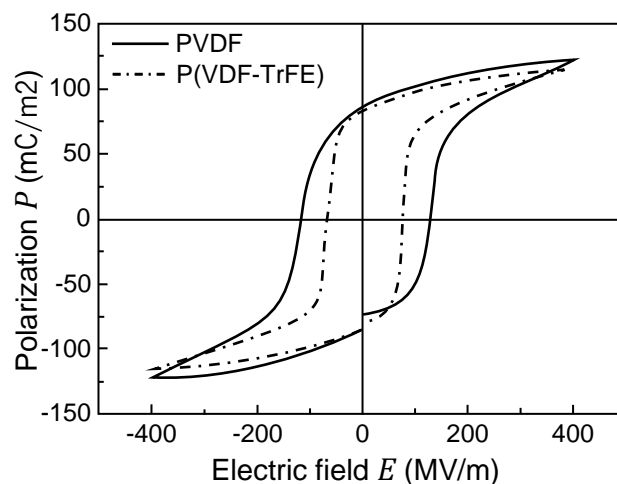
Figure 4.13. **Typical *P-E* hysteresis loop for PVDF and P(VDF-TrFE).** Reprinted from (Chen et al., 2010), *Journal of Applied Polymer Science*, vol. *116*(6), copyright © 2010 Wiley Periodicals, Inc. with permission from John Wiley and Sons.

In contact poling, electrodes are placed in the material, either by direct contact, conductive ink printing, or using a conductive liquid. Then, a high DC voltage differential is applied between the electrodes to polarize the material (Marshall et al., 2008; Tang et al., 1997). Vacuum or an insulating fluid are often used to prevent electric arc (Ramadan et al., 2014).
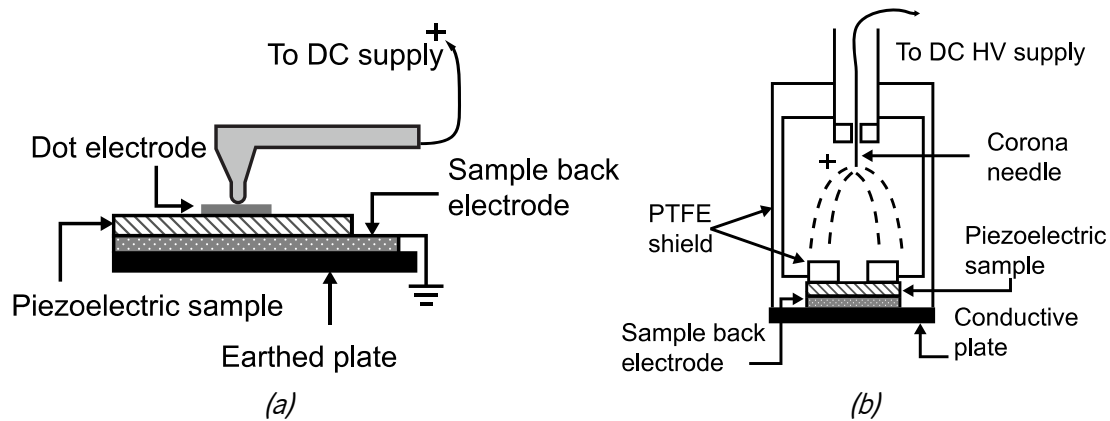
Figure 4.14.   Apparatus for poling of ferroelectric polymer materials: *(a)* contact poling and *(b)* corona poling. Reprinted from *Thin Solid Films*, vol. *516*(15), (Marshall et al., 2008), "Corona poling of highly (001)/(100)-oriented lead zirconate titanate thin films", pp. 4679-4684, copyright © 2007 Elsevier B.V., with permission from Elsevier.

Corona poling, on the other hand, comprises a corona discharge which ionizes the air particles and deposits electric charges directly on the surface of the material (Marshall et al., 2008; R. S. Martins et al., 2014). It is necessary to heat the air to enable the corona discharge, which also increases dipole mobility (Ramadan et al., 2014).

Either way, the created electric field must be higher than the coercive field of the material, which usually is in the range of 50 to 120 MV/m for PVDF and about 100 MV/m for P(VDF-TrFE) at room temperature, but it gets lower when the material is heated (R. S. Martins et al., 2014; Tsutsumi et al., 2005).

The existence of non-polar phases in PVDF also determines whether it is polarizable or not. PVDF crystalizes into the non-polar α-phase, but it must be stretched first to induce phase transformation to the polar β-phase (Arrigoni et al., 2020). Surprisingly, P(VDF-TrFE) directly crystallizes into a polar phase, and no non-polar phases of P(VDF-TrFE) have been reported (Arrigoni et al., 2020).

A method for simultaneous stretching and static electric poling (SSSEP) of PVDF has been reported (Huan et al., 2007; Kaura et al., 1991), and, based on a 3D fused filament fabrication (FFF) printer, it has also been developed electric poling-assisted additive manufacturing (EPAM), as visible in Figure 4.15 (C. Lee & Tarbutton, 2014; Tarbuttona et al., 2017). Unpoled α-phase PVDF is fed to the nozzle, but the high electric field applied while extruding, crystalizing and stretching results in a mostly poled β-phase printed PVDF (Hartono et al., 2016; Tarbuttona et al., 2017).

To simplify manufacturing process of poling, Ting et al. (2013) reported surface poling, involving only single-layer electrodes using an interdigitated pattern, as shown in Figure 4.16, for applications such as bending sensors. However, the polarization is weaker.
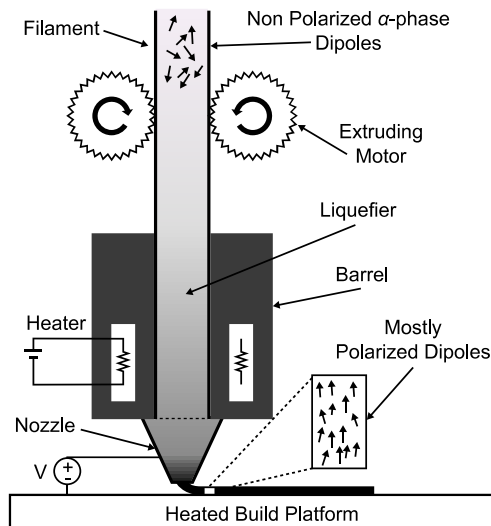
Figure 4.15. 3D-printing PVDF using an FFF printer with EPAM technique: the filament feed is unpoled PVDF in the α-phase, but the printed filament is mostly β-phase poled PVDF. Reprinted from *Procedia Manufacturing*, vol. *10*, (Tarbuttona et al., 2017), copyright © 2017 The Authors, Published by Elsevier B.V., under Creative Commons BY-NC-ND 4.0 license (https://creativecommons.org/licenses/by-nc-nd/4.0).
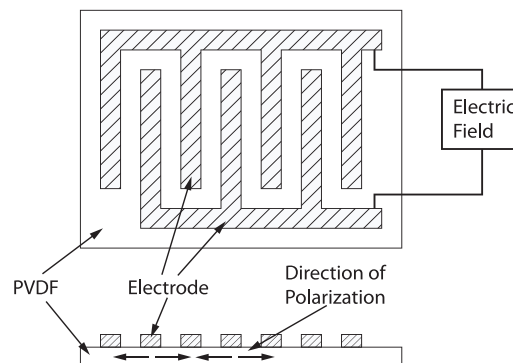
Figure 4.16. Surface poling using interdigitated pattern electrodes. Reprinted from (Ting et al., 2013), copyright © Taylor & Francis Group, LLC.

4.2. APPLICATIONS BASED ON PIEZOELECTRIC POLYMER FILMS

Only a handful of polymers are known to be piezoelectric, from which PVDF, PVDF copolymers and terpolymers stand out due to interesting characteristics such as flexibility, robustness, low weight, heat

resistance, etc., and, the most important, high piezoelectric coefficient (P. Martins et al., 2014). Some examples of applications range from multitouch surfaces, to energy harvesting systems, acoustic transducers or motion sensors (Ramadan et al., 2014). Nevertheless, the piezoelectric coefficient of PVDF and PVDF copolymer films can be improved by modification of the composite for specific target applications, as is for energy harvesting (L. Wu et al., 2014).

There exist several prototypes of piezoelectric polymer solutions, ranging from sensors, to actuators, energy harvesters, and there are some commercial products as well. Next there will be presented some examples of applications.

4.2.1. Sensors

More than a decade ago, Reis et al. (2010) proposed the use of piezoelectric elements in the development of touchscreens with a glass surface, using acoustic pulse recognition to determine the location of finger touch, as shown in Figure 4.17. Sensors made of PVDF film sense the vibrations of created by the fingers when touching the glass.
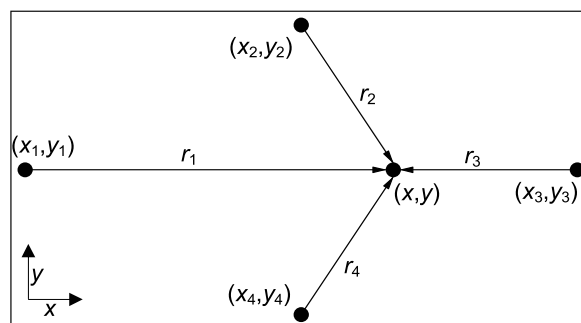
Figure 4.17. Calculation of the touch position using four piezoelectric sensors. Reprinted from (Reis et al., 2010), copyright © 2010, IEEE.

However, besides just the touch location, piezoelectric materials have been proposed to account for the force of the touch, giving the user a 3D form of interaction (S Gao et al., 2016). Figure 4.18 shows one of the proposed approaches. However, the technical challenges that such touch panels pose in terms of unstable force-voltage responsivity and in isolating the signals due to crosstalking issues have kept piezoelectric sensors away from touchscreens (Shuo Gao & Wu, 2019).
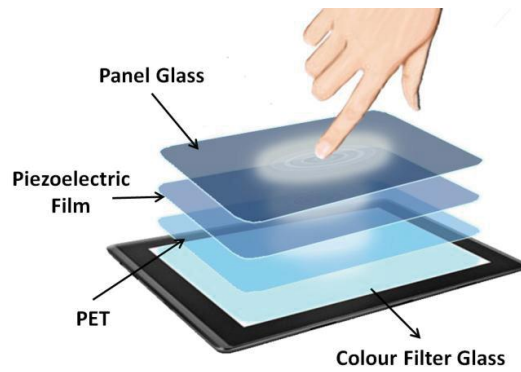
Figure 4.18. Piezoelectric-based touchscreen. Reprinted from (S Gao et al., 2016), copyright © 2016, IEEE.

In the search for new forms of interaction with digital devices, Rendl et al. (2016) fabricated a foldable display cover named FlexCase, that can used together with a smartphone, as shown in Figure 4.19.

(a)

(b)

(c)

(d)
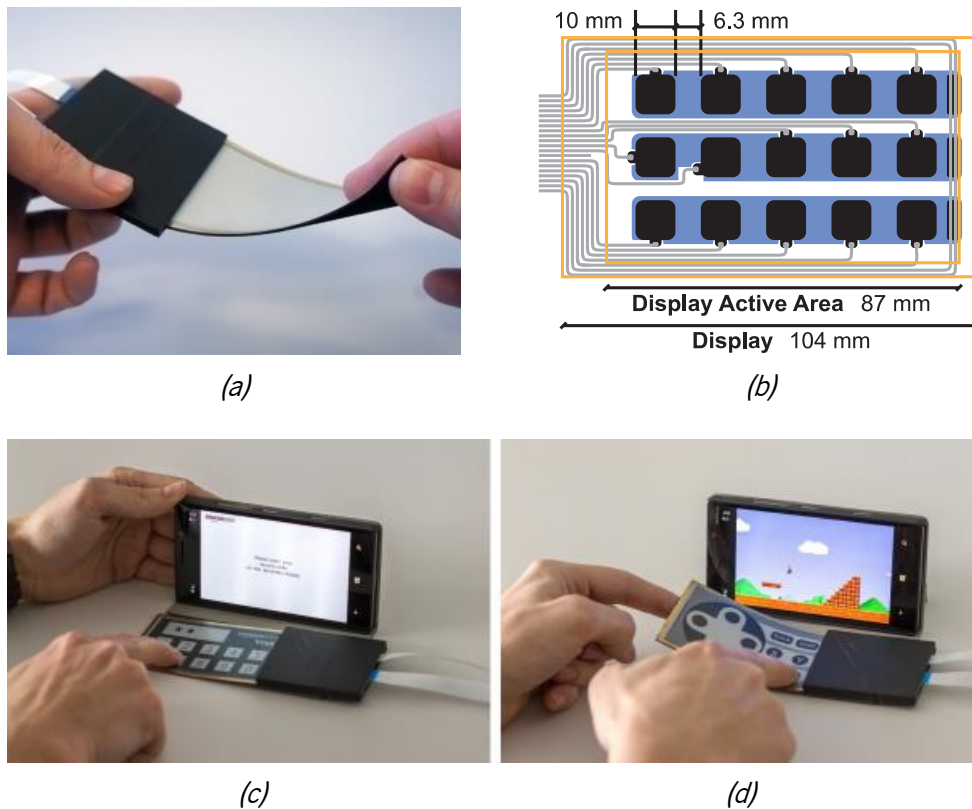
Figure 4.19. FlexCase consists in *(a)* an electrophoretic display with *(b)* a piezoelectric matrix underneath, for extended user interaction with a smartphone using *(c)* touch buttons and *(d)* bend sensing. Republished with permission of ACM (Association for Computing Machinery), from *Proceedings of the 2016 CHI Conference on Human Factors in Computing Systems*, (Rendl et al., 2016), copyright © 2016 ACM.

The system is composed by an e-paper display with a matrix of 3×5 piezoelectric polymer sensors under beneath. The display works as a dynamic keypad, updating its menu accordingly to the content

displayed in the smartphone. The piezoelectric sensors can detect individual pressure, or be used globally to determine film bending, using a film bending reconstruction algorithm. Applications include increased experience e-paper reading and interaction, 3D manipulation in applications and games, or easier copy-and-paste handling.

Piezoelectric sensors have been prepared for wearable devices, such as the pulse wave velocity (PWV) sensor designed by Katsuura et al. (2017). The device is intended for use in the human's wrist, as shown in Figure 4.20a. It is composed by a PVDF sensor array (Figure 4.20b) that can measure the blood pumping and determine its velocity based on the time that the blood pulse takes to reach each of the sensors. Since measuring the blood pressure is sensitive by nature, the authors introduced 1 mm-thick silicone pads between each piezoelectric sensor and the skin, and in the back of the sensor they created a small air cushion on the back of the piezoelectric film composite to reduce noise and improve readability.
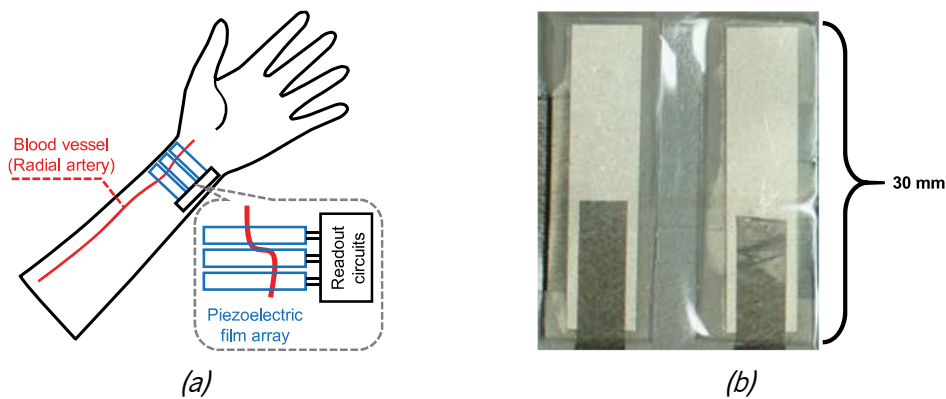
**Figure 4.20.   Wearable sensor array for pulse wave velocity (PWV) measurement:
(a) concept based on PVDF sensors, and (b) fabricated sensors.** Reprinted
from (Katsuura et al., 2017), copyright © 2017, IEEE.

Vibration sensors have been commercially available by TE Connectivity[1] using PVDF films for simple prototyping, as visible in Figure 4.21. These sensors consist in a piece of poled PVDF film with silver ink electrodes printed on its surfaces. They are flexible and can withstand high shock overload, and can be dotted with or without mass, depending on the frequency of response and sensitivity desired. These sensors are primarily used to detect continuous vibration or impacts, presenting below 1 % non-linearity, and high sensitivity.

---

1 TE Connectivity official website: https://www.te.com.

(a)   *(b)*
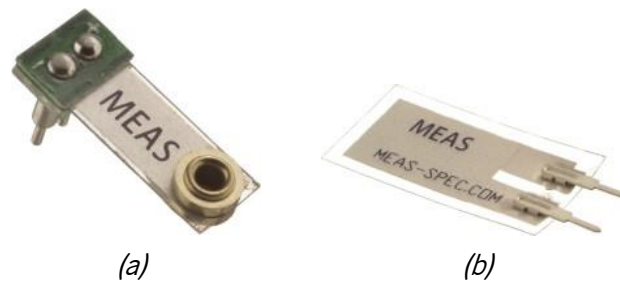
Figure 4.21. Piezoelectric film sensors from TE Connectivity for vibration sensing *(a)* with mass and *(b)* without mass.

Lu et al. (2018) created a 4 × 4 piezoelectric strain sensor array using PVDF polymer film, as shown in Figure 4.22. Aluminum was deposited on both sides of a 50 μm-thick PVDF film, which underwent photolithography and wet etching processes to create the electrodes according to a mask. The area of each electrode was 1.4 mm2. A PDMS substrate functioned as a stiff support where the prepared PVDF was placed. The matrix disposition of the electrodes was done by creating conductive traces for rows and columns, and terminal wires were connected with silver glue. A PDMS layer was applied on each side of the device as packaging, providing protection, and helping to distributing pressure homogeneously. According to the authors, all of the 16 sensors showed similar performances, with a precision of 2.9 mV/kPa, being able to reach up to 300 mV with a delay lower than 2 ms after pressure being applied, making it a ultra-fast and ultra-sensitive strain sensor.

(a)   *(b)*
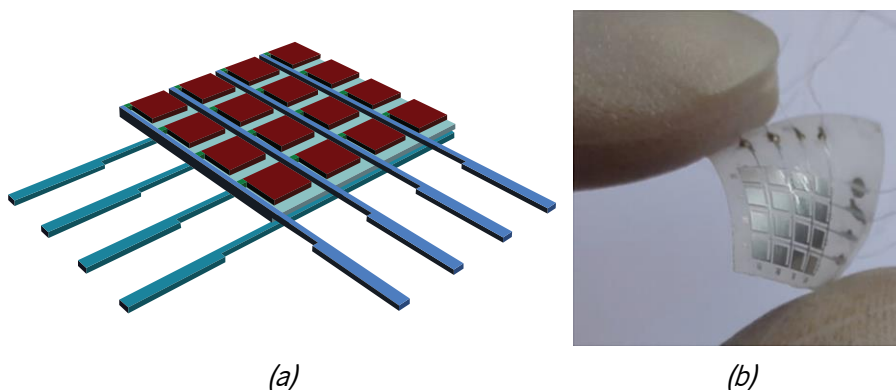
Figure 4.22. PVDF sensor array: *(a)* schematic and *(b)* implemented of the real. Reprinted from *Nanoscale Research Letters*, vol. *13*(1), "Ultra-sensitive strain sensor based on flexible poly(vinylidene fluoride) piezoelectric film", (K. Lu et al., 2018), copyright © 2018, The Authors, under Creative Commons BY 4.0 license (https://creativecommons.org/licenses/by/4.0/).

To increase output power and sensitivity, J.-H. Lee et al. (2015) designed a pyramidal micropattern on the surface of a P(VDF-TrFE) film. Without increasing the d_{33}, the authors were able to generate up to

5 times larger output when compared to flat films. To prove their achievements, the presented work mentioned the creation of self-powered pressure sensors.

Q. Li et al. (2019) applied a piezoelectric sensor on the measurement of the velocity of fluids without affecting the fluid's velocity. It consisted in a PVDF film sensor placed parallel with the flow in a pipe, as shown in Figure 4.23. The pipe had a diameter of 16 cm, and the PVDF sensor had dimensions of 14 × 10.8 cm. A simulation was performed to assess how the turbulence affected the sensor, and the results validated by experimentation. The obtained voltage generated by the PVDF film was proportional to the flow velocity, which demonstrated the applicability of the designed system.

Piezoelectric sensors have also been used in buildings structural health monitoring systems, such as the projected system by Cui & Zhao (2021) to detect strain damages in beams, using groups of PVDF film sensors, as shown in Figure 4.24.
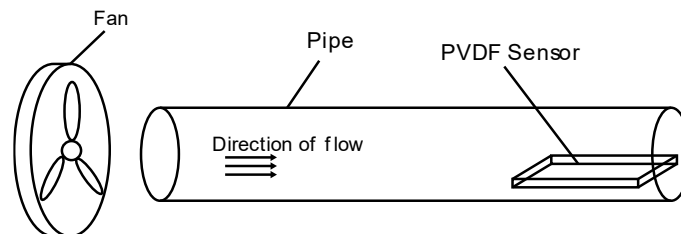
Figure 4.23.   PVDF sensor for fluid velocity measurement. Reprinted from *Sensors*, vol. *19*(7), (Q. Li et al., 2019), copyright © 2019 by the authors, under Creative Commons BY 4.0 license (https://creativecommons.org/licenses/by/4.0).

(a)

(b)
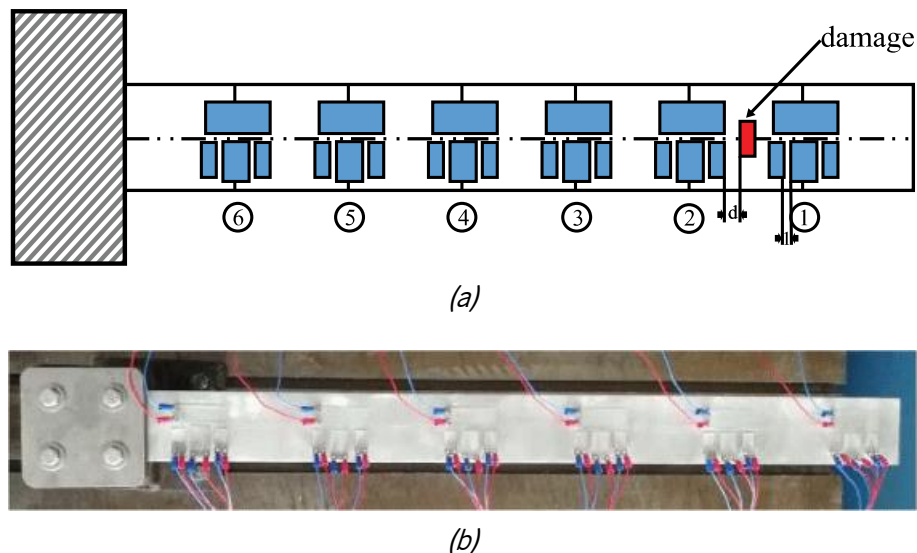
Figure 4.24.   Piezoelectric combined sensors for cantilever damage identification: *(a)* schematic and *(b)* real implementation. Republished with permission of IOP Publishing, Ltd., from *Measurement Science and Technology*, (Cui & Zhao, 2021), vol. *32*(11), copyright © 2021 IOP Publishing Ltd.; permission conveyed through Copyright Clearance Center, Inc.

The resonant frequency of each beam of a building changes when that beam is deformed or is cracked, and the sensors, despite the authors do not specify the electronic system to read the sensors, reckon the deformation of the beam based on the resonant frequency. The system uses natural building vibrations as excitation for the sensors. The PVDF sensors were coated with aluminum to create the electrodes, and wire terminals were cold-pressed on the film. The authors claim to be able to detect not only a damaged beam, but the location of the damage as well.

4.2.2. Actuators

In terms of actuators, the most common form of use of piezoelectric polymer materials is for sonic and ultra-sonic reproduction, due to weak physical response of PVDF polymer and PVDF copolymers at low frequencies (C. S. Lee et al., 2003; M. Martins et al., 2012; M. S. Martins et al., 2017; Street et al., 2020; Sugimoto et al., 2009). Piezoelectric actuators outperform electromagnetic ones in low powers (Uchino, 2008). Nevertheless, some projects have been able to use piezoelectric polymers with other materials in order to create slow-motion actuators (Correia et al., 2019; Dias et al., 2015; Mejri et al., 2016).

Casset et al. (2017) presented a P(VDF-TrFE) film loudspeaker, using multiple actuators with different diameters, as shown in Figure 4.25b. The substrate was a PEN foil, as visible in Figure 4.25a, with $125\,\mu m$ of thickness, and the piezoelectric film was $4.7\,\mu m$. The electrodes were poly(3,4-ethylenedioxythiophene) polystyrene sulfonate (PEDOT:PSS) with $800\,nm$. The P(VDF-TrFE) polymer was annealed for $120\,s$ in an infrared oven at $135\,°C$.

The resonant frequency was $993\,Hz$, and the device was driven with an audio signal of $70\,V$. The authors refer that the system produces satisfying audio and music, with a performance of $35\,dB$ at $1\,m$ away from the sensor.

(a)   (b)
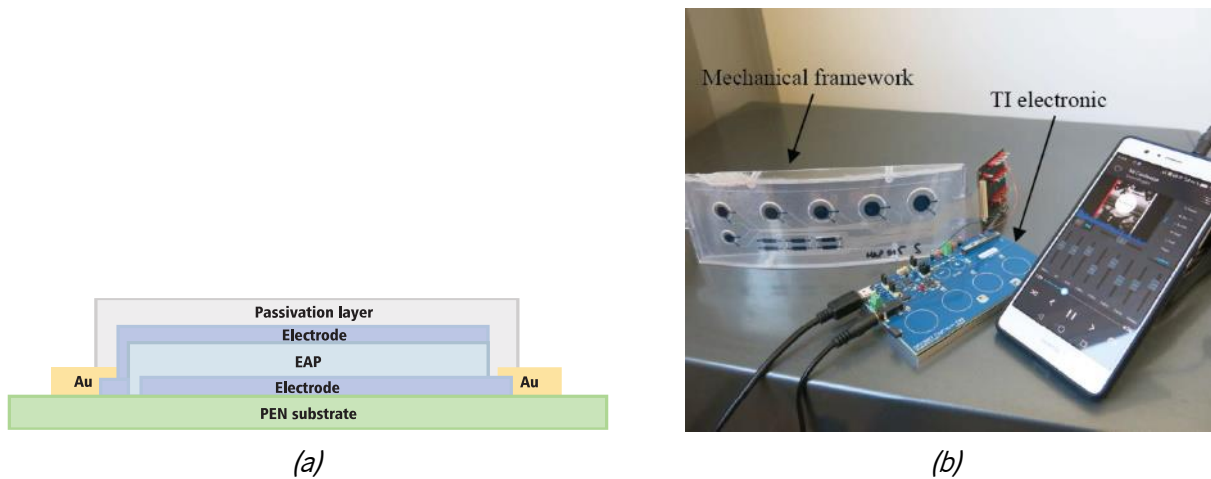
Figure 4.25.   P(VDF-TrFE) film loudspeaker: *(a)* topology and *(b)* implemented system.
Reprinted from (Casset et al., 2017), copyright © 2017, IEEE.

In another project, Street et al. (2020) developed a bimorph piezoelectric polymer speaker with an increase in loudness when compared to single layer polymer speakers. The designed prototype included two speakers for comparison: a single layer speaker and a bimorph speaker comprising two speakers bonded back-to-back, using P(VDF-TrFE). This prototype has been entirely made in flexible materials, recurring to printing techniques, as visible in Figure 4.26. The substrate was a layer of polyimide (PI) and the electrodes were made of gold. Contrarily to many other applications, this speaker operated mainly through the piezoelectric coefficient d_{31}, which causes the film to expand laterally when in a presence of a voltage along its thickness. However, as the substrate has difficulty in accompanying the P(VDF-TrFE) film during the expansion, it creates an asymmetry that converts the expansion into a plane-motion, creating sound.

Figure 4.26.   Bimorph P(VDF-TrFE) speaker with flexible and printed electronics.
Reprinted from (Street et al., 2020), copyright © 2020 IEEE.

An ultrasonic system for underwater communication with capability of reaching up to 1.5 MHz was designed by M. S. Martins et al. (2017), using two PVDF films as acoustic actuator. Figure 4.27 shows the actuator glued to a semicircular shape metal. The device was powered by a 12 V supply, and when a signal with frequency of 1 MHz was applied on it, it produced an output higher than 130 dB with a power consumption of 37.5 mW. This proves the applicability of the piezoelectric actuator in underwater communication systems. The project developed by Wu et al. (2020) has also attained similar results, but with higher resonant frequency.
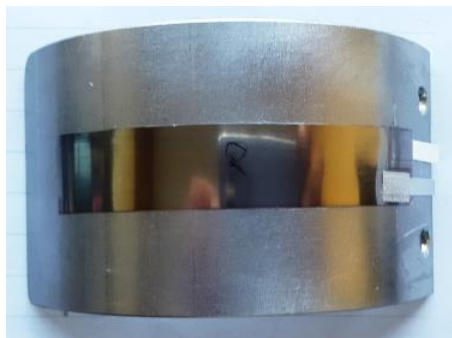
Figure 4.27. PVDF film actuator glued to a curved stainless-steel surface for high frequency acoustic underwater communication. Reprinted from (M. S. Martins et al., 2017), copyright © 2017, IEEE.

An interesting form of actuation using piezoelectric polymer films is through haptic devices, capable of providing mechanical feedback to the user when the finger is touching the device (Emgin et al., 2019; Van Duong et al., 2019; S. H. Yoon et al., 2019). The device created by S. H. Yoon et al. (2019) is a flexible multilayer piezoelectric composite, as shown in Figure 4.28, composed of 25 layers of PVDF stacked upon each other, for increased vibration. The device had an active area of 12 mm × 14 mm with 2 mm of thickness, prepared by screen-printing technique. The haptic actuator could be powered up to 400 V, but the authors found that users were able to identify haptic sensations with a voltage as low as 150 V. Several types of waves and frequencies were tested, such as sine, square and sawtooth waves, with frequencies of 160 Hz and 430 Hz.
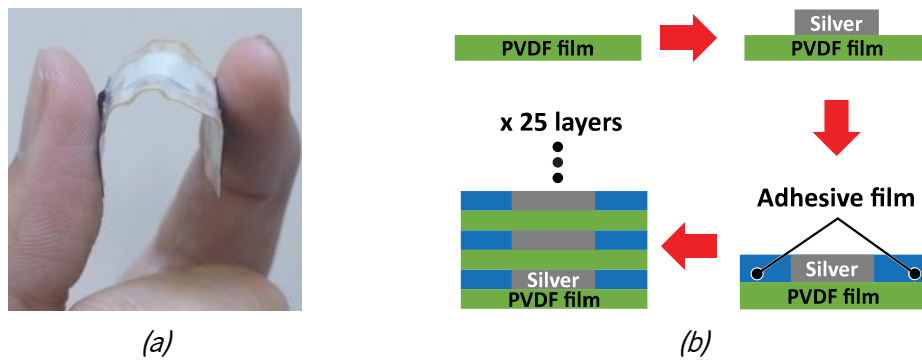
Figure 4.28. HapSense: *(a)* a flexible haptic device *(b)* composed by 25 layers of PVDF film. Republished with permission of ACM (Association for Computing Machinery), from *Proceedings of the 32nd Annual ACM Symposium on User Interface Software and Technology*, (S. H. Yoon et al., 2019), copyright © 2019 ACM.

Polylactic acid (PLA) is a biodegradable polymer (Curry et al., 2018) which does not show piezoelectricity, but the two chiral isomers poly-L-lactide acid (PLLA) and poly-D-lactide acid (PDLA) do. Moreover, PLLA films present spontaneous polarization, thus no poling treatment is necessary (Tajitsu, 2016). Recurring to PLA material, Tajitsu (2016) created a piezoelectric actuator with PLLA and PDLA. A new approach for the fabrication of PLLA film was developed which reached a shear piezoelectric coefficient of 16 pC/N, about three times higher than for conventional PLLA films. Gold electrodes were deposited on the surfaces of the PLLA film, and a demonstration of the applicability of the material was showed by making a plastic ball with mass of 3.2 g spin on the top of a rolled PLLA film, shown in Figure 4.29. A sine wave with amplitude of 250 V was applied on the electrodes, which caused the film to propagate a surface acoustic wave, resulting in the ball spinning at different velocities and directions, depending on the frequency applied. A maximum speed of 200 revolutions per minute (rpm) was attained at a driven signal of 12 kHz.

Additionally to this experiment, the author attempted an improve in the performance of the developed actuator, by using a PDLA/PLLA multilayer film. Due to chirality, PLLA and PDLA exhibit piezoelectric constants with opposite signs, and the author took advantage of that particularity by stacking up to 200 layers. Each layer was 14 μm-thick, composed by a PDLA film with aluminum electrode on bottom and a PLLA film with aluminum electrode on top, forming a pair of electrodes with a PDLA/PLLA bimorph composite in between. This time, a laptop with mass of 2.1 kg was placed on top of the PDLA/PLLA multilayer actuator, and it started rotating with when a sine wave with 12.8 kHz and 150 V peak-to-peak. This system was tested for 20 h with the laptop maintain a constant speed of 100 rpm.
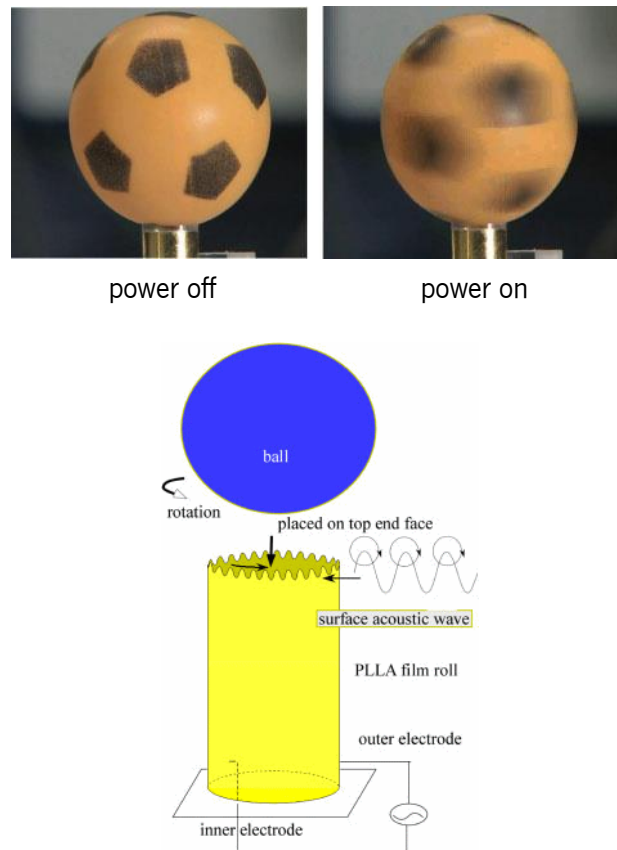
Figure 4.29. PLLA film actuator, spinning a plastic ball on the top end face. Republished by written permission of IOP Publishing, Ltd., from *Japanese Journal of Applied Physics*, (Tajitsu, 2016), vol. *55*(4S), copyright © 2016 The Japan Society of Applied Physics.

To create slow motion actuators using piezoelectric materials, Mejri et al. (2016) combined PVDF particles with ionic liquid, creating a film that bends accordingly to the applied electric field. The functioning of the system lies on the principle that anions have larger size than cations, and when the ions are sorted due to an external electric field, the film experiences a deforming force. The result is visible in Figure 4.30.
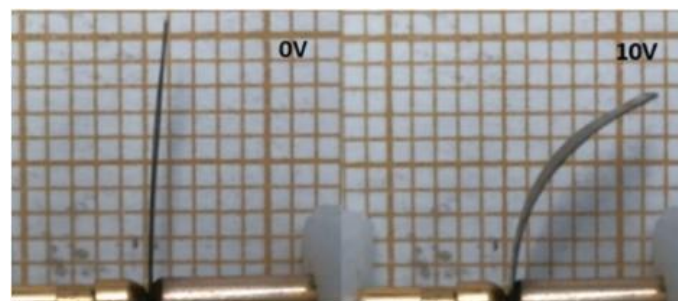
Figure 4.30. Displacement of an ionic liquid/PVDF when a voltage is applied on the film. Reprinted from *Journal of Non-Crystalline Solids*, vol. *453*, (Mejri et al., 2016), "Effect of anion type in the performance of ionic liquid/poly(vinylidene fluoride) electromechanical actuators", pp. 8-15, copyright 2016 Elsevier B.V., with permission from Elsevier.

4.2.3. Energy harvesters

Piezoelectricity has been used in nanogenerators to produce electrical energy from mechanical sources, and piezoelectric energy harvesters (PEHs) have been increasing in the area of small electronics, mainly because of flexibility, robustness and easier to fabricate, when compared to traditional piezoelectric ceramics. Applications for PEHs range from wind energy harvesting (S. Li & Lipson, 2009), to biomedical devices (S. Yoon & Cho, 2014; Yu et al., 2016), rain power energy harvesters (Rajeev et al., 2020) or wearable devices (Dutta et al., 2018), among others (Pedro Costa, Nunes-Pereira, et al., 2019).

In a prototype presented by Mahanty et al. (2017) it has been developed a flexible sponge-like nanogenerator, based on P(VDF-HFP) film, etched by zinc oxide (ZnO) nanoparticles (NPs), without any poling treatment due to the self-poling chemical structure of P(VDF-HFP). The device presents high sensitivity of 1 µV/Pa and is demonstrated for a self-powered wireless device.

In another project, a PEH device was developed by Shan et al. (2015) to scavenge energy from a moving fluid, as shown in Figure 4.31. The prototype used a piezoelectric beam (M8514-P2[1], Smart Material Corp.) made of aligned rectangular piezoceramic fibers, also known as a macro fiber composite (MFC). Though this is not a polymer, due to its microstructure composition, it has reached a nearly polymer behavior in terms of flexibility. The MFC was attached to a PVC beam in order to adjust the damping ratio and resonant frequency. For a water speed of 0.5 m/s, this system has reached a peak power of 1.32 µW and a power density of 1.1 mW/m2.
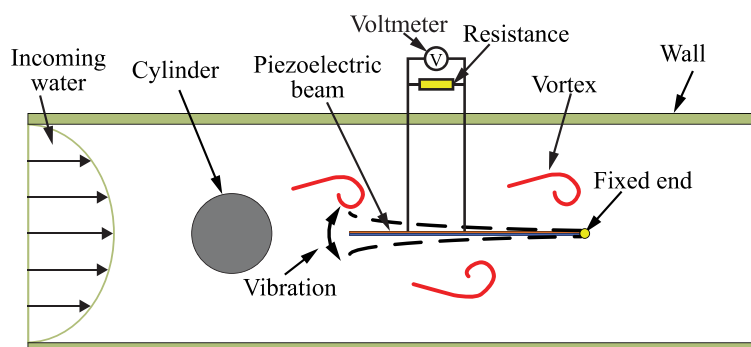
Figure 4.31.   Piezoelectric energy harvester made of PVDF to extract energy from water vortex. Reprinted from *Ceramics International*, vol. *41*, (Shan et al., 2015), "Novel energy harvesting: A macro fiber composite piezoelectric energy harvester in the water vortex", pp. S763 - S767, copyright © 2015 Elsevier Ltd. And Techna Group S.r.l., with permission from Elsevier.

---

1 See the product in manufacturer catalogue: https://www.smart-material.com/MFC-product-P2.html

The combination of piezoelectric with other effects has been used for increased energy harvesting. For example, Rajeev et al. (2020) fabricated a device to scavenge piezo and triboelectric energy from rain droplets, yielding 16 V and 15.4 nA with a device with area of 2.25 cm2, and X. Wang et al. (2016) for wearable applications. On the other hand, Gusarov et al. (2015) combined the piezoelectric and pyroelectric effects to increase the thermal energy harvested by a device, using two shape-memory alloy (SMA) stripes attached to a PVDF film to better thermally deform the PVDF film, as shown in Figure 4.32, resulting in electrical energy obtained not only by the pyroelectric effect itself, but also through the piezoelectric effect subsequent from the deformation induced by the SMAs. The material must be configured with additive polarities for both effects for maximum energy scavenge, contrarily to touch and hover sensors (Rendl et al., 2012). The authors report that the output voltage of this system was increased by 75 % when compared to the PVDF film alone, and the output energy was also increased by 200 %.
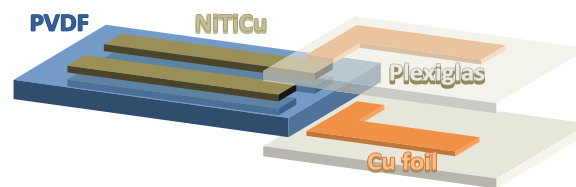
Figure 4.32. Schematic drawing of the PVDF film with two SMAs for piezoelectric-added thermal energy harvesting. Reprinted from (Gusarov et al., 2015), copyright © 2015, IEEE.

Another type of energy harvesting devices are magnetoelectric (ME) transducers. ME composites have a piezoelectric and a magnetostrictive materials (Pedro Costa, Nunes-Pereira, et al., 2019). A magnetostrictive material is a smart material that suffers a deforming force when in presence of a magnetic field. Through the physical coupling of the magnetostrictive material with a piezoelectric material, a ME device can convert changing magnetic fields into electric charge, as shown in Figure 4.33. Both are reversible effects, therefore ME composites can be of interest in sensors and actuators as well. ME energy harvesters can operate as wireless power supply for devices, gathering energy from mobile base stations, Wi-Fi routers, radio and TV transmitters, among others (Pedro Costa, Nunes-Pereira, et al., 2019).
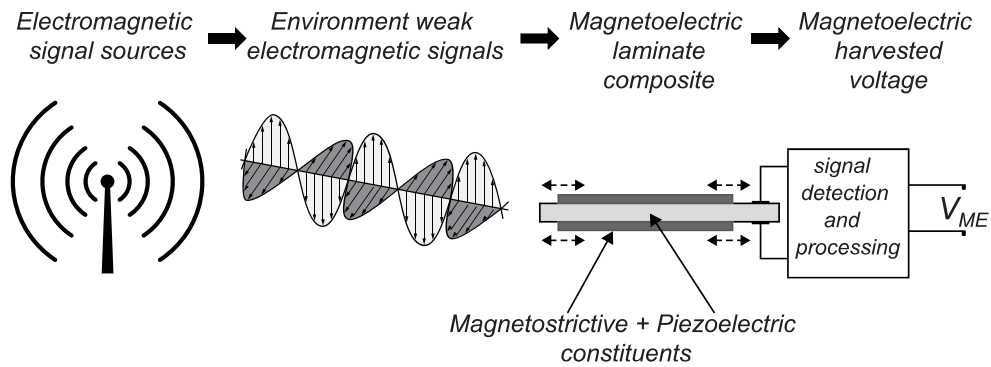
Figure 4.33. Schematic representation of the energy-harvesting process for a magnetoelectric device. Weak electromagnetic signals deform the magnetostrictive material, which deforms the piezoelectric material and produces an output voltage V_{ME} (V). Republished with permission of IOP Publishing, Ltd., from *Smart Materials and Structures*, (Lasheras et al., 2015), vol. *24*(6), copyright © 2015 IOP Publishing Ltd.; permission conveyed through Copyright Clearance Center, Inc.

Zaeimbashi et al. (2021) created an ultra-compact ME energy harvester for implantable medical devices, with size of 250×174 µm. The magnetostrictive layer was iron-gallium-boron, and the piezoelectric layer aluminum nitride. The device was conceived with two resonant frequencies, one at 2.51 GHz to scavenge energy from radio frequency (RF) communication, and another at 63.6 MHz for neural recording. Additionally, the authors also implemented transmit and receive communication wirelessly, at a fixed distance of 8 mm.

4.3. EXPERIMENTAL WORK

One prototype was prepared based on the piezoelectric technology:

–   A PVDF piezoelectric film prototype for touch and bending sensing, and audio reproduction (N. Castro et al., 2017; S. Gonçalves, Pereira, et al., 2019; S. Gonçalves, Serrado-Nunes, et al., 2019b).

This prototype is going to be discussed next.

4.3.1. Piezoelectric sensing and audio transducer prototype

The objective of this prototype was to use PVDF films in the creation of sensors and actuators recurring to the piezoelectric effect, through printing technologies. In this work it is demonstrated the fabrication of a device using a PVDF film with printed electronics. Electrodes and terminals were screen-printed with silver nanoparticles (NP) ink. An array with six squares was used for touch and bending sensors, as well as for audio reproduction. The implemented circuits were analyzed, and the results presented.

This work is covered by a journal article (S. Gonçalves, Serrado-Nunes, et al., 2019b) and two conference posters (N. Castro et al., 2017; S. Gonçalves, Pereira, et al., 2019). Accompanying the journal article, a video demonstrating the system in operation is also available in the supporting information section of the publication[1].

4.3.1.1. Materials

To prepare a PVDF piezoelectric film device, commercial poled PVDF film with 110 μm of thickness was acquired from Measurement Specialties (now TE Connectivity) with reference 3-1003352-0. Conductive silver NPs ink for screen printing was purchased from Novacentrix with reference Metalon HPS-021LV. The screen-printing mesh used was from Sefar, with 65 threads/cm, and a homemade screen printer was utilized to print the layouts. Thermal treatment of materials was performed on a JP Selecta 2005165 oven. Digital multimeter used to take measurements was a Fluke 117. Piezoelectric coefficient of PVDF films d_{33} was measured with an APC YE2730A instrument.

4.3.1.2. Touchpad fabrication

An array with six squares of 4 cm2 organized in 2 rows was used for the layout of the device, as shown in Figure 4.34, for screen printing. First, the bottom layer was printed on a PVDF film with silver ink and dried for 6 h at room temperature. Then, the top layer was printed, and the film was put in the oven for 1 h at 80 °C. The bottom layer was not immediately cured because the PVDF film gets slightly deformed during the process, which would make the aligning of the top layer impossible. Figure 4.35 shows the printed device after leaving the oven.

---

1 Link of the demo video: https://pubs.acs.org/doi/suppl/10.1021/acsaelm.9b00363/suppl_file/el9b00363_si_002.mp4
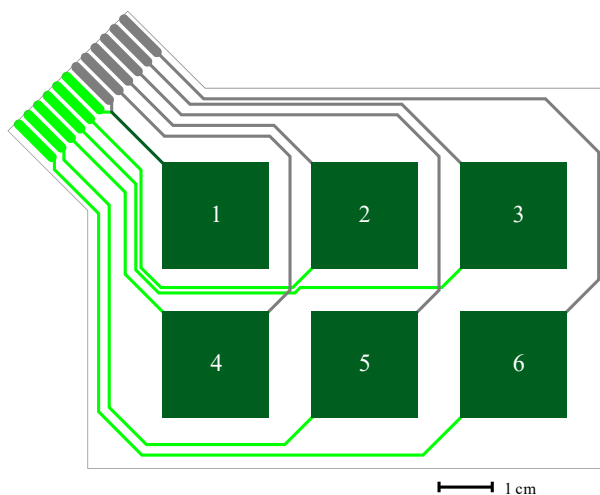
Figure 4.34. Layout of the array with 6 squares for screen printing (light green is bottom layer, gray is top layer, and dark green is both). Reprinted with permission from (S. Gonçalves, Serrado-Nunes, et al., 2019b), copyright © 2019 American Chemical Society.
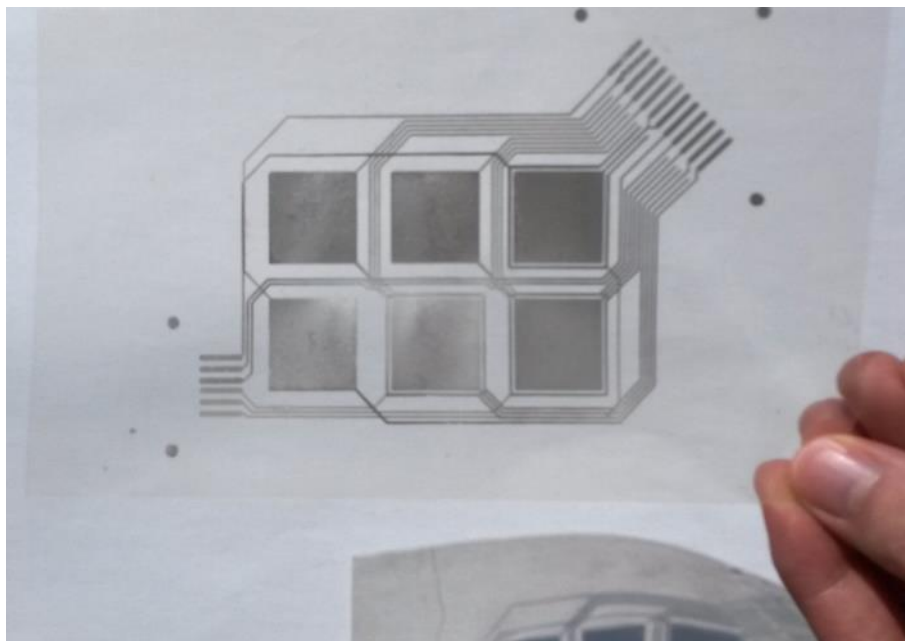
Figure 4.35. Aspect of the PVDF film with silver NP printed electrodes and terminals.

Electrical measurements on the printed film were performed to evaluate quality of the printed circuit, and once everything was confirmed to be fine, a layer of adhesive PET film was applied on each side of the film except on the terminals, to protect the silver ink from corrosion and oxidation, as well as to prevent direct electrical contact with the electrodes. Finally, clincher connecters were inserted (Amphenol FCI 65801-012LF), perforating the PVDF film.

4.3.1.3. Model of the sensors

It is often seen a piezoelectric device just generically represented as in Figure 4.36*a*. According to Equation (4.1), the displaced charge in a piezoelectric device is proportional to the force exerted on it. Therefore, a piezoelectric device behaves not as a *voltage* source nor a current source, but a charge source, as represented in Figure 4.36*b* by Q_p (C) But, since the current flowing on a circuit is the derivative of charge over time, we can represent the piezoelectric device as controlled current source, as presented in Figure 4.36*c*. The overlapping electrodes create a capacitance, which can be represented by capacitor C_p (F), and the wiring and terminals create an impedance, represented here by the resistor R_p (Ω). Instead of a current source, it is also possible to use a voltage source through the Thévenin's theorem, but it would result in a more complex controlled voltage source.
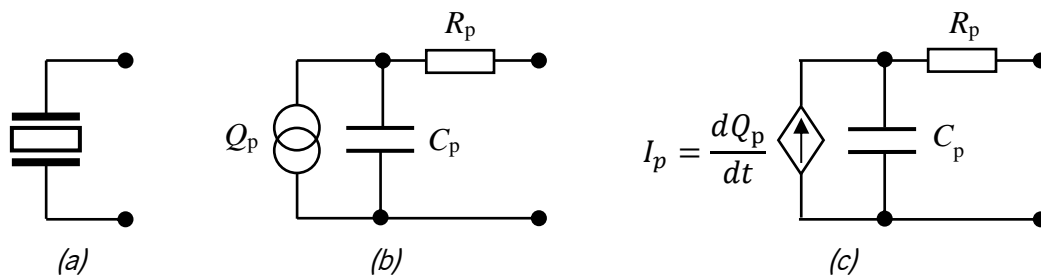
Figure 4.36. Equivalent model of a piezoelectric sensor: *(a)* representation of an ideal piezoelectric device; *(b)* real piezoelectric device works as charge source, with electrodes creating a capacitance C_p and terminals a resistance R_p; *(c)* charge source represented by equivalent controlled current source.
Reprinted with permission from (S. Gonçalves, Serrado-Nunes, et al., 2019b), copyright © 2019 American Chemical Society.

Together, capacitor C_p and resistor R_p create a low-pass filter (LPF), according to the transfer function of the piezoelectric device $H_p(s)$ in the Laplace complex domain s:

$$H_p(s) = \frac{Q_{out}(s)}{Q_p(s)} = \frac{1}{\frac{s}{\omega_p} + 1}, \qquad \omega_p = \frac{1}{C_p R_p} \tag{4.5}$$

where $Q_p(s)$ is the displaced electric charge, $Q_{out}(s)$ the total electric charge capable of leaving the piezoelectric device through the terminals, and ω_p (rad/s) the cutoff frequency of the LPF (Alexander & Sadiku, 2001, Chapter 14). Details about the calculation of the transfer function are available in Appendix A.1.

4.3.1.4. Electrical circuit for sensing

Several topologies exist for reading piezoelectric sensors, but the most common are the voltage mode amplifier and the charge mode amplifier (Karki, 2000). The first configures the sensor in open-circuit and is used when the amplifier is very close to the sensor because of susceptibility to noise, and the later drives the sensor to a short-circuit, a more complex type of circuit, but useful when the amplifier and the sensor are apart. Differential signaling is another improvement that can significantly reduce noise (Bartolome, 2010).

In this work, it was decided to use the charge mode amplifier with a band-pass filter (BPF) to block both electrostatic DC noise and the $50/60$ Hz grid noise. In Figure 4.37*a* is shown the used circuit with single-ended signaling. Differential signaling mode was also experimented, as visible in Figure 4.37*b*. Due to the very high gain of this circuit and input current concerns, the chosen operational amplifier was MCP6021 from Microchip.

(a)   *(b)*
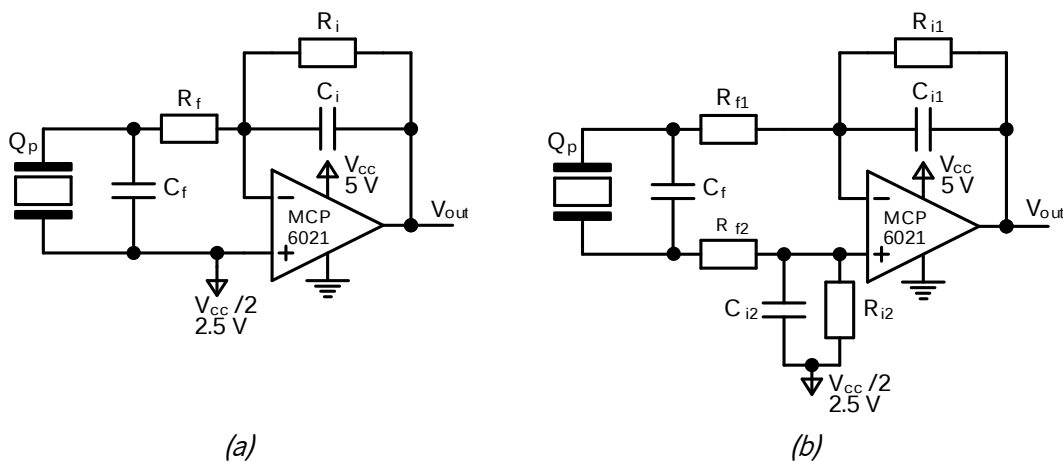
Figure 4.37. Piezoelectric sensor connected to a charge amplifier with a BPF in
***(a)* single-ended signaling and *(b)* differential signaling.** *(a)* Adapted with permission from (S. Gonçalves, Serrado-Nunes, et al., 2019b), copyright © 2019 American Chemical Society.

In the single-ended signaling circuit, the capacitor C_i integrates the signal from the piezoelectric sensor, and the amplifier converts it to voltage, therefore the output voltage V_{out} is proportional to the generated charge by the piezoelectric sensor Q_p. Resistor R_i together with capacitor C_i create a high-pass

filter (HPF). And the other pair constituted by resistor R_f and capacitor C_f create a low-pass filter (LPF), resulting in a band-pass filter (BPF). The transfer function $H_{pfi}(s)$ of this circuit is given by:

$$H_{pfi}(s) = \frac{V_{out}(s)}{Q_p(s)} = -\frac{sR_i}{\left(\frac{s}{\omega_p} + 1\right)\left(\frac{s}{\omega_f} + 1\right)\left(\frac{s}{\omega_i} + 1\right)},$$

$$\omega_p \cong \frac{1}{C_pR_p}, \qquad \omega_f \cong \frac{1}{C_fR_f}, \qquad \omega_i = \frac{1}{C_iR_i}$$

(4.6)

where ω_p, ω_f and ω_i (rad/s) are the cutoff angular frequencies of the filter of the piezoelectric sensor, the LPF on the input, and the HPF of integration, respectively. To obtain the cutoff frequencies f_p, f_f and f_i (Hz) is simply done by solving the equation:

$$\omega = 2\pi f$$

(4.7)

The gain A (V/C) of the circuit is given by:

$$A = -\frac{1}{C_i}$$

(4.8)

The negative sign indicates signal inversion. The transfer function of the circuit $H_{pfi}(s)$ has three poles, and can be decomposed in three parts, $H_p(s)$, $H_f(s)$ and $H_i(s)$. Further explanation can be found in Appendix A (Alexander & Sadiku, 2001, Chapter 14).

The power supply of the circuit Vcc was 5 V provided by a USB port. To avoid using dual power supply, the $Vcc/2$ was given as reference for the operational amplifier, so, the output voltage V_{out} is averaged at 2.5 V.

For the differential signaling circuit, the same transfer functions still apply, but attention must be paid to make both pins of the piezoelectric sensor to feel the same impedance. Therefore, the following conditions must be verified:

$$R_{f1} = R_{f2} = \frac{R_f}{2}, \qquad C_{i1} = C_{i2} = \frac{C_i}{2}, \qquad R_{i1} = R_{i2} = 2R_i$$

(4.9)

The input filter resistor R_f has to be split in two, and the integration R_i C_i pair was duplicated to the bottom pin of the piezoelectric sensor. The integration now is done by two capacitors (C_{i1} and C_{i2}), and as they are in parallel from the sensor's point of view, their capacitance must be halved, and the same happens with resistors (R_{i1} and R_{i2}), so their value must be twice as high.

A total of six identical circuits were replicated to simultaneously read the six sensors. A Microchip ATmega328P microcontroller was used, with a clock frequency of 8 MHz. Each of the outputs of the amplifiers was connected to a channel of the ADC of the microcontroller. The ADC was configured to acquire 8-bit samples at a rate of 7,300 samples per second (sps) (approx. 1.2 ksps for each channel).

The acquired data was then sent via UART at a baud rate of 115,200 bps and converted to USB (using an FTDI FT232RL) and connected to a computer where a Java graphical application displayed and stored the data.

4.3.1.5. <u>Electrical circuit for actuating</u>

The use the converse piezoelectric effect in a PVDF film actuator, it is necessary to apply higher voltage signals, particularly in smaller film transducers. Street et al. (2020) used 40 V in a bimorph P(VDF-TrFE) acoustic transducer, and Sugimoto et al. (2009) used only 9 V, but in an A4-sized PVDF film.

In this project, to keep up with simplicity, the audio source was the 3.5 mm audio jack from a tablet, smartphone or computer. Connecting it directly to the PVDF film would result in an inaudible sound reproduction. So, a mini-transformer was used, with relation of $1{:}38$ (HAHN reference BV 201 0142), as shown in Figure 4.38.

1:38
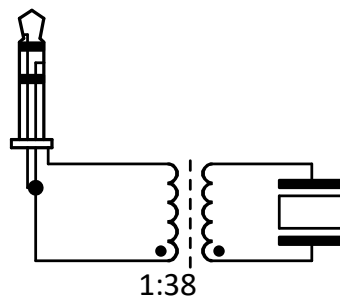
Figure 4.38.   Piezoelectric transducer connected to the 3.5 mm audio jack.

However, this approach can overload the audio output from the device, limiting the output power applied to the piezoelectric actuator. To improve efficiency, it is possible to insert an amplification module after the 3.5 mm audio jack, but as the system exhibited satisfactory response without it, it was not used.

4.3.1.6. <u>Results and discussion</u>

Before screen printing the layout in the PVDF film, the d_{33} coefficient was measured, which was -23 pC/N. After printing the layout on a PVDF film and curing the ink, the d_{33} obtained was -21 pC/N, which means that the thermal annealing did not depole the PVDF film. It was measured the electrical resistance between each of the electrodes and their terminals. The minimum registered value was $2.3\ \Omega$ for each pair of electrodes, and the maximum was $11.0\ \Omega$. Next, the capacitance of each sensor was measured, which was between to 590 to 610 pF. The obtained value for capacitance is higher than expected, which was attributed to fact of the PVDF being poled (Bhunia et al., 2016), but the manufacturer of the PVDF film does not publish the dielectric constant of the material.

The parameters considered for touch and bending sensors are listed in Table 4.7.

Table 4.7.   Considered parameters for the filters of the touch and bending piezoelectric sensors.

Sensor	R_p	C_p	R_f	C_f	R_i	C_i	f_p (LPF)	f_i (HPF)	f_f (LPF)	$\|A\|$ (V/C)
Touch	11 Ω	610 pF	480 kΩ	33 nF	100 MΩ	300 pF	24.2 MHz	5.3 Hz	9.9 Hz	190 dB
Bending	11 Ω	610 pF	2 MΩ	33 nF	1.5 GΩ	660 pF	24.2 MHz	0.16 Hz	2.4 Hz	184 dB

The saturation frequency of the developed piezoelectric sensor is very high (24.2 MHz). The circuit for touch detection was projected with higher gain since the displaced charge on touch is usually lower. For the touch sensor, the implemented BPF had a band gap between 5.3 Hz to 9.9 Hz, while the bending sensor has a slower response, and therefore, the chosen band gap was between 0.16 Hz to 2.4 Hz. The Bode plot of the circuits was calculated based on the transfer function $H_{pfi}(s)$ in terms of amplitude $|H_{pfi}(s)|$ and phase shift φ (Alexander & Sadiku, 2001, Chapter 14), as observable in Figure 4.39.

Touch sensor circuit

(a)

(b)

Bending sensor circuit

(c)

(d)
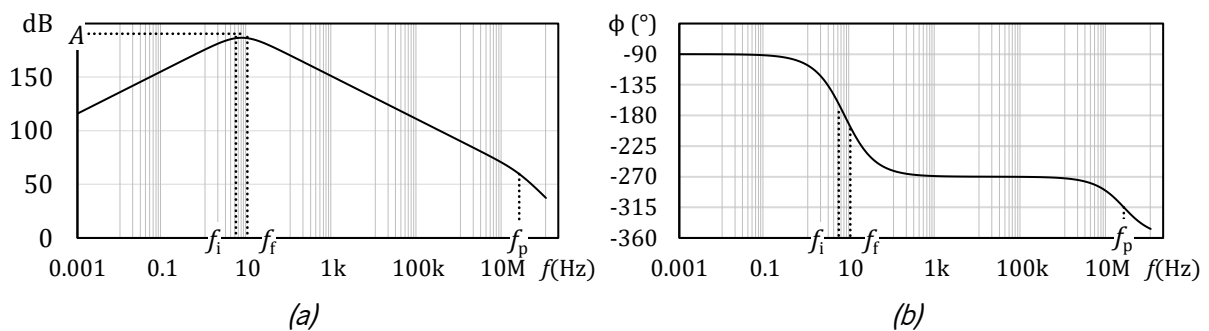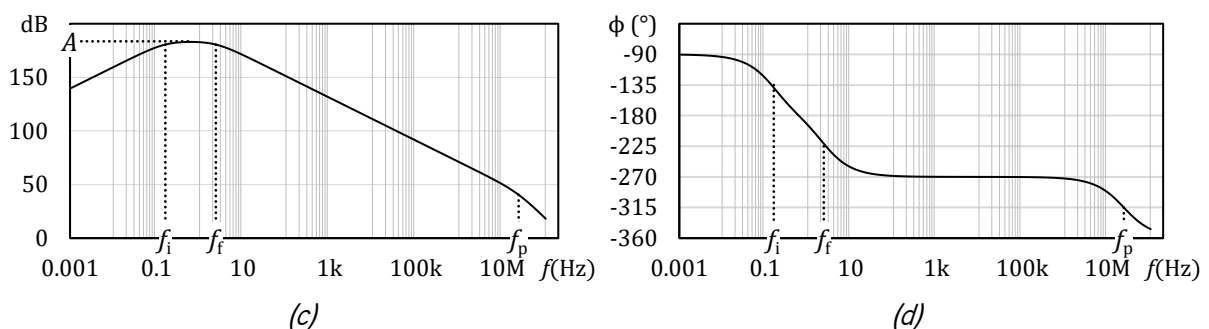
Figure 4.39.   Bode plot of the transfer function for touch and bending sensor circuits: *(a)* amplitude and *(b)* phase shift of touch sensor; *(c)* amplitude and *(d)* phase shift of bending sensor.

In most applications, the differential signaling circuit has improved noise rejection, compared to single-ended signaling. However, in this specific case, the single-ended signaling circuit has one advantage: since one of the electrodes of the PVDF film is directly connected to the voltage reference of 2.5 V, if this electrode is facing towards the side of user interaction, it can be used as shield for the human finger. This is not possible in the differential signaling topology, and, as the human finger is closer to one of the electrodes, it unbalances the common mode noise rejection. This has been confirmed by the experimental results, driving the operational amplifier to saturation when touching the sensor with a finger. For this reason, only the single-ended signaling results are shown next.

The narrow passing-band of the touch sensing circuit creates a response composed by pulses, as shown in Figure 4.40*a*. When the user presses the sensor, it destabilizes the charge in the piezoelectric sensor, storing that energy in the integrating capacitor, but that charge immediately drains through the parallel resistor. When the user releases the sensor, the same happens but with inverse polarity. Figure 4.40*b* shows several touch and release events. The intensity of the touch can be determined by the peak value.

(a)   *(b)*
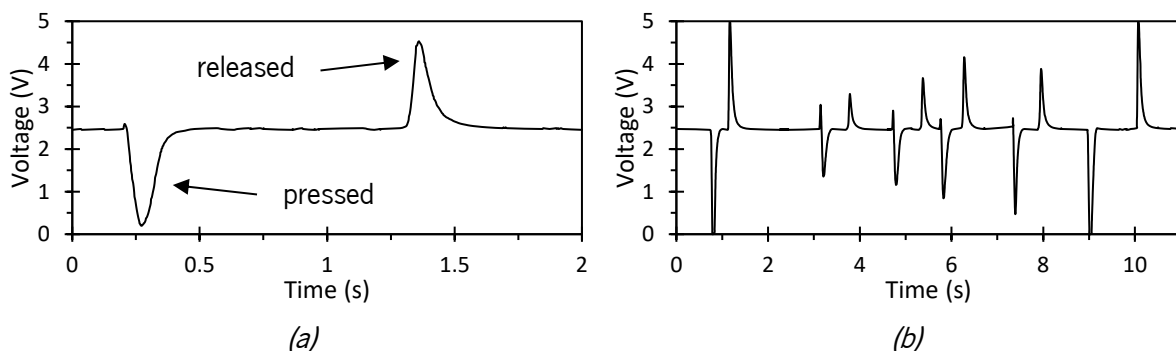
Figure 4.40.   Touch sensor's response: *(a)* single press and release event, and *(b)* sequence of several touches with different forces.

In the bending sensor a different approach was followed because the bending of the film can be slower or faster, more intense or weaker. It was attempted to increase the time constant of the HPF, giving the user time to unbend the sensor meanwhile. This is the reason why the cutoff frequency of the HPF was set so low. This is visible in Figure 4.41, where it is distinguishable the HPF cutoff from the user unbending the sensor. It has been noticed that the amplifier easily reaches saturation when bending the sensor more sharply. Increasing the capacitance of the integrating capacitor could easily solve this, as well as reducing amplifier drift rate. However, it comes at a cost of less accuracy.

Acquiring data from all of the sensors of the array simultaneously showed some crosstalking due to the vibration of the whole film when pressing only one of the sensors. This is shown in Figure 4.42, where

the PVDF film is side by side with the computer's screen displaying the readout of the sensors. A demonstrating video is also available in the supporting information section of the publication (S. Gonçalves, Serrado-Nunes, et al., 2019b)[1].
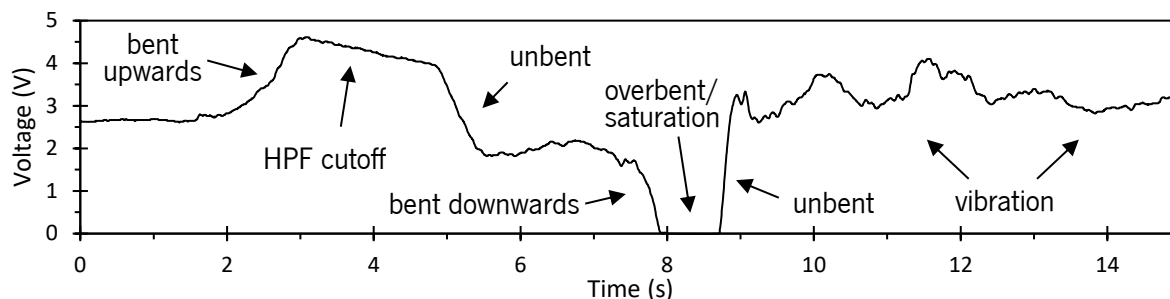
Figure 4.41. Bending sensor's response.
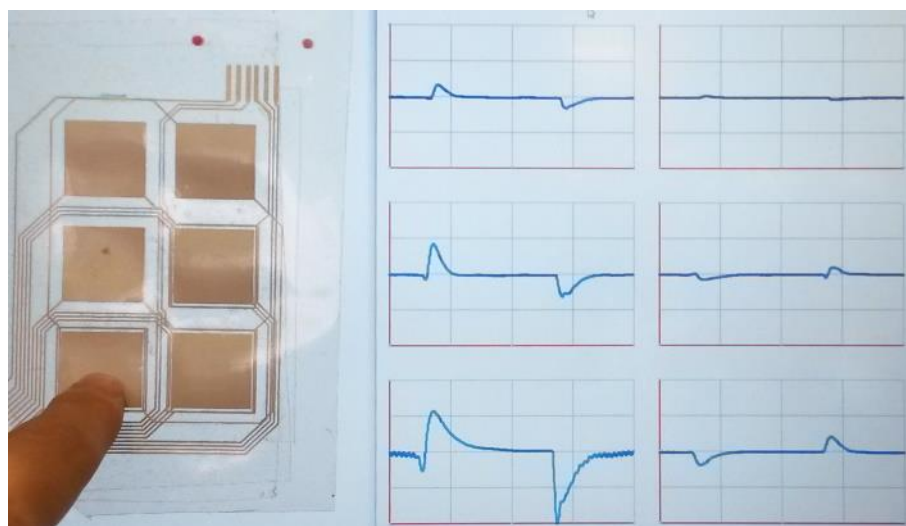
Figure 4.42. Sensor array by the side of the computer's screen during one touch and release event on one of the sensors.

Relatively to the sound reproduction, all the piezoelectric devices were driven together, using the 3.5 mm audio jack from a computer as source, with the signal amplified in voltage through the transformer.

The PVDF was slightly curved to operate as a diaphragm (Sugimoto et al., 2009). Sharp beeps and instrumental music were clearly audible. Voice reproduction got distorted but still understandable. In Figure 4.43 is shown the spectral performance of the developed device, and it is visible the weak response on the low frequency. The best response was around 7 kHz. Measurements were taken with a smartphone approximately 7 cm away from the film.

---

1 Link of the demo video: https://pubs.acs.org/doi/suppl/10.1021/acsaelm.9b00363/suppl_file/el9b00363_si_002.mp4
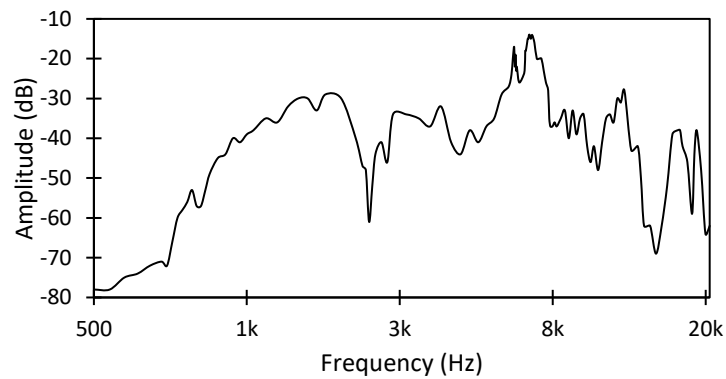
Figure 4.43.   Acoustic performance of the PVDF film.

Additionally, an improve in the quality of the reproduced sound was achieved by using more than one transformer simultaneously. Placing up to three transformers in parallel significantly reduced distortion and increased volume of the reproduced voice.

4.3.1.7. <u>Conclusions</u>

This work described the fabrication of piezoelectric sensors and actuators based on PVDF films and printed electronics. Electrodes were printed using silver ink by screen-printing technique, creating an array of six transducers.

It has been developed the mathematical model for the devices to operate as sensors, and a circuit based on a charge amplifier and a LPF was proposed. A variation of the charge amplifier was also studied for differential signaling, but it proved to be not as effective as the single-ended signaling. The sensors were prepared for touch and for bending operations, being the BPF set to 5.3 – 9.9 Hz and 0.16 – 2.4 Hz, respectively. Noise was mostly eliminated from the sensors and it was possible to detect pressing and releasing events along with their intensity, as well as bending and unbending directions.

The developed piezoelectric film was also used for acoustic reproduction, being connected to the audio jack of a computer and then to an elevating transformer to amplify the voltage applied on the electrodes. For the acoustic vibration to reach audible volume, it was necessary to bend the piezoelectric film lightly, in other to make it act as a diaphragm. Music was possible to hear, but voice got slightly distorted because the piezoelectric film showed good response only to higher frequencies, particularly higher than 1 kHz, being the best response registered at around 7 kHz. Piezoelectric sensors and are promissory for the development of TUIs since they are being considered as an augmenting technology for capacitive touch displays (Arokia Nathan et al., 2019), and piezoelectric actuators for haptic systems, such as to aid visually impaired people (W. Yang et al., 2021), among others.

5. PIEZORESISTIVE FILMS

The piezoresistive effect is the variation of the electrical resistance of a material when suffering a deformative force (W.-T. Park, 2012). It is a phenomenon first reported by William Thomson in 1856 (Barlian et al., 2009) in iron and copper under elongation, and only in 1938 the first piezoresistive sensor was developed (Barlian et al., 2009). A half century later, progress in piezoresistivity have been mostly focused on silicon strain gauges and microelectromechanical system (MEMS) devices (Barlian et al., 2009).

Nowadays, piezoresistivity involves a much broader range of materials, including polymer composites, such as elastomers (Georgopoulou & Clemens, 2020), foams (Panahi-Sarmad et al., 2020), fibers (Irfan et al., 2021), paper (Ren et al., 2012), fabric (Castano & Flatau, 2014) or natural polymers (Wan et al., 2021), among others.

Flexible and stretchable piezoresistive materials can be classified in three categories: conductive polymer composites, porous conductive materials, and architected conductive materials (Jing Li et al., 2020). These materials are illustrated in Figure 5.1.
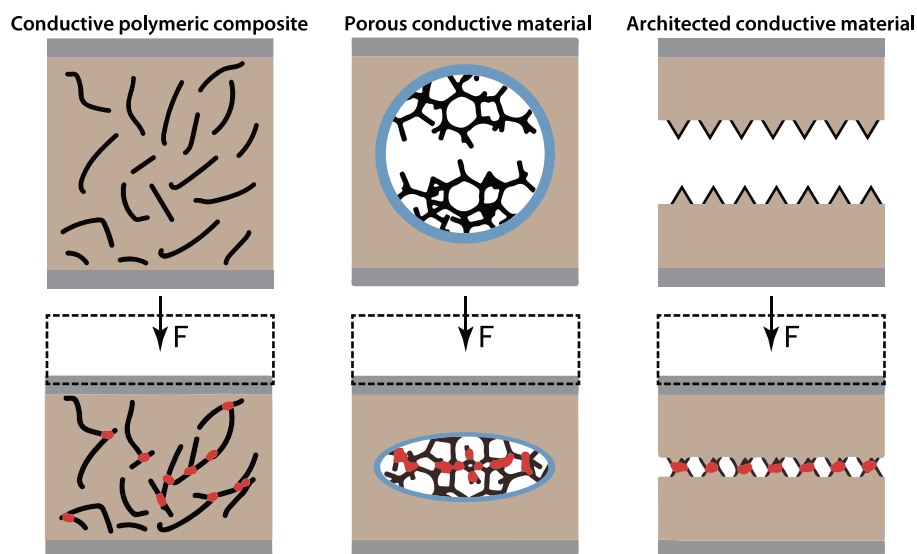
Figure 5.1. **Schematic representation of the different forms of piezoresistivity.** Reprinted from *Journal of The Electrochemical Society*, vol. *167*(3), (Jing Li et al., 2020), copyright © 2020 The Authors(s), under Creative Commons BY 4.0 license (https://creativecommons.org/licenses/by/4.0).

Conductive polymeric composites are constituted by a blend of stretchable polymers with conductive materials, so that the deformation of the composite leads to a rearrangement of the connection between the conductive materials, changing resistivity (Jing Li et al., 2020). Porous conductive materials have a specific microscopic 3D-structure of conductive materials that adjusts the conductive paths when under

stress (Jing Li et al., 2020). And architected conductive materials possess a macroscopic mechanical architecture that facilitates the electrical contact between different composite layers (Jing Li et al., 2020).

The most common types of applications for piezoresistive materials are force, pressure and deformation sensors (T. Yang et al., 2017), requiring properties that traditional piezoresistive silicon or metal-based sensors lack, despite of higher accuracy and sensibility, and that polymer composites can provide, in particular, flexibility and stretchability (B. F. Gonçalves et al., 2016). Other advantages are low-cost fabrication, the possibility for tailoring the properties of the composites according to specific requirements, and the easy integration into devices (Amjadi et al., 2016; B. F. Gonçalves et al., 2016).

Increasing demanding fields of application of piezoresistive polymers range from building structure monitoring (Das & Saha, 2018), to human motion monitoring (Y. Hu et al., 2018), biomedical applications (Y. Lu et al., 2019), robotics (Stassi et al., 2014), wearables (T. Yang et al., 2017), or user touch interfacing (Yue & Moussa, 2018), among others (Saggio et al., 2015).

Carbonaceous nanofillers are the most studied type of fillers in the development of piezoresistive polymer composites (Chung, 2020; Ke et al., 2021), namely CNTs, multi-walled carbon nanotubes (MWCNTs) (M. Wang et al., 2017), carbon nanofibers (J.-Z. Xu et al., 2014), graphene (Liu et al., 2017) or carbon black nanoparticles (Nalon et al., 2020). Nevertheless, other less investigated fillers include silver nanowires (SNWs) (Ahmed et al., 2019), silver nanoparticles (Shen et al., 2020) or iron oxide nanoparticles (Vipulanandan & Mohammed, 2015), among others.

The sensitivity of a piezoresistive material is determined by the gauge factor (GF), which correlates the electrical resistivity variation of the material with the mechanical strain. The GF of a piezoresistive material is given by:

$$GF = \frac{\Delta R/R}{\varepsilon} \tag{5.1}$$

in which $\Delta R/R$ is the resistance change ratio and ε is the mechanical stain (Barlian et al., 2009). The gauge factor of piezoresistive metal foil strain gauges is about 2 (N. Hu et al., 2013), but it can reach up to 100 or more in polymer/CNT composites (Ke et al., 2018), due to the high stretchability of polymer composites.

The polymer base material is responsible for many of the properties of the composite. There has been applications using several types of polymer materials, such as thermosets (Bouhamed et al., 2017; Xiaohan Cao et al., 2017; Yanlei Wang et al., 2018), thermoplastics (P Costa et al., 2016; Tsonos et al., 2015) or thermoplastic elastomers (B. F. Gonçalves et al., 2016; Liu et al., 2017), among others, each attaining different properties in terms of sensitivity, linearity and hysteresis, stretchability, biocompatibility

and even self-healing. Given the functionality of these polymer composites, efforts have been made for the introduction of these materials into low-cost industrial manufacturing processes (Duan et al., 2020).

This chapter is mostly covered by the publications of the candidate (Pedro Costa, Gonçalves, et al., 2019; J.R. Dios et al., 2019; Jose R Dios et al., 2020; Reizabal et al., 2019, 2020).

5.1. APPLICATIONS BASED ON PIEZORESISTIVE POLYMER FILMS

One of the first applications of piezoresistive polymeric composites, and that has been largely industrialized, is the development of electrostatic and electromagnetic shielding (Panahi-Sarmad et al., 2020), such as the material under the registered trademark Velostat (also known as Linqstat), often used in packaging of electrostatic sensitive devices. However, in this type of applications, the piezoresistive effect is not actually interesting, but rather the conductive capacity of the material.

Pointner et al. (2020) presented a project named Knitted RESi, based on a piezoresistive yarn, which resulted in a stretchable and robust textile due to the knitted structure. Using intersecting yarns, the system is able to detect pressure applied on the intersections, operating in the same principle as force-sensing resistors (FSR)s.

Another project using conductive fabric is the smart carpet, developed by Zhou et al. (2017). It consists of a three-layer assembly, with metallic fibers woven intro polyester substrate for top and bottom layers, and a CarboTex layer in the middle layer, which is a carbonated polymer fabric. The designed prototype has dimensions of 1.8×0.8 m, and is arranged in 120 rows $\times 54$ columns for piezoresistive sensing. In Figure 5.2 is shown the prototype that can be easily placed under a normal carpet. The objective of this system is to monitor people waking on the device and to identify them based on the individual steps and morphing footprint. The system was tested with 13 participants, attaining an identification success rate of 76.9 %.

(a)   *(b)*

Figure 5.2.   Piezoresistive sensing carpet: *(a)* fabric-based sensor and *(b)* operating under a real carpet. Reprinted from (Zhou et al., 2017), copyright © 2017, IEEE.

The previously mentioned prototype Keppi (in section 2.1.2) for self-reporting of user pain (Adams et al., 2018) has found an interesting way to embed a piezoresistive sensor, by using conductive foam and copper electrodes in the inner section of the device (see Figure 2.13), preventing the device from being excessively deformed and presenting erroneous response, as happened in their first prototype, due to placing the piezoresistive sensor more close to the surface.

B. F. F. Gonçalves et al. (2017) developed a method for the fabrication of water-based piezoresistive sensors, based on the thermoplastic poly(vinyl alcohol) (PVA), a water-soluble polymer. The authors reinforced the polymer with multi-walled carbon nanotubes (MWCNTs) to achieve piezoresistivity. To test the developed composite, a conductive layout with interdigitated areas was printed on a PVA substrate where the piezoresistive ink was deposited, through screen-printing and spray-printing techniques. The authors achieved a gauge factor of 3.

Damalerio et al. (2018) recurred to piezoresistive sensors made of carbon paste for early extravasation detection during intravenous cannulation, using non-invasive methods. Extravasation during intravenous cannulation might happen when the injected fluid into a vein leaks, leading to swelling of the skin. Fabricated devices as the ones shown in Figure 5.3 are attached to the skin in the likely region for the extravasation to happen, being able to detect the swelling of the skin. An initial prototype made of gold electrodes was designed, but the expensive fabrication prevents the devices to be discardable. The following approach used carbon paste that was screen-printed directly on a flexible medical adhesive film. The devices are disposable and look like the normal hospital adhesives, except the wire for the terminals, being not very difficult their use in hospital environment.
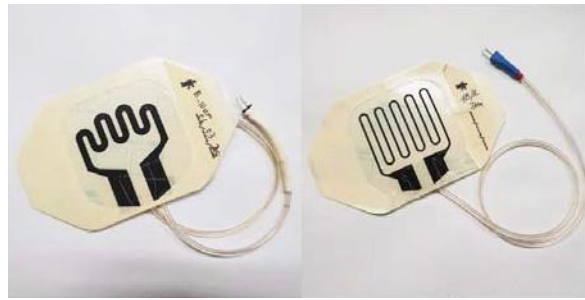
Figure 5.3. **Non-invasive piezoresistive sensors for extravasation detection during intravenous canulation.** Reprinted from (Damalerio et al., 2018), copyright © 2018, IEEE.

Intead of printing single sensors, H. F. Castro et al. (2018) developed a fully printed Wheatstone bridge, as shown in Figure 5.4, suitable for strain sensing applications. A PET substrate was used, where silver nanoparticles ink was printed. The authors developed a piezoresistive ink based on styrene-*b*-(ethylene-co-butylene)-*b*-styrene (SEBS) with MWCNTs nanofillers. After being fabricated, the sensor presented no repeatability, but after 50 bending cycles, the sensor sharted showing a linear response with the apllied pressure.
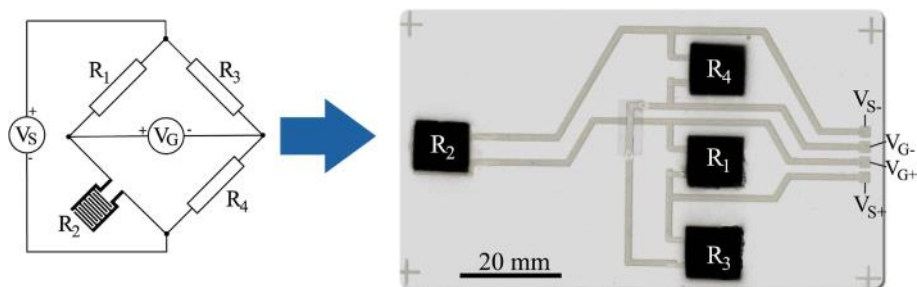
Figure 5.4. **Printed Wheatstone bridge with piezoresistive sensor.** Reprinted from *Additive Manufacturing*, vol. 20, (H. F. Castro et al., 2018), "Printed Wheatstone bridge with embedded polymer based piezoresistive sensors for strain sensing applications", pp. 119-125, copyright © 2018 Elsevier B.V., with permission from Elsevier.

Other devices have also been designed and simulated using piezoresistive polymer materials, such as in accelerometers (Verma & Ansari, 2019) or particles detection systems. The work developed by Agarwal et al. (2018) consists in a cantilever system capable of detecting fatty acid-binding protein. The piezoresistive cantilever gets deformed due to the molecular adsorption-induced surface stress in the presence of specific antibody-antigen, as represented in Figure 5.5. The fabricated microcantilever had a size of 220 ×110 µm, and was made of SU-8 epoxy and carbon black. According to the authors, the obtained piezoresistive response was proportional to the concentration of the fatty acid-binding protein.

<center>(a)   (b)</center>
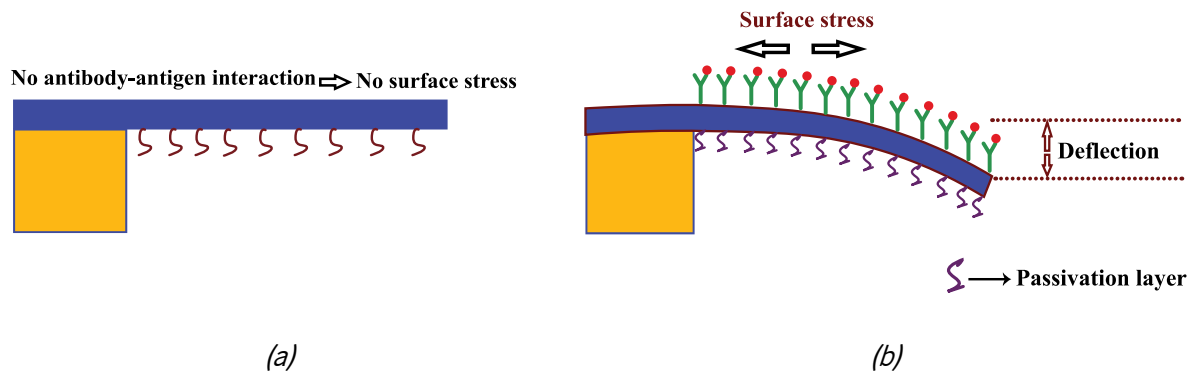
Figure 5.5.   Fatty acid-binding protein detection cantilever sensor: *(a)* no particles detected and *(b)* deflection caused by particles. Reprinted by permission from Springer Nature Customer Service Centre GmbH: Springer Nature, *Applied Nanoscience*, vol. *8*(5), "Detection of heart-type fatty acid-binding protein (h-FABP) using piezoresistive polymer microcantilevers functionalized by a dry method", (Agarwal et al., 2018), copyright © 2018, Springer-Verlag GmbH Germany, part of Springer Nature.

In the user interaction field, Hwang et al. (2019) reported a transparent sensing device capable of distinguish between touch and pressure, using capacitive and piezoresistive technologies, respectively. It contains an array of 4 × 4 sensors, allowing to create several command buttons. The device can be applied in wearable electronics or stretchable displays. In Figure 5.6*a* is shown the touch sensor array device attached to a human wrist. The device is composed by several layers, as visible in Figure 5.6*b*.

<center>(a)   (b)</center>
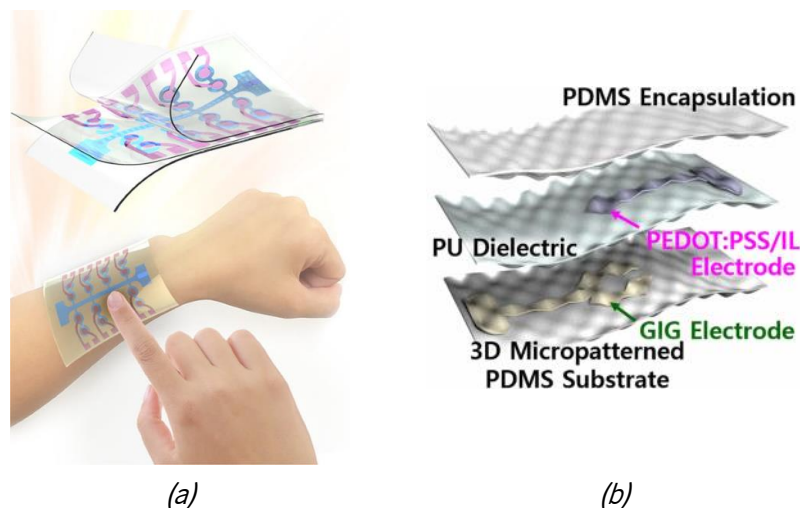
Figure 5.6.   Wearable touch and pressure piezoresistive device: *(a)* attached to a human wrist and *(b)* layers composing the device. Reprinted from *NPG Asia Materials*, vol. *11*(1), (Hwang et al., 2019), copyright © 2019, The Authors(s), under Creative Commons BY 4.0 license (https://creativecommons.org/licenses/by/4.0).

The device comprises a 3D microstructure pattern for increased sensitivity and stretchability. The bottom layer is the substrate that was used as support for the remaining layers. It comprised a

3D-micropatterned PDMS layer, and then an ultra-thin multilayer sheet of gold/ITO/gold (GIG) to operate as electrode. A polyurethane (PU) layer acted as dielectric material, and on top of it, a PEDOT:PSS/ionic liquid electrode. A final layer of PDMS encapsulated the whole device. For the capacitive sensing, it was taken into account the mutual capacitance between the two electrodes, but the top electrode was actually piezoresistive too. Therefore, when pressed, it changes the series resistance of the capacitive sensor, allowing to detect pressure in addition to touch. The authors compared the results of the 3D-micropatterned device with a similar non-micropatterned, and concluded that the 3D micropattern was responsible for the piezoresistivity of the top electrode, since the planar device showed no piezoresistivity. To demonstrate that the device worked as intended, an experiment was made with the user successfully controlling a small remote vehicle with the developed sensor array.

On the other hand, paper is a natural substrate for wearables and human contact. The work proposed by L. Gao et al. (2019) involves piezoresistive sensors based on a smooth surface nanocellulose paper substrate. Silver interdigitated electrodes were first printed on it using direct writing technique. The piezoresistive material was based on porous tissue paper with rough surface, and coated with SNWs, using dip-drying method. The piezoresistive material was placed on top of the electrodes, and an adhesive paper encapsulation fixed everything in place. The sensor is shown in Figure 5.7. When pressed, the conductive microfibers of the tissue paper/SNW are pressed against the interdigitated electrodes, changing resistance. The produced device is entirely made of green flexible electronics, paving the way to low-cost disposable sensors for electronic skin.
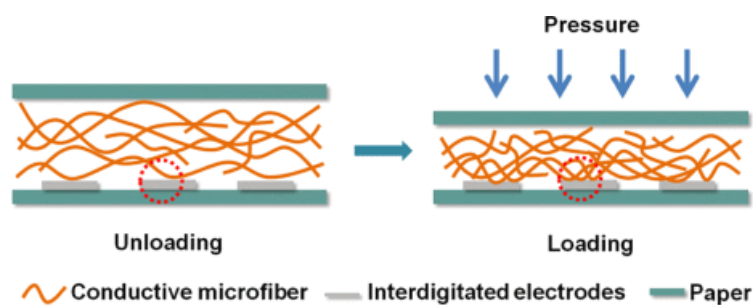
Figure 5.7. **Schematic of a paper-based piezoresistive sensor.** Reprinted with permission from (L. Gao et al., 2019), copyright © 2019, American Chemical Society.

5.2. Experimental work

Four different prototypes were prepared based on the piezoresistive technology:

– An array of 8 pressure sensors based on the inclusion of CNTs on PVDF, SEBS and thermoplastic polyurethane (TPU) for walking detection (J.R. Dios et al., 2019);

– A composite based on polylactic acid (PLA) reinforced with CNTs for deformation sensing applied on an endoscope (Jose R Dios et al., 2020);

– A highly stretchable and sensitive SEBS and graphene-based composite applied on the fingers of a glove (Pedro Costa, Gonçalves, et al., 2019);

– A piezoresistive touchpad for drawing and writing digitalization.

These prototypes are going to be discussed next.

Attempts to develop piezoresistive sensors based on natural materials, namely silk fibroin (SF), were made (Reizabal et al., 2019, 2020), but with rather unexpected results, such as the electrochemical effect[1], which, although it constitutes important scientific advance, was found not to fit in the content of this thesis, and therefore, is not going to be further discussed.

5.2.1. Walking prototype with an array of PVDF, SEBS and TPU reinforced with CNTs pressure sensors

The objective of this work was to demonstrate the applicability of different polymer materials for the fabrication of piezoresistive sensors, namely polyvinylidene fluoride (PVDF), thermoplastic polyurethane (TPU) and styrene-*b*-(ethylene-co-butylene)-*b*-styrene (SEBS). To provide conductive properties to the polymers, they were reinforced with CNTs in different quantities. The developed materials were experimented on a human walking detection sensing device, with each of the fabricated polymer composite films being integrated in a sensor. As expected, increasing the CNTs concentration increases the conductivity of the composite. However, it might reduce the piezoresistive effect.

The used polymers had different properties, being PVDF rigid, and TPU and SEBS flexible and stretchable. Nevertheless, all the polymers were capable of identifying and measuring the walking movement, although with different piezoresistive responses for the different sensors.

---

1 Demo video showing the use of the electrochemical effect in SF-based composites: https://youtu.be/IFRe1eibhDE

This is work is covered by the publication (J.R. Dios et al., 2019), and a demo video is also available in the supplementary data of the article[1].

5.2.1.1. Materials

SEBS was supplied by Dynasol Gestión S.A. (reference 6110), PVDF from Solvay Inc. (reference 6010), and TPU from Lubrizol (reference Estane 2103-70A). CNTs were furnished by Nanocyl (reference NC7000). DMF solvent was acquired from Carlo Erba Reagents, and cyclopentyl methyl ether (CPME) from Scharlau.

Conductive silver ink was obtained from Novacentrix (reference HPS-21LV), and the PET film from Lohmann Technologies UK Ltd. (reference Melinex with 100 µm of thickness). Conductive z-axis adhesive tape was from 3M (reference 9703).

5.2.1.2. Samples preparation

The green solvent CPME was used for SEBS (B. F. Gonçalves et al., 2016), and DMF solvent for PVDF (Ribeiro et al., 2018) and TPU (Zheng et al., 2017) films preparation. First, the CNTs powder was mixed with the respective solvent with a ratio of 0.5, 1, 2 and 5 wt.% for PVDF, and 2 and 5 wt.% for SEBS and TPU. The mixtures were put in an ultrasound bath for 3 h for good CNTs dispersion. Then the polymers were added to the CNTs solutions: 1 g of SEBS for each 6 mL of CPME; 1 g of PVDF for each 9.5 mL of DMF; and 1 g of TPU for each 7 mL of DMF. The solutions followed a magnetic stir for 2 h at room temperature. The fabrication of the films was performed by pouring the solutions in a glass and spread with a doctor blade. Solvent evaporation was done overnight at room temperature for the SEBS-based composite, and at 210 °C for 15 min for the TPU and the PVDF-based ones. After full solvent dry out, the obtained thicknesses were between 35 to 80 µm.

5.2.1.3. Device fabrication

To test the produced films for piezoresistive operation an array of 8 sensors was created. Interdigitated patterns were used for the sensors, where a sample of each prepared film were deposited, as shown in Figure 5.8. Each sensor has an individual terminal and a common terminal. The interdigitated sensors were 9.3×5.5 mm, with a 300 µm interdigitated gap.

---

[1] Demo video available in the supporting information of the article: https://ars.els-cdn.com/content/image/1-s2.0-S026635381931293X-mmc2.mp4

Conductive Pattern   **Piezoresistive Matrix**
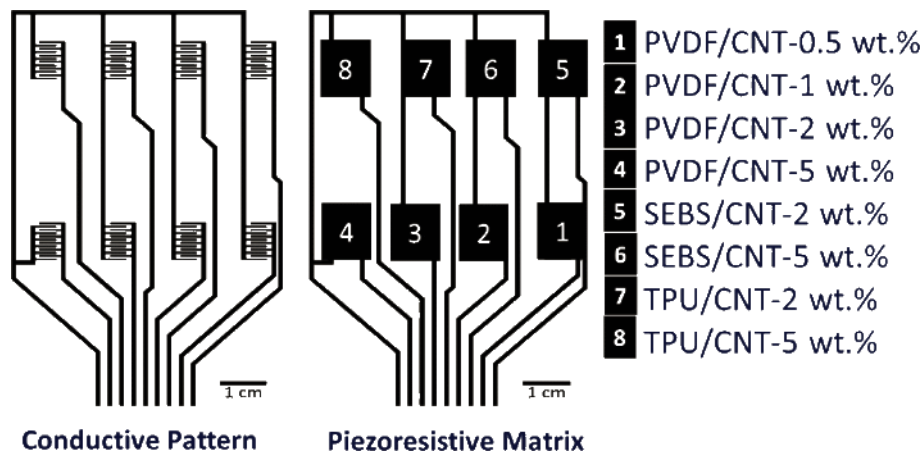
Figure 5.8.   Pattern used for the array of piezoresistive sensors. Reprinted with permission from (J.R. Dios et al., 2019), copyright © 2019 Elsevier Ltd. All rights reserved.

The layout was printed with silver ink on the PET film by screen-printing technique. The film was placed in the oven for 1 h at 120 °C to cure and sinter the ink. Then, the prepared films were placed over the interdigitates and secured with tape. To connect the array of sensors with the external circuit, a flexible flat cable (FFC) was attached to the terminals using the conductive z-axis adhesive tape.

A large piece of polyurethane foam was placed on top of the sensors, together with a 1 cm-thick plastic board, to make the pressure on the sensors uniform.

5.2.1.4. Electrical circuit

To read the 8 sensors, a current source was implemented with an instrumentation amplifier (IA), and an analog multiplexer (AMux) to permutate through all of the sensors, as visible in Figure 5.9.
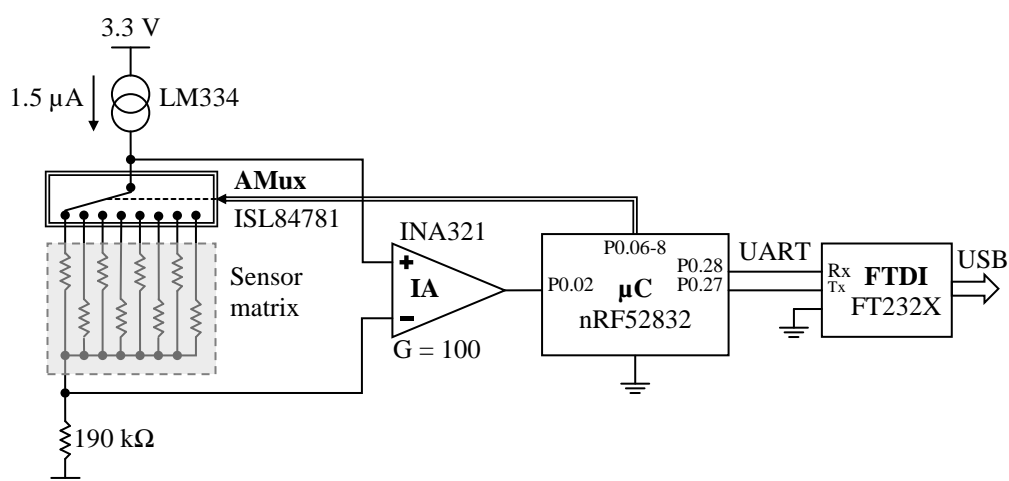
Figure 5.9.   Schematic representation of the electrical circuit implemented to read the 8-sensor array. Reprinted with permission from (J.R. Dios et al., 2019). Copyright © 2019 Elsevier Ltd. All rights reserved.

A current source of 1.5 µA (Texas Instruments LM334) ensures a constant current on the sensors, to granting linearity of the voltage drop. The analog multiplexer (Intersil ISL84781) selects the sensor to be read, and the instrumentation amplifier (Texas Instruments INA321) amplifies the voltage drop of the selected sensor, with a gain of 100. The 190 kΩ in the negative input of the instrumentation amplifier instrumentation amplifier ensures that input voltage is higher than the minimum operating voltage. The used microcontroller (µC) was a Nordic Semiconductor (nRF52832), which controlled the analog multiplexer selection and acquired the voltage output from the instrumentation amplifier through the inbuilt ADC at a rate of 100 sps, with 8 bits. The microcontroller sends the acquired data via UART to an FTDI (FT232X), converting it to USB and connecting to a computer where a Java application plots the data.

5.2.1.5. <u>Results and discussion</u>

An application as a pressure floor sensor was used to evaluate the developed sensor array, where a person walks over the sensors, as shown in Figure 5.10.

Figure 5.10. Sensor array in operation as walking detection device.

Sensors were considered to be submitted to the same pressure, due to the foam and plastic board on top. From the prepared composites, the PVDF-based one was rigid, while the TPU and SEBS were soft and flexible, and the SEBS was also very adherent to surfaces. In addition, due to the differences in the wt.% of CNTs, different results were expected for the different sensors.

When the sensors are not being pressed, since they were simply placed on the interdigitated patterns, their connection with the electrodes is very poor, normally causing the instrumentation amplifier to saturate (at around 3 V). When pressing the sensors, the contact with between the polymer composites and the electrodes increases, reducing resistance. Therefore, this prototype does not evaluate the piezoresistive response of the polymer composites alone, but also the mechanical piezoresistive behavior.

Figure 5.11 shows the result of the output voltage for the sensors during operation as a walking detection device. A demo video is also available in the supplementary data of the article[1] (J.R. Dios et al., 2019).
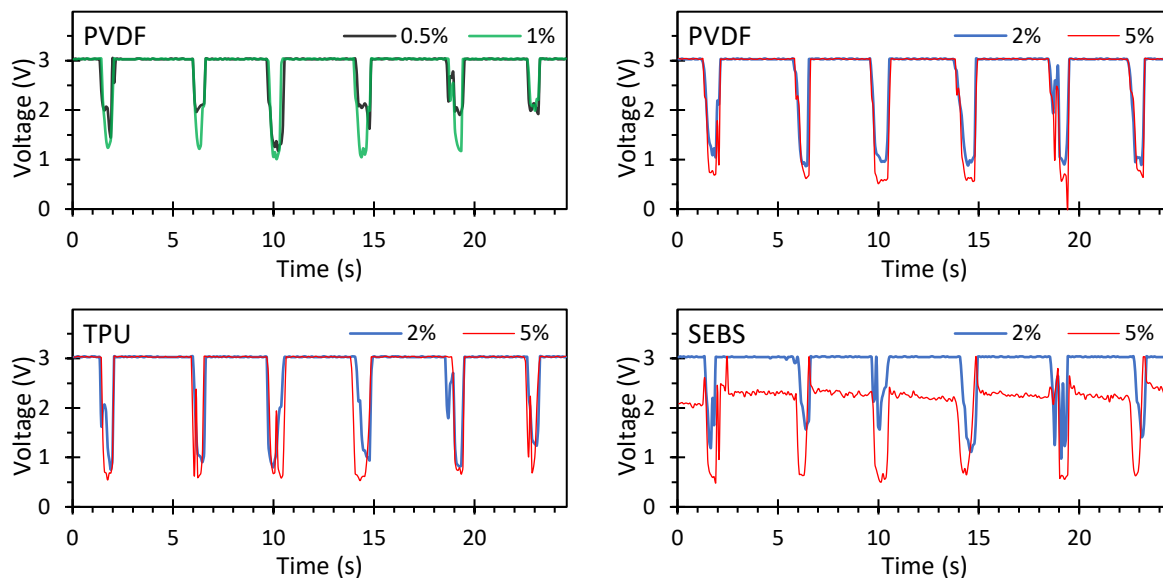
Figure 5.11. Output voltage of the sensors during user operation as a walking detection device.

In the PVDF-based composite, the CNTs wt.% is particularly noticeable for the 0.5 and 1 wt.% concentrations. But for the 2 and 5 wt.%, only a slight difference in conductivity is visible. Similar results show the TPU-based composite sensors. However, for the SEBS-based composite, the behavior was very different. Due to its adherent property, it is visible that the sensor with 5 wt.% of CNTs never causes the saturation of the instrumentation amplifier, meaning that composite film never fully detaches from the electrodes. Probably the same happens with the 2 wt.% one, but as it has lower conductivity, it is still enough to cause the saturation of the instrumentation amplifier. The lower conductivity of the 2 wt.% samples is evident because of the negative peaks not as significant as in the 5 wt.% CNTs sample.

Towards these results, it is concluded that any of the developed sensors is suitable to monitor the walking movements.

In this work, particular emphasis is given to the SEBS-based composite sensor, since the utilized solvent for this material, CPME, is an environmentally friendly chemical, contributing this work towards the eco-sustainability (B. F. Gonçalves et al., 2016).

---

1 Demo video available in the supporting information of the article: https://ars.els-cdn.com/content/image/1-s2.0-S026635381931293X-mmc2.mp4

The chemical and mechanical stability of PVDF is higher, but the stretchability of SEBS and TPU is considerably higher, being PVDF-based composite sensors more indicated for rigid piezoresistive applications, and SEBS and TPU for flexible ones.

5.2.1.6. <u>Conclusions</u>

Polymeric composite films from rigid (PVDF) to stretchable (TPU and SEBS), with reinforced CNTs have been studied. The inclusion of CNTs provided materials with electrical properties, allowing the development of piezoresistive materials.

Polymeric matrix composites from rigid (PVDF) to stretchable (TPU and SEBS) have been studied reinforced with CNT to provide electrical properties that allow the development of piezoresistive materials. Different filler contents with 2 and 5 wt.% were experimented for each material. Additionally, for PVDF-based composite it was used 0.5 and 1 wt.%, too.

An electronic application was developed for human walking detection, consisting in 8 interdigitated sensing areas, where a different composite film was deposited in each. The implemented system allowed for measuring all the sensors in real-time, and displaying it in a computer.

Although exhibiting different piezoresistive responses, all the polymers were capable of identifying and measuring the walking movement of a human.

This work demonstrated the relevance of the integration of the fabricated composite sensors in the future applications.

5.2.2. Endoscope prototype with PLA reinforced with CNTs for deformation sensing

The development of polymer-based composites in the last years has led to a whole new generation of electronic devices, such as sensors, actuators, electromagnetic shielding, energy systems, and self-healing materials (Chung, 2019). Biopolymers are receiving a growing attention for the lower environmental impact, such as the polylactic acid (PLA) (Farah et al., 2016) due to the mechanical properties, environmental stability and biocompatibility (Ning et al., 2018; Scaffaro et al., 2018). PLA can be functionalized through the reinforcement of specific particles in order to create electroactive devices, such as sensors (Scaffaro et al., 2018).

The present work proposes the fabrication of piezoresistive film sensors based on PLA for stretching detection. Functionalization of the polymer is carried out by the inclusion of CNTs, giving the composite an electrical behavior.

To assess the functionality of the developed devices, an endoscope is used as a case study, where the CNTs/PLA sensors are attached to the tip of the endoscope to detect orientation and amplitude of bending. The variation of the electrical resistance of the sensors is low, thus a robust electronic solution was developed based on a Wheatstone bridge with a current source and a differential amplifier to successfully measure the variation of the sensors.

The system was tested and the applicability of the developed sensors to measure the endoscope during bending was demonstrated. Although the application involving an endoscope can hardly be considered a user interface nor a TUI, the project is still pertinent since the developed sensors and electronics can integrate any other type of devices specifically designed for user interfacing, in a very similar approach as the bend and twist sensor tapes developed by Balakrishnan et al. (1999) or Dementyev et al. (2015).

This prototype resulted in a journal article (Jose R Dios et al., 2020), and a demo video is also available in the footnote link[1].

5.2.2.1. Materials

PLA was acquired from NatureWorks Ingeo (reference 3052D), and CNTs were purchased from Nanocyl (reference NC7000). To dissolve the polymer, dichloromethane (DCM) was used, which is an industrial solvent, and the least toxic of the chlorinated solvents (Tobiszewski & Namieśnik, 2015), not classified as affecting the ozone according to the Montreal Protocol. Conductive carbon glue utilized was Electric Paint from Bare Conductive).

5.2.2.2. Sample preparation

A solution consisting in CNTs (6 wt.% relatively to the PLA) dispersed in 8 mL of DCM solvent was prepared and placed in ultrasound bath for 3 h to achieve good dispersion and deagglomeration of the CNTs. Then, 2 g of PLA were added to the solution, which was magnetically stirred at room temperature for 2 h. The polymer film was created by solvent casting technique on a glass and dried for 12 h at 20 °C. After complete solvent evaporation, the resulting film had a thickness between 37 to 47 μm.

---

1 Link of the demo video: https://youtu.be/rh42SO5ItQE

5.2.2.3. Device fabrication

The prepared PLA reinforced with CNTs film was tested for bending sensing in the tip of an endoscope, which can allow the operator to perceive the movements of the endoscope when inside the patient's body.

The film was cut in four stripes with dimensions of 35 × 5 mm. Each stripe was attached to the outer side of endoscope, as shown in Figure 5.19*a*. For each piezoresistive stripe, two pieces of adhesive copper foil were glued to the endoscope, and the film stripes were connected to them using the conductive glue. In the copper foil pieces was soldered a 30 AWG wire, and the wires wrapped around the endoscope or passed through the interior of it. Figure 5.19*b* shows the real assemblage.

(a)   *(b)*
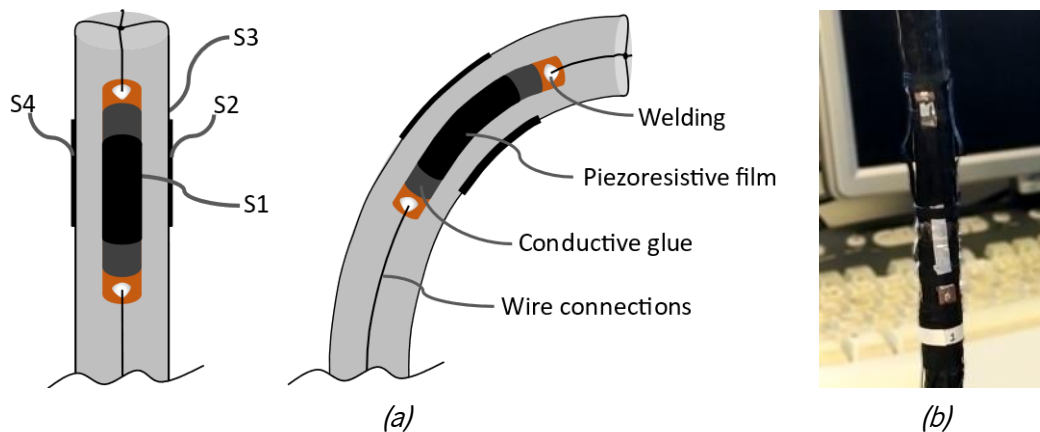
Figure 5.12.   Endoscope with piezoresistive sensors: *(a)* schematic representation and *(b)* real implementation. *(a)* Reprinted with permission from (Jose R Dios et al., 2020), copyright © 2020 WILEY-VCH GmbH.

After the sensors were placed in the endoscope, measurements to survey the resistance of the sensors were made and their resistance change during endoscope bending. The obtained value was between 40 to 50 kΩ for the initial resistance, with a variation lower than 1 kΩ.

5.2.2.4. Electrical circuit

Since the variation of these sensors is very small (lower than 2 %), a more sophisticated electric circuit was necessary. A current source with a differential amplifier was used, as shown in Figure 5.13. The constant current source makes the voltage drop in the sensor linear with its resistance. A resistive Wheatstone bridge provides the offset voltage to the differential amplifier, being amplified only the resistance change in the sensor. Four equal electrical circuits were prototyped, one for each sensor. The downside of the developed circuit is the necessity for its physical calibration through the trimmer potentiometers, which were all multi-turn with 12 turns (84WR100KLF from TT Electronics).
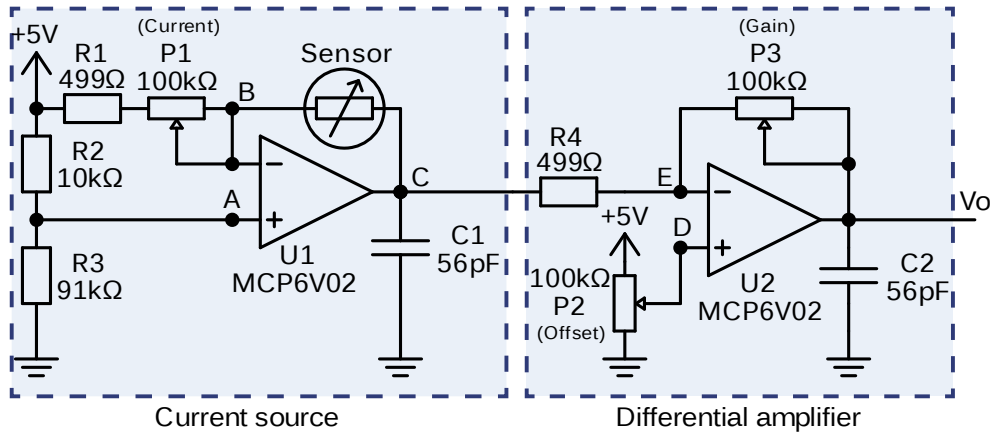
Figure 5.13. Implemented circuit to measure the resistance of the sensors. Reprinted with permission from (Jose R Dios et al., 2020), copyright © 2020 WILEY-VCH GmbH.

The circuit was powered with 5 V from the USB power. The operational amplifiers used were Microchip MCP6V02. The circuit was projected to allow at least 0.5 V margin from the supply limits (0.5 to 4.5 V) in the inputs of the operational amplifiers. The voltage in nodes A and B is 4.5 V (by R2 and R3 voltage divider). R1 limits the maximum current in the sensor (to avoid overcurrent), and P1 sets the current for the constant current source. P2 establishes the voltage to be subtracted from the current source output (this allows to remove the voltage corresponding to the base resistance of the sensor). And P3, together with R4, define the gain (G) of the circuit.

The output voltage V_o is linear with the resistance, and is given by:

$$V_o = V_{offset} + G \cdot R_{sensor} \tag{5.2}$$

in which R_{sensor} (Ω) is the resistance of the sensor, and V_{offset} (V) and G can be calculated as follows:

$$V_{offset} = V_D + \frac{P_3}{R_4}(V_D - V_A), \qquad G = \frac{P_3}{R_4} \cdot \frac{5 - V_A}{R_1 + P_1} \tag{5.3}$$

being V_A and V_D the voltages at nodes A and D, respectively.

The tuning of the three potentiometers is very sensitive because of the high gain of the amplifier. The calibration of the circuit should be performed as follows:

- Bend the corresponding sensor to its maximum resistance position and adjust P1 so that the voltage in node C reaches 0.5 V;

- Unbend the sensor back to its position of minimum resistance, and adjust P2 until voltage in node D is equal to node C;

- Once again, bend the sensor to its maximum resistance, and adjust P3 until the output voltage Vo is 4.5 V.

After correctly calibrated, the output voltage Vo will swing between 0.5 V (sensor at minimum resistance) to 4.5 V (sensor at maximum resistance).

Following the differential amplifier stage, the output voltages of the 4 sensors were connected to a microcontroller (Microchip ATmega328P) running at 16 MHz. The inbuilt ADC of the microcontroller was used to acquire samples at a rate of 9.8 ksps and with 8 bits of significance, but averaging each 500 samples to reduce noise. Data was then sent to a computer via a USB to UART converter, where a Java application showed the data acquired by the sensors in an interactive interface.

5.2.2.5. <u>Results and discussion</u>

To test the developed system, it was set up the endoscope and circuit as visible in Figure 5.14. The computer displayed the data acquired from the sensors in two different modes: plotting the raw data (Figure 5.14*a*) and showing a graphical representation of the sensors using rectangles (Figure 5.14*b*), in which the amplitude registered by each sensor is given by the color of the rectangle.

(a)   *(b)*
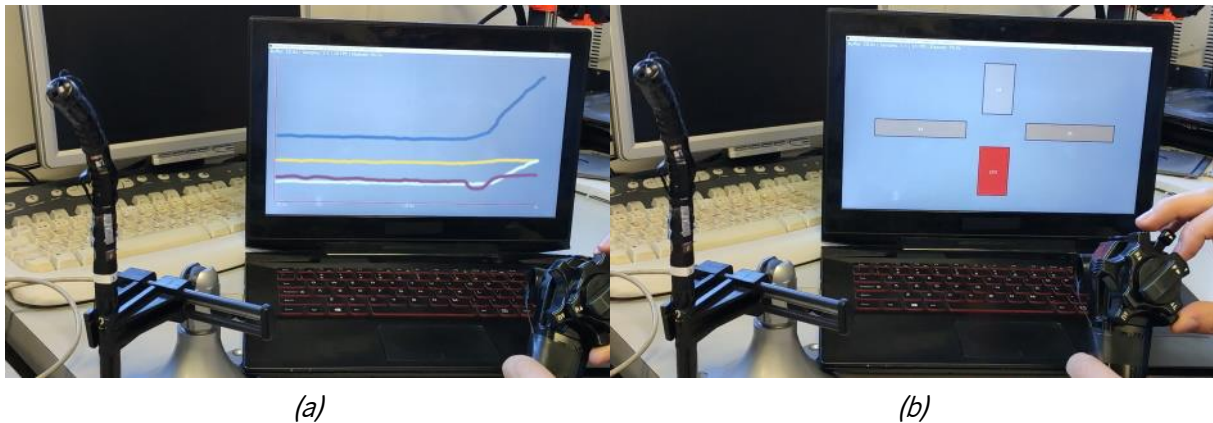
Figure 5.14. Endoscope prototype in operation: *(a)* plotting the output voltage and *(b)* showing a graphical representation of the movement. Reprinted with permission from (Jose R Dios et al., 2020), copyright © 2020 WILEY-VCH GmbH.

A demo video of the system can be watched using the footnote link[1].

The output voltages of the circuit relative to each sensor are shown in the graph of Figure 5.15. It is possible to identify correctly the direction of the movement of the endoscope by analyzing which sensors are being stretched. Yet, the graph also allows to take conclusions about the calibration of the circuits, particularly in the case of the sensor S4, which registers a minimum voltage of around 3 V. This indicates that the tunning for the offset potentiometer is slightly off, which is also the cause of it reaching the saturation of the amplifier. For the sensor S3, a little less of gain would be enough to prevent saturation.

---

1 Link of the demo video: https://youtu.be/rh42O5ItQE
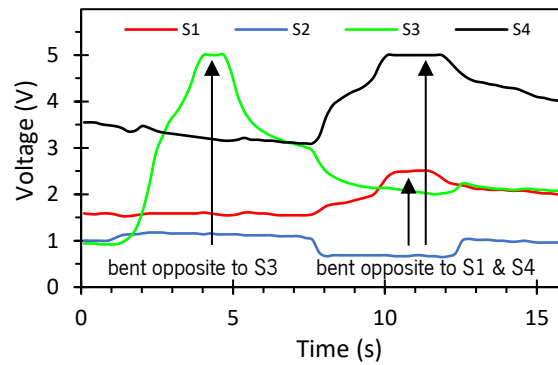
Figure 5.15. Response of the piezoresistive sensors in the endoscope. Reprinted with permission from (Jose R Dios et al., 2020), copyright © 2020 WILEY-VCH GmbH.

Nevertheless, despite the complexity, the implemented circuit proved to be very efficient in detecting the small variations in the resistance of the sensors.

Regarding the sensors, when stretched, the resistance increased quickly, but it was noticeable that they would not instantly recover when returning back to the unstretched state, as we can see by the curves of S3 and S4: the rise is much faster than the drop.

Relatively to the physical properties of the sensors, the PLA-based composite sensors were very fragile and, though being somewhat stretchable, easy to tear. Therefore, to attach them to the endoscope, it was necessary to choose a proper location where the endoscope did not bend excessively, otherwise the film stripes would easily tear apart. Also, a fragility of the PLA film is its tendency to wrinkle and get scratches that weaken the film. For these reasons, the endoscope was not the best application for the CNTs/PLA film sensors. More suitable applications for this type of sensors are applications involving short deformations, where full potential can be taken from the precision of these sensors without compromising their physical integrity.

5.2.2.6. Conclusions

Piezoresistive sensors were fabricated by doctor blade technique through the inclusion of CNTs with PLA polymer. Four sensors were attached the tip of an endoscope for real-time monitoring of the motion of the endoscope when inside of a patient's body. The variation of the electrical resistance of the sensors was lower than 2 %. An improved version of the resistive Wheatstone bridge was implemented using a constant current source to linearize the output, and a differential amplifier (a simplified version of the instrumentation amplifier) to amplify only the variation of the sensors. The tunning of the circuit was performed for each sensor, and the output voltage was acquired by a microcontroller and sent to a computer.

The response of the sensors was suitable, being easy to identify the bending orientation and intensity of the endoscope. It was noticed a delay in the capacity of the sensors to recover the initial state after being stretched. However, the developed sensors were fragile and easy to tear, and probably not best suited for an endoscope application, but to applications involving smaller deformations. An endoscope, which shows large deformations, is probably best fitted with an elastomer-based composite film.

Nonetheless, the applicability of the developed materials is wide, whether for diagnosis tools or for user interfacing (which an endoscope certainly is not), in platforms such as 3D bend and twist sensing tapes (Balakrishnan et al., 1999; Dementyev et al., 2015).

5.2.3. Glove prototype with SEBS and graphene-based composites for stretch sensing

Carbonaceous composites with tailored electroactive properties enable the creation of high-performance polymer-based sensors. There is an increasing need for highly stretchable and compressible piezoresistive materials (Liu et al., 2017, 2016). Applications for polymer piezoresistive polymer-based materials range from structural health monitoring (Das & Saha, 2018), mechanical and biomedical applications (Y. Lu et al., 2019; Stassi et al., 2014), wearables (T. Yang et al., 2017), and human and robotic interface devices (Y. Hu et al., 2018; Trung et al., 2017).

In this work, a composite film based on styrene-*b*-(ethylene-co-butylene)-*b*-styrene (SEBS) with reduced graphene oxide (rGO) was developed and tested for piezoresistive stretching sensors. SEBS is a thermoplastic elastomer, so the developed composite shows very high stretchability and piezoresistive sensibility. Additionally, CPME solvent was used, which is considered to be eco-friendly. To demonstrate the applicability of the developed composite, a hand glove prototype was implemented, capable of monitoring the movement of each finger.

This work is covered by the publication (Pedro Costa, Gonçalves, et al., 2019). A demo video is also available in the supporting information of the article[1].

---

1 Demo video available in the supporting information: https://pubs.acs.org/doi/suppl/10.1021/acsami.9b19294/suppl_file/am9b19294_si_001.mp4

5.2.3.1. Materials

SEBS copolymer was acquired from Dynasol Elastomers (reference Dyne 108C), rGO with 99 % of purity was obtained from The Graphene Box, and the used solvent was CPME, furnished by Carlo Erba Reagents. CPME is considered an environmentally friendly solvent. Conductive glue utilized was Electric Paint from Bare Conductive). Ultrasonic bath equipment was ATU ATM40-3LCD. Digital multimeter used was a Fluke 117.

5.2.3.2. Sample preparation

To prepare the sample, rGO was dissolved in 12 mL of CPME with a concentration of 4 wt.%, and dispersed in an ultrasound bath for 3 h at room temperature. Then, 2 g of SEBS was added to the solution, and mixed under magnetic stirring for 2 h at 30 °C. Then, the solution was poured on a glass and a composite film was fabricated by doctor blade technique. After 12 h at room temperature, the solvent was fully evaporated, the film was peeled off from the glass. It presented a thickness between 30 to 60 μm.

5.2.3.3. Fabrication of the device

The rGO/SEBS composite is very flexible and stretchable due to the elastomeric property of SEBS. A glove was used for prototyping, to sensorize the fingers. A strip with dimension of 12 ×0.8 cm was cut and attached on the outer side of each of the glove's fingers, as shown in Figure 5.16. The strips were properly secured with adhesive black tape.
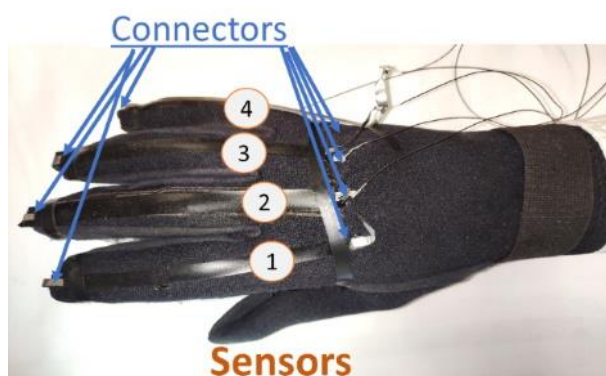
Figure 5.16. Glove with rGO/SEBS strip sensors on the fingers. Reprinted with permission from (Pedro Costa, Gonçalves, et al., 2019), copyright © 2019, American Chemical Society.

To connect film strips to the electric circuit, aluminum foils were attached to the endings of the strips, with conductive glue. Thin flexible wires attach to the aluminum foils mechanically and connect to the

external circuit. It is not a robust solution that does not give the user the freedom to move the hand away freely, but it is sufficient to demonstrate the electrical results.

5.2.3.4. Electrical circuit

These sensors are expected to show a large variation in resistance, since they have an elastomeric base and are highly stretched in the glove application. Measurements with a multimeter on the terminals of the sensors indicate an initial resistance around 10 to 20 MΩ. Therefore, a simple circuit was implemented with only a resistor voltage divider, shown in Figure 5.17. A 10 MΩ resistor was placed in series with the sensor, producing an intermediate voltage that is roughly half of the voltage supply.
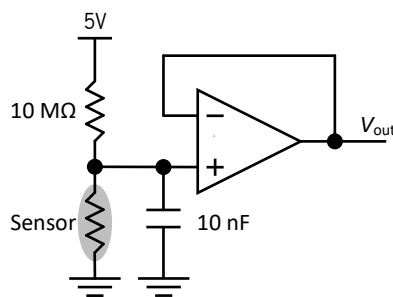
Figure 5.17. Electric circuit used to read each sensor. Reprinted with permission from (Pedro Costa, Gonçalves, et al., 2019), copyright © 2019, American Chemical Society.

A 10 nF capacitor was placed in parallel with the sensor to create a low-pass filter (LPF), filtering the $50/60$ Hz grid noise and acting as anti-aliasing filter. The cutoff frequency of the LPF filter is given by:

$$f_{\text{cutoff}} = \frac{1}{2\pi RC} \tag{5.4}$$

in which R (Ω) is the resistance of the sensor in parallel with the 10 MΩ, and C (F) is the capacitance of the capacitor of the filter. Thus, f_{cutoff} is between 1.6 to 3.2 Hz, depending on the resistance of the sensor.

A voltage follower amplifier (Microchip MCP6024) provides impedance isolation. The output voltage V_{out} is connected to the analog pins of a microcontroller (Microchip ATmega328P), where the inbuilt ADC converts data to digital with 8 bits. The microcontroller sends the data to a computer, through a USB to UART converter (CH340), where a Java application plots the graph of each sensor.

It is important to draw attention to the non-linearity of the measured output voltage. To obtain a linear measurement, it was used the Ohm's law to estimate the resistance of the sensors based on the read voltage, by software.

5.2.3.5. <u>Results and discussion</u>

The developed prototype, although with rudimentary assemblage, allowed to read the movement of the fingers of the user. Figure 5.18 shows the output voltage V_{out} (V) for each sensor being displayed on the screen of the computer when the user is interacting with the glove. As expected, the voltage rises when the finger is bent.
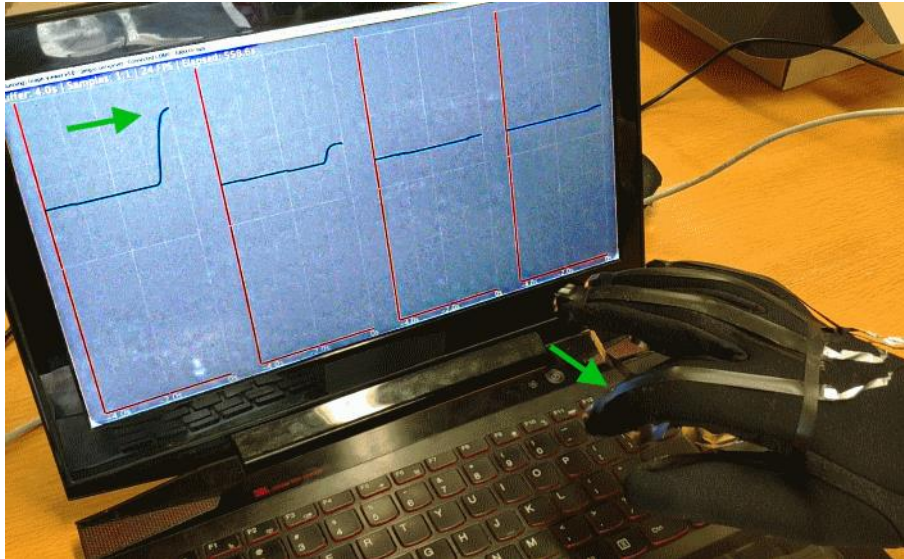
Figure 5.18.   User interacting with the glove, and the output voltage of the sensors being displayed in the screen of the computer.

Based on the voltage, the resistance of the sensors was calculated. In Figure 5.19 is shown the resistance variation of the sensors during individual finger bending and simultaneous bending of all fingers. The difference in the maximum value for the sequential to the simultaneous finger bending is related to the user's inability to bend the fingers individually as much as when closing the hand, due to human anatomy.

(a)   *(b)*
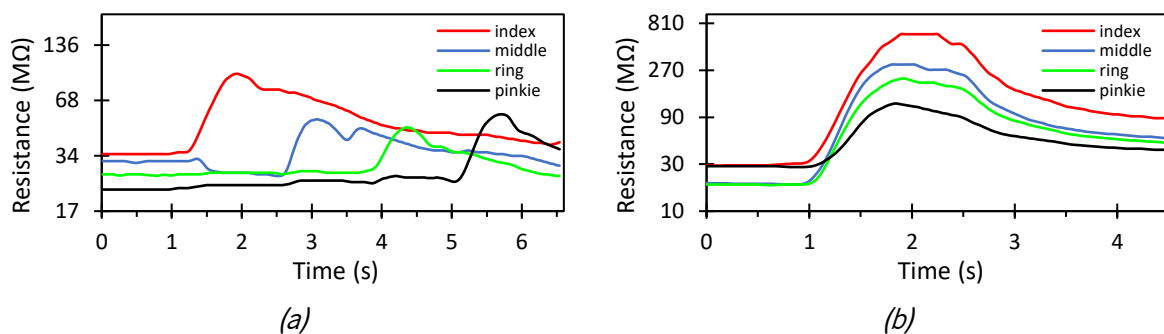
Figure 5.19.   Resistance measured for each sensor when all fingers are bent *(a)* sequentially and *(b)* simultaneously.

It is visible that the initial resistance of the sensors is between 20 to 30 MΩ, and that the sensors respond with very large change in the resistance, reaching up to 800 MΩ. This provides good sensibility and allows for very simple circuits. However, the recovery of the sensors after being stretched is not instantaneous, taking up to minutes to fully reach the initial resistance. This is caused by the slow motion of SEBS after being elongated. Nonetheless, it is possible to eliminate the slow recovery by software, comparing the theoretical recovery of the film with the actual measured value.

5.2.3.6. Conclusions

The developed polymer composite with the inclusion of graphene-based material in SEBS showed excellent properties for sensing materials, such as flexibility, stretchability and resistance variation. The green solvent CPME was used, a common request in material developments nowadays. The large piezoresistive response obtained made it easier to do the instrumentation of the sensors with simple circuits, such as the used resistive voltage divider. The functioning of the material has been demonstrated in an application involving a glove to determine the bending position of each finger. The downside of the developed composite sensors was the inability for the sensor quickly recover to the initial resistance value it has been heavily stretched, sometimes reaching up to minutes.

Nevertheless, the high stretchability of the developed composite and the corresponding acquisition system are very important in the development of shape-changing sensing interfaces.

5.2.4. Piezoresistive touchpad prototype for drawing and writing digitalization

In this prototype, the main objective was the demonstration of a proof-of-the-concept of a platform capable of digitalizing the drawing or writing with a normal pen or pencil, and that could fit in the cover of a book. Other projects use special pens (Jing et al., 2017; Shintani et al., 2021) or smartphone cameras (Burie et al., 2015) to digitalize handwriting.

A multi-layer platform was fabricated based on printed electronics and Velostat and EeonTex piezoresistive films, with an air gap separating the top from bottom layers. It was used the 4-wire touch technology to read the touch location and pressure. Since this was a proof-of-the-concept platform, it was projected for single touch detection, which does not allow the user to place the hand on the platform

while writing or drawing. The produced prototype had an A5-size surface with thickness of 2.3 mm, being flexible enough to be fitted on the cover of a book.

It was possible to digitalize the user writing or drawing on the piezoresistive platform with a pen, but the produced system deserves improvements to increase accuracy. This is an important technology to have available in the development of TUIs, since it can be considered itself a TUI.

5.2.4.1. <u>Materials</u>

In this experiment, the PET film was used was acquired from Lohmann Technologies UK Ltd. (reference Melinex with 100 μm of thickness), silver ink for screen-printing was obtained from DuPont (reference 5025), and piezoresistive films used were Velostat and EeonTex. Velostat was purchased from Adafruit (reference 1361) and EeonTex fabric from Sparkfun (reference COM-14111). Polypropylene film with 500 μm of thickness was acquired from Stapes (reference 179418). *z*-axis conductive adhesive tape was from 3M (reference 9703).

A JP Selecta oven, model 2005165, was used for thermal treatment. The apparatus for screen printing was homemade, and the polyester mesh used had $62/64$ threads/cm.

5.2.4.2. <u>Touchpad fabrication</u>

To quickly explore the fabrication of this platform, a printed layout from a previous project was used, which served as a quick proof-of-the-concept of this platform without the need of ordering a new screen tile. Thus, the geometry used was not optimal. The reused tile was from a large capacitive touchpad with dimensions of 20×14 cm, and 19 rows $\times$ 27 columns electrodes in the diamond pattern.

First, top and bottom layers were screen-printed on a PET film each, and thermally annealed for 30 min at 120 °C. However, for the 4-wire resistive touchpad topology, only the first and last rows and columns are used. Thus, a 50 μm adhesive film was glued on top of the electrodes to disable them, leaving just the first and last rows and columns. On them, *z*-axis conductive adhesive tape was placed so that a Velostat film could connect the first to the last rows and columns. These are the first three top and bottom layers shown in Figure 5.20. The Velostat films, due to their resistive characteristic, have the function of linearly distribute the electric field imposed by the electrodes.

PET (100 μm)

Printed silver (10 μm)

Velostat (100 μm)

EeonTex (800 μm)

z-axis conductive
tape (50 μm)

Air gap

PP (500 μm)
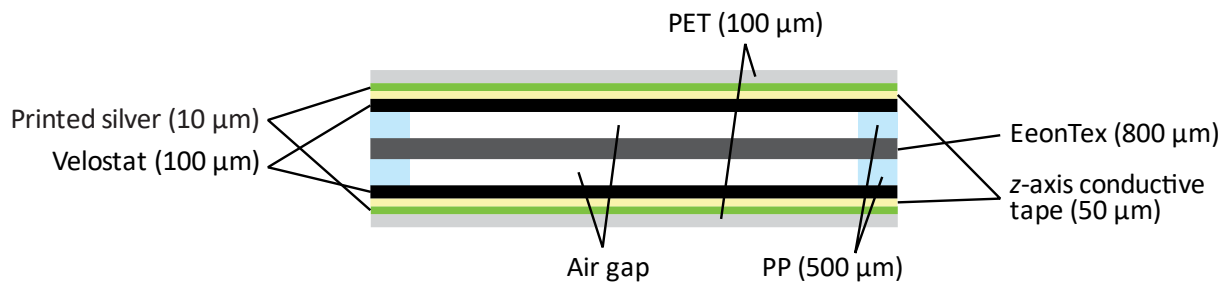
Figure 5.20. Layers constituting the piezoresistive platform.

Then, a separator between the top and bottom layers was necessary to build and prevent them from randomly touching each other. It was achieved by the use of two thick polypropylene (PP) frames, with thickness of 500 μm, and a piezoresistive EeonTex textile in between. The several layers were manually tensioned and attached to the PP frames with super glue, which kept the correct tension in the top and bottom layers. Any eventual connection from the top to the bottom layers is very weak, unless the user intentionally presses it. Finally, 1 mm-pitch flexible flat cables (FFCs) were attached to the printed terminals using *z*-axis conductive adhesive tape.

Figure 5.21 shows the assembled prototype.
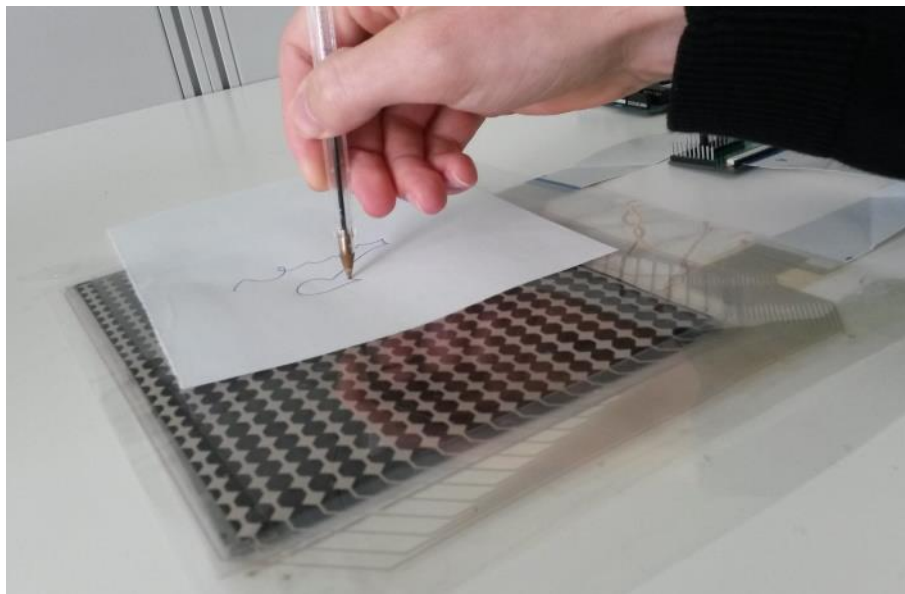
Figure 5.21. Aspect of the assembled piezoresistive platform.

A sheet of paper is supposed to be placed on top of the platform for the user to write in. It is important to notice that the used polymer films do not get scratched during the user writing or drawing, which is particularly important for the PET and Velostat layers, and ensures that the prototype does not quickly degrade with use.

5.2.4.3. <u>Electrical circuit</u>

To control the piezoresistive platform, a microcontroller (µC) from Microchip (ATmega328P) was used. It converts the pressure applied on the piezoresistive platform by the user to digital data, including coordinates of the touch point and pressure level. The four wires of the platform were directly connected to the analog pins of the microcontroller, without the need for any extra hardware, as shown in Figure 5.22.The acquired data is then sent to a computer via USB, using a converter CH340. In the computer, an application in Java draws the read points in real-time.
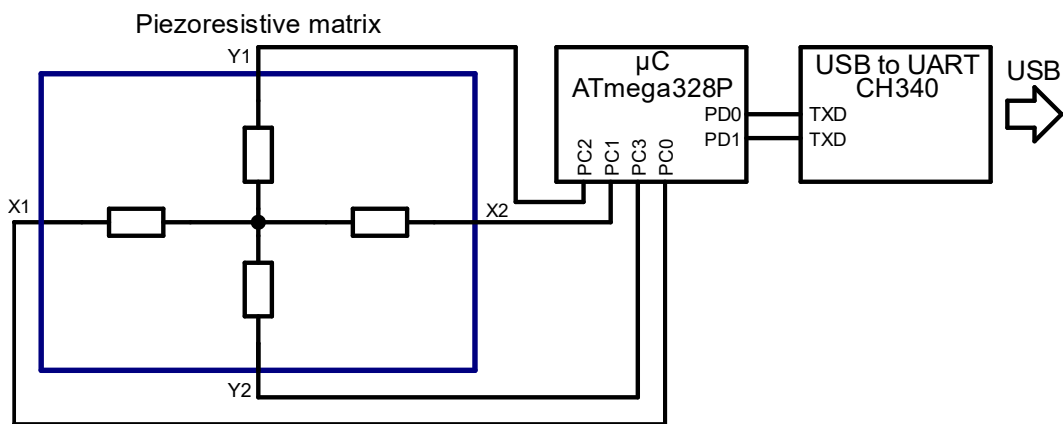
Figure 5.22. Electrical circuit for the piezoresistive platform.

The piezoresistive matrix is operated using a simple principle. Initially, a voltage differential of 5 V is applied from pin X1 to X2, while pins Y1 and Y2 are set to high impedance state. During this moment, pin Y1 performs an analog read with the ADC. Since no current flows into or out of the pin, it will pick the corresponding voltage present on the location where the user is pressing the platform. This gives the coordinate of the touch in the *x*-axis. To obtain the coordinate in the *y*-axis, it is done the same procedure, the but with the electric field developed across Y1 to Y2.

It is also very important to estimate the pressure exerted on the piezoresistive matrix, because when the user is not pressing it, it will just read any random point coordinates. Therefore, when pressure is below a certain threshold, that point is discarded. To measure the pressure, it is developed a voltage differential of 5 V from X1 to Y1 pins while X2 and Y2 pins are configured to high impedance state. The difference between the analog read from pin X2 to pin Y2 gives a value inversely proportional to the pressure.

To reduce noise on detection, each sample sent to the computer is the actually the average of four samples. Coordinates and pressure transfer to the computer were implemented using 1 byte of data (0 – 255 range). Coordinates were sent as read, but pressure was calculated using the expression

255 – (ADC(X2) – ADC(Y2)) to make it proportional to the exerted pressure in the platform, in which ADC() was the value obtained from the conversion of the ADC.

5.2.4.4. <u>Results and discussion</u>

The fabricated piezoresistive platform is flexible and physically robust, as visible in Figure 5.23, as proposed in the initial objectives. It can be fitted in the cover or back cover of a notebook, where flexibility is necessary without compromising the functionality of the system.
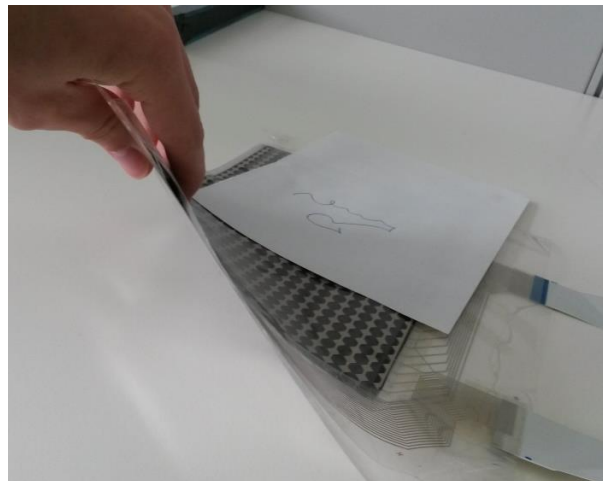
Figure 5.23.   Flexibility of the piezoresistive platform.

However, the drawing and writing digitalization still deserve improvements. It is possible to correlate the digitalized image to the original, as seen in Figure 5.24, but the digitalized image is still not very truthful. It is possible to identify the tendency of the matrix to a specific spot, by the gray blur in the image. This is the average of the several locations where the top and bottom layers touch, probably due to the manual assembly of the platform, but also an indicator that the air gap is not being as effective as initially projected.

Velostat is a very flexible film, showing some stretchability as well. However, it can be deformed permanently when stretched. And, in fact, it has been noticed that the Velostat film developed wrinkles after being tensioned and attached to the PET film, making it to become slightly loose. Moreover, the PET film, which holds the Velostat film, has also turned slightly loose. As a consequence, when the tip of the pen or pencil slides over the piezoresistive platform, it drags the PET and Velostat films together with it, which shifts the position of the perceived touch. This is particularly visible in the drawn star on the bottom left corner, which was the begin and end of the trace done with the pen. In the digitalized shape, the end did not coincide with the begin, though it did on paper. Same happened on the bottom right corner. When

the pen changed direction, it pulled the PET and Velostat films in different direction, resulting in overlapping lines that were not supposed to be overlapped.

(a)   (b
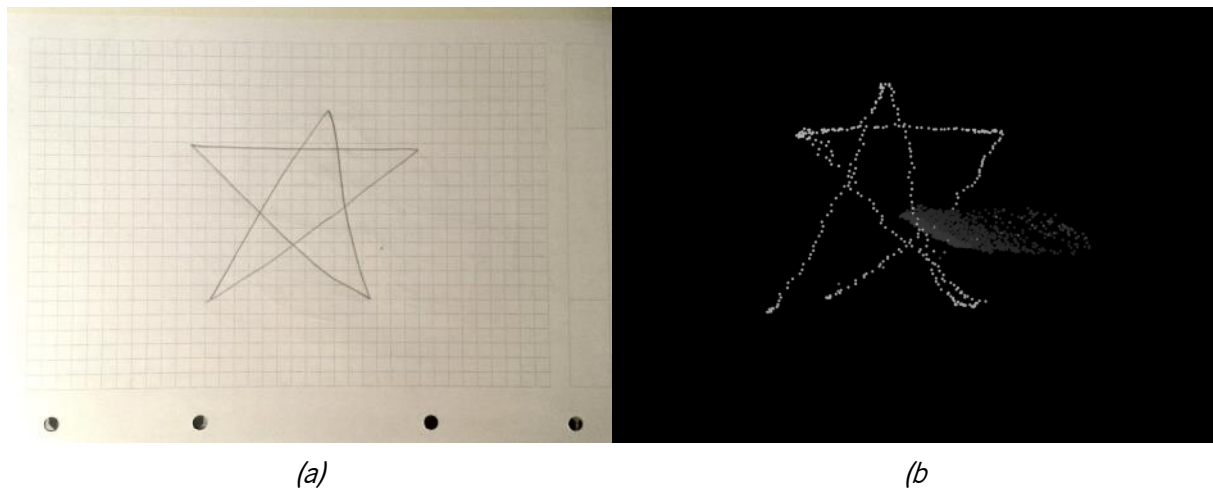
Figure 5.24.   Digitalized image using the piezoresistive platform: *(a)* original drawn by the user on paper, and *(b)* result of image digitalized.

Another reason for the distortion of the digitalized image might be linked to the possibly of the sheet resistance of Velostat do not be uniform. A linearizing conductive pattern constituted by parallel lines printed on the back of the Velostat film can improve this.

In terms of usability, one major advantage for this platform would be to allow the user to place the hand on the platform while writing. This can be done by the use of multitouch technology.

5.2.4.5. <u>Conclusions</u>

In this experiment, it has been fabricated a flexible piezoresistive platform based on the 4-wire technology capable of digitalizing the drawing or writing with a pen or pencil on top of it. The platform was composed by a stack of different layers, using Velostat and EeonTex piezoresistive films, and others, and an air gap separating the top and bottom layers, with a total thickness of about 2.3 mm. A microcontroller was used to acquire the touch locations and pressure, and data was sent to a computer.

The fabricated platform was capable of digitalizing a pressing finger or the tip of a pen or pencil, but the digitalized image lacks accuracy, which can be overcome by the research of better piezoresistive materials, the improvement of the air gap separator, and more precise assembly.

6. CASE STUDY: THE HYBRID BOOK

To demonstrate the integration of the developed materials in a single application, it is proposed the fabrication of a prototype platform combining the three technologies focused on this thesis: capacitive, piezoelectric and piezoresistive.

To elaborate a case study prototype, several hypothesis were considered, from flexible game controllers (Rendl et al., 2014), to flexible tape controllers (Balakrishnan et al., 1999; Dementyev et al., 2015), wearables (Jones, 2019), hybrid books (Q. Li & Wang, 2016), roll up devices (Gomes et al., 2018), or wrapping devices (Drogemuller et al., 2021), among others. Yet, the platform that seemed more natural to employ the developed materials throughout this thesis was the book, since books are a platform where flexibility is essential, and that have been around for centuries the way we know them today, still with very little innovations. Nowadays, children usually find traditional physical books alone less interesting than the digital ones or a combination of the two (Cesário et al., 2016). This grants the opportunity to revolutionize the traditional physical book, making them more appealing to children by interactivity, just as in the Electronic Popables (Qi & Buechley, 2010).

Furthermore, a previous project of the lab team named Bridging Book[1] (A. C. Figueiredo, Pinto, Branco, et al., 2013; Pinto et al., 2013) consisting in a traditional picture book complemented by a tablet attained success as hybrid book, resulting in a patent (A. C. P. De Figueiredo et al., 2014). This inspiring book-form prototype is a representative example of the versatility and possibility of the application of the developed materials and technologies.

Therefore, a simple hybrid book was developed consisting on a few pages with embedded electroactive polymer films, as shown in Figure 6.1, which will be presented next[2].

---

1 Demo video of Bridging Book available at: https://vimeo.com/engagelab/bridgingbook
2 Demo video of the developed hybrid book available at: https://youtu.be/vDwr-BfbtH0

Figure 6.1.   Developed hybrid book demonstrator, with a 1 euro coin for reference.

6.1. CONTEXT AND FEATURES

Different prototypes based on different technologies and applications have been shown throughout the document. At this stage, it is a necessary to integrate all technologies together in a functional prototype to demonstrate the coherence and the possibilities of the developed work. The hybrid book seemed the appropriate application, where the features of the developed materials, such as thinness, lightweight and flexibility, can be also an advantage.

Some of the previously developed prototypes were selected and adapted for a case study demonstration. Therefore, a themeless book was designed, composed by white paper sheets, where the

electroactive printed films were attached to the sheets with tape. Three main sheets composed the book, one for each technology. Figure 6.2 shows the structure of the hybrid book application. In the first page, a capacitive matrix sensor was designed, which controls the audio played in the second page using a piezoelectric film. The last page, the third, was actually the back cover of the book, where a piezoresistive touchpad was used to digitalize writing and sent to a smartphone via Bluetooth.
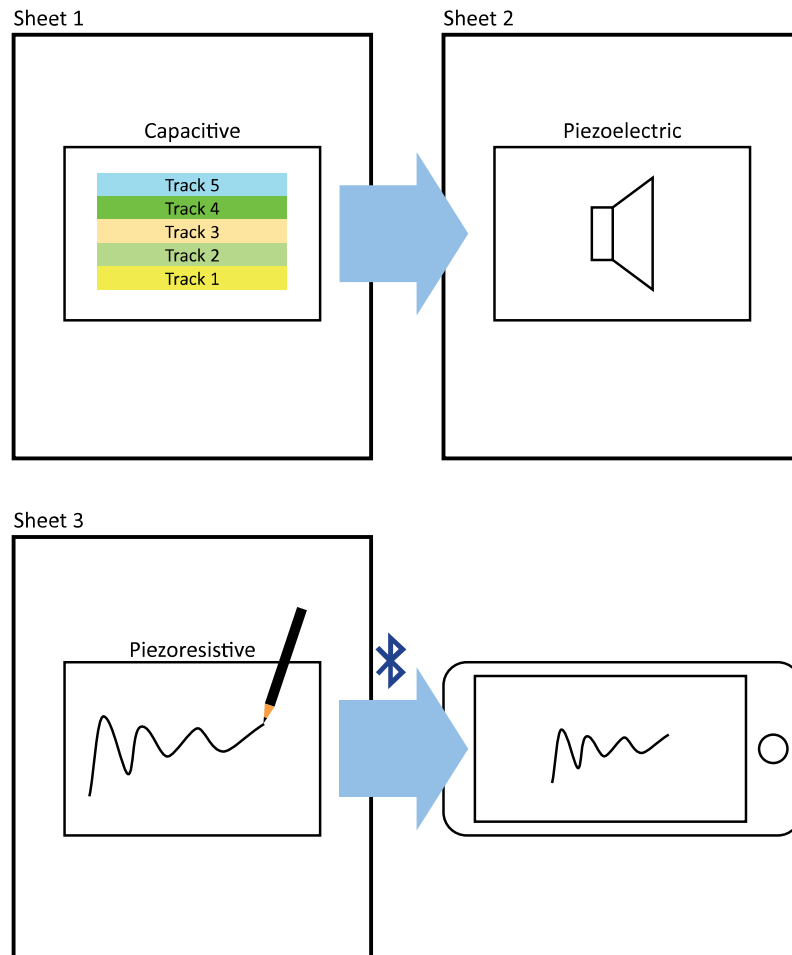
Figure 6.2. **Proposed structure for the hybrid book integrating the three technologies explored in the thesis.**

The major effort was placed on the electronic sensors and actuators as form of interaction, and no effort was placed into miniaturizing the electronic systems to control the sensors and actuators so that they could fit in the book's cover or spine, since that is an already standard among the industry through the use of flexible PCBs and surface-mount technology (SMT) devices, and would pose no improvements to the state of the art other than from the user interface's point of view. As a result, from the developed hybrid book, there were wires and flexible flat cables (FFCs) coming out, connecting to an external electronic circuit.

In the first page, the capacitive matrix was divided into 5 buttons, each of them associated with an audio track. Consequently, when the user touches one of the buttons, the corresponding audio track starts to play. Touching again the same button stops the playback. Table 6.1 lists the selected audio tracks. Simplified version of the songs was used, based on the instrumental with only one simultaneous note, to simplify the playback circuit and data storage. Likewise, instead of harmonical audio sinewaves, single square waves were generated. Audio data was converted from Musical Instrument Digital Interface (MIDI) format to note frequencies and durations using the free online tool provided by Andy Tran called Midi to Arduino[1]. Furthermore, generated code was manipulated in order to store data in an array.

Table 6.1.   Songs associated to the audio tracks.

Track	Song	Composer
1	A Portuguesa	Alfredo Keil
2	Game of Thrones Theme	Ramin Djawadi
3	Canon Rock	JerryC
4	Super Mario Bros Theme	Koji Kondo
5	Himno del Athletic Club	José de Olaizola & Feliciano Beobide

Relatively to the piezoresistive interface, pressure exerted by a finger or pen is digitalized and sent to a smartphone via Bluetooth, as a form of expansibility of the book's functionality. Despite research for multitouch piezoresistive touchpads has been going on, only single-touch were specified for this interface.

Electrical energy for the prototype is supplied by a 9 V battery (6LR61).

6.2. PROTOTYPE FABRICATION

The book was prepared with 2.5 mm-thick bulk cardboard, and cut into two 250 × 283 mm size panels for the cover. A decorative 50 μm-thick polypropylene (PP) adhesive film was used to line the book

---

1 Midi to Arduino tool website, by Andy Tran: https://extramaster.net/tools/midiToArduino/

cover. Inside the book, 4 sheets of A4-sized white paper were glued together with the cover, forming pages. In some of the pages, printed polymer films were attached with tape, as described in the following.

6.2.1. Capacitive-based film

The fabricated capacitive touchpad was similar to the one described in section 3.3.2, using the same materials and methodology, with the exception of the imprinted layout and form of connection. The diamond outer frame pattern (Peng, 2019) was used, which has the same principle of working than the diamond pattern, but with an empty center. It is a form of economizing silver ink without affecting performance. The terminals were also upgraded to 1 mm pitch, allowing the connection to an FFC using *z*-axis adhesive tape (3M 9703). Figure 6.3 shows the fabricated capacitive matrix. Five stripes of colored paper were glued to the matrix to help the user identify the defined touch areas.
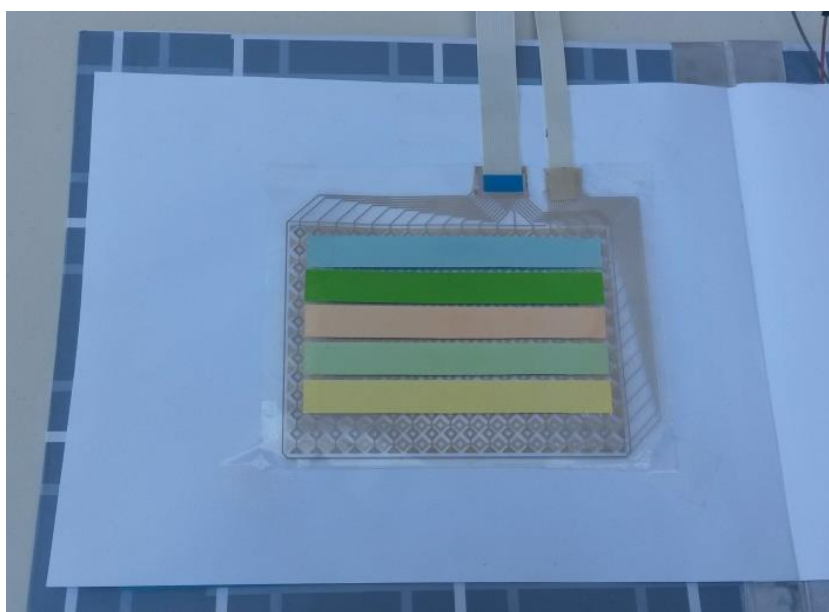
Figure 6.3.   Capacitive matrix attached to a sheet of the book, with colored stripes of paper to identify the touch areas.

In this context, due to the simplicity of the application, the electronic sensing was performed by self-capacitance measurements, eliminating the need for a dedicated capacitive controller IC. Instead, measurements were achieved directly by the digital pins of the microcontroller, and picking only on the necessary matrix terminals due to the microcontroller's limited pin availability and computational power.

6.2.2. Piezoelectric-based film

The used piezoelectric film actuator for audio reproduction was a PVDF film fabricated through the same method and materials as described in section 4.3.1. Figure 6.4 shows the piezoelectric film attached to a book sheet using tape. Only one pair of electrodes were connected, since no significative improvements were noticed when connecting more than one pair. And, as this prototype was prepared for a 2.54 mm pitch clincher, two wires were coming out of it. To make the piezoelectric film less visible to the user, it was incased within two paper sheets.
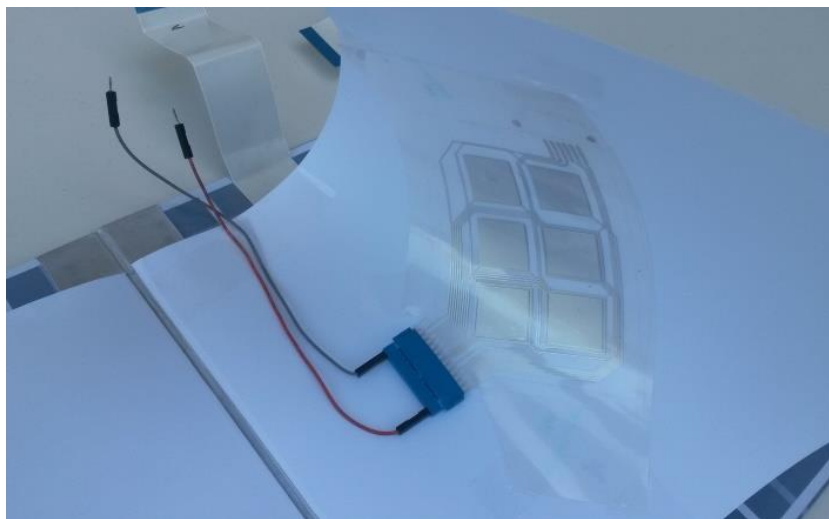
Figure 6.4.   Piezoelectric matrix attached to a book sheet.

6.2.3. Piezoresistive platform

The piezoresistive platform selected to use in the book is the same as described in section 5.2.4. Since it is less flexible than the others, it was glued to the back cover of the book, as shown in Figure 6.5. However, instead of a USB connection to a computer, Bluetooth data transfer was used to display the digitalized writing in a smartphone. Consequently, the used microcontroller was altered to an Espressif ESP32-WROOM-32U, equipped with internal Bluetooth and Wi-Fi radio communication.
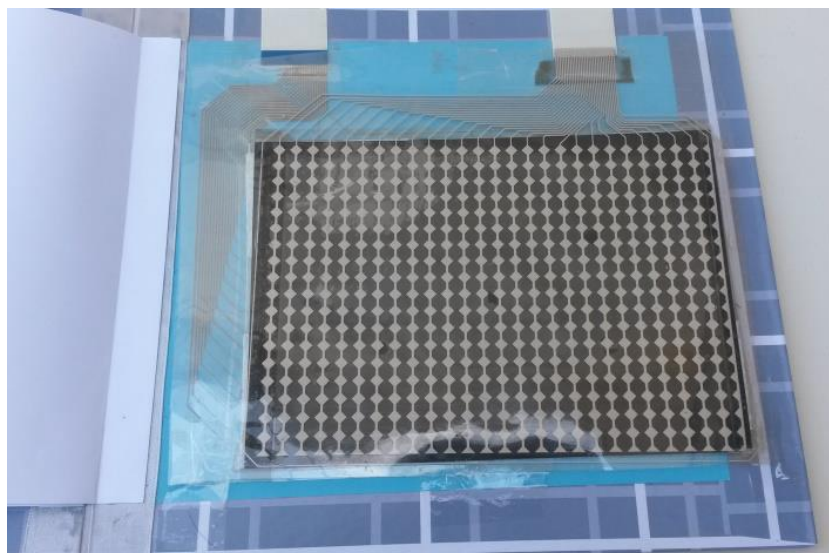
Figure 6.5.   Piezoresistive platform attached to the back cover of the book.

6.3. ELECTRICAL CIRCUIT

Figure 6.6 displays the schematic of the electrical circuit implemented in the hybrid book case study. Two microcontrollers (µCs) were used: a Microchip ATmega328P for the capacitive sensing and piezoelectric actuation; and an Espressif ESP32-WROOM-32U for the piezoresistive sensing and Bluetooth communication. It would be possible to perform all the tasks only with the later one, but it would imply to do carry out the porting of the previously developed code.

In the self-capacitive matrix sensing, one source pin (PD2) was common to all the lines, and 5 sensing pins (PD3 - 7) were used to measure each of the lines. Initially, as indicated in Figure 6.7b, all the pins are reset. A short delay of 1 µs ensures the electrodes discharge. Then, the sensing pins are changed to high impedance state and the source pin is set to 5 V, allowing the matrix electrodes to be slowly charged through 10 MΩ resistors, and while the sensing pins continuously monitor the pins' state. Added capacitive loading exerted by a touching finger slows the charging rate. When all the pins of the matrix have transited to high logic level, it is calculated the amount of time taken. Although the pins are read using polling, the introduced delay is in the order of hundreds of µs, not enough to alter the audio playback. Due to the noisy nature of capacitive sensing, each capacitive sample takes 200 acquisitions, and each acquisition is intercalated with audio signal update, as visible in Figure 6.7a.
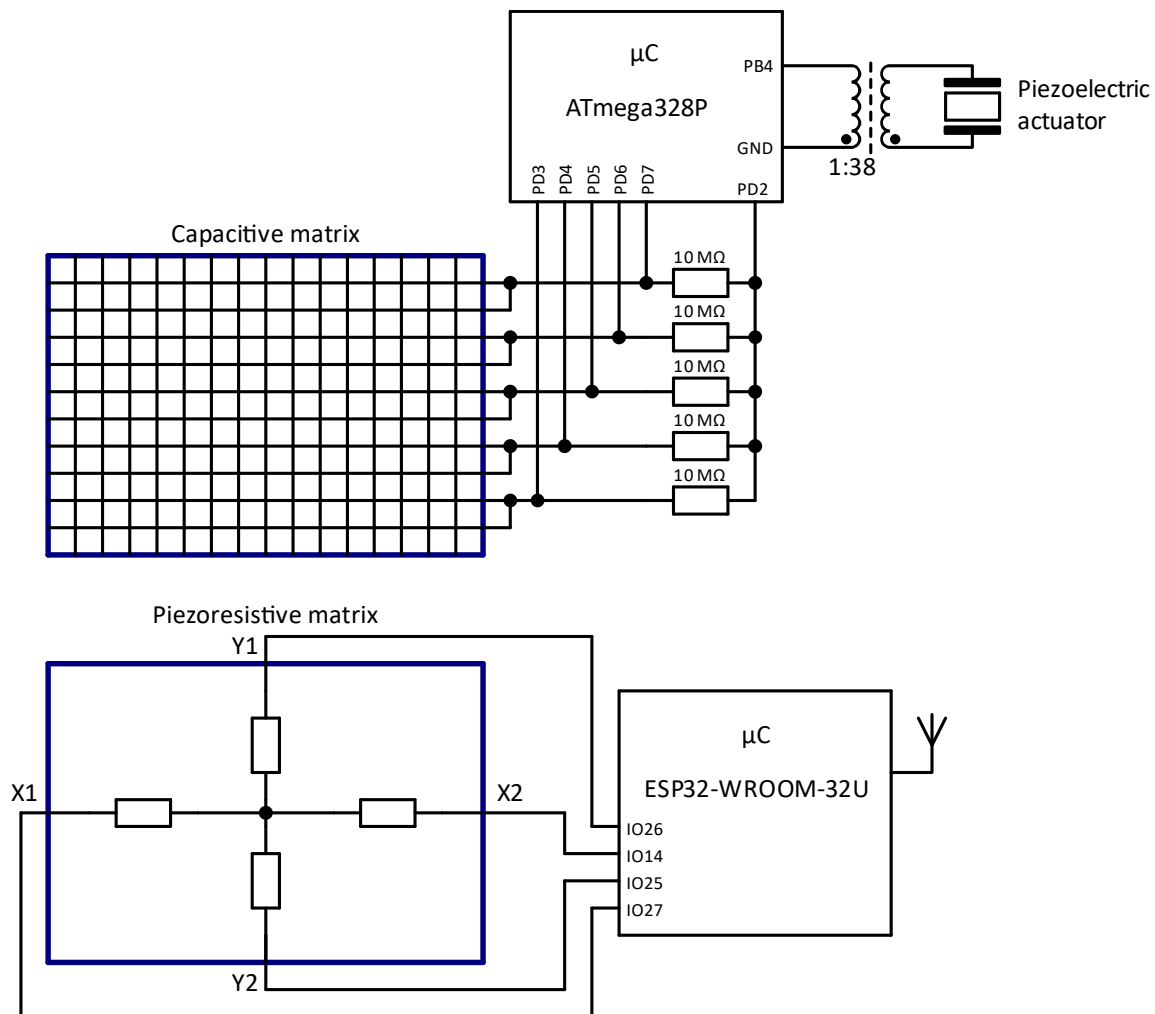
Figure 6.6.   Implemented circuit for the hybrid book.

On the first 2 s of execution of the microcontroller, it is performed a software calibration of the capacitive sensors, noting the maximum and minimum values read, and based on that it is stipulated a baseline for each sensor, and a touch threshold. Moreover, the maximum value continues to be updated throughout the entire execution of the microcontroller to take into account the real amplitude of the sensors during touching. To assess touches in the matrix, it is executed a software debouncing by comparing the signals from all the sensors by their amplitude, and checking if the highest one keeps its state for 500 ms, at least.

Audio playback is done by hardware, using a timer of the microcontroller, through a pulse-width modulation (PWM) signal technique, width duty cycle of 50 % and variable frequency. The audio data is stored as an array of note frequencies and durations, therefore, it does not lock the microcontroller processing capability.

(a)   (b)
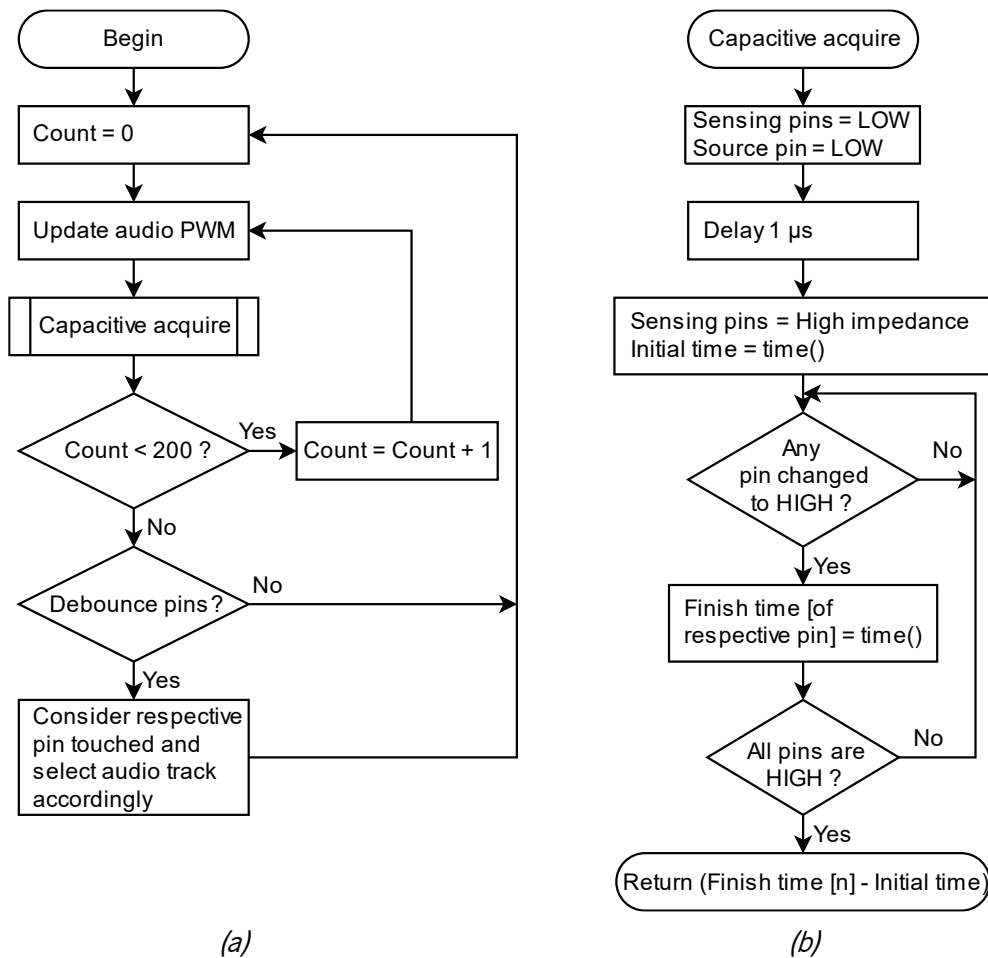
Figure 6.7.   Flowchart for the Microchip ATmega328P for self-capacitance touch matrix and piezoelectric sound actuation: *(a)* overall cycle and *(b)* single touch sample acquisition.

Relatively to the piezoresistive sensing matrix, it is a 4-wire touchpad topology, thus it was implemented a 4-wire data acquisition (NXP Semiconductors, 2008). The flowchart of execution is shown in Figure 6.8.

To improve stability of measured signals, each sample was determined by the average of 40 acquisitions for the coordinates and 20 for the pressure level, considering opposite symmetrical measurements.

Data is sent via Bluetooth to a smartphone running Android operating system, where a Java application reads and displays the acquired points. The communication protocol is based in American Standard Code for Information Interexchange (ASCII) characters, in the format described in Table 6.2. The application running on the smartphone dims the points' color based on the reported pressure, and if the value is lower than 100 it does not draw them.
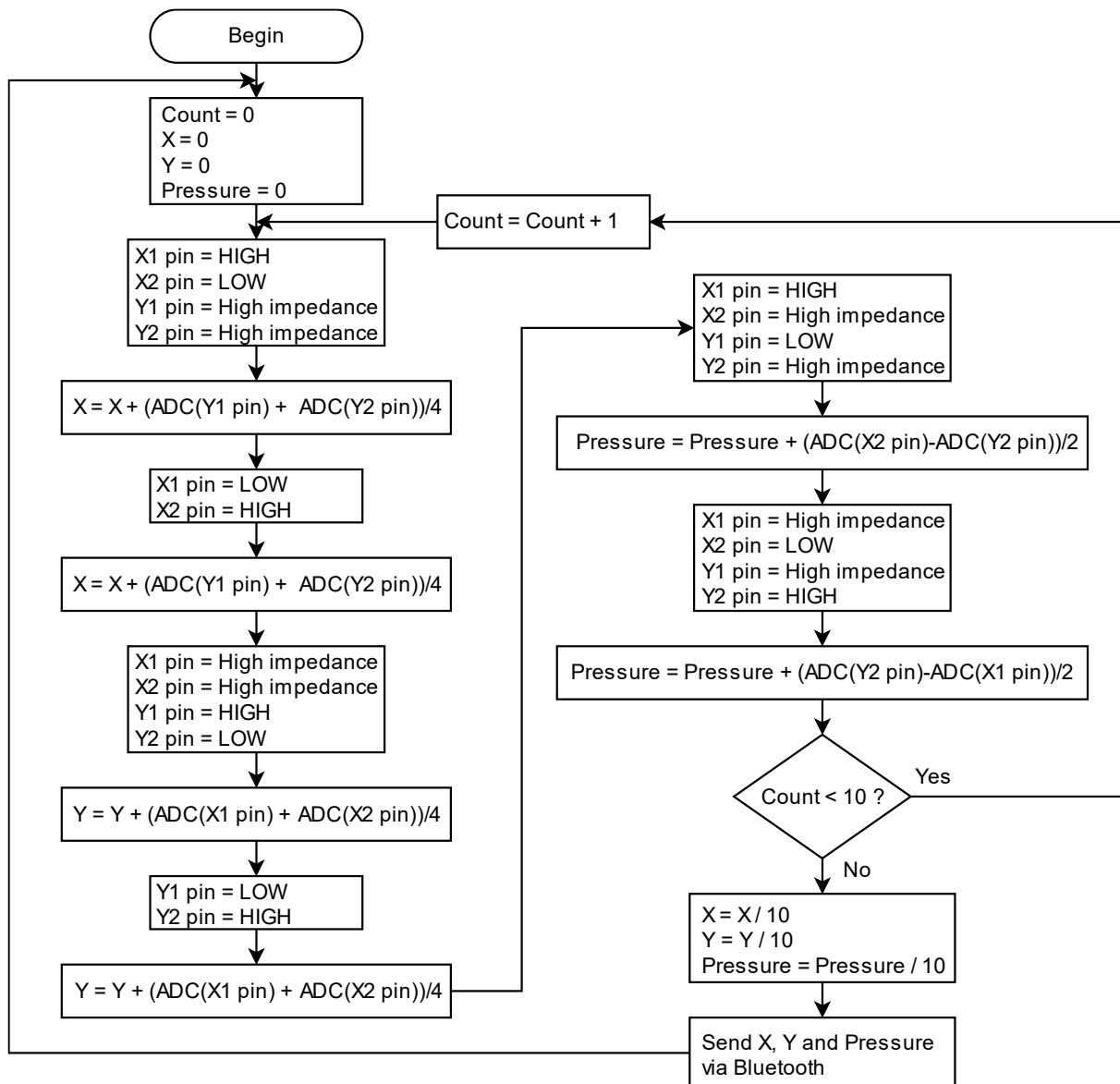
Figure 6.8. Flowchart for the Espressif ESP32-WROOM-32U for the piezoresistive touch matrix and Bluetooth data transfer.

Table 6.2. Packets of the Bluetooth communication protocol for writing display on a smartphone.

Packet
...
[*row*],[*col*],[*press*]
[*row*],[*col*],[*press*]
[*row*],[*col*],[*press*]
...

[*row*] is the abscissa of the touch point (0 – 1023)

[*col*] is the ordinate of the touch point (0 – 1023)

[*press*] is the pressure of the touch point (0 – 255)

6.4. RESULTS AND DISCUSSION

A demo video of the developed prototype under operation is available in the footnote link[1].

The self-capacitance measurements taken on the capacitive matrix are very susceptible to noise, particularly if any electric charge is present nearby the electrodes, such as electronic equipment, electrostatic materials or power supply ripple, etc. Notwithstanding, the implemented software method for data acquisition has also its limitations: the high impedance input of sensing pins might still allow current to flow into the pin, changing the charge build up rate on the electrodes; due to software implementation, the microcontroller has a limited timestamp precision of 4 µs; and the concurring tasks executing in the microcontroller at any specific moment. For these reasons, efficient filtering systems had to be implemented in order to obtain valid measurements.

Figure 6.9 shows the readout data from the self-capacitive sensors after filtering. The baseline is determined by the minimum sample occurred in the first 2 s, and it is subtracted to the acquired samples. Then, based on the historic maximum for each sensor, the acquired sample is converted to the same scale as the other sensors (here shown as an amplitude from 0 – 255).
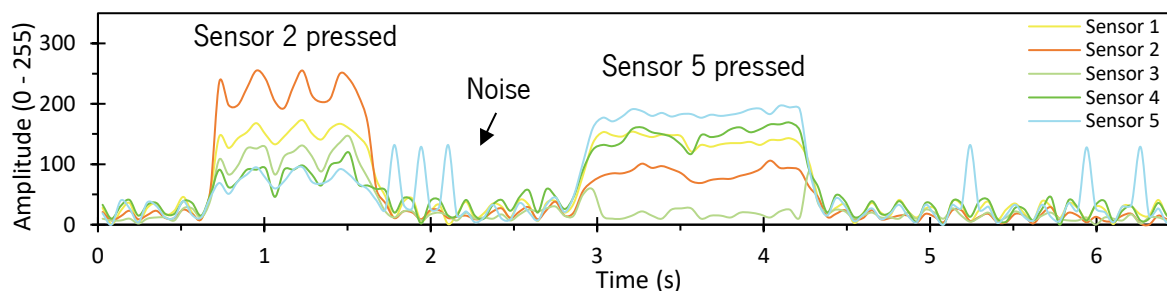
Figure 6.9.   **Readout of the self-capacitive sensors after filtering, during finger touches.**

A touch threshold is set at 50 % of each sensor's range. The system considers a touch on one of the sensors when its amplitude is higher than the others, as well as higher than the touch threshold for a defined time of 500 ms or more.

The system has been capable of successfully operate with the paper sheet with the capacitive matrix bent, but recalibration is necessary every time the sheet changes shape, thus not being possible to dynamically bend the sheet during capacitive sensing operation.

Relatively to the piezoelectric actuation film, it has been pointed out that it performs better at higher frequencies than at lower ones, particularly higher than 1 kHz. Therefore, when choosing the audio tracks

---

1 Demo video of the developed hybrid book available at: https://youtu.be/vDwr-BfbtH0

for this demonstration it was given preference to melodies with less bass notes. To reach satisfying playback audio volume, the user should bend slightly the paper sheet with the piezoelectric film, to make it act as a diaphragm. However, in this application, that can be done easily. The major downside of this technology is related to the playback volume, which, though perfectly audible, it can get quickly suppressed by a loud-speaking person.

A higher playback volume can be achieved by altering the size of the piezoelectric film, the dimensions of the electrodes, the thickness of the piezoelectric film or even the shape of it, in order to manipulate the resonant frequency (Measurement Specialties Inc., 1999). But, as obvious, creating a multilayer stack might be the solution producing better outcome (Street et al., 2020; Tajitsu, 2016).

In the case of the piezoresistive platform, it has been possible to digitalize writing with a pen or finger on the platform to a smartphone, as shown in Figure 6.10. The developed piezoelectric platform is comfortable to touch, with a slight softness in the initial touch, but getting stiff when applying pressure, resembling a sheet of paper. Since it has been secured to the back cover of the book, which help to keep the layers stretched, it performs better than the piezoresistive platform alone one a table.
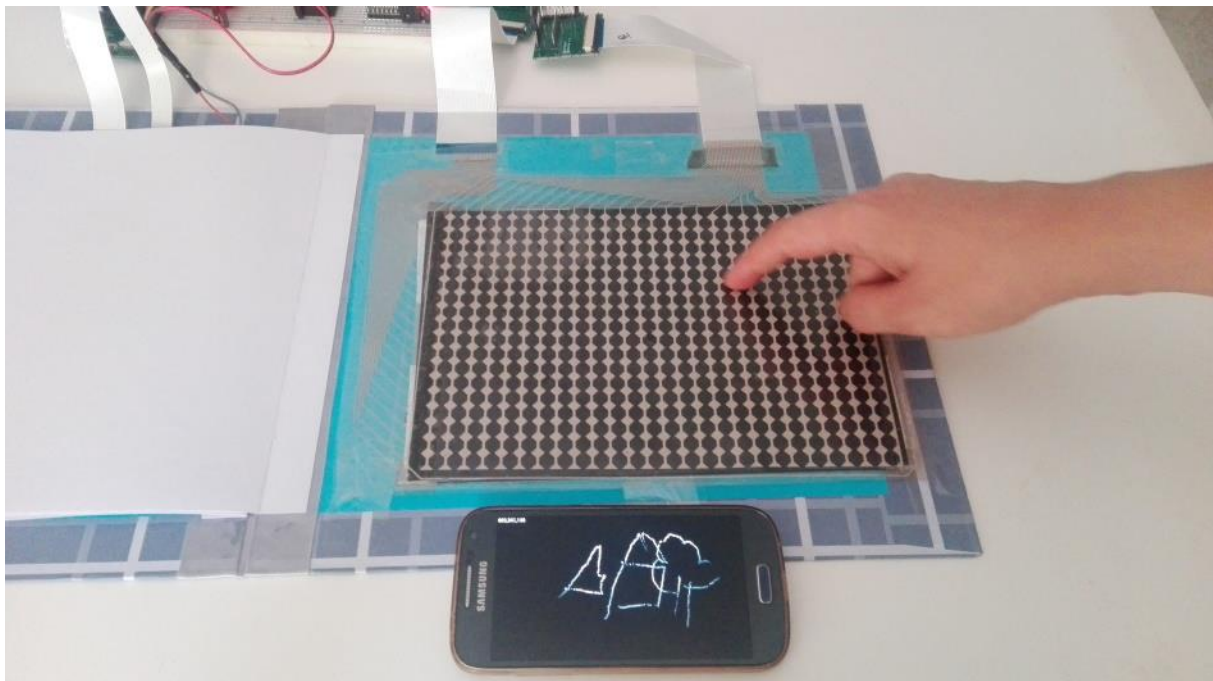
Figure 6.10.   Example of a drawing with a finger on the piezoresistive platform, and displayed on a smartphone.

The difference between drawing with a finger or with a pen or pencil lies on the pressed area and applied pressure. Since the finger has a larger area, when it presses against the platform it facilitates the passage of current through the piezoresistive fabric inner layer, and the system shows higher accuracy than with a sharp tip pen or pencil, as visible in Figure 6.11a and Figure 6.11b, respectively. The traces

are smoother for the finger, being better identifiable what it has been drawn. The cause might be the small undulation of the EeonTex, which the sharp tip of a pen or pencil does not press uniformly. This indicates that a better material is necessary to replace the EeonTex layer. Nevertheless, drawing with a pen or pencil on a sheet of paper above the platform is easier, as the drawing becomes visible in the paper.

<center>(a)   (b)</center>
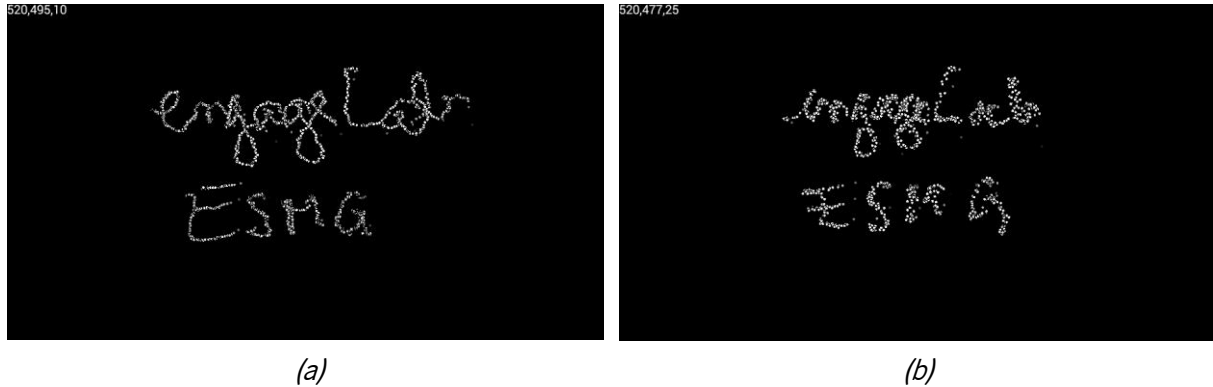
Figure 6.11. **Screenshot of the smartphone after writing on the piezoresistive platform *(a)* with a finger and *(b)* with a pencil.**

Nevertheless, it is worth noting that the developed piezoresistive platform is robust enough to show no loss of accuracy when drawing with 5 or more sheets of paper on top of it. In fact, at times, a couple of sheets of paper increased accuracy of digitalized drawing, probably because it spreads the applied force on the tip of the pen or pencil onto a slightly larger area.

From the several users experimenting with this platform, it is a unanimous opinion that multitouch would be a major improvement to its usability, mainly for allowing users to rest their hand on the platform while writing.

6.5. CONCLUSIONS

A hybrid book prototype has been presented as a form of the integration of materials from studied technologies, combining a capacitive touchpad, a piezoelectric film for acoustic actuation, and a piezoresistive platform for drawing and writing digitalization. The structure for the book was defined, giving

each of the included technologies a specific application. The developed materials were attached to the book sheets with tape. A demonstrating video of the developed prototype is available in the footnote link[1].

The first sheet was the capacitive touchpad, which was divided into 5 capacitive touch buttons, each of them associated to a specific audio melody, which once touched triggers the audio playback on the piezoelectric film. The method for sensing the capacitive electrodes with digital pins of a microcontroller was described, as well as the filtering and debouncing, presenting the acquired signals from the electrodes.

The piezoelectric film was on the next book sheet. PVDF film was used to successfully playback audio melodies according to the capacitive touch selection. The user must bend this sheet slightly for the piezoelectric film act as a diaphragm and reproduce louder sounds. The actuation for the piezoelectric film was given by a microcontroller using PWM, which was then amplified in voltage by a transformer to drive the piezoelectric film.

For the piezoresistive platform, it integrated the last sheet of the book, which was actually the back cover. The intent of this platform is to allow the user to digitalize drawing or writing. It is composed by several layers of piezoresistive films and fabrics, and air gaps separating them. It uses a 4-wire topology, allowing the top and bottom layers to touch each other when pressure is applied on them. The measurement of the signals is performed by the analog pins of a microcontroller. The acquired signals are sent to a smartphone via Bluetooth. It has several improvements to be done in the future, such as improving the air gap separator, the resistive deposition on the top and bottom layers, and allow for multitouch.

The hybrid book proved to be platform where the several film technologies could be exhibited and potentialized. It is also a platform that can take great advantage of the flexible materials developed. Moreover, the integration of capacitive, piezoelectric and piezoresistive materials in a hybrid book is definitely an advance in the state of the art.

---

1 Demo video of the developed hybrid book available at: https://youtu.be/vDwr-BfbtH0

7. CONCLUSIONS AND FUTURE WORK

The project explored novel materials that can be used for interaction with electronic platforms, recurring to polymer films and printed electronics. Three main technologies were used, namely capacitive, piezoelectric and piezoresistive.

Prototypes were implemented for each technology, evincing the versatility of the developed polymer-based materials for sensor and actuator applications, with advantages such as simple integration and processing, as well as flexibility.

To demonstrate the integrability and the potential of the developed materials, a final prototype was developed as a case study, consisting in a hybrid book with features based on the three studied technologies.

7.1. CONCLUSIONS

The change of the interface paradigm in the recent years is outlining the future of HCI through more immersive experiences, diminishing the dependence on the user to provide commands via keyboard and mouse, and to expect the outcome on a screen. The concept of ubiquitous and transparent computation has been around for some decades already, but limitations of the available materials and their functionalities has been preventing the concept to gain practical applications (Ishii et al., 2012; Weiser, 1991). However, recent advances in the development of smart and electroactive materials, allowing sensors and actuators embedded in traditional everyday use objects, are leading to a new generation of platforms. We are assisting to the arising of smart objects that are surrounding us, perceiving commands through sensing interaction floors, walls, textiles or multitouch surfaces, among others (Ishii & Ullmer, 1997), and displaying information through shape, color and texture (Coelho & Maes, 2009; Coelho & Zigelbaum, 2011).

In this sense, this work focused on the development of new forms of sensors and actuators capable of coping with the progress in interactive systems, based on polymer films with electroactive response

such as capacitive, piezoelectric and piezoresistive. Electroactive response was obtained through the inclusion of nanoparticles (NPs), such as metallic or carbonaceous, together with printed electronics.

Table 7.1 summarizes the main characteristics of the developed sensors throughout this project.

Table 7.1.   Comparison of the technologies used in this project.

Property	Capacitive		Piezoelectric	Piezoresistive	
	Using fringing	**Deformable dielectric**		**Individual sensors/array**	**4-wire matrix**
Sensed bodies	Only conductors	Any	Any	Any	Any
Smallest detectable body	Usually 5 mm ø (fingertip)	About 2 mm ø (limited by sensor size)	Any (as long as it causes vibration on the sensor)	About 2 mm ø (limited by sensor size)	0.5 mm ø, or less
Proximity detection	Yes	No	Possible, using the pyroelectric effect	No	No
Pressure detection	Estimated	Yes	Yes	Yes	Yes
Stretch detection	No	No	No	Yes	No
Precision	Very high	High	Medium	Medium	Low
Repeatability	Very high	High	Very High	Medium	Medium
Time to recover	Low	Low	Low	High	Low
Sensitive to temperature	No	No	Yes	No	No
Sensitivity to electrostatic induction	High	Low	Medium	Low	No
Calibration needed	Yes	Yes	Self-calibrating	Yes	No
Electronic circuit	Very complex	Complex	Very complex	Simple	Very simple
Flexibility	Very high	High	Very high	Very high	Medium

Capacitive technology the was most beneficial on the development of touch sensors where no force was necessary to apply on the touchscreen, allowing the finger to easily slide over the platform without inducing friction. However, measurement of pressure is only estimated, based on the area of the finger

in contact with the sensor. On the other hand, piezoresistive sensors require a pressure to be applied on it, which, although measuring real pressure instead of estimated, are not as pleasant options for operations involving touch button applications, but perfect for sensors involving stretching. In turn, piezoelectric technology is more suitable for bending detection, and it shows a huge potential for applications, because of the versatility in providing energy harvesting, sensors and actuators capabilities. Also, the pyroelectric effect can be used as a sensor to detect an approaching finger (Rendl et al., 2012). Furthermore, the possibility of piezoelectrics to simultaneously operate as sensor and actuator broadens the possibilities. Nonetheless, piezoelectric devices require more complex electronics and it is a technology that still has to be improved in polymers.

In the present work, prototypes based on capacitive, piezoelectric and piezoresistive technologies were developed, each for specific applications.

Different topologies were pursued to obtain capacitive prototypes, with particular emphasis on those using the fringing effect or the deformation of the dielectric to measure touches or pressure. The first approach was based on the development of a single touch button sensor made of resin/ITO composites using self-capacitance measurements (Mendes-Felipe et al., 2020). Then, this application was expanded into a PET film-based matrix with multitouch capability, using mutual-capacitance measurements (N. Castro et al., 2017; Nunes et al., 2017). Both of these prototypes were only able to measure touch of the fingers, not being possible to detect non-conductive materials or the applied pressure. Subsequently, a different approach was pursued by developing a prototype with a principle of operation based on the deformation of the dielectric, which brings the electrodes closer when pressure is applied on the sensor. The used material for the dielectric was P(VDF-TrFE-CFE), a flexible film with high dielectric constant. This enabled to detect the pressure exerted by any object, including non-conductive ones, as well as the intensity of the applied pressure (Pereira et al., 2021).

Using the piezoelectric technology, a prototype was prepared based on PVDF films that can operate both as sensor or actuator (N. Castro et al., 2017; S. Gonçalves, Pereira, et al., 2019; S. Gonçalves, Serrado-Nunes, et al., 2019b). The system is capable of detecting any vibration resulting from touching or bending the film, with a circuit tuned for the desired type of sensor. Simultaneously, the device can also work as acoustic actuator by applying a high voltage (HV) signal to the electrodes.

The fabricated prototypes based on piezoresistive technology mostly consisted in the arrangement of different types of polymers with specific properties reinforced with carbonaceous materials. An initial study was conducted where CNTs were included in three polymers, namely PVDF, SEBS and TPU, and material samples were placed on top of the interdigitated layout electrodes, being the piezoresistive

response obtained by the mechanical contact between the samples and the electrodes (J.R. Dios et al., 2019). The several samples were integrated in a walking detection device, where different responses were observed for different samples, but all were able to detect the movement of the user. Another prototype was then developed base on PLA/CNT composites, capable of exhibiting the piezoresistive effect itself when deformed (Jose R Dios et al., 2020). This composite material was applied on the tip of a human endoscope to allow healthcare professionals to get the data about the real deformation of the endoscope when inside the patient, which, despite not being an interactive platform, is still as relevant since the developed materials can easily integrate one. Although good results were obtained, yet with small electrical variation, the mechanical strength of the composite limited the maximum range of deformation for the endoscope. However, in another experiment, both the mechanical stretchability and electrical response were improved, recurring to rGO/SEBS composites, which is highly stretchable, and, therefore, exhibits a large piezoresistive response. In fact, the stretchability allowed the application of the composite on the fingers of a glove to identify finger movements of the user (Pedro Costa, Gonçalves, et al., 2019). The downside of the piezoresistive composites was the sometimes high recovery time, while in the piezoresistive sensors by mechanical contact the recovery time was much quicker. Efforts were put into developing environmentally friendly piezoresistive composites based on silk fibroin (SF)/silver nanowires (SNWs), where an electrochemical behavior was observed (Reizabal et al., 2019, 2020). The last piezoresistive prototype consisted in a touchpad platform for human writing digitalization, prepared by a multilayer assemblage of different polymer films, with a 4-wire topology. This platform was mostly fabricated recurring to commercial materials, but that can be improved by specifically optimized materials.

To conclude, a final prototype consisting in a hybrid book was presented as case study for the developed materials and technologies. It featured a capacitive touch matrix, a piezoelectric acoustic actuator, and a piezoresistive touchpad, each embedded on different paper sheets. This prototype shows the potential for the developed technologies to integrate a single platform and complement each other's functionalities, providing a more immersive experience to the user.

Often, the capacitive, piezoelectric and piezoresistive technologies investigated in this thesis are interchangeable in terms of user interaction. For example, deformation sensors can be fabricated using piezoelectric or piezoresistive technologies, or touch sensors by any of capacitive, piezoresistive or piezoelectric. The overlapping of technologies is important because different technologies have different forms of operation, which might be or not effective for specific applications, depending on each case.

Hence, ultimately, it is possible to reduce the number of technologies applied on the hybrid book to two, or even to one, namely piezoelectric.

The current thesis interconnects the important subject of tangibility of interfaces with some novel types of materials that technological advances are making available. This work represents a significant contribution to the state of the art on advanced materials development and technology applicability. Therefore, this is an ongoing project that requires further research in order to facilitate the application of the developed technologies and materials, as well as to enable industrial applications of it. Thus, next will be presented some insights for future developments.

7.2. FUTURE WORK

Throughout the research process, materials and prototype devices have been developed. Yet, nevertheless, as the systems were implemented, more improvements and innovations were foreseen. For the continuity of the current project, recommendations for future improvements are discussed in the following.

In the capacitive polymer matrix, besides the clincher connector, the most problematic was the sensitivity to electrostatic induction due to the triboelectric effect. This was particularly emphasized by the PET polymer film used as substrate, which, contrarily to glass, is an electron acceptor and builds up an electric charge in contact with the human skin (Khandelwal et al., 2021; R. Zhang & Olin, 2020). Therefore, the most necessary improvement on this prototype is the application of a coating using an electron donor material, close to that of the human skin. Another important improvement for capacitive materials is the direct printing of the conductive layout on an environmentally friendly substrate, such as paper. Paper-based composites are a growing alternative to polymers, since cellulose is also tunable in terms of properties by the inclusion of particles (Lizundia et al., 2020).

Several improvements can be performed on the developed PVDF film, particularly when embedded on the hybrid book. An improved layout, such as the shown in Figure 7.1, can fabricated to contain bending sensors in the margins and contemplate larger area for sound reproduction, in the center.

The bending sensors allow to use the shape of the sheets as form of interaction, such as bookmark pinning (Rendl et al., 2014).
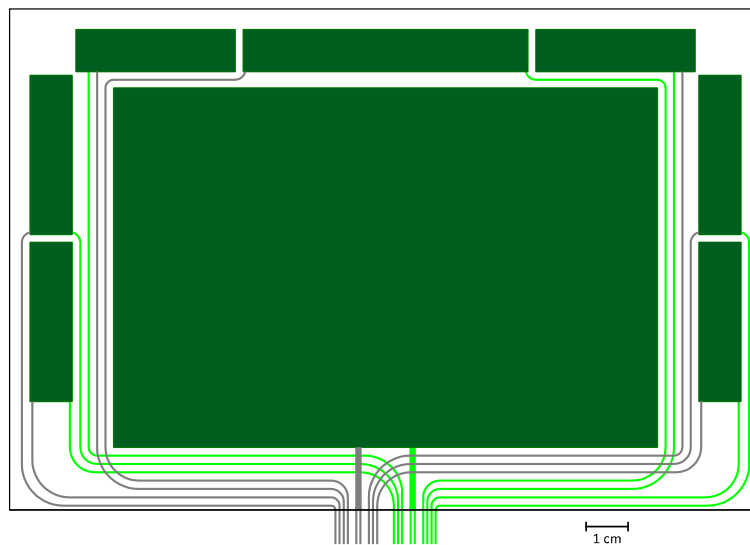
Figure 7.1.   Layout for dual function piezoelectric film: 7 bending sensors on the borders and a sound actuator in the center (light green – bottom layer; gray – top layer; dark green – bottom and top layers).

The audio transducer is expected to increase the playback volume. However, it is not expected that it solves the inaudibility of the reproduced audio when the film is lying flat. Moreover, increasing the applied voltage, creating a multilayer film (Street et al., 2020), or applying a more rigid coating on the PVDF film (Sugimoto et al., 2009) can also result in increased sound volume. Furthermore, additional research on the resonant frequency of the PVDF film is needed, evaluating the sound propagation velocity in the piezoelectric film, together with its size and thickness, as well as the influence of the electrodes (C. S. Lee et al., 2003). Probably, a solution to the problem of the piezoelectric film not responding well when lying flat, is the use of two polymer films with printed coils for electromagnetic actuation, in a topology similar to the one implemented by Preindl et al. (2020) using conductive fabric. However, this is a challenging approach due to the precision limit for large inductors printing as well as the higher power requirements.

In the developed piezoresistive polymer composites with the inclusion of CNTs or rGO, the most necessary improvement is the response curve of the sensors, which often take too long for the resistance to recover to initial value after stretching the composite film. This is linked to the interaction between the polymer and the nanoparticles, which need molecular rearrangements to reestablish resistivity. Therefore, future research on this topic must focus on the selection of other polymers and nanoparticles to mitigate this behavior.

In the piezoresistive platform, several improvements are necessary, such as multitouch support and highly increase precision, and hand rejection, among others. Multitouch can be achieved by implementing electrodes associated in rows and columns. However, the design suggested in Figure 7.2*a* can be an interesting solution specific for writing digitalization, using only a few analog pins. This layout is based on the assumption that there is a gap between the hand to the tip of the pen of at least 2 cm, making the hand and the tip of the pen always land in different areas. Alternatively, a capacitive matrix can also be applied on top of the piezoresistive platform to allow the system to subtract the hand.

To highly increase precision, it is necessary to investigate the sources of non-linearities. The Velostat layer has been noticed to wrinkle over time, therefore, it should be replaced by another polymer solution such as directly print a piezoresistive ink on top of the electrodes, eliminating the need for the connection through the *z*-axis conductive tape. The separator between top and bottom layers needs to be changed to a structure as shown in Figure 7.2*b*, printed in an fused filament fabrication (FFF) 3D printer with 20 µm of thickness in PLA. The internal piezoresistive fabric can also be source of some noise due to the wavy structure of the EeonTex film. It can be replaced by a stretchable piezoresistive EeonTex fabric, such as the COM-14112 by Sparkfun.

(a)   (b)
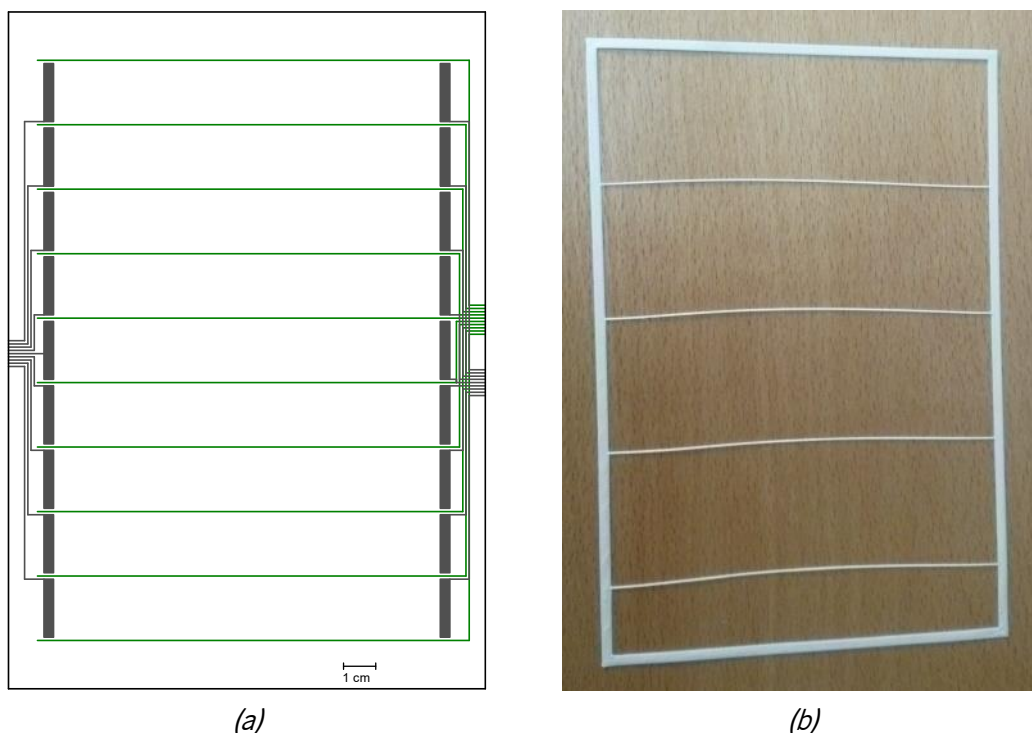
Figure 7.2.   Layout for multitouch matriz, composed by 9 single touch areas: *(a)* disposition of the electrodes and *(b)* 3D-printed PLA separator with 20 µm of thickness.

Relatively to the pursue of new polymer materials from natural sources, as the attempt performed using sink fibroin (SF), more efforts should be allocated to finding a green natural solution for the fabrication of piezoresistive sensors. Furthermore, the electrochemical effect resulting from the developed SF/SNW composites should be further investigated, since it represents huge potential.

Finally, to develop a case study prototype with more compact and clean aspect, several improvements are suggested.

The capacitive touch matrix can be directly printed with silver ink on paper instead of on a PET film that is glued to the paper sheet. The cellulose of the paper can be manipulated to attain low porosity and improve performance of the conductive silver traces. Printing method should be screen printing, because this is the method that deposits larger amount of ink on the paper.

A neat appearance of the book should be pursued, recurring to flexible PCBs and low-profile surface-mount technology (SMT) devices, capable of fitting in the hard cover of the book. Also, energy requirements must be evaluated and reduced to minimum in order to allow the system to operate with a coin battery that can also fit together with the remaining circuitry in the cover.

To reduce the required hardware and simplify the system technologically, it is possible to reduce the amount of technologies, such as substituting the capacitive sensor by piezoresistive or piezoelectric alternatives.

Finally, performing an optical character recognition (OCR) on the data acquired from the piezoresistive platform and store it as a digital information, easing digital operations such as copy & paste, find, or reading out loud through a text-to-speech conversion, among others.

8. REFERENCES

3M. (2009). *Selection of grounding, EMI shielding and attachment 3M™ electrically conductive adhesive transfer tapes (ECATT)*. https://multimedia.3m.com/mws/media/581129O/selection-of-grounding-emi-shielding-attachment-3mtm-ecatt.pdf

3M. (2013). *Touch technology brief: Projected capacitive technology*. https://multimedia.3m.com/mws/media/788463O/tech-brief-projected-capacitive-technology.pdf

Abliz, D., Duan, Y., Steuernagel, L., Xie, L., Li, D., & Ziegmann, G. (2013). Curing methods for advanced polymer composites - A review. *Polymers and Polymer Composites*, *21*(6), 341–348. https://doi.org/10.1177/096739111302100602

Achenbach, S., Haluzan, D. T., Klymyshyn, D. M., Börner, M., & Mohr, J. (2014). Large tuning ratio high aspect ratio variable capacitors using leveraged bending. *Microsystem Technologies*, *20*(10), 1807–1813. https://doi.org/10.1007/s00542-013-1940-7

Adams, A. T., Murnane, E. L., Adams, P., Elfenbein, M., Chang, P. F., Sannon, S., Gay, G., & Choudhury, T. (2018). Keppi: A tangible user interface for self-reporting pain. *Proceedings of the 2018 CHI Conference on Human Factors in Computing Systems*, 1–13. https://doi.org/10.1145/3173574.3174076

Agarwal, D. K., Prasad, A., Vinchurkar, M., Gandhi, S., Prabhakar, D., Mukherji, S., & Rao, V. R. (2018). Detection of heart-type fatty acid-binding protein (h-FABP) using piezoresistive polymer microcantilevers functionalized by a dry method. *Applied Nanoscience*, *8*(5), 1031–1042. https://doi.org/10.1007/s13204-018-0723-y

Ageyeva, T., Horváth, S., & Kovács, J. G. (2019). In-mold sensors for injection molding: On the way to Industry 4.0. *Sensors*, *19*(16), 3551. https://doi.org/10.3390/s19163551

Ahmed, M. F., Li, Y., & Zeng, C. (2019). Stretchable and compressible piezoresistive sensors from auxetic foam and silver nanowire. *Materials Chemistry and Physics*, *229*, 167–173. https://doi.org/10.1016/j.matchemphys.2019.03.015

Akhtar, H., & Kakarala, R. (2014). A methodology for evaluating accuracy of capacitive touch sensing grid patterns. *Journal of Display Technology*, *10*(8), 672–682. https://doi.org/10.1109/JDT.2014.2312975

Akhtar, H., Kemao, Q., & Kakarala, R. (2017). A review of sensing technologies for small and large-scale touch panels. In A. K. Asundi (Ed.), *Fifth International Conference on Optical and Photonics Engineering* (Vol. 10449, pp. 209–221). SPIE. https://doi.org/10.1117/12.2270631

Aleeva, Y., & Pignataro, B. (2014). Recent advances in upscalable wet methods and ink formulations for printed electronics. *Journal of Materials Chemistry C*, *2*(32), 6436–6453. https://doi.org/10.1039/C4TC00618F

Alexander, C. K., & Sadiku, M. N. O. (2001). *Fundamentals of electric circuits* (5th ed.). McGraw-Hill. https://www.mheducation.com/highered/product/fundamentals-electric-circuits-alexander-sadiku/M9781260226409.html

Amjadi, M., Kyung, K.-U., Park, I., & Sitti, M. (2016). Stretchable, skin-mountable, and wearable strain sensors and their potential applications: A review. *Advanced Functional Materials*, *26*(11), 1678–1698. https://doi.org/10.1002/adfm.201504755

Andrusyk, A. (2011). Piezoelectric effect in rochelle salt. In M. Lallart (Ed.), *Ferroelectrics - Physical Effects* (pp. 195–220). IntechOpen Limited. https://doi.org/10.13140/2.1.4242.0168

Arefin, M. S., Bulut Coskun, M., Alan, T., Redoute, J.-M., Neild, A., & Rasit Yuce, M. (2014). A microfabricated fringing field capacitive pH sensor with an integrated readout circuit. *Applied Physics Letters*, *104*(22), 223503-1-223503–223504. https://doi.org/10.1063/1.4881263

Arrigoni, A., Brambilla, L., Bertarelli, C., Serra, G., Tommasini, M., & Castiglioni, C. (2020). P(VDF-TrFE) nanofibers: structure of the ferroelectric and paraelectric phases through IR and Raman spectroscopies. *RSC Advances*, *10*(62), 37779–37796. https://doi.org/10.1039/D0RA05478J

Baglio, S., Castorina, S., Ganci, G., & Savalli, N. (2004). A high sensitivity conditioning circuit for capacitive sensors including stray effects compensation and dummy sensors approach. *Proceedings of the 21st IEEE Instrumentation and Measurement Technology Conference (IEEE Cat. No.04CH37510)*, *2*, 1542-1545 Vol.2. https://doi.org/10.1109/IMTC.2004.1351359

Balakrishnan, R., Fitzmaurice, G., Kurtenbach, G., & Singh, K. (1999). Exploring interactive curve and surface manipulation using a bend and twist sensitive input strip. *Proceedings of the 1999 Symposium on Interactive 3D Graphics*, 111–118. https://doi.org/10.1145/300523.300536

Bare Conductive. (2017). *Electric Paint - Technical Data Sheet*. https://www.bareconductive.com/wp-content/uploads/2020/05/2020.05.ElectricPaint-TechDataSheet.pdf

Barlian, A. A., Park, W.-T., Mallon, J. R., Rastegar, A. J., & Pruitt, B. L. (2009). Review: Semiconductor piezoresistance for microsystems. *Proceedings of the IEEE*, *97*(3), 513–552. https://doi.org/10.1109/JPROC.2009.2013612

Barrett, G., & Omote, R. (2010). Projected-capacitive touch technology. *Information Display*, *26*(3), 16–21. https://doi.org/10.1002/j.2637-496X.2010.tb00229.x

Bartolome, E. (2010). Signal conditioning for piezoelectric sensors. *Analog Design Journal*, 24–31. https://www.ti.com/lit/an/slyt369/slyt369.pdf

Bauman, C. (2007, December). How to select a surface-capacitive touch-screen controller. *Information Display*, *23*, 32–36. https://walkermobile.com/December_2007_ID_Selecting_Surface_Capacitive_Touch_Screen_Controller.pdf

Berni, A., Mennig, M., & Schmidt, H. (2004). Doctor blade. In M. A. Aegerter & M. Mennig (Eds.), *Sol-Gel Technologies for Glass Producers and Users* (pp. 89–92). Springer US. https://doi.org/10.1007/978-0-387-88953-5_10

Bhunia, R., Das, S., Dalui, S., Hussain, S., Paul, R., Bhar, R., & Pal, A. K. (2016). Flexible nano-ZnO/polyvinylidene difluoride piezoelectric composite films as energy harvester. *Applied Physics A*, *122*(7), 637. https://doi.org/10.1007/s00339-016-0161-1

Boem, A., & Troiano, G. M. (2019). Non-rigid HCI: A review of deformable interfaces and input. *Proceedings of the 2019 on Designing Interactive Systems Conference*, 885–906. https://doi.org/10.1145/3322276.3322347

Bouhamed, A., Al-Hamry, A., Müller, C., Choura, S., & Kanoun, O. (2017). Assessing the electrical behaviour of MWCNTs/epoxy nanocomposite for strain sensing. *Composites Part B: Engineering*, *128*, 91–99. https://doi.org/10.1016/j.compositesb.2017.07.005

Bowen, C. R., Taylor, J., LeBoulbar, E., Zabek, D., Chauhan, A., & Vaish, R. (2014). Pyroelectric materials and devices for energy harvesting applications. *Energy & Environmental Science*, *7*(12), 3836–3856. https://doi.org/10.1039/C4EE01759E

Braun, A., Zander-Walz, S., Krepp, S., Rus, S., Wichert, R., & Kuijper, A. (2016). CapTap: Combining capacitive gesture recognition and acoustic touch detection. *Proceedings of the 3rd International Workshop on Sensor-Based Activity Recognition and Interaction*. https://doi.org/10.1145/2948963.2948969

Briand, D., Oprea, A., Courbat, J., & Bârsan, N. (2011). Making environmental sensors on plastic foil. *Materials Today*, *14*(9), 416–423. https://doi.org/10.1016/S1369-7021(11)70186-9

Burie, J. C., Chazalon, J., Coustaty, M., Eskenazi, S., Luqman, M. M., Mehri, M., Nayef, N., Ogier, J. M., Prum, S., & Rusiñol, M. (2015). ICDAR2015 competition on smartphone document capture and OCR (SmartDoc). *2015 13th International Conference on Document Analysis and Recognition (ICDAR)*, 1161–1165. https://doi.org/10.1109/ICDAR.2015.7333943

Buxton, B. (2010). 31.1: Invited paper: A touching story: A personal perspective on the history of touch interfaces past and future. *SID Symposium Digest of Technical Papers*, *41*(1), 444–448. https://doi.org/10.1889/1.3500488

Callister, W. D., & Rethwisch, D. G. (2010). *Materials science and engineering: An introduction* (8th ed.). John Wiley & Sons, Inc. https://www.wiley.com/en-pt/Materials+Science+and+Engineering:+An+Introduction,+10th+Edition-p-9781119405498

Cao, Xiaohan, Wei, X., Li, G., Hu, C., Dai, K., Guo, J., Zheng, G., Liu, C., Shen, C., & Guo, Z. (2017). Strain sensing behaviors of epoxy nanocomposites with carbon nanotubes under cyclic deformation. *Polymer*, *112*, 1–9. https://doi.org/10.1016/j.polymer.2017.01.068

Cao, Xuan, Lau, C., Liu, Y., Wu, F., Gui, H., Liu, Q., Ma, Y., Wan, H., Amer, M. R., & Zhou, C. (2016). Fully screen-printed, large-area, and flexible active-matrix electrochromic displays using carbon nanotube thin-film transistors. *ACS Nano*, *10*(11), 9816–9822. https://doi.org/10.1021/acsnano.6b05368

Cartwright, W., Crampton, J., Gartner, G., Miller, S., Mitchell, K., Siekierska, E., & Wood, J. (2001). Geospatial information visualization user interface issues. *Cartography and Geographic Information Science*, *28*(1), 45–60. https://doi.org/10.1559/152304001782173961

Casset, F., Poncet, P., Latour, A., Laroche, B., Bouchet, S., & Fanget, S. (2017). Ultra-thin polymer loudspeaker based on electro active polymer actuation. *2017 19th International Conference on Solid-State Sensors, Actuators and Microsystems (TRANSDUCERS)*, 2051–2054. https://doi.org/10.1109/TRANSDUCERS.2017.7994476

Castano, L. M., & Flatau, A. B. (2014). Smart fabric sensors and e-textile technologies: A review. *Smart Materials and Structures*, *23*(5), 53001. https://doi.org/10.1088/0964-1726/23/5/053001

Castro, H. F., Correia, V., Pereira, N., Costab, P., Oliveiraa, J., & Lanceros-Méndez, S. (2018). Printed Wheatstone bridge with embedded polymer based piezoresistive sensors for strain sensing applications. *Additive Manufacturing*, *20*, 119–125. https://doi.org/10.1016/j.addma.2018.01.004

Castro, H. F., Correia, V., Sowade, E., Mitra, K. Y., Rocha, J. G., Baumann, R. R., & Lanceros-Méndez, S. (2016). All-inkjet-printed low-pass filters with adjustable cutoff frequency consisting of resistors, inductors and transistors for sensor applications. *Organic Electronics*, *38*, 205–212. https://doi.org/10.1016/j.orgel.2016.08.025

Castro, H. F., Sowade, E., Rocha, J. G., Alpuim, P., Lanceros-Méndez, S., & Baumann, R. R. (2014). All-inkjet-printed bottom-gate thin-film transistors using UV curable dielectric for well-defined source-drain electrodes. *Journal of Electronic Materials*, *43*(7), 2631–2636. https://doi.org/10.1007/s11664-014-3143-0

Castro, N., Gonçalves, S., Nunes, J. S., Pereira, N., Correia, V., & Lanceros-Méndez, S. (2017, February 21–22). *Development of printed interactive surfaces based on electroactive polymers* [Poster presentation]. Printed and Flexible Electronics Congress 2017, London, United Kingdom. http://www.globalengage.co.uk/electronics/pr17.html#posters

Cecchetto, J., Fernandes, F. C. B., Lopes, R., & Bueno, P. R. (2017). The capacitive sensing of NS1 Flavivirus biomarker. *Biosensors and Bioelectronics*, *87*, 949–956. https://doi.org/10.1016/j.bios.2016.08.097

Centro ALGORITMI. (2013, November 16). *engageLab was awarded the World Technology Award 2013*. http://algoritmi.uminho.pt/engagelab-was-awarded-the-worldtechnology-award-2013/

Cesário, V., Freitas, P., Pimentel, D., & Nisi, V. (2016). Children's books: Paper vs digital, what do they prefer? *Proceedings of the The 15th International Conference on Interaction Design and Children*, 625–630. https://doi.org/10.1145/2930674.2936004

Chen, S., Yao, K., Tay, F. E. H., & Chew, L. L. S. (2010). Comparative investigation of the structure and properties of ferroelectric poly(vinylidene fluoride) and poly(vinylidene fluoride–trifluoroethylene) thin films crystallized on substrates. *Journal of Applied Polymer Science*, *116*(6), 3331–3337. https://doi.org/10.1002/app.31794

Choi, S., Han, J., Kim, S., Heo, S., & Lee, G. (2011). ThickPad: A hover-tracking touchpad for a laptop. *Proceedings of the 24th Annual ACM Symposium Adjunct on User Interface Software and Technology*, 15–16. https://doi.org/10.1145/2046396.2046405

Chung, D. D. L. (2019). A review of multifunctional polymer-matrix structural composites. *Composites Part B: Engineering*, *160*, 644–660. https://doi.org/10.1016/j.compositesb.2018.12.117

Chung, D. D. L. (2020). A critical review of piezoresistivity and its application in electrical-resistance-based strain sensing. *Journal of Materials Science*, *55*(32), 15367–15396. https://doi.org/10.1007/s10853-020-05099-z

Cleary, F. (2019). *Capacitive touch sensor design guide*. http://ww1.microchip.com/downloads/en/DeviceDoc/AN2934-Capacitive-Touch-Sensor-Design-Guide-00002934A.pdf

Coelho, M., & Maes, P. (2009). Shutters: A permeable surface for environmental control and communication. *Proceedings of the 3rd International Conference on Tangible and Embedded Interaction*, 13–18. https://doi.org/10.1145/1517664.1517671

Coelho, M., & Zigelbaum, J. (2011). Shape-changing interfaces. *Personal and Ubiquitous Computing*, *15*(2), 161–173. https://doi.org/10.1007/s00779-010-0311-y

Correia, D. M., Barbosa, J. C., Costa, C. M., Reis, P. M., Esperança, J. M. S. S., de Zea Bermudez, V., & Lanceros-Méndez, S. (2019). Ionic liquid cation size-dependent electromechanical response of ionic liquid/poly(vinylidene fluoride)-based soft actuators. *The Journal of Physical Chemistry C*, *123*(20), 12744–12752. https://doi.org/10.1021/acs.jpcc.9b00868

Costa, C. M., Kundu, M., Dias, J. C., Nunes-Pereira, J., Botelho, G., Silva, M. M., & Lanceros-Méndez, S. (2019). Mesoporous poly(vinylidene fluoride-co-trifluoroethylene) membranes for lithium-ion battery separators. *Electrochimica Acta*, *301*, 97–106. https://doi.org/10.1016/j.electacta.2019.01.178

Costa, P., Ribeiro, S., & Lanceros-Mendez, S. (2015). Mechanical vs. electrical hysteresis of carbon nanotube/styrene–butadiene–styrene composites and their influence in the electromechanical response. *Composites Science and Technology*, *109*, 1–5. https://doi.org/10.1016/j.compscitech.2015.01.006

Costa, P, Nunes-Pereira, J., Oliveira, J., Silva, J., Moreira, J. A., Carabineiro, S. A. C., Buijnsters, J. G., & Lanceros-Mendez, S. (2017). High-performance graphene-based carbon nanofiller/polymer composites for piezoresistive sensor applications. *Composites Science and Technology*, *153*, 241–252. https://doi.org/10.1016/j.compscitech.2017.11.001

Costa, P, Silva, J., & Lanceros Mendez, S. (2016). Strong increase of the dielectric response of carbon nanotube/poly(vinylidene fluoride) composites induced by carbon nanotube type and pre-treatment. *Composites Part B: Engineering*, *93*, 310–316. https://doi.org/10.1016/j.compositesb.2016.03.010

Costa, Pedro, Gonçalves, S. A. P., Mora, H., Carabineiro, S. A. C., Viana, J. C., & Lanceros-Mendez, S. (2019). Highly sensitive piezoresistive graphene-based stretchable composites for sensing applications. *ACS Applied Materials & Interfaces*, *11*(49), 46286–46295. https://doi.org/10.1021/acsami.9b19294

Costa, Pedro, Nunes-Pereira, J., Pereira, N., Castro, N., Gonçalves, S., & Lanceros-Mendez, S. (2019). Recent progress on piezoelectric, pyroelectric, and magnetoelectric polymer-based energy-harvesting devices. *Energy Technology*, *7*(7), 1800852. https://doi.org/10.1002/ente.201800852

Cui, H., & Zhao, F. (2021). Damage identification for a beam structure based on a PVDF piezoelectric film combined sensor. *Measurement Science and Technology*, *32*(11), 115105. https://doi.org/10.1088/1361-6501/ac1150

Curie, J., & Curie, P. (1880). *Développement par compression de l'électricité polaire dans les cristaux hémièdres à faces inclinées* [Development by compression of polar electricity in hemihedral crystals with inclined faces]. *Bulletin de La Société Minéralogique de France*, *3*(4), 90–93. https://doi.org/10.3406/bulmi.1880.1564

Curry, E. J., Ke, K., Chorsi, M. T., Wrobel, K. S., Miller, A. N., Patel, A., Kim, I., Feng, J., Yue, L., Wu, Q., Kuo, C.-L., Lo, K. W.-H., Laurencin, C. T., Ilies, H., Purohit, P. K., & Nguyen, T. D. (2018). Biodegradable piezoelectric force sensor. *Proceedings of the National Academy of Sciences*, *115*(5), 909–914. https://doi.org/10.1073/pnas.1710874115

Damalerio, R. B., Lim, R., Chen, W., Choong, D. S. W., & Cheng, M.-Y. (2018). Evaluation of piezoresistive polymer-based traces for non-invasive sensor patch. *2018 IEEE 20th Electronics Packaging Technology Conference (EPTC)*, 55–58. https://doi.org/10.1109/EPTC.2018.8654338

Darcovich, K., & Kutowy, O. (1988). Surface tension considerations for membrane casting systems. *Journal of Applied Polymer Science*, *35*(7), 1769–1778. https://doi.org/10.1002/app.1988.070350705

Das, S., & Saha, P. (2018). A review of some advanced sensors used for health diagnosis of civil engineering structures. *Measurement*, *129*, 68–90. https://doi.org/10.1016/j.measurement.2018.07.008

Davison, B. (2010). Techniques for robust touch sensing design. *AN1334 Microchip Technology Inc.*, 1–30. http://ww1.microchip.com/downloads/en/DeviceDoc/00001334B.pdf

de Gans, B.-J., Duineveld, P. C., & Schubert, U. S. (2004). Inkjet printing of polymers: State of the art and future developments. *Advanced Materials*, *16*(3), 203–213. https://doi.org/10.1002/adma.200300385

Dearden, A. L., Smith, P. J., Shin, D.-Y., Reis, N., Derby, B., & O'Brien, P. (2005). A low curing temperature silver ink for use in ink-jet printing and subsequent production of conductive tracks. *Macromolecular Rapid Communications*, *26*(4), 315–318. https://doi.org/10.1002/marc.200400445

Dehsari, H. S., Michels, J. J., & Asadi, K. (2017). Processing of ferroelectric polymers for microelectronics: from morphological analysis to functional devices. *Jounal of Materials Chemistry C*, *5*(40), 10490–10497. https://doi.org/10.1039/C7TC01495C

Dementyev, A., Kao, H.-L. (Cindy), & Paradiso, J. A. (2015). SensorTape: Modular and programmable 3D-aware dense sensor network on a tape. *Proceedings of the 28th Annual ACM Symposium on User Interface Software & Technology*, 649–658. https://doi.org/10.1145/2807442.2807507

Dempsey, S. J., Szablewski, M., & Atkinson, D. (2015). Tactile sensing in human–computer interfaces: The inclusion of pressure sensitivity as a third dimension of user input. *Sensors and Actuators A: Physical*, *232*, 229–250. https://doi.org/10.1016/j.sna.2015.05.025

Dias, J. C., Lopes, A. C., Magalhães, B., Botelho, G., Silva, M. M., Esperança, J. M. S. S., & Lanceros-Mendez, S. (2015). High performance electromechanical actuators based on ionic liquid/poly(vinylidene fluoride). *Polymer Testing*, *48*, 199–205. https://doi.org/10.1016/j.polymertesting.2015.10.012

Dias, J. C., Martins, M. S., Ribeiro, S., Silva, M. M., Esperança, J. M. S. S., Ribeiro, C., Botelho, G., Costa, C. M., & Lanceros-Mendez, S. (2016). Electromechanical actuators based on poly(vinylidene fluoride) with $[N_{1112(OH)}][NTf_2]$ and $[C_2mim]$ $[C_2SO_4]$. *Journal of Materials Science*, *51*(20), 9490–9503. https://doi.org/10.1007/s10853-016-0193-0

Dios, J.R., Garcia-Astrain, C., Gonçalves, S., Costa, P., & Lanceros-Méndez, S. (2019). Piezoresistive performance of polymer-based materials as a function of the matrix and nanofiller content to walking detection application. *Composites Science and Technology*, *181*, 107678. https://doi.org/10.1016/j.compscitech.2019.107678

Dios, Jose R, Gonzalo, B., Tubio, C. R., Cardoso, J., Gonçalves, S., Miranda, D., Correia, V., Viana, J. C., Costa, P., & Lanceros-Méndez, S. (2020). Functional piezoresistive polymer-composites based on polycarbonate and polylactic acid for deformation sensing applications. *Macromolecular Materials and Engineering*, 2000379. https://doi.org/10.1002/mame.202000379

Drogemuller, A., Walsh, J., Smith, R. T., Adcock, M., & Thomas, B. H. (2021). Turning everyday objects into passive tangible controllers. *Proceedings of the Fifteenth International Conference on Tangible, Embedded, and Embodied Interaction*. https://doi.org/10.1145/3430524.3442460

Du, L. (2016). An overview of mobile capacitive touch technologies trends. *ArXiv*, *abs/1612.0*. http://arxiv.org/abs/1612.08227

Duan, L., D'hooge, D. R., & Cardon, L. (2020). Recent progress on flexible and stretchable piezoresistive strain sensors: From design to application. *Progress in Materials Science*, *114*, 100617. https://doi.org/10.1016/j.pmatsci.2019.100617

Dutta, B., Kar, E., Bose, N., & Mukherjee, S. (2018). NiO@SiO2/PVDF: A flexible polymer nanocomposite for a high performance human body motion-based energy harvester and tactile e-skin mechanosensor. *ACS Sustainable Chemistry & Engineering*, *6*(8), 10505–10516. https://doi.org/10.1021/acssuschemeng.8b01851

Ellingford, C., Zhang, R., Wemyss, A. M., Zhang, Y., Brown, O. B., Zhou, H., Keogh, P., Bowen, C., & Wan, C. (2020). Self-healing dielectric elastomers for damage-tolerant actuation and energy harvesting. *ACS Applied Materials & Interfaces*, *12*(6), 7595–7604. https://doi.org/10.1021/acsami.9b21957

Emgin, S. E., Aghakhani, A., Sezgin, T. M., & Basdogan, C. (2019). HapTable: An interactive tabletop providing online haptic feedback for touch gestures. *IEEE Transactions on Visualization and Computer Graphics*, *25*(9), 2749–2762. https://doi.org/10.1109/TVCG.2018.2855154

Fan, W., Lok, B. K., Lai, F. K., & Wei, J. (2017). Evaluation of printed capacitive touch sensors for touch panel. *2017 IEEE 19th Electronics Packaging Technology Conference (EPTC)*, 1–4. https://doi.org/10.1109/EPTC.2017.8277586

Farah, S., Anderson, D. G., & Langer, R. (2016). Physical and mechanical properties of PLA, and their functions in widespread applications — A comprehensive review. *Advanced Drug Delivery Reviews*, *107*, 367–392. https://doi.org/10.1016/j.addr.2016.06.012

Ferreira, I., Brás, B., Martins, J. I., Correia, N., Barquinha, P., Fortunato, E., & Martins, R. (2011). Solid-state paper batteries for controlling paper transistors. *Electrochimica Acta*, *56*(3), 1099–1105. https://doi.org/10.1016/j.electacta.2010.10.018

Figueiredo, A. C., Pinto, A. L., Branco, P., Zagalo, N., & Coquet, E. (2013). Bridging book: A not-so-electronic children's picturebook. *Proceedings of the 12th International Conference on Interaction Design and Children - IDC '13*, 569–572. https://doi.org/10.1145/2485760.2485867

Figueiredo, A. C., Pinto, A. L., Zagalo, N., & Branco, P. (2013). Bridging Book: A not-so-electronic children picturebook. *CHI '13 Extended Abstracts on Human Factors in Computing Systems*, 2801–2802. https://doi.org/10.1145/2468356.2479519

Figueiredo, A. C. P. De, Pinto, A. L. J., Branco, P. S. O., & Zagalo, N. T. (2014). *Interactive book electronic system and operation method thereof* (Patent No. US 9,965,050 B2). United States Patent and Trademark Office (USPTO). https://patents.google.com/patent/US9965050B2/en

Follmer, S., Leithinger, D., Olwal, A., Cheng, N., & Ishii, H. (2012). Jamming user interfaces: Programmable particle stiffness and sensing for malleable and shape-changing devices. *Proceedings of the 25th Annual ACM Symposium on User Interface Software and Technology*, 519–528. https://doi.org/10.1145/2380116.2380181

Frecker, M. I., & Aguilera, W. M. (2003). Analytical modeling of a segmented unimorph actuator using electrostrictive P(VDF-TrFE) copolymer. *Smart Materials and Structures*, *13*(1), 82–91. https://doi.org/10.1088/0964-1726/13/1/010

Fukada, E. (2000). History and recent progress in piezoelectric polymers. *IEEE Transactions on Ultrasonics, Ferroelectrics, and Frequency Control*, *47*(6), 1277–1290. https://doi.org/10.1109/58.883516

Fulay, P., & Lee, J.-K. (2016). *Electronic, magnetic, and optical materials* (Y. Gogotsi (ed.); 2nd ed.). CRC Press. https://www.routledge.com/Electronic-Magnetic-and-Optical-Materials/Fulay-Lee/p/book/9781498701693

Gao, L., Zhu, C., Li, L., Zhang, C., Liu, J., Yu, H.-D., & Huang, W. (2019). All paper-based flexible and wearable piezoresistive pressure sensor. *ACS Applied Materials & Interfaces*, *11*(28), 25034–25042. https://doi.org/10.1021/acsami.9b07465

Gao, S, Arcos, V., & Nathan, A. (2016). Piezoelectric vs. capacitive based force sensing in capacitive touch panels. *IEEE Access*, *4*, 3769–3774. https://doi.org/10.1109/ACCESS.2016.2591535

Gao, Shuo, & Wu, L. (2019). Why piezoelectric material is unsuccessful in interactive displays: Challenges in high detection accuracy. *IEEE Consumer Electronics Magazine*, *8*(4), 28–31. https://doi.org/10.1109/MCE.2019.2892264

Georgakilas, V., Gournis, D., Tzitzios, V., Pasquato, L., Guldi, D. M., & Prato, M. (2007). Decorating carbon nanotubes with metal or semiconductor nanoparticles. *Jounal of Materials Chemistry*, *17*(26), 2679–2694. https://doi.org/10.1039/B700857K

Georgopoulou, A., & Clemens, F. (2020). Piezoresistive elastomer-based composite strain sensors and their applications. *ACS Applied Electronic Materials*, *2*(7), 1826–1842. https://doi.org/10.1021/acsaelm.0c00278

Gerard, C., & Desmulliez, P. Y. M. (2012). Inkjet printing of conductive materials: A review. *Circuit World*, *38*(4), 193–213. https://doi.org/10.1108/03056121211280413

Gomes, A., Priyadarshana, L. L., Visser, A., Carrascal, J. P., & Vertegaal, R. (2018). Magicscroll: A rollable display device with flexible screen real estate and gestural input. *Proceedings of the 20th International Conference on Human-Computer Interaction with Mobile Devices and Services*. https://doi.org/10.1145/3229434.3229442

Gonçalves, B. F., Costa, P., Oliveira, J., Ribeiro, S., Correia, V., Botelho, G., & Lanceros-Mendez, S. (2016). Green solvent approach for printable large deformation thermoplastic elastomer based piezoresistive sensors and their suitability for biomedical applications. *Journal of Polymer Science Part B: Polymer Physics*, *54*(20), 2092–2103. https://doi.org/10.1002/polb.24118

Gonçalves, B. F. F., Oliveira, J., Costa, P., Correia, V., Martins, P., Botelho, G., & Lanceros-Mendez, S. (2017). Development of water-based printable piezoresistive sensors for large strain applications. *Composites Part B: Engineering*, *112*, 344–352. https://doi.org/10.1016/j.compositesb.2016.12.047

Gonçalves, S., Pereira, N., Correia, V., & Lanceros-Méndez, S. (2019, March 19–21). *Multitouch printed touchscreens based on piezoelectric polymers* [Poster presentation]. LOPEC 2019, Munich, Germany. http://program.lopec.com/#!contentsessions/36021

Gonçalves, S., Serrado-Nunes, J., Oliveira, J., Pereira, N., Hilliou, L., Costa, C. M., & Lanceros-Méndez, S. (2019a). *ACS Applied Electronic Materials*, *1*(8) [Cover image]. https://pubs.acs.org/pb-assets/images/_journalCovers/aaembp/aaembp_v001i008-3.jpg

Gonçalves, S., Serrado-Nunes, J., Oliveira, J., Pereira, N., Hilliou, L., Costa, C. M., & Lanceros-Méndez, S. (2019b). Environmentally friendly printable piezoelectric inks and their application in the development of all-printed touch screens. *ACS Applied Electronic Materials*, *1*(8), 1678–1687. https://doi.org/10.1021/acsaelm.9b00363

Greaves, R. W., & Lamb, D. R. (1971). Observation of the inverse piezoelectric effect in polyethylene while under a polarising field. *Journal of Materials Science*, *6*(1), 74–79. https://doi.org/10.1007/BF00550294

Grosse-Puppendahl, T., Berghoefer, Y., Braun, A., Wimmer, R., & Kuijper, A. (2013). OpenCapSense: A rapid prototyping toolkit for pervasive interaction using capacitive sensing. *2013 IEEE International Conference on Pervasive Computing and Communications (PerCom)*, 152–159. https://doi.org/10.1109/PerCom.2013.6526726

Grosse-Puppendahl, T., Braun, A., Kamieth, F., & Kuijper, A. (2013). Swiss-Cheese Extended: An object recognition method for ubiquitous interfaces based on capacitive proximity sensing. *Proceedings of the SIGCHI Conference on Human Factors in Computing Systems*, 1401–1410. https://doi.org/10.1145/2470654.2466186

Grosse-Puppendahl, T., Holz, C., Cohn, G., Wimmer, R., Bechtold, O., Hodges, S., Reynolds, M. S., & Smith, J. R. (2017). Finding common ground: A survey of capacitive sensing in human-computer interaction. *Proceedings of the 2017 CHI Conference on Human Factors in Computing Systems*, 3293–3315. https://doi.org/10.1145/3025453.3025808

Guo, C., Yu, Y., & Liu, J. (2014). Rapidly patterning conductive components on skin substrates as physiological testing devices via liquid metal spraying and pre-designed mask. *Journal of Materials Chemistry B*, *2*(35), 5739–5745. https://doi.org/10.1039/C4TB00660G

Gusarov, B., Gimeno, L., Gusarova, E., Viala, B., Boisseau, S., & Cugat, O. (2015). Flexible composite thermal energy harvester using piezoelctric PVDF polymer and shape memory alloy. *IEEE Solid-State Sensors, Actuators and Microsystems (TRANSDUCERS)*, 722–725. https://doi.org/10.1109/TRANSDUCERS.2015.7181025

Hajian, S., Zhang, X., Maddipatla, D., Narakathu, B. B., Rodriguez-Labra, J. I., Blair, R. G., & Atashbar, M. Z. (2019). Flexible capacitive humidity sensor based on fluorinated graphene. *2019 IEEE SENSORS*, 1–4. https://doi.org/10.1109/SENSORS43011.2019.8956564

Harley, J. A., & Orsley, T. J. (2009). *Single layer mutual capacitance sensing systems, device, components and methods* (Patent No. US 2009/0194344 A1). United States Patent and Trademark Office (USPTO). https://patents.google.com/patent/US20090194344A1

Harrison, J. S., & Ounaies, Z. (2002). Piezoelectric polymers. In *Encyclopedia of Polymer Science and Technology* (Vol. 3, pp. 474–498). American Cancer Society. https://doi.org/10.1002/0471440264.pst427

Hartono, A., Darwin, Ramli, Satira, S., Djamal, M., & Herman. (2016). Electric field poling 2G V/m to improve piezoelectricity of PVDF thin film. *AIP Conference Proceedings*, *1719*(1), 30021. https://doi.org/10.1063/1.4943716

Heywang, W., Lubitz, K., & Wersing, W. (2008). Piezoelectricity: Evolution and future of a technology. In W. Heywang, K. Lubitz, & W. Wersing (Eds.), *Springer Series in Materials Science* (1st ed., Vol. 114). Springer-Verlag Berlin Heidelberg. https://doi.org/10.1007/978-3-540-68683-5

Higashihata, Y., Sako, J., & Yagi, T. (1981). Piezoelectricity of vinylidene fluoride-trifluoroethylene copolymers. *Ferroelectrics*, *32*(1), 85–92. https://doi.org/10.1080/00150198108238678

Ho, T.-K., Lee, C.-Y., Tseng, M.-C., & Kwok, H.-S. (2009). 32.3: Simple single-layer multi-touch projected capacitive touch panel. *SID Symposium Digest of Technical Papers*, *40*(1), 447–450. https://doi.org/10.1889/1.3256812

Hoch, D., & Badaye, M. (2017). *Capacitive sensing pattern* (Patent No. US 9,740,348 B2). United States Patent and Trademark Office (USPTO). https://patents.google.com/patent/US9740348B2

Hoeng, F., Denneulin, A., & Bras, J. (2016). Use of nanocellulose in printed electronics: A review. *Nanoscale*, *8*, 13131–13154. https://doi.org/10.1039/C6NR03054H

Holman, D., & Vertegaal, R. (2008). Organic user interfaces: Designing computers in any way, shape, or form. *Communications of the ACM*, *51*(6), 48–55. https://doi.org/10.1145/1349026.1349037

Hong, C.-H., Jae-Heon, S., Ju, B.-K., Kim, K.-H., Park, N.-M., Kim, B.-S., & Cheong, W.-S. (2013). Index-matched indium tin oxide electrodes for capactivie touch screen panel applications. *Journal of Nanoscience and Nanotechnology*, *13*(11), 7756–7759. https://doi.org/10.1166/jnn.2013.7814

Hösel, M., Søndergaard, R. R., Angmo, D., & Krebs, F. C. (2013). Comparison of fast roll-to-roll flexographic, inkjet, flatbed, and rotary screen printing of metal back electrodes for polymer solar cells. *Advanced Engineering Materials*, *15*(10), 995–1001. https://doi.org/10.1002/adem.201300011

Hu, L., Zhong, J., Tian, Y., Zheng, X., Cheng, J., & Pu, Z. (2019). Study on properties of barium titanate/polyethersulfone dielectric composites prepared by physical dispersion method. *Journal of Materials Science: Materials in Electronics*, *30*(1), 221–229. https://doi.org/10.1007/s10854-018-0284-6

Hu, N., Itoi, T., Akagi, T., Kojima, T., Xue, J., Yan, C., Atobe, S., Fukunaga, H., Yuan, W., Ning, H., Surina, Liu, Y., & Alamusi. (2013). Ultrasensitive strain sensors made from metal-coated carbon nanofiller/epoxy composites. *Carbon*, *51*, 202–212. https://doi.org/10.1016/j.carbon.2012.08.029

Hu, Y., Zhao, T., Zhu, P., Zhang, Y., Liang, X., Sun, R., & Wong, C.-P. (2018). A low-cost, printable, and stretchable strain sensor based on highly conductive elastic composites with tunable sensitivity for human motion monitoring. *Nano Research*, *11*(4), 1938–1955. https://doi.org/10.1007/s12274-017-1811-0

Huan, Y., Liu, Y., & Yang, Y. (2007). Simultaneous stretching and static electric field poling of poly(vinylidene fluoride-hexafluoropropylene) copolymer films. *Polymer Engineering & Science*, *47*(10), 1630–1633. https://doi.org/10.1002/pen.20843

Huang, Q., & Zhu, Y. (2019). Printing conductive nanomaterials for flexible and stretchable electronics: A review of materials, processes, and applications. *Advanced Materials Technologies*, *4*(5), 1800546. https://doi.org/10.1002/admt.201800546

Hussaini, S., Jiang, H., Walsh, P., MacSweeney, D., & Makinwa, K. A. A. (2018). A 15nW per button noise-immune readout IC for capacitive touch sensor. *ESSCIRC 2018 - IEEE 44th European Solid State Circuits Conference (ESSCIRC)*, 190–193. https://doi.org/10.1109/ESSCIRC.2018.8494283

Hwang, B.-U., Zabeeb, A., Trung, T. Q., Wen, L., Lee, J. D., Choi, Y.-I., Lee, H.-B., Kim, J. H., Han, J. G., & Lee, N.-E. (2019). A transparent stretchable sensor for distinguishable detection of touch and pressure by capacitive and piezoresistive signal transduction. *NPG Asia Materials*, *11*(1), 23. https://doi.org/10.1038/s41427-019-0126-x

Irfan, M. S., Khan, T., Hussain, T., Liao, K., & Umer, R. (2021). Carbon coated piezoresistive fiber sensors: From process monitoring to structural health monitoring of composites – A review. *Composites Part A: Applied Science and Manufacturing*, *141*, 106236. https://doi.org/10.1016/j.compositesa.2020.106236

Ishii, H. (2008). Tangible Bits: Beyond pixels. *Proceedings of the 2nd International Conference on Tangible and Embedded Interaction*, xv–xxv. https://doi.org/10.1145/1347390.1347392

Ishii, H., Lakatos, D., Bonanni, L., & Labrune, J.-B. (2012). Radical Atoms: Beyond Tangible Bits, toward transformable materials. *Interactions*, *19*(1), 38–51. https://doi.org/10.1145/2065327.2065337

Ishii, H., & Ullmer, B. (1997). Tangible Bits: Towards seamless interfaces between people, bits and atoms. *Proceedings of the SIGCHI Conference on Human Factors in Computing Systems CHI 97*, *39*, 234–241. https://doi.org/10.1145/258549.258715

Jaffe, H., & Berlincourt, D. A. (1965). Piezoelectric transducer materials. *Proceedings of the IEEE*, *53*(10), 1372–1386. https://doi.org/10.1109/PROC.1965.4253

Jang, Y., Park, Y. D., Lim, J. A., Lee, H. S., Lee, W. H., & Cho, K. (2006). Patterning the organic electrodes of all-organic thin film transistors with a simple spray printing technique. *Applied Physics Letters*, *89*(18), 183501. https://doi.org/10.1063/1.2372583

Ji, H., Li, H., Huang, Z., Wang, B., & Li, H. (2014). Measurement of gas-liquid two-phase flow in micro-pipes by a capacitance sensor. *Sensors*, *14*(12), 22431–22446. https://doi.org/10.3390/s141222431

Jing, L., Dai, Z., & Zhou, Y. (2017). Wearable handwriting recognition with an inertial sensor on a finger nail. *2017 14th IAPR International Conference on Document Analysis and Recognition (ICDAR)*, *01*, 1330–1337. https://doi.org/10.1109/ICDAR.2017.219

Jones, L. (2019). A co-design toolkit for wearable e-textiles. *Adjunct Proceedings of the 2019 ACM International Joint Conference on Pervasive and Ubiquitous Computing and Proceedings of the 2019 ACM International Symposium on Wearable Computers*, 363–366. https://doi.org/10.1145/3341162.3349303

Joo, Y., Yoon, J., Ha, J., Kim, T., Lee, S., Lee, B., Pang, C., & Hong, Y. (2017). Highly sensitive and bendable capacitive pressure sensor and its application to 1 V operation pressure-sensitive transistor. *Advanced Electronic Materials*, *3*(4), 1600455. https://doi.org/10.1002/aelm.201600455

Jung, S.-H., Kim, J.-J., & Kim, H.-J. (2012). High performance inkjet printed phosphorescent organic light emitting diodes based on small molecules commonly used in vacuum processes. *Thin Solid Films*, *520*(23), 6954–6958. https://doi.org/10.1016/j.tsf.2012.07.084

Kamel, T. M., & de With, G. (2008). Poling of hard ferroelectric PZT ceramics. *Journal of the European Ceramic Society*, *28*(9), 1827–1838. https://doi.org/10.1016/j.jeurceramsoc.2007.11.023

Kaneswaran, K., & Arshak, K. (2009). Capacitive interfaces for navigation of electric powered wheelchairs. In C. T. Lim & J. C. H. Goh (Eds.), *13th International Conference on Biomedical Engineering* (pp. 1153–1157). Springer Berlin Heidelberg. https://doi.org/10.1007/978-3-540-92841-6_283

Kao, K. C. (2004). 4 - Ferroelectrics, piezoelectrics, and pyroelectrics. In K. C. Kao (Ed.), *Dielectric Phenomena in Solids* (pp. 213–282). Academic Press. https://doi.org/10.1016/B978-012396561-5/50014-1

Karki, J. (2000). Signal conditioning piezoelectric sensors. In *Application Report SLOA033A*. Texas Instruments Incorporated. https://www.ti.com/lit/an/sloa033a/sloa033a.pdf

Katsuura, T., Izumi, S., Yoshimoto, M., Kawaguchi, H., Yoshimoto, S., & Sekitani, T. (2017). Wearable pulse wave velocity sensor using flexible piezoelectric film array. *2017 IEEE Biomedical Circuits and Systems Conference (BioCAS)*, 1–4. https://doi.org/10.1109/BIOCAS.2017.8325551

Kaura, T., Nath, R., & Perlman, M. M. (1991). Simultaneous stretching and corona poling of PVDF films. *Journal of Physics D: Applied Physics*, *24*(10), 1848–1852. https://doi.org/10.1088/0022-3727/24/10/020

Kawai, H. (1969). The piezoelectricity of poly (vinylidene Fluoride). *Japanese Journal of Applied Physics*, *8*(7), 975–976. https://doi.org/10.1143/JJAP.8.975

Ke, K., Solouki Bonab, V., Yuan, D., & Manas-Zloczower, I. (2018). Piezoresistive thermoplastic polyurethane nanocomposites with carbon nanostructures. *Carbon*, *139*, 52–58. https://doi.org/10.1016/j.carbon.2018.06.037

Ke, K., Yue, L., Shao, H., Yang, M.-B., Yang, W., & Manas-Zloczower, I. (2021). Boosting electrical and piezoresistive properties of polymer nanocomposites via hybrid carbon fillers: A review. *Carbon*, *173*, 1020–1040. https://doi.org/10.1016/j.carbon.2020.11.070

Kellogg, B., Talla, V., & Gollakota, S. (2014). Bringing gesture recognition to all devices. *11th USENIX Symposium on Networked Systems Design and Implementation (NSDI 14)*, 303–316. https://www.usenix.org/conference/nsdi14/technical-sessions/presentation/kellogg

Khan, S., Dang, W., Lorenzelli, L., & Dahiya, R. (2015). Flexible pressure sensors based on screen-printed P(VDF-TrFE) and P(VDF-TrFE)/MWCNTs. *IEEE Transactions on Semiconductor Manufacturing*, *28*(4), 486–493. https://doi.org/10.1109/TSM.2015.2468053

Khan, S., Lorenzelli, L., & Dahiya, R. S. (2015). Technologies for printing sensors and electronics over large flexible substrates: A review. *IEEE Sensors Journal*, *15*(6), 3164–3185. https://doi.org/10.1109/JSEN.2014.2375203

Khan, Y., Thielens, A., Muin, S., Ting, J., Baumbauer, C., & Arias, A. C. (2020). A new frontier of printed electronics: Flexible hybrid electronics. *Advanced Materials*, *32*(15), 1905279. https://doi.org/10.1002/adma.201905279

Khandelwal, G., Maria Joseph Raj, N. P., & Kim, S.-J. (2021). Materials beyond conventional triboelectric series for fabrication and applications of triboelectric nanogenerators. *Advanced Energy Materials*, *11*(33), 2101170. https://doi.org/10.1002/aenm.202101170

Kim, J., Kumar, R., Bandodkar, A. J., & Wang, J. (2017). Advanced materials for printed wearable electrochemical devices: A Review. *Advanced Electronic Materials*, *3*(1), 1600260. https://doi.org/10.1002/aelm.201600260

Kim, W., Oh, H., Kwak, Y., Park, K., Ju, B.-K., & Kim, K. (2015). Development of a carbon nanotube-based touchscreen capable of multi-touch and multi-forse sensing. *Sensors*, *15*(11), 28732–28741. https://doi.org/10.3390/s151128732

King, T. G., Preston, M. E., Murphy, B. J. M., & Cannell, D. S. (1990). Piezoelectric ceramic actuators: A review of machinery applications. *Precision Engineering*, *12*(3), 131–136. https://doi.org/10.1016/0141-6359(90)90084-C

Kisić, M., Blaž, N., Žlebič, Č., Živanov, L., & Huđik, A. (2017). Flexible polyimide based capacitive displacement sensor. *2017 40th International Spring Seminar on Electronics Technology (ISSE)*, 1–4. https://doi.org/10.1109/ISSE.2017.8000995

Ko, S. H., Pan, H., Grigoropoulos, C. P., Luscombe, C. K., Fréchet, J. M. J., & Poulikakos, D. (2007). All-inkjet-printed flexible electronics fabrication on a polymer substrate by low-temperature high-resolution selective laser sintering of metal nanoparticles. *Nanotechnology*, *18*(34), 1–8. https://doi.org/10.1088/0957-4484/18/34/345202

Krebs, F. C. (2009). Fabrication and processing of polymer solar cells: A review of printing and coating techniques. *Solar Energy Materials and Solar Cells*, *93*(4), 394–412. https://doi.org/10.1016/j.solmat.2008.10.004

Kwon, O., An, J., & Hong, S. (2018). Capacitive touch systems with styli for touch sensors: A review. *IEEE Sensors Journal*, *18*(12), 4832–4846. https://doi.org/10.1109/JSEN.2018.2830660

Lantada, A. D. (2012). *Handbook of active materials for medical devices: Advances and applications* (1st ed.). Jenny Stanford Publishing. https://www.routledge.com/Handbook-of-Active-Materials-for-Medical-Devices-Advances-and-Applications/Lantada/p/book/9789814303361

Lasheras, A., Gutiérrez, J., Reis, S., Sousa, D., Silva, M., Martins, P., Lanceros-Mendez, S., Barandiarán, J. M., Shishkin, D. A., & Potapov, A. P. (2015). Energy harvesting device based on a metallic glass/PVDF magnetoelectric laminated composite. *Smart Materials and Structures*, *24*(6), 65024. https://doi.org/10.1088/0964-1726/24/6/065024

Lee, C. S., Kim, J. Y., Lee, D. E., Koo, Y. K., Joo, J., Han, S., Beag, Y. W., & Koh, S. K. (2003). Organic based flexible speaker through enhanced conductivity of PEDOT/PSS with various solvents. *Synthetic Metals*, *135–136*, 13–14. https://doi.org/10.1016/S0379-6779(02)01026-3

Lee, C., & Tarbutton, J. A. (2014). Electric poling-assisted additive manufacturing process for PVDF polymer-based piezoelectric device applications. *Smart Materials and Structures*, *23*(9), 95044. https://doi.org/10.1088/0964-1726/23/9/095044

Lee, J.-H., Yoon, H.-J., Kim, T. Y., Gupta, M. K., Lee, J. H., Seung, W., Ryu, H., & Kim, S.-W. (2015). Micropatterned P(VDF-TrFE) film-based piezoelectric nanogenerators for highly sensitive self-powered pressure sensors. *Advanced Functional Materials*, *25*(21), 3203–3209. https://doi.org/10.1002/adfm.201500856

Li, J. H., Hong, R. Y., Li, M. Y., Li, H. Z., Zheng, Y., & Ding, J. (2009). Effects of ZnO nanoparticles on the mechanical and antibacterial properties of polyurethane coatings. *Progress in Organic Coatings*, *64*(4), 504–509. https://doi.org/10.1016/j.porgcoat.2008.08.013

Li, Jiangyu, Liu, Y., Zhang, Y., Cai, H.-L., & Xiong, R.-G. (2013). Molecular ferroelectrics: Where electronics meet biology. *Physical Chemistry Chemical Physics*, *15*(48), 20786–20796. https://doi.org/10.1039/C3CP52501E

Li, Jing, Fang, L., Sun, B., Li, X., & Kang, S. H. (2020). Review – Recent progress in flexible and stretchable piezoresistive sensors and their applications. *Journal of The Electrochemical Society*, *167*(3), 37561. https://doi.org/10.1149/1945-7111/ab6828

Li, Q., & Wang, Q. (2016). Ferroelectric polymers and their energy-related applications. *Macromolecular Chemistry and Physics*, *217*(11), 1228–1244. https://doi.org/10.1002/macp.201500503

Li, Q., Xing, J., Shang, D., & Wang, Y. (2019). A flow velocity measurement method based on a PVDF piezoelectric sensor. *Sensors*, *19*(7). https://doi.org/10.3390/s19071657

Li, R.-Z., Hu, A., Zhang, T., & Oakes, K. D. (2014). Direct writing on paper of foldable capacitive touch pads with silver nanowire inks. *ACS Applied Materials & Interfaces*, *6*(23), 21721–21729. https://doi.org/10.1021/am506987w

Li, S., & Lipson, H. (2009). Vertical-stalk flapping-leaf generator for wind energy harvesting. *ASME 2009 Conference on Smart Materials, Adaptive Structures and Intelligent Systems*, *2*, 611–619. https://doi.org/10.1115/SMASIS2009-1276

Liu, H. (刘虎), Huang, W. (黄文举), Gao, J. (高嘉辰), Dai, K. (代坤), Zheng, G. (郑国强), Liu, C. (刘春太), Shen, C. (申长雨), Yan, X. (闫星如), Guo, J. (郭江), & Guo, Z. (郭战虎). (2016). Piezoresistive behavior of porous carbon nanotube-thermoplastic polyurethane conductive nanocomposites with ultrahigh compressibility. *Applied Physics Letters*, *108*(1), 11904. https://doi.org/10.1063/1.4939265

Liu, H., Dong, M., Huang, W., Gao, J., Dai, K., Guo, J., Zheng, G., Liu, C., Shen, C., & Guo, Z. (2017). Lightweight conductive graphene/thermoplastic polyurethane foams with ultrahigh compressibility for piezoresistive sensing. *Journal of Materials Chemistry C*, *5*(1), 73–83. https://doi.org/10.1039/C6TC03713E

Lizundia, E., Puglia, D., Nguyen, T.-D., & Armentano, I. (2020). Cellulose nanocrystal based multifunctional nanohybrids. *Progress in Materials Science*, *112*, 100668. https://doi.org/10.1016/j.pmatsci.2020.100668

Lu, K., Huang, W., Guo, J., Gong, T., Wei, X., Lu, B.-W., Liu, S.-Y., & Yu, B. (2018). Ultra-sensitive strain sensor based on flexible poly(vinylidene fluoride) piezoelectric film. *Nanoscale Research Letters*, *13*(1), 83. https://doi.org/10.1186/s11671-018-2492-7

Lu, Y., Biswas, M. C., Guo, Z., Jeon, J.-W., & Wujcik, E. K. (2019). Recent developments in bio-monitoring via advanced polymer nanocomposite-based wearable strain sensors. *Biosensors and Bioelectronics*, *123*, 167–177. https://doi.org/10.1016/j.bios.2018.08.037

Luo, C., Borkar, M. A., Redfern, A. J., & McClellan, J. H. (2012). Compressive sensing for sparse touch detection on capacitive touch screens. *IEEE Journal on Emerging and Selected Topics in Circuits and Systems*, *2*(3), 639–648. https://doi.org/10.1109/JETCAS.2012.2217033

Ma, S., Ribeiro, F., Powell, K., Lutian, J., Møller, C., Large, T., & Holbery, J. (2015). Fabrication of novel transparent touch sensing device via drop-on-demand inkjet printing technique. *ACS Applied Materials & Interfaces*, *7*(39), 21628–21633. https://doi.org/10.1021/acsami.5b04717

Mahanty, B., Ghosh, S. K., Garain, S., & Mandal, D. (2017). An effective flexible wireless energy harvester/sensor based on porous electret piezoelectric polymer. *Materials Chemistry and Physics*, *186*, 327–332. https://doi.org/10.1016/j.matchemphys.2016.11.003

Marshall, J. M., Zhang, Q., & Whatmore, R. W. (2008). Corona poling of highly (001)/(100)-oriented lead zirconate titanate thin films. *Thin Solid Films*, *516*(15), 4679–4684. https://doi.org/10.1016/j.tsf.2007.08.039

Martins, M., Correia, V., Cabral, J. M., Lanceros-Mendez, S., & Rocha, J. G. (2012). Optimization of piezoelectric ultrasound emitter transducers for underwater communications. *Sensors and Actuators A: Physical*, *184*, 141–148. https://doi.org/10.1016/j.sna.2012.06.008

Martins, M. S., Barardo, C., Matos, T., Gonçalves, L. M., Cabral, J., Silva, A., & Jesus, S. M. (2017). High frequency wide beam PVDF ultrasonic projector for underwater communications. *OCEANS 2017 - Aberdeen*, 1–5. https://doi.org/10.1109/OCEANSE.2017.8084677

Martins, P., Lopes, A. C., & Lanceros-Mendez, S. (2014). Electroactive phases of poly(vinylidene fluoride): Determination, processing and applications. *Progress in Polymer Science*, *39*(4), 683–706. https://doi.org/10.1016/j.progpolymsci.2013.07.006

Martins, P., Moya, X., Caparrós, C., Fernandez, J., Mathur, N. D., & Lanceros-Mendez, S. (2013). Large linear anhysteretic magnetoelectric voltage coefficients in $CoFe_2O_4$/polyvinylidene fluoride 0–3 nanocomposites. *Journal of Nanoparticle Research*, *15*(8), 1–6. https://doi.org/10.1007/s11051-013-1825-9

Martins, Pedro, & Lanceros-Méndez, S. (2013). Polymer-based magnetoelectric materials. *Advanced Functional Materials*, *23*(27), 3371–3385. https://doi.org/10.1002/adfm.201202780

Martins, R. S., Gonçalves, R., Azevedo, T., Rocha, J. G., Nóbrega, J. M., Carvalho, H., & Lanceros-Mendez, S. (2014). Piezoelectric coaxial filaments produced by coextrusion of poly(vinylidene fluoride) and electrically conductive inner and outer layers. *Journal of Applied Polymer Science*, *131*(17). https://doi.org/10.1002/app.40710

Masunaga, S., Xu, X., Terabe, H., Shibuta, K., & Shibata, H. (2017). A paper book type input device for page navigation in digital documents. *IEICE Transactions on Electronics*, *E100.C*(11), 984–991. https://doi.org/10.1587/transele.E100.C.984

Mazzeo, A. D., Kalb, W. B., Chan, L., Killian, M. G., Bloch, J.-F., Mazzeo, B. A., & Whitesides, G. M. (2012). Paper-based, capacitive touch pads. *Advanced Materials*, *24*(21), 2850–2856. https://doi.org/10.1002/adma.201200137

McIntosh, R. B., Mauger, P. E., & Patterson, S. R. (2006). Capacitive transducers with curved electrodes. *IEEE Sensors Journal*, *6*(1), 125–138. https://doi.org/10.1109/JSEN.2005.854137

Measurement Specialties Inc. (1999). *Piezo film sensors technical manual*. https://www.sparkfun.com/datasheets/Sensors/Flex/MSI-techman.pdf

Mehling, V., Tsakmakis, C., & Gross, D. (2007). Phenomenological model for the macroscopical material behavior of ferroelectric ceramics. *Journal of the Mechanics and Physics of Solids*, *55*(10), 2106–2141. https://doi.org/10.1016/j.jmps.2007.03.008

Mejri, R., Dias, J. C., Hentati, S. B., Martins, M. S., Costa, C. M., & Lanceros-Mendez, S. (2016). Effect of anion type in the performance of ionic liquid/poly(vinylidene fluoride) electromechanical actuators. *Journal of Non-Crystalline Solids*, *453*, 8–15. https://doi.org/10.1016/j.jnoncrysol.2016.09.014

Mendes-Felipe, C., Barbosa, J. C., Gonçalves, S., Pereira, N., Costa, C. M., Vilas-Vilela, J. L., & Lanceros-Mendez, S. (2020). High dielectric constant UV curable polyurethane acrylate/indium tin oxide composites for capacitive sensing. *Composites Science and Technology*, *199*, 108363. https://doi.org/10.1016/j.compscitech.2020.108363

Minari, T., Kanehara, Y., Liu, C., Sakamoto, K., Yasuda, T., Yaguchi, A., Tsukada, S., Kashizaki, K., & Kanehara, M. (2014). Room-temperature printing of organic thin-film transistors with π-junction gold nanoparticles. *Advanced Functional Materials*, *24*(31), 4886–4892. https://doi.org/10.1002/adfm.201400169

Mishra, S., Unnikrishnan, L., Nayak, S. K., & Mohanty, S. (2019). Advances in piezoelectric polymer composites for energy harvesting applications: A systematic review. *Macromolecular Materials and Engineering*, *304*(1), 1800463. https://doi.org/10.1002/mame.201800463

Mohammed, A., & Pecht, M. (2016). A stretchable and screen-printable conductive ink for stretchable electronics. *Applied Physics Letters*, *109*(18), 184101. https://doi.org/10.1063/1.4965706

Molina-Lopez, F., Briand, D., & de Rooij, N. F. (2012). All additive inkjet printed humidity sensors on plastic substrate. *Sensors and Actuators B: Chemical*, *166–167*, 212–222. https://doi.org/10.1016/j.snb.2012.02.042

Moorthy, P., Honauer, M., Hornecker, E., & Mühlenberend, A. (2017). Hello World: A children's touch and feel books enhanced with DIY electronics. *Proceedings of the 16th International Conference on Mobile and Ubiquitous Multimedia*, 481–488. https://doi.org/10.1145/3152832.3157811

Moretti, G., Papini, G. P. R., Righi, M., Forehand, D., Ingram, D., Vertechy, R., & Fontana, M. (2018). Resonant wave energy harvester based on dielectric elastomer generator. *Smart Materials and Structures*, *27*(3), 35015. https://doi.org/10.1088/1361-665x/aaab1e

Moretti, G., Rosset, S., Vertechy, R., Anderson, I., & Fontana, M. (2020). A review of dielectric elastomer generator systems. *Advanced Intelligent Systems*, *2*(10), 2000125. https://doi.org/10.1002/aisy.202000125

Nair, N. M., Daniel, K., Vadali, S. C., Ray, D., & Swaminathan, P. (2019). Direct writing of silver nanowire-based ink for flexible transparent capacitive touch pad. *Flexible and Printed Electronics*, *4*(4), 45001. https://doi.org/10.1088/2058-8585/ab4b04

Nalon, G. H., Ribeiro, J. C. L., de Araújo, E. N. D., Pedroti, L. G., de Carvalho, J. M. F., Santos, R. F., & Aparecido-Ferreira, A. (2020). Effects of different kinds of carbon black nanoparticles on the piezoresistive and mechanical properties of cement-based composites. *Journal of Building Engineering*, *32*, 101724. https://doi.org/10.1016/j.jobe.2020.101724

Nathan, A, Ahnood, A., Cole, M. T., Lee, S., Suzuki, Y., Hiralal, P., Bonaccorso, F., Hasan, T., Garcia-Gancedo, L., Dyadyusha, A., Haque, S., Andrew, P., Hofmann, S., Moultrie, J., Chu, D., Flewitt, A. J., Ferrari, A. C., Kelly, M. J., Robertson, J., ... Milne, W. I. (2012). Flexible electronics: The next ubiquitous platform. *Proceedings of the IEEE*, *100*(Special Centennial Issue), 1486–1517. https://doi.org/10.1109/JPROC.2012.2190168

Nathan, Arokia, Sharma, P., Tsangarides, C. P., Li, J., Cheng, X., & Astley, M. R. (2019). 42.2: Invited paper: Multi-force touch technology augmenting capacitive touch in displays. *SID Symposium Digest of Technical Papers*, *50*(S1), 472–475. https://doi.org/10.1002/sdtp.13532

Ning, C., Zhou, Z., Tan, G., Zhu, Y., & Mao, C. (2018). Electroactive polymers for tissue regeneration: Developments and perspectives. *Progress in Polymer Science*, *81*, 144–162. https://doi.org/10.1016/j.progpolymsci.2018.01.001

Nunes-Pereira, J., Costa, P., & Lanceros-Mendez, S. (2018). 3.9 Piezoelectric energy production. In I. Dincer (Ed.), *Comprehensive Energy Systems* (Vol. 3, pp. 380–415). Elsevier. https://doi.org/10.1016/B978-0-12-809597-3.00324-2

Nunes, J. S. J. S., Castro, N., Gonçalves, S., Pereira, N., Correia, V., & Lanceros-Mendez, S. (2017). Marked object recognition multitouch screen printed touchpad for interactive applications. *Sensors*, *17*(12), 1–9. https://doi.org/10.3390/s17122786

NXP Semiconductors. (2008). *AN10675 Interfacing 4-wire and 5-wire resistive touchscreens to the LPC247x*. https://www.nxp.com/docs/en/application-note/AN10675.pdf

Ou, J., Skouras, M., Vlavianos, N., Heibeck, F., Cheng, C.-Y., Peters, J., & Ishii, H. (2016). aeroMorph - Heat-sealing inflatable shape-change materials for interaction design. *Proceedings of the 29th Annual Symposium on User Interface Software and Technology - UIST '16*, 121–132. https://doi.org/10.1145/2984511.2984520

Paiva, M. C., Novais, R. M., Araújo, R. F., Pederson, K. K., Proença, M. F., Silva, C. J. R., Costa, C. M., & Lanceros-Méndez, S. (2010). Organic functionalization of carbon nanofibers for composite applications. *Polymer Composites*, *31*(3), 369–376. https://doi.org/10.1002/pc.20813

Panahi-Sarmad, M., Noroozi, M., Abrisham, M., Eghbalinia, S., Teimoury, F., Bahramian, A. R., Dehghan, P., Sadri, M., & Goodarzi, V. (2020). A comprehensive review on carbon-based polymer nanocomposite foams as electromagnetic interference shields and piezoresistive sensors. *ACS Applied Electronic Materials*, *2*(8), 2318–2350. https://doi.org/10.1021/acsaelm.0c00490

Park, S. W., Das, P. S., Chhetry, A., & Park, J. Y. (2017). A flexible capacitive pressure sensor for wearable respiration monitoring system. *IEEE Sensors Journal*, *17*(20), 6558–6564. https://doi.org/10.1109/JSEN.2017.2749233

Park, W.-T. (2012). Piezoresistivity. In B. Bhushan (Ed.), *Encyclopedia of Nanotechnology* (pp. 2111–2117). Springer Netherlands. https://doi.org/10.1007/978-90-481-9751-4_222

Peng, T. (2019). *Mutual capacitance sensing array* (Patent No. US 10,386,976 B2). United States Patent and Trademark Office (USPTO). https://patents.google.com/patent/US10386976B2

Pereira, N., Gonçalves, S., Barbosa, J. C., Gonçalves, R., Tubio, C. R., Vilas-Vilela, J. L., Costa, C. M., & Lanceros-Mendez, S. (2021). High dielectric constant poly(vinylidene fluoride-trifluoroethylene-chlorofluoroethylene) for capacitive pressure and bending sensors. *Polymer*, *214*, 123349. https://doi.org/10.1016/j.polymer.2020.123349

Pintér, Á., & Dénes, I. (2015). Interface circuit for measuring small capacitance changes in sensor networks. *IET Science, Measurement & Technology*, *9*(5), 570–578. https://doi.org/10.1049/iet-smt.2014.0221

Pinto, A. L., Zagalo, N., Sylla, C., Freed, N., Figueiredo, A. C., Qi, J., Branco, P., & Coquet, E. (2013). Bridging Books: The printed book as a support for digital experiences. *Proceedings of the 12th International Conference on Interaction Design and Children*, 606–609. https://doi.org/10.1145/2485760.2485891

Pohl, H., Hettig, M., Karras, O., Öztürk, H., & Rohs, M. (2015). CapCouch: Home control with a posture-sensing couch. *Adjunct Proceedings of the 2015 ACM International Joint Conference on Pervasive and Ubiquitous Computing and Proceedings of the 2015 ACM International Symposium on Wearable Computers*, 229–232. https://doi.org/10.1145/2800835.2800932

Pointner, A., Preindl, T., Mlakar, S., Aigner, R., & Haller, M. (2020). Knitted RESi: A highly flexible, force-sensitive knitted textile based on resistive yarns. *ACM SIGGRAPH 2020 Emerging Technologies*. https://doi.org/10.1145/3388534.3407292

Porto Canal. (2012). *Investigadores da UMinho recebem prémio internacional no Nepal - Entrevista Porto Canal* [Researchers from UMinho are awarded international prize in Nepal - Interview Porto Canal]. [Live interview video]. https://youtu.be/f8RhupnjxjA

Posch, I. (2021). Crafting Stories: Smart and electronic textile craftsmanship for interactive books. *Proceedings of the Fifteenth International Conference on Tangible, Embedded, and Embodied Interaction*. https://doi.org/10.1145/3430524.3446076

Preindl, T., Honnet, C., Pointner, A., Aigner, R., Paradiso, J. A., & Haller, M. (2020). Sonoflex: Embroidered speakers without permanent magnets. In *Proceedings of the 33rd Annual ACM Symposium on User Interface Software and Technology* (pp. 675–685). Association for Computing Machinery. https://doi.org/10.1145/3379337.3415888

Pruvost, M., Smit, W. J., Monteux, C., Poulin, P., & Colin, A. (2019). Polymeric foams for flexible and highly sensitive low-pressure capacitive sensors. *Npj Flexible Electronics*, *3*(1), 7. https://doi.org/10.1038/s41528-019-0052-6

Purnendu, Novack, S. M., Acome, E., Keplinger, C., Alistar, M., Gross, M. D., Bruns, C., & Leithinger, D. (2021). Electriflow: Soft electrohydraulic building blocks for prototyping shape-changing interfaces. *Designing Interactive Systems Conference 2021*, 1280–1290. https://doi.org/10.1145/3461778.3462093

Qi, J., & Buechley, L. (2010). Electronic Popables: Exploring paper-based computing through an interactive pop-up book. *Proceedings of the Fourth International Conference on Tangible, Embedded, and Embodied Interaction*, 121–128. https://doi.org/10.1145/1709886.1709909

Rajan, K., Roppolo, I., Chiappone, A., Bocchini, S., Perrone, D., & Chiolerio, A. (2016). Silver nanoparticle ink technology: State of the art. *Nanotechnology, Science and Applications*, *2016:9*, 1–13. https://doi.org/10.2147/NSA.S68080

Rajeev, S. P., John, S. K., Cherian, R., Karumuthil, S. C., & Varghese, S. (2020). Next-generation rooftop tribo–piezo electric energy harvesting from rain power. *Applied Nanoscience*, *10*(3), 679–686. https://doi.org/10.1007/s13204-019-01184-1

Ramadan, K. S., Sameoto, D., & Evoy, S. (2014). A review of piezoelectric polymers as functional materials for electromechanical transducers. *Smart Materials and Structures*, *23*(3). https://doi.org/10.1088/0964-1726/23/3/033001

Ratti, C., Wang, Y., Ishii, H., Piper, B., & Frenchman, D. (2004). Tangible user interfaces (TUIs): A novel paradigm for GIS. *Transactions in GIS*, *8*(4), 407–421. https://doi.org/10.1111/j.1467-9671.2004.00193.x

Reale, A., La Notte, L., Salamandra, L., Polino, G., Susanna, G., Brown, T. M., Brunetti, F., & Di Carlo, A. (2015). Spray coating for polymer solar cells: An up-to-date overview. *Energy Technology*, *3*(4), 385–406. https://doi.org/10.1002/ente.201402180

Reis, S., Correia, V., Martins, M., Barbosa, G., Sousa, R. M., Minas, G., Lanceros-Mendez, S., & Rocha, J. G. (2010). Touchscreen based on acoustic pulse recognition with piezoelectric polymer sensors. *2010 IEEE International Symposium on Industrial Electronics*, 516–520. https://doi.org/10.1109/ISIE.2010.5637672

Reizabal, A., Gonçalves, S., Brito-Pereira, R., Costa, P., Costa, C. M., Pérez-Álvarez, L., Vilas-Vilela, J. L., & Lanceros-Méndez, S. (2019). Optimized silk fibroin piezoresistive nanocomposites for pressure sensing applications based on natural polymers. *Nanoscale Advances*, *1*(6), 2284–2292. https://doi.org/10.1039/C8NA00417J

Reizabal, A., Gonçalves, S., Pereira, N., Costa, C., Perez-Alvarez, L., Vilas, J. L., & Lanceros-Mendez, S. (2020). Optically transparent silk fibroin/silver nanowire composites for piezoresistive sensing and object recognitions. *Jounal of Materials Chemistry C*. https://doi.org/10.1039/D0TC03428B

Ren, T.-L., Tian, H., Xie, D., & Yang, Y. (2012). Flexible graphite-on-paper piezoresistive sensors. *Sensors*, *12*(5), 6685–6694. https://doi.org/10.3390/s120506685

Rendl, C., Greindl, P., Haller, M., Zirkl, M., Stadlober, B., & Hartmann, P. (2012). PyzoFlex: Printed piezoelectric pressure sensing foil. *Proceedings of the 25th Annual ACM Symposium on User Interface Software and Technology*, 509–518. https://doi.org/10.1145/2380116.2380180

Rendl, C., Kim, D., Fanello, S., Parzer, P., Rhemann, C., Taylor, J., Zirkl, M., Scheipl, G., Rothländer, T., Haller, M., & Izadi, S. (2014). FlexSense: A transparent self-sensing deformable surface. *Proceedings of the 27th Annual ACM Symposium on User Interface Software and Technology*, 129–138. https://doi.org/10.1145/2642918.2647405

Rendl, C., Kim, D., Parzer, P., Fanello, S., Zirkl, M., Scheipl, G., Haller, M., & Izadi, S. (2016). FlexCase: Enhancing mobile interaction with a flexible sensing and display cover. In *Proceedings of the 2016 CHI Conference on Human Factors in Computing Systems* (pp. 5138–5150). Association for Computing Machinery. https://doi.org/10.1145/2858036.2858314

Ribeiro, C., Costa, C. M., Correia, D. M., Nunes-Pereira, J., Oliveira, J., Martins, P., Gonçalves, R., Cardoso, V. F., & Lanceros-Méndez, S. (2018). Electroactive poly(vinylidene fluoride)-based structures for advanced applications. *Nature Protocols*, *13*(4), 681–704. https://doi.org/10.1038/nprot.2017.157

Ribeiro, C., Sencadas, V., Correia, D. M., & Lanceros-Méndez, S. (2015). Piezoelectric polymers as biomaterials for tissue engineering applications. *Colloids and Surfaces B: Biointerfaces*, *136*, 46–55. https://doi.org/10.1016/j.colsurfb.2015.08.043

Ricoh Europe PLC. (2016). *Ricoh announces development of new industrial print head using thin film PZT actuator*. https://www.ricoh-europe.com/news-events/news/ricoh-announces-development-of-new-industrial-print-head-using-thin-film-pzt-actuator.html

Rim, Y. S., Bae, S.-H., Chen, H., De Marco, N., & Yang, Y. (2016). Recent progress in materials and devices toward printable and flexible sensors. *Advanced Materials*, *28*(22), 4415–4440. https://doi.org/10.1002/adma.201505118

Rivadeneyra, A., Salmerón, J. F., Palma, A. J., López-Villanueva, J. A., Agudo-Acemel, M., & Capitan-Vallvey, L. F. (2015). Comparative study of printed capacitive sensors. *2015 10th Spanish Conference on Electron Devices (CDE)*, 1–4. https://doi.org/10.1109/CDE.2015.7087485

Rus, S., Grosse-Puppendahl, T., & Kuijper, A. (2014). Recognition of bed postures using mutual capacitance sensing. In E. Aarts, B. de Ruyter, P. Markopoulos, E. van Loenen, R. Wichert, B. Schouten, J. Terken, R. Van Kranenburg, E. Den Ouden, & G. O'Hare (Eds.), *Ambient Intelligence* (pp. 51–66). Springer International Publishing. https://doi.org/10.1007/978-3-319-14112-1_5

Saggio, G., Riillo, F., Sbernini, L., & Quitadamo, L. R. (2015). Resistive flex sensors: A survey. *Smart Materials and Structures*, *25*(1), 13001. https://doi.org/10.1088/0964-1726/25/1/013001

Sappati, K. K., & Bhadra, S. (2018). Piezoelectric polymer and paper substrates: A review. *Sensors*, *18*(11), 3605. https://doi.org/10.3390/s18113605

Scaffaro, R., Maio, A., Lo Re, G., Parisi, A., & Busacca, A. (2018). Advanced piezoresistive sensor achieved by amphiphilic nanointerfaces of graphene oxide and biodegradable polymer blends. *Composites Science and Technology*, *156*, 166–176. https://doi.org/10.1016/j.compscitech.2018.01.008

Scheipl, G., Zirkl, M., Stadlober, B., Groten, J., Jakopic, G., Krenn, J. R., Sawatdee, A., Bodö, P., & Andersson, P. (2009). Fabrication, characterization and modeling of PVDF based organic IR-sensors for human body recognition. *SENSORS, 2009 IEEE*, 1252–1255. https://doi.org/10.1109/ICSENS.2009.5398379

Schmidt, A. (2017). The world is not flat: Shape-changing user interfaces - An interview with Anne Roudaut, Kasper Hornbæk, and Hiroshi Ishii. *IEEE Pervasive Computing*, *16*(4), 47–49. https://doi.org/10.1109/MPRV.2017.3971122

Schmitz, M., Steimle, J., Huber, J., Dezfuli, N., & Mühlhäuser, M. (2017). Flexibles: Deformation-aware 3D-printed tangibles for capacitive touchscreens. *Proceedings of the 2017 CHI Conference on Human Factors in Computing Systems*, 1001–1014. https://doi.org/10.1145/3025453.3025663

Schneider, B., Wallace, J., Blikstein, P., & Pea, R. (2013). Preparing for future learning with a tangible user interface: The case of neuroscience. *IEEE Transactions on Learning Technologies*, *6*(2), 117–129. https://doi.org/10.1109/TLT.2013.15

Schoessler, P., Leigh, S., Jagannath, K., van Hoof, P., & Ishii, H. (2015). Cord UIs: Controlling devices with augmented cables. *Proceedings of the Ninth International Conference on Tangible, Embedded, and Embodied Interaction*, 395–398. https://doi.org/10.1145/2677199.2680601

Shaer, O., & Hornecker, E. (2010). Tangible user interfaces: Past, present, and future directions. *Foundations and Trends® in Human–Computer Interaction*, *3*(1–2), 4–137. https://doi.org/10.1561/1100000026

Shan, X., Song, R., Liu, B., & Xie, T. (2015). Novel energy harvesting: A macro fiber composite piezoelectric energy harvester in the water vortex. *Ceramics International*, *41*, S763–S767. https://doi.org/10.1016/j.ceramint.2015.03.219

Shen, X., Zheng, L., Tang, R., Nie, K., Wang, Z., Jin, C., & Sun, Q. (2020). Double-network hierarchical-porous piezoresistive nanocomposite hydrogel sensors based on compressive cellulosic hydrogels deposited with silver nanoparticles. *ACS Sustainable Chemistry & Engineering*, *8*(19), 7480–7488. https://doi.org/10.1021/acssuschemeng.0c02035

Shigemune, H., Maeda, S., Cacucciolo, V., Iwata, Y., Iwase, E., Hashimoto, S., & Sugano, S. (2017). Printed paper robot driven by electrostatic actuator. *IEEE Robotics and Automation Letters*, *2*(2), 1001–1007. https://doi.org/10.1109/LRA.2017.2658942

Shintani, M., Lee, J. H., & Okamoto, S. (2021). Digital pen for handwritten alphabet recognition. *2021 IEEE International Conference on Consumer Electronics (ICCE)*, 1–4. https://doi.org/10.1109/ICCE50685.2021.9427700

Soleimani, V., Raji, M. R. A., & Golshan, M. A. (2011). Converting every surface to touchscreen. *2011 7th Iranian Conference on Machine Vision and Image Processing*, 1–5. https://doi.org/10.1109/IranianMVIP.2011.6121587

Song, A., Han, Y., Hu, H., & Li, J. (2014). A novel texture sensor for fabric texture measurement and classification. *IEEE Transactions on Instrumentation and Measurement*, *63*(7), 1739–1747. https://doi.org/10.1109/TIM.2013.2293812

Stassi, S., Cauda, V., Canavese, G., & Pirri, C. F. (2014). Flexible tactile sensing based on piezoresistive composites: A review. *Sensors*, *14*(3), 5296–5332. https://doi.org/10.3390/s140305296

Street, R. A., Mei, P., Krusor, B., Lujan, R., Karatay, E., Pierre, A., Schwartz, D. E., Kor, S., & Ready, S. E. (2020). Audio system fabricated with flexible hybrid electronics. *IEEE Transactions on Electron Devices*, *67*(3), 1270–1276. https://doi.org/10.1109/TED.2020.2967242

Subramanian, V., Chang, J. B., de la Fuente Vornbrock, A., Huang, D. C., Jagannathan, L., Liao, F., Mattis, B., Molesa, S., Redinger, D. R., Soltman, D., Volkman, S. K., & Qintao Zhang. (2008). Printed electronics for low-cost electronic systems: Technology status and application development. *ESSCIRC 2008 - 34th European Solid-State Circuits Conference*, 17–24. https://doi.org/10.1109/ESSCIRC.2008.4681785

Sugimoto, T., Ono, K., Ando, A., Kurozumi, K., Hara, A., Morita, Y., & Miura, A. (2009). PVDF-driven flexible and transparent loudspeaker. *Applied Acoustics*, *70*(8), 1021–1028. https://doi.org/10.1016/j.apacoust.2009.03.007

Suikkola, J., Björninen, T., Mosallaei, M., Kankkunen, T., Iso-Ketola, P., Ukkonen, L., Vanhala, J., & Mäntysalo, M. (2016). Screen-printing fabrication and characterization of stretchable electronics. *Scientific Reports*, *6*(1), 25784. https://doi.org/10.1038/srep25784

Sylla, C., Ângelo, P., Coutinho, C., Branco, P., Zagalo, N., & Coquet, E. (2011). Is it a book... is it a game? No, it is TOK. In A. Moreira, M. J. Loureiro, A. Balula, F. Nogueira, L. Pombo, L. Pedro, & P. Almeida (Eds.), *Old Meets New: Media in Education – Proceedings of the 61st International Council of Educational Media and the XIII International Symposium on Computers in Education (ICEM&SIIE'2011) Joint Conference* (pp. 902–904). http://hdl.handle.net/1822/14801

Sylla, C., Branco, P., Coutinho, C., Coquet, E., & Skaroupka, D. (2011). TOK: A tangible interface for storytelling. *CHI '11 Extended Abstracts on Human Factors in Computing Systems*, 1363–1368. https://doi.org/10.1145/1979742.1979775

Sylla, C., Branco, P., & Coutinho, C. P. (2011). Developing a tangible interface for storytelling. In U. Ellen Yi-Luen Do (Georgia Tech, U. Gross, Mark D. (Carnegie Mellon University, & P. Ian Oakley (University of Madeira (Eds.), *TEI '11, Work-in-Progress Workshop* (pp. 43–48). http://tei.acm.org/2011/11/TEI-WIP-final-compressed.pdf

Sylla, C., Coutinho, C., & Branco, P. (2015). Play platforms for children's creativity. In N. Zagalo & P. Branco (Eds.), *Creativity in the Digital Age* (pp. 223–243). Springer London. https://doi.org/10.1007/978-1-4471-6681-8_12

Sylla, C., Figueiredo, A. C., Pinto, A. L., Branco, P., & Zagalo, N. (2014). Merging physical and digital white canvas to unleash children's creativity. *Proceedings of the 2014 Workshops on Advances in Computer Entertainment Conference*. https://doi.org/10.1145/2693787.2693807

Sylla, C., Gonçalves, S., Branco, P., & Coutinho, C. (2013). Peter piper picked a peck of pickled peppers: An interface for playful language exploration. *CHI'13 Extended Abstracts on Human Factors in Computing Systems*, 3127–3130. https://doi.org/10.1145/2468356.2479627

Sylla, C., Gonçalves, S., Branco, P., & Coutinho, C. (2012). t-words: Playing with sounds and creating narratives. In A. Nijholt, T. Romão, & D. Reidsma (Eds.), *Advances in Computer Entertainment* (Vol. 7624, pp. 565–568). Springer Berlin Heidelberg. https://doi.org/10.1007/978-3-642-34292-9_60

Sylla, C., Gonçalves, S., Brito, P., Branco, P., & Coutinho, C. (2013). A tangible platform for mixing and remixing narratives. *Lecture Notes in Computer Science (Including Subseries Lecture Notes in Artificial Intelligence and Lecture Notes in Bioinformatics)*, *8253 LNCS*, 630–633. https://doi.org/10.1007/978-3-319-03161-3_69

Sylla, C., Gonçalves, S., Brito, P., Branco, P., & Coutinho, C. (2012). t-books: Merging traditional storybooks with electronics. *Proceedings of the 11th International Conference on Interaction Design and Children*, 323–326. https://doi.org/10.1145/2307096.2307157

Tajitsu, Y. (2016). Development of environmentally friendly piezoelectric polymer film actuator having multilayer structure. *Japanese Journal of Applied Physics*, *55*(4S), 04EA07. https://doi.org/10.7567/jjap.55.04ea07

Tan, Z., Jiang, H., Zhang, H., Tang, X., Xin, H., & Nihtianov, S. (2021). Power-efficiency evolution of capacitive sensor interfaces. *IEEE Sensors Journal*, *21*(11), 12457–12468. https://doi.org/10.1109/JSEN.2020.3035109

Tang, H., Taboada, J. M., Cao, G., Li, L., & Chen, R. T. (1997). Enhanced electro-optic coefficient of nonlinear optical polymer using liquid contact poling. *Applied Physics Letters*, *70*(5), 538–540. https://doi.org/10.1063/1.118333

Tarbuttona, J., Leb, T., Helfrichb, G., & Kirkpatrickb, M. (2017). Phase transformation and shock sensor response of additively manufactured piezoelectric PVDF. *Procedia Manufacturing*, *10*, 982–989. https://doi.org/10.1016/j.promfg.2017.07.089

Tausiff, M., Ouakad, H. M., & Alqahtani, H. (2020). Global nonlinear dynamics of MEMS arches actuated by fringing-field electrostatic field. *Arabian Journal for Science and Engineering*, *45*(7), 5959–5975. https://doi.org/10.1007/s13369-020-04588-2

Tentzeris, M. M. (2013). Inkjet-printed antennas, sensors and circuits on paper substrate. *IET Microwaves, Antennas & Propagation*, *7*(10), 858-868(10). https://doi.org/10.1049/iet-map.2012.0685

Tian, L., Song, A., & Chen, D. (2017). Image-based haptic display via a novel pen-shaped haptic device on touch screens. *Multimedia Tools and Applications*, *76*(13), 14969–14992. https://doi.org/10.1007/s11042-017-4387-5

Ting, Y., Gunawan, H., Chiu, C.-W., & Zhong, J.-Z. (2013). A new approach for surface poling of polyvinylidene fluoride (PVDF). *Ferroelectrics*, *446*(1), 18–27. https://doi.org/10.1080/00150193.2013.820978

Tobiszewski, M., & Namieśnik, J. (2015). Scoring of solvents used in analytical laboratories by their toxicological and exposure hazards. *Ecotoxicology and Environmental Safety*, *120*, 169–173. https://doi.org/10.1016/j.ecoenv.2015.05.043

Trung, T. Q., Duy, L. T., Ramasundaram, S., & Lee, N.-E. (2017). Transparent, stretchable, and rapid-response humidity sensor for body-attachable wearable electronics. *Nano Research*, *10*(6), 2021–2033. https://doi.org/10.1007/s12274-016-1389-y

Tsonos, C., Pandis, C., Soin, N., Sakellari, D., Myrovali, E., Kripotou, S., Kanapitsas, A., & Siores, E. (2015). Multifunctional nanocomposites of poly(vinylidene fluoride) reinforced by carbon nanotubes and magnetite nanoparticles. *EXPRESS Polymer Letters*, *9*(12), 1104–1118. https://doi.org/10.3144/expresspolymlett.2015.99

Tsutsumi, N., Ueyasu, A., Sakai, W., & Chiang, C. K. (2005). Crystalline structures and ferroelectric properties of ultrathin films of vinylidene fluoride and trifluoroethylene copolymer. *Thin Solid Films*, *483*(1), 340–345. https://doi.org/10.1016/j.tsf.2004.12.033

Tulachan, B., Meena, S. K., Rai, R. K., Mallick, C., Kusurkar, T. S., Teotia, A. K., Sethy, N. K., Bhargava, K., Bhattacharya, S., Kumar, A., Sharma, R. K., Sinha, N., Singh, S. K., & Das, M. (2014). Electricity from the silk cocoon membrane. *Scientific Reports*, *4*(1), 5434. https://doi.org/10.1038/srep05434

Tung, H.-T., Chen, I.-G., Kempson, I. M., Song, J.-M., Liu, Y.-F., Chen, P.-W., Hwang, W.-S., & Hwu, Y. (2012). Shape-controlled synthesis of silver nanocrystals by X-ray irradiation for inkjet printing. *ACS Applied Materials & Interfaces*, *4*(11), 5930–5935. https://doi.org/10.1021/am3015718

Tung, Y.-C., Cheng, T. Y., Yu, N.-H., Wang, C., & Chen, M. Y. (2015). FlickBoard: Enabling trackpad interaction with automatic mode switching on a capacitive-sensing keyboard. *Proceedings of the 33rd Annual ACM Conference on Human Factors in Computing Systems*, 1847–1850. https://doi.org/10.1145/2702123.2702582

Tzou, H. S., Lee, H.-J., & Arnold, S. M. (2004). Smart materials, Precision sensors/actuators, smart structures, and structronic systems. *Mechanics of Advanced Materials and Structures*, *11*(4–5), 367–393. https://doi.org/10.1080/15376490490451552

Uchino, K. (2008). Piezoelectric actuators 2006. *Journal of Electroceramics*, *20*(3), 301–311. https://doi.org/10.1007/s10832-007-9196-1

Vallgårda, A., & Redström, J. (2007). Computational composites. *Proceedings of the SIGCHI Conference on Human Factors in Computing Systems*, *522*, 513–522. https://doi.org/10.1145/1240624.1240706

Valtonen, M., Vuorela, T., Kaila, L., & Vanhala, J. (2012). Capacitive indoor positioning and contact sensing for activity recognition in smart homes. *Journal of Ambient Intelligence and Smart Environments*, *4*, 305–334. https://doi.org/10.3233/AIS-2012-0158

Van Duong, Q., Nguyen, V. P., Domingues Dos Santos, F., & Choi, S. T. (2019). Localized fretting-vibrotactile sensations for large-area displays. *ACS Applied Materials & Interfaces*, *11*(36), 33292–33301. https://doi.org/10.1021/acsami.9b09691

Vella, S., Smithson, C. S., Halfyard, K., Shen, E., & Chrétien, M. (2019). Integrated capacitive sensor devices aerosol jet printed on 3D objects. *Flexible and Printed Electronics*. https://doi.org/10.1088/2058-8585/ab59c0

Verma, G. K., & Ansari, M. Z. (2019). Design and simulation of piezoresistive polymer accelerometer. *IOP Conference Series: Materials Science and Engineering*, *561*, 12128. https://doi.org/10.1088/1757-899x/561/1/012128

Villar, N., Cletheroe, D., Saul, G., Holz, C., Regan, T., Salandin, O., Sra, M., Yeo, H.-S., Field, W., & Zhang, H. (2018). Project Zanzibar: A portable and flexible tangible interaction platform. In *Proceedings of the 2018 CHI Conference on Human Factors in Computing Systems* (pp. 1–13). Association for Computing Machinery. https://doi.org/10.1145/3173574.3174089

Vipulanandan, C., & Mohammed, A. (2015). Smart cement modified with iron oxide nanoparticles to enhance the piezoresistive behavior and compressive strength for oil well applications. *Smart Materials and Structures*, *24*(12), 125020. https://doi.org/10.1088/0964-1726/24/12/125020

Vyas, D., Poelman, W., Nijholt, A., & De Bruijn, A. (2012). Smart material interfaces: A new form of physical interaction. *CHI '12 Extended Abstracts on Human Factors in Computing Systems*, 1721–1726. https://doi.org/10.1145/2212776.2223699

Walker, G. (2012). A review of technologies for sensing contact location on the surface of a display. *Journal of the Society for Information Display*, *20*(8), 413–440. https://doi.org/10.1002/jsid.100

Walker, G. (2014). Touch sensing. In *Interactive Displays* (pp. 27–105). John Wiley & Sons, Ltd. https://doi.org/10.1002/9781118706237.ch2

Wan, C., Zhang, L., Yong, K.-T., Li, J., & Wu, Y. (2021). Recent progress in flexible nanocellulosic structures for wearable piezoresistive strain sensors. *Jounal of Materials Chemistry C*, *9*(34), 11001–11029. https://doi.org/10.1039/D1TC02360H

Wang, D. (2014). *FDC1004: Basics of capacitive sensing and applications*.
    https://www.ti.com/lit/an/snoa927/snoa927.pdf

Wang, G., Cheng, T., Do, Y., Yang, H., Tao, Y., Gu, J., An, B., & Yao, L. (2018). Printed paper actuator:
    A low-cost reversible actuation and sensing method for shape changing interfaces. In *Proceedings
    of the 2018 CHI Conference on Human Factors in Computing Systems* (pp. 1–12). Association for
    Computing Machinery. https://doi.org/10.1145/3173574.3174143

Wang, L., Liu, T., Peng, X., Zeng, W., Jin, Z., Tian, W., Gao, B., Zhou, Y., Chu, P. K., & Huo, K. (2018).
    Highly stretchable conductive glue for high-performance silicon anodes in advanced lithium-ion
    batteries. *Advanced Functional Materials*, *28*(3), 1704858.
    https://doi.org/10.1002/adfm.201704858

Wang, M., Zhang, K., Dai, X.-X., Li, Y., Guo, J., Liu, H., Li, G.-H., Tan, Y.-J., Zeng, J.-B., & Guo, Z.
    (2017). Enhanced electrical conductivity and piezoresistive sensing in multi-wall carbon
    nanotubes/polydimethylsiloxane nanocomposites via the construction of a self-segregated
    structure. *Nanoscale*, *9*(31), 11017–11026. https://doi.org/10.1039/C7NR02322G

Wang, X., Yang, B., Liu, J., Zhu, Y., Yang, C., & He, Q. (2016). A flexible triboelectric-piezoelectric hybrid
    nanogenerator based on P(VDF-TrFE) nanofibers and PDMS/MWCNT for wearable devices.
    Scientific Reports, *6*(1), 36409. https://doi.org/10.1038/srep36409

Wang, Y, Zhou, X., Chen, Q., Chu, B., & Zhang, Q. (2010). Recent development of high energy density
    polymers for dielectric capacitors. *IEEE Transactions on Dielectrics and Electrical Insulation*,
    17(4), 1036–1042. https://doi.org/10.1109/TDEI.2010.5539672

Wang, Yanlei, Wang, Y., Wan, B., Han, B., Cai, G., & Li, Z. (2018). Properties and mechanisms of self-
    sensing carbon nanofibers/epoxy composites for structural health monitoring. *Composite
    Structures*, *200*, 669–678. https://doi.org/10.1016/j.compstruct.2018.05.151

Wang, Z. L., & Kang, Z. C. (1998). *Functional and smart materials: Structural evolution and structure
    analysis* (1st ed.). Springer, Boston, MA. https://doi.org/10.1007/978-1-4615-5367-0

Węgrzyn, W. (2012). *Elektrobiblioteka*.
    https://web.archive.org/web/20191207054322/http://www.elektrobiblioteka.net/

Weiser, M. (1991, September 1). The computer for the 21st century. *Scientific American*, *265*(3), 94–
    104. https://doi.org/10.1038/scientificamerican0991-94

Wessely, M., Tsandilas, T., & Mackay, W. E. (2016). Stretchis: Fabricating highly stretchable user
    interfaces. *Proceedings of the 29th Annual Symposium on User Interface Software and
    Technology*, 697–704. https://doi.org/10.1145/2984511.2984521

Wu, L., Alamusi, Xue, J., Itoi, T., Hu, N., Li, Y., Yan, C., Qiu, J., Ning, H., Yuan, W., & Gu, B. (2014).
    Improved energy harvesting capability of poly(vinylidene fluoride) films modified by reduced
    graphene oxide. *Journal of Intelligent Material Systems and Structures*, *25*(14), 1813–1824.
    https://doi.org/10.1177/1045389X14529609

Wu, T., Jin, H., Dong, S., Xuan, W., Xu, H., Lu, L., Fang, Z., Huang, S., Tao, X., Shi, L., Liu, S., & Luo, J.
    (2020). A flexible film bulk acoustic resonator based on β-phase polyvinylidene fluoride polymer.
    Sensors, *20*(5). https://doi.org/10.3390/s20051346

Wu, W. (2017). Inorganic nanomaterials for printed electronics: A review. *Nanoscale*, *9*(22), 7342–
    7372. https://doi.org/10.1039/C7NR01604B

Wu, Y., & Huang, T. (2018). Design of high precision capacitance displacement sensor. *2018 IEEE 3rd Advanced Information Technology, Electronic and Automation Control Conference (IAEAC)*, 83–87. https://doi.org/10.1109/IAEAC.2018.8577635

Xie, L., Antle, A. N., & Motamedi, N. (2008). Are tangibles more fun? Comparing children's enjoyment and engagement using physical, graphical and tangible user interfaces. *Proceedings of the 2nd International Conference on Tangible and Embedded Interaction*, 191–198. https://doi.org/10.1145/1347390.1347433

Xu, J.-Z., Zhong, G.-J., Hsiao, B. S., Fu, Q., & Li, Z.-M. (2014). Low-dimensional carbonaceous nanofiller induced polymer crystallization. *Progress in Polymer Science*, *39*(3), 555–593. https://doi.org/10.1016/j.progpolymsci.2013.06.005

Xu, T.-B. (2016). 7 - Energy harvesting using piezoelectric materials in aerospace structures. In F.-G. Yuan (Ed.), *Structural health monitoring (SHM) in aerospace structures* (pp. 175–212). Woodhead Publishing. https://doi.org/10.1016/B978-0-08-100148-6.00007-X

Yagi, T., Higashihata, Y., Fukuyama, K., & Sako, J. (1984). Piezoelectric properties of rolled vinylidene fluoride and trifluoroethylene copolymer. *Ferroelectrics*, *57*(1), 327–335. https://doi.org/10.1080/00150198408012771

Yagi, T., & Tatemoto, M. (1979). A fluorine-19 NMR study of the microstructure of vinylidene fluoride–trifluoroethylene copolymers. *Polymer Journal*, *11*(6), 429–436. https://doi.org/10.1295/polymj.11.429

Yang, P., Tian, F., & Ohki, Y. (2014). Dielectric properties of poly(ethylene terephthalate) and poly(ethylene 2,6-naphthalate). *IEEE Transactions on Dielectrics and Electrical Insulation*, *21*(5), 2310–2317. https://doi.org/10.1109/TDEI.2014.004416

Yang, T., Xie, D., Li, Z., & Zhu, H. (2017). Recent advances in wearable tactile sensors: Materials, sensing mechanisms, and device performance. *Materials Science and Engineering: R: Reports*, *115*, 1–37. https://doi.org/10.1016/j.mser.2017.02.001

Yang, W., Huang, J., Wang, R., Zhang, W., Liu, H., & Xiao, J. (2021). A survey on tactile displays for visually impaired people. *IEEE Transactions on Haptics*, 1. https://doi.org/10.1109/TOH.2021.3085915

Yang, X., Wang, Y., & Qing, X. (2019). A flexible capacitive sensor based on the electrospun PVDF nanofiber membrane with carbon nanotubes. *Sensors and Actuators A: Physical*, *299*, 111579. https://doi.org/10.1016/j.sna.2019.111579

Yang, Y.-J., Cheng, M.-Y., Chang, W.-Y., Tsao, L.-C., Yang, S.-A., Shih, W.-P., Chang, F.-Y., Chang, S.-H., & Fan, K.-C. (2008). An integrated flexible temperature and tactile sensing array using PI-copper films. *Sensors and Actuators A: Physical*, *143*(1), 143–153. https://doi.org/10.1016/j.sna.2007.10.077

Yoon, S., & Cho, Y.-H. (2014). A skin-attachable flexible piezoelectric pulse wave energy harvester. *Journal of Physics: Conference Series*, *557*, 12026. https://doi.org/10.1088/1742-6596/557/1/012026

Yoon, S. H., Ma, S., Lee, W. S., Thakurdesai, S., Sun, D., Ribeiro, F. P., & Holbery, J. D. (2019). HapSense: A soft haptic I/O device with uninterrupted dual functionalities of force sensing and vibrotactile actuation. *Proceedings of the 32nd Annual ACM Symposium on User Interface Software and Technology*, 949–961. https://doi.org/10.1145/3332165.3347888

Yu, Y., Sun, H., Orbay, H., Chen, F., England, C. G., Cai, W., & Wang, X. (2016). Biocompatibility and in vivo operation of implantable mesoporous PVDF-based nanogenerators. *Nano Energy*, *27*, 275–281. https://doi.org/10.1016/j.nanoen.2016.07.015

Yue, S., & Moussa, W. A. (2018). A piezoresistive tactile sensor array for touchscreen panels. *IEEE Sensors Journal*, *18*(4), 1685–1693. https://doi.org/10.1109/JSEN.2017.2776936

Zaeimbashi, M., Nasrollahpour, M., Khalifa, A., Romano, A., Liang, X., Chen, H., Sun, N., Matyushov, A., Lin, H., Dong, C., Xu, Z., Mittal, A., Martos-Repath, I., Jha, G., Mirchandani, N., Das, D., Onabajo, M., Shrivastava, A., Cash, S., & Sun, N. X. (2021). Ultra-compact dual-band smart NEMS magnetoelectric antennas for simultaneous wireless energy harvesting and magnetic field sensing. *Nature Communications*, *12*(1), 3141. https://doi.org/10.1038/s41467-021-23256-z

Zaitsev, I. O., Levytskyi, A. S., & Kromplyas, B. A. (2019). Capacitive distance sensor with coplanar electrodes for large turbogenerator core clamping system. *2019 IEEE 39th International Conference on Electronics and Nanotechnology (ELNANO)*, 644–647. https://doi.org/10.1109/ELNANO.2019.8783916

Zhang, B., Xiang, Z., Zhu, S., Hu, Q., Cao, Y., Zhong, J., Zhong, Q., Wang, B., Fang, Y., Hu, B., Zhou, J., & Wang, Z. (2014). Dual functional transparent film for proximity and pressure sensing. *Nano Research*, *7*(10), 1488–1496. https://doi.org/10.1007/s12274-014-0510-3

Zhang, Q., Niu, S., Wang, L., Lopez, J., Chen, S., Cai, Y., Du, R., Liu, Y., Lai, J.-C., Liu, L., Li, C.-H., Yan, X., Liu, C., Tok, J. B.-H., Jia, X., & Bao, Z. (2018). An elastic autonomous self-healing capacitive sensor based on a dynamic dual crosslinked chemical system. *Advanced Materials*, *30*(33), 1801435. https://doi.org/10.1002/adma.201801435

Zhang, R., & Olin, H. (2020). Material choices for triboelectric nanogenerators: A critical review. *EcoMat*, *2*(4), e12062. https://doi.org/10.1002/eom2.12062

Zhang, Yang, Laput, G., & Harrison, C. (2017). Electrick: Low-cost touch sensing using electric field tomography. *Proceedings of the 2017 CHI Conference on Human Factors in Computing Systems*, 1–14. https://doi.org/10.1145/3025453.3025842

Zhang, Yubai, Shi, G., Qin, J., Lowe, S. E., Zhang, S., Zhao, H., & Zhong, Y. L. (2019). Recent progress of direct ink writing of electronic components for advanced wearable devices. *ACS Applied Electronic Materials*, *1*(9), 1718–1734. https://doi.org/10.1021/acsaelm.9b00428

Zhao, T., Jiang, W., Niu, D., Liu, H., Chen, B., Shi, Y., Yin, L., & Lu, B. (2017). Flexible pyroelectric device for scavenging thermal energy from chemical process and as self-powered temperature monitor. *Applied Energy*, *195*, 754–760. https://doi.org/10.1016/j.apenergy.2017.03.097

Zhao, X., Xu, S., & Liu, J. (2017). Surface tension of liquid metal: role, mechanism and application. *Frontiers in Energy*, *11*(4), 535–567. https://doi.org/10.1007/s11708-017-0463-9

Zheng, Y., Li, Y., Dai, K., Liu, M., Zhou, K., Zheng, G., Liu, C., & Shen, C. (2017). Conductive thermoplastic polyurethane composites with tunable piezoresistivity by modulating the filler dimensionality for flexible strain sensors. *Composites Part A: Applied Science and Manufacturing*, *101*, 41–49. https://doi.org/10.1016/j.compositesa.2017.06.003

Zhou, B., Singh, M. S., Doda, S., Yildirim, M., Cheng, J., & Lukowicz, P. (2017). The carpet knows: Identifying people in a smart environment from a single step. *2017 IEEE International Conference on Pervasive Computing and Communications Workshops, PerCom Workshops 2017*, 527–532. https://doi.org/10.1109/PERCOMW.2017.7917618

Zhu, X. (2010). Piezoelectric ceramics materials: Processing, properties, characterization, and applications. In W. G. Nelson (Ed.), *Piezoelectric Materials: Structure, Properties and Applications* (pp. 1–36). Nova Science Publishers Inc. http://www.novapublishers.org/catalog/product_info.php?products_id=29257

Zimmerman, T. G., Smith, J. R., Paradiso, J. A., Allport, D., & Gershenfeld, N. (1995). Applying electric field sensing to human-computer interfaces. *Proceedings of the SIGCHI Conference on Human Factors in Computing Systems*, 280–287. https://doi.org/10.1145/223904.223940

9. APPENDICES

The following appendices follow:

APPENDIX A   **Calculation of transfer functions for piezoelectric sensing**

Here is shown the expansion of the transfer functions used for the piezoelectric device.

Figure A.1 shows the implemented circuit for touch and bending sensors.
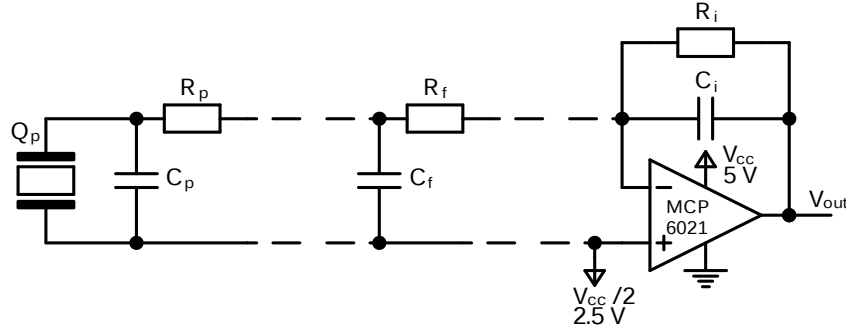
Figure A.1.   Charge amplifier with piezoelectric sensor.

It can be divided into three modules:
-   The piezoelectric sensor (Q_p, R_p and C_p – creating a 1st order LPF);
-   The input filter (R_f and C_f – creating a 1st order LPF);
-   And the amplifying integrating stage (operational amplifier, R_i and C_i – creating a 1st order HPF with gain).

The transfer functions $H_p(s)$, $H_f(s)$ and $H_i(s)$ for the piezoelectric sensor, input filter and amplifying integrating stage, respectively. Obviously, any combination of modules has an associated combination of transfer functions, for example $H_{pfi}(s)$ to refer the transfer function of the whole circuit.

Initially, it will be calculated the transfer function of each individual module, and then the global transfer function.

A.1.   **Transfer function of the piezoelectric device**

Objective: Calculate $H_p(s) = \frac{Q_{out}(s)}{Q_p(s)}$ of the piezoelectric sensor in short-circuit (since the charge amplifier sets its inputs in short-circuit) from Figure A.2.
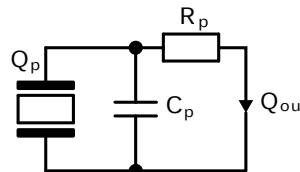
Figure A.2.   Piezoelectric sensor in short-circuit.

First, let's calculate the voltage of the piezoelectric V_p:

$$V_p(s) = \frac{1}{sC_p + \frac{1}{R_p}} I_p(s) = \frac{R_p}{sC_pR_p + 1} I_p(s) \tag{A.1}$$

Then, the output current:

$$I_{out}(s) = \frac{V_p(s)}{R_p} = \frac{\frac{R_p}{sC_pR_p + 1}I_p(s)}{R_p} = \frac{1}{sC_pR_p + 1}I_p(s) \tag{A.2}$$

Since charge is the integral of current over time:

$$Q(s) = \frac{1}{s}I(s) - i(0) \tag{A.3}$$

Considering null initial conditions $i(0) = 0$, then:

$$H_p(s) = \frac{Q_{out}(s)}{Q_p(s)} = \frac{\frac{1}{s}I_{out}(s)}{\frac{1}{s}I_p(s)} = \frac{I_{out}(s)}{I_p(s)} \tag{A.4}$$

Finally, substituting Equation (A.2) in Equation (A.4):

$$H_p(s) = \frac{Q_{out}(s)}{Q_p(s)} = \frac{1}{\frac{s}{\omega_p} + 1}, \qquad \omega_p = \frac{1}{C_pR_p} \tag{A.5}$$

A.2. Transfer function of the input LPF

Objective: Calculate $H_f(s) = \frac{Q_{out}(s)}{Q_{in}(s)}$ of the input LPF in short-circuit (since the charge amplifier sets its inputs in short-circuit) from Figure A.3.
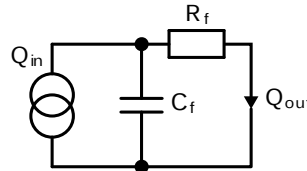
Figure A.3. Input filter with output in short-circuit.

This is the same as the previous case (section A.1), so the transfer function is similar:

$$H_f(s) = \frac{Q_{out}(s)}{Q_{in}(s)} = \frac{1}{\frac{s}{\omega_f} + 1}, \qquad \omega_f = \frac{1}{C_fR_f} \tag{A.6}$$

A.3. Transfer function of the charge amplifier

Objective: Calculate $H_i(s) = \frac{V_{out}(s)}{Q_{in}(s)}$ of the charge amplifyer with HPF from Figure A.4.
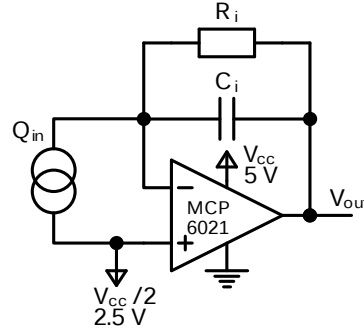
Figure A.4. Charge amplifier stage, which is just an integrator, with HPF.

First, let's calculate the output voltage of the amplifier V_{out}:

$$V_{out}(s) = -\frac{1}{sC_i + \dfrac{1}{R_i}} I_{in}(s) = -\frac{R_i}{sC_iR_i + 1} I_{in}(s) \tag{A.7}$$

Since current is just the derivative of charge over time, then:

$$I_{in}(s) = sQ_{in}(s) + q_{in}(0) \tag{A.8}$$

Considering null initial conditions $q_{in}(0) = 0$, then:

$$V_{out}(s) = -\frac{sR_i}{sC_iR_i + 1} Q_{in}(s) \tag{A.9}$$

Now, calculating the transfer function:

$$H_i(s) = \frac{V_{out}(s)}{Q_{in}(s)} = -\frac{sR_i}{sC_iR_i + 1} \tag{A.10}$$

Converting to the general zeros/poles form:

$$\boxed{H_i(s) = \frac{V_{out}(s)}{Q_{in}(s)} = -\frac{sR_i}{\dfrac{s}{\omega_i} + 1}, \qquad \omega_i = \frac{1}{C_iR_i}} \tag{A.11}$$

A.4. Transfer function of the piezoelectric sensor with charge amplifier.

Objective: Calculate $H_{pfi}(s) = \frac{V_{out}(s)}{Q_p(s)}$ of the whole circuit from Figure A.2.

Attention: The transfer function of this circuit cannot be simply calculated by multiplying $H_p(s)$, $H_f(s)$, and $H_i(s)$ because the piezoelectric sensor and the input filter modules are not isolated from each other in terms of current. Not only the input filter module excerces a variable load on the piezoelectric sensor, but also the piezoelectric sensor can actually sink current from the input filter. This changes their cuttoff frequencies. However an approximation is:

$$H_{pf}(s) \cong H_p(s) \cdot H_f(s), \qquad \text{only if } \omega_p \text{ and } \omega_f \text{ are very different.} \tag{A.12}$$
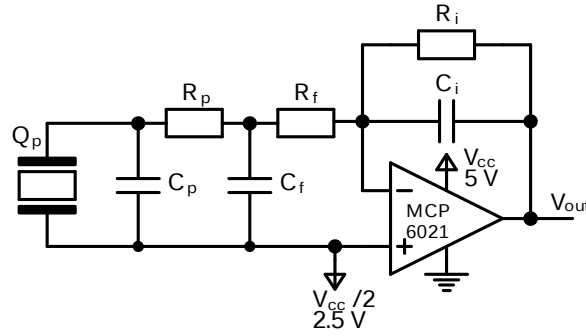
Figure A.5.   Piezoelectric sensor with a charge amplifier circuit.

The same does not happen with the amplifying stage module because the inputs of the operational amplifier are kept very stable as long as the operational amplifier does not reach saturation. Therefore:

$$H_{\mathrm{pfi}}(s) = H_{\mathrm{pf}}(s) \cdot H_{\mathrm{i}}(s) \tag{A.13}$$

To calculate $H_{\mathrm{pf}}(s) = \frac{Q_{\mathrm{out}}(s)}{Q_{\mathrm{p}}(s)}$ it is necessary to analyze the piezoelectric and the input filter modules as a whole 2nd order LPF.

First, let's calculate the voltage in the piezoelectric sensor V_{p}:

$$V_{\mathrm{p}}(s) = \cfrac{1}{sC_{\mathrm{p}} + \cfrac{1}{R_{\mathrm{p}} + \cfrac{1}{sC_{\mathrm{f}} + \cfrac{1}{R_{\mathrm{f}}}}}} I_{\mathrm{p}}(s) = \cfrac{1}{sC_{\mathrm{p}} + \cfrac{1}{R_{\mathrm{p}} + \cfrac{R_{\mathrm{f}}}{sC_{\mathrm{f}}R_{\mathrm{f}} + 1}}} I_{\mathrm{p}}(s)$$

$$= \cfrac{1}{sC_{\mathrm{p}} + \cfrac{sC_{\mathrm{f}}R_{\mathrm{f}} + 1}{sC_{\mathrm{f}}R_{\mathrm{f}}R_{\mathrm{p}} + R_{\mathrm{p}} + R_{\mathrm{f}}}} I_{\mathrm{p}}(s)$$

$$= \frac{sC_{\mathrm{f}}R_{\mathrm{f}}R_{\mathrm{p}} + R_{\mathrm{p}} + R_{\mathrm{f}}}{s^2 C_{\mathrm{p}}C_{\mathrm{f}}R_{\mathrm{f}}R_{\mathrm{p}} + sC_{\mathrm{p}}R_{\mathrm{p}} + sC_{\mathrm{p}}R_{\mathrm{f}} + sC_{\mathrm{f}}R_{\mathrm{f}} + 1} I_{\mathrm{p}}(s) \tag{A.14}$$

Now let's calculate the output current I_{out} from the input filter module:

$$I_{\mathrm{out}}(s) = \frac{V_{\mathrm{p}}(s) - I_{R_{\mathrm{p}}}(s)R_{\mathrm{p}}}{R_{\mathrm{f}}} = \frac{V_{\mathrm{p}}(s) - (I_{\mathrm{p}}(s) - V_{\mathrm{p}}(s) \cdot sC_{\mathrm{p}})R_{\mathrm{p}}}{R_{\mathrm{f}}}$$

$$= \frac{-I_{\mathrm{p}}(s)R_{\mathrm{p}} + (1 + sC_{\mathrm{p}}R_{\mathrm{p}})V_{\mathrm{p}}(s)}{R_{\mathrm{f}}}$$

$$= \frac{-I_{\mathrm{p}}(s)R_{\mathrm{p}} + (1 + sC_{\mathrm{p}}R_{\mathrm{p}})\dfrac{sC_{\mathrm{f}}R_{\mathrm{f}}R_{\mathrm{p}} + R_{\mathrm{p}} + R_{\mathrm{f}}}{s^2 C_{\mathrm{p}}C_{\mathrm{f}}R_{\mathrm{f}}R_{\mathrm{p}} + sC_{\mathrm{p}}R_{\mathrm{p}} + sC_{\mathrm{p}}R_{\mathrm{f}} + sC_{\mathrm{f}}R_{\mathrm{f}} + 1} I_{\mathrm{p}}(s)}{R_{\mathrm{f}}}$$

$$= \frac{-R_{\mathrm{p}} + (1 + sC_{\mathrm{p}}R_{\mathrm{p}})\dfrac{sC_{\mathrm{f}}R_{\mathrm{f}}R_{\mathrm{p}} + R_{\mathrm{p}} + R_{\mathrm{f}}}{s^2 C_{\mathrm{p}}C_{\mathrm{f}}R_{\mathrm{f}}R_{\mathrm{p}} + sC_{\mathrm{p}}R_{\mathrm{p}} + sC_{\mathrm{p}}R_{\mathrm{f}} + sC_{\mathrm{f}}R_{\mathrm{f}} + 1} I_{\mathrm{p}}(s)}{R_{\mathrm{f}}}$$

$$= \frac{-R_{\mathrm{p}} + \dfrac{sC_{\mathrm{f}}R_{\mathrm{f}}R_{\mathrm{p}} + R_{\mathrm{p}} + R_{\mathrm{f}} + s^2 C_{\mathrm{f}}C_{\mathrm{p}}R_{\mathrm{f}}R_{\mathrm{p}}^2 + sC_{\mathrm{p}}R_{\mathrm{p}}^2 + sC_{\mathrm{p}}R_{\mathrm{f}}R_{\mathrm{p}}}{s^2 C_{\mathrm{p}}C_{\mathrm{f}}R_{\mathrm{f}}R_{\mathrm{p}} + sC_{\mathrm{p}}R_{\mathrm{p}} + sC_{\mathrm{p}}R_{\mathrm{f}} + sC_{\mathrm{f}}R_{\mathrm{f}} + 1} I_{\mathrm{p}}(s)}{R_{\mathrm{f}}} \tag{A.15}$$

$$= \frac{-s^2 C_p C_f R_f R_p^2 - s C_p R_p^2 - s C_p R_f R_p - s C_f R_f R_p - R_p + \frac{s C_f R_f R_p + R_p + R_f + s^2 C_f C_p R_f R_p^2 + s C_p R_p^2 + s C_p R_f R_p}{s^2 C_p C_f R_f R_p + s C_p R_p + s C_p R_f + s C_f R_f + 1} I_p(s)}{R_f}$$

$$= \frac{\frac{-s^2 C_p C_f R_f R_p^2 - s C_p R_p^2 - s C_p R_f R_p - s C_f R_f R_p - R_p + s C_f R_f R_p + R_p + R_f + s^2 C_f C_p R_f R_p^2 + s C_p R_p^2 + s C_p R_f R_p}{s^2 C_p C_f R_f R_p + s C_p R_p + s C_p R_f + s C_f R_f + 1} I_p(s)}{R_f}$$

$$= \frac{\frac{-\cancel{s^2 C_p C_f R_f R_p^2} - \cancel{s C_p R_p^2} - \cancel{s C_p R_f R_p} - \cancel{s C_f R_f R_p} - \cancel{R_p} + \cancel{s C_f R_f R_p} + \cancel{R_p} + R_f + \cancel{s^2 C_f C_p R_f R_p^2} + \cancel{s C_p R_p^2} + \cancel{s C_p R_f R_p}}{s^2 C_p C_f R_f R_p + s C_p R_p + s C_p R_f + s C_f R_f + 1} I_p(s)}{R_i} \tag{A.16}$$

$$I_{\text{out}}(s) = \frac{1}{s^2 C_p C_f R_f R_p + s C_p R_p + s C_p R_f + s C_f R_f + 1} I_p(s) \tag{A.17}$$

And now we can calculate $H_{\text{pf}}(s)$:

$$\boxed{H_{\text{pf}}(s) = \frac{I_{\text{out}}(s)}{I_p(s)} = \frac{Q_{\text{out}}(s)}{Q_p(s)} = \frac{1}{s^2 C_p C_f R_f R_p + s C_p R_p + s C_p R_f + s C_f R_f + 1}} \tag{A.18}$$

However, in this expression it is not very easy to calculate the poles. So, let's expand the divisor onto its poles:

$$s^2 C_p C_f R_f R_p + s C_p R_p + s C_p R_f + s C_f R_f + 1 = k(s-a)(s-b) \tag{A.19}$$

and find the k, a and b constants:

$$s^2 C_p C_f R_p R_f + s C_p R_p + s C_p R_f + s C_f R_f + 1 = ks^2 - ksb - ksa + kab$$

$$= \begin{cases} C_p C_f R_p R_f = k \\ C_p R_p + C_p R_f + C_f R_f = -kb - ka \\ 1 = kab \end{cases}$$

$$= \begin{cases} C_p R_p + C_p R_f + C_f R_f = -C_p C_f R_p R_f (b+a) \\ 1 = C_p C_f R_p R_f ab \end{cases}$$

$$= \begin{cases} C_p R_p + C_p R_f + C_f R_f = -C_p C_f R_p R_f b - \cancel{C_p C_f R_p R_f} \dfrac{1}{\cancel{C_p C_f R_p R_f} b} \\ a = \dfrac{1}{C_p C_i R_p R_i b} \end{cases}$$

$$= \begin{cases} C_p R_p + C_p R_f + C_f R_f + C_p C_f R_p R_f b = -\dfrac{1}{b} \end{cases}$$

$$= \begin{cases} C_p C_f R_p R_f b^2 + (C_p R_p + C_p R_f + C_f R_f) b + 1 = 0 \end{cases}$$

$$= \begin{cases} b = \dfrac{-C_p R_p - C_p R_f - C_f R_f \pm \sqrt{(C_p R_p + C_p R_f + C_f R_f)^2 - 4 C_p C_f R_p R_f}}{2 C_p C_f R_p R_f} \end{cases} \tag{A.20}$$

The $\pm$ sign means that a and b can be swapped. So, let's just pick one option:

$$= \begin{cases} k = C_pC_fR_pR_f \\[2mm] b = \dfrac{-C_pR_p - C_pR_f - C_fR_f + \sqrt{\left(C_pR_p + C_pR_f + C_fR_f\right)^2 - 4C_pC_fR_pR_f}}{2C_pC_fR_pR_f} \\[4mm] a = \dfrac{-C_pR_p - C_pR_f - C_fR_f - \sqrt{\left(C_pR_p + C_pR_f + C_fR_f\right)^2 - 4C_pC_fR_pR_f}}{2C_pC_fR_pR_f} \end{cases} \tag{A.21}$$

Substituting k, a and b in Equation (A.19):

$$k(s-a)(s-b) = C_pC_fR_pR_f \left(s - \frac{-C_pR_p - C_pR_f - C_fR_f - \sqrt{\left(C_pR_p + C_pR_f + C_fR_f\right)^2 - 4C_pC_fR_pR_f}}{2C_pC_fR_pR_f} \right) \times$$

$$\times \left(s - \frac{-C_pR_p - C_pR_f - C_fR_f + \sqrt{\left(C_pR_p + C_pR_f + C_fR_f\right)^2 - 4C_pC_fR_pR_f}}{2C_pC_fR_pR_f} \right) \tag{A.22}$$

Getting back to the transfer function $H_{pf}(s)$ from Equation (A.18):

$$H_{pf}(s) = \frac{1}{s^2 C_pC_fR_fR_p + sC_pR_p + sC_pR_f + sC_fR_f + 1} = \frac{1}{k(s-a)(s-b)} = \frac{1}{kab\left(\frac{s}{-a}+1\right)\left(\frac{s}{-b}+1\right)}$$

$$= \frac{1}{C_pC_fR_pR_f \frac{-C_pR_p - C_pR_f - C_fR_f - \sqrt{\left(C_pR_p + C_pR_f + C_fR_f\right)^2 - 4C_pC_fR_pR_f}}{2C_pC_fR_pR_f} \cdot \frac{-C_pR_p - C_pR_f - C_fR_f + \sqrt{\left(C_pR_p + C_pR_f + C_fR_f\right)^2 - 4C_pC_fR_pR_f}}{2C_pC_fR_pR_f}} \times$$

$$\times \frac{1}{\left(\frac{s}{-a}+1\right)\left(\frac{s}{-b}+1\right)} = \frac{1}{\frac{(-C_pR_p - C_pR_f - C_fR_f)^2 - \sqrt{\left(C_pR_p + C_pR_f + C_fR_f\right)^2 - 4C_pC_fR_pR_f}}{4C_pC_fR_pR_f}^2} \frac{1}{\left(\frac{s}{-a}+1\right)\left(\frac{s}{-b}+1\right)}$$

$$= \frac{1}{\frac{(-C_pR_p - C_pR_f - C_fR_f)^2 - (C_pR_p + C_pR_f + C_fR_f)^2 + 4C_pC_fR_pR_f}{4C_pC_fR_pR_f}} \frac{1}{\left(\frac{s}{-a}+1\right)\left(\frac{s}{-b}+1\right)} = \frac{1}{\left(\frac{s}{-a}+1\right)\left(\frac{s}{-b}+1\right)} \tag{A.23}$$

Substituting $-a$ and $-b$ by the angular frequencies ω_p and ω_f:

$$\boxed{\begin{aligned} H_{pf}(s) &= \frac{I_{out}(s)}{I_{in}(s)} = \frac{Q_{out}(s)}{Q_{in}(s)} = \frac{1}{\left(\frac{s}{\omega_p}+1\right)\left(\frac{s}{\omega_f}+1\right)}, \\[4mm] \omega_p &= \frac{C_pR_p + C_pR_f + C_fR_f + \sqrt{\left(C_pR_p + C_pR_f + C_fR_f\right)^2 - 4C_pC_fR_pR_f}}{2C_pC_fR_pR_f}, \\[4mm] \omega_f &= \frac{C_pR_p + C_pR_f + C_fR_f - \sqrt{\left(C_pR_p + C_pR_f + C_fR_f\right)^2 - 4C_pC_fR_pR_f}}{2C_pC_fR_pR_f} \end{aligned}} \tag{A.24}$$

However, if one of the frequencies ω_p and ω_f is much greater than the other, the corresponding pair of R_x and C_x will dominate over the remaining terms, and it is possible to approximate the values of ω_p and ω_f to:

$$\omega_p \cong \frac{1}{R_pC_p}, \qquad \omega_f \cong \frac{1}{R_fC_f} \tag{A.25}$$

Now, getting back to the original multiplication of transfer functions, from Equation (A.13):

$$H_{\text{pfi}}(s) = H_{\text{pf}}(s) \cdot H_{\text{i}}(s)$$ (A.26)

and substituting $H_{\text{pf}}(s)$ and $H_{\text{i}}(s)$ from Equations (A.24) and (A.11), respectively:

$$
\begin{aligned}
H_{pfi}(s) &= -\frac{s\mathrm{R_i}}{\left(\frac{s}{\omega_{\mathbf{p}}}+1\right)\left(\frac{s}{\omega_{\mathbf{f}}}+1\right)\left(\frac{s}{\omega_{\mathbf{i}}}+1\right)}, \\[2mm]
\omega_{\mathrm{p}} &= \frac{\mathrm{C_pR_p} + \mathrm{C_pR_f} + \mathrm{C_fR_f} + \sqrt{\left(\mathrm{C_pR_p} + \mathrm{C_pR_f} + \mathrm{C_fR_f}\right)^2 - 4\mathrm{C_pC_fR_pR_f}}}{2\mathrm{C_pC_fR_pR_f}}, \\[2mm]
\omega_{\mathrm{f}} &= \frac{\mathrm{C_pR_p} + \mathrm{C_pR_f} + \mathrm{C_fR_f} - \sqrt{\left(\mathrm{C_pR_p} + \mathrm{C_pR_f} + \mathrm{C_fR_f}\right)^2 - 4\mathrm{C_pC_fR_pR_f}}}{2\mathrm{C_pC_fR_pR_f}}, \\[2mm]
\omega_{\mathrm{i}} &= \frac{1}{\mathrm{C_iR_i}}
\end{aligned}
$$ (A.27)

Or, for very different values of ω_{p} and ω_{f}:

$$
\begin{aligned}
H_{\mathbf{pfi}}(s) &= -\frac{s\mathrm{R_i}}{\left(\frac{s}{\omega_{\mathbf{p}}}+1\right)\left(\frac{s}{\omega_{\mathbf{f}}}+1\right)\left(\frac{s}{\omega_{\mathbf{i}}}+1\right)}, \\[2mm]
\omega_{\mathrm{p}} &\cong \frac{1}{\mathrm{C_pR_p}}, \qquad \omega_{\mathrm{f}} \cong \frac{1}{\mathrm{C_fR_f}}, \qquad \omega_{\mathrm{i}} = \frac{1}{\mathrm{C_iR_i}}
\end{aligned}
$$ (A.28)

To calculate the gain A of the transfer function $H_{\text{pfi}}(s)$ can be just calculated by $H_{\text{i}}(s)$, since this is the only expression that has a zero:

$$A = \lim_{s \to \infty} H_{\text{i}}(s) = \lim_{s \to \infty} -\frac{s\mathrm{R_i}}{s\mathrm{C_iR_i} + 1} = \lim_{s \to \infty} -\frac{s\mathrm{R_{\cancel{i}}}}{s\mathrm{C_iR_{\cancel{i}}}} = -\frac{1}{\mathrm{C_i}}$$ (A.29)